U.PORTO

DOCTORATE
PATHOLOGY AND MOLECULAR GENETICS

UNRAVELLING THE ROLE OF HEPARAN SULFATE PROTEOGLYCANS IN CELL COMMUNICATION AND GASTRIC CANCER PROGRESSION

Juliana Poças

D

2023



U.PORTO Juliana Poças. **UNRAVELLING THE ROLE OF HEPARAN SULFATE PROTEOGLYCANS IN CELL COMMUNICATION AND GASTRIC CANCER PROGRESSION**

UNRAVELLING THE ROLE OF HEPARAN SULFATE PROTEOGLYCANS IN CELL COMMUNICATION AND GASTRIC CANCER PROGRESSION

JULIANA POÇAS

INSTITUTO DE **CIÊNCIAS BIOMÉDICAS ABEL SALAZAR**



JULIANA POÇAS

UNRAVELLING THE ROLE OF HEPARAN SULFATE PROTEOGLYCANS IN CELL COMMUNICATION AND GASTRIC CANCER PROGRESSION

Tese de Candidatura ao grau de Doutor em Patologia e Genética Molecular submetida ao Instituto de Ciências Biomédicas Abel Salazar da Universidade do Porto.

Porto

2023

JULIANA POÇAS

UNRAVELLING THE ROLE OF HEPARAN SULFATE PROTEOGLYCANS IN CELL COMMUNICATION AND GASTRIC CANCER PROGRESSION

Supervisor – Ana Maria Rodrigues Leite de Magalhães

Category – Assistant Professor

Affiliation – Instituto de Ciências Biomédicas Abel Salazar (ICBAS-UP) da Universidade do Porto; Instituto de Investigação e Inovação em Saúde (i3S) da Universidade do Porto.

Co-supervisor – Celso Albuquerque Reis

Category – Head of Glycobiology in cancer group; Coordinator Researcher

Affiliation – Instituto de Investigação e Inovação em Saúde (i3S) da Universidade do Porto; Instituto de Ciências Biomédicas Abel Salazar (ICBAS-UP) da Universidade do Porto.

Co-supervisor – Mattias Belting

Category – Head of Tumor Microenvironment group; Professor and senior consultant of oncology

Affiliation – Department of Clinical Sciences, Lund, Lund University, Sweden; Department of Immunology Genetics and Pathology, Uppsala, Uppsala University, Sweden.

Funding

The candidate was funded through a PhD fellowship (SFRH/BD/137319/2018) awarded by the Portuguese Foundation for Science and Technology (FCT) of the Portuguese Ministry of Science, Technology and Higher Education.

This work was supported through FEDER funds through the Operational Programme for Competitiveness Factors (COMPETE 2020), Programa Operacional de Competitividade e Internacionalização (POCI), Programa Operacional Regional do Norte (Norte 2020) and by National Funds through the Portuguese Foundation for Science and Technology (FCT) (POCI-01-0145-FEDER-028489).











“The most important thing is to never stop questioning.”

Albert Einstein

Declaration

In compliance with the terms of the n.º 2, alínea a) do artigo 31º do Decreto-Lei n.º 115/2013 de 7 de Agosto, the work developed under the scope of this thesis and hereby presented is published in peer-reviewed scientific journals, submitted or in preparation for submission, as further detailed:

Published scientific articles (included in this thesis):

Poças J, Marques C, Gomes C, Otake AH, Pinto F, Ferreira M, Silva T, Faria-Ramos I, Matos R, Ribeiro AR, Senra E, Cavadas B, Batista S, Maia J, Macedo JA, Lima L, Afonso LP, Ferreira JA, Santos LL, Polónia A, Osório H, Belting M, Reis CA, Costa-Silva B, Magalhães A. Syndecan-4 is a maestro of gastric cancer cell invasion and communication that underscores poor survival. Proc Natl Acad Sci U S A. 2023 May 16;120(20):e2214853120. doi: 10.1073/pnas.2214853120.

Poças J and Belting M. Analysis of Extracellular Vesicle-Associated Proteoglycans. In: Karamanos, N.K. (eds) Proteoglycans. Methods in Molecular Biology. 2023, vol 2619. Humana, New York, NY. https://doi.org/10.1007/978-1-0716-2946-8_10.

Published dataset:

Poças J, Osório H, Magalhães A. Identification and quantification of proteins from MKN74 WT and SDC4 KO cells and EVs. The PRoteomics IDEntifications (PRIDE) database. www.ebi.ac.uk/pride/ archive/projects/PXD035679. Deposited 1 August 2022.

Other publications, as co-author, within this thesis scope:

Faria-Ramos I, **Poças J**, Marques C, Santos-Antunes J, Macedo G, Reis CA, Magalhães A. Heparan Sulfate Glycosaminoglycans: (Un)Expected Allies in Cancer Clinical Management. *Biomolecules*. 2021; 11(2):136. https://doi.org/10.3390/biom11020136.

Marques C, **Poças J**, Gomes C, Faria-Ramos I, Reis CA, Vivès RR, Magalhães A. Glycosyltransferases EXTL2 and EXTL3 cellular balance dictates heparan sulfate biosynthesis and shapes gastric cancer cell motility and invasion. J Biol Chem. 2022 Nov;298(11):102546. doi: 10.1016/j.jbc.2022.102546.

Freitas D, Balmaña M, **Poças J,** Campos D, Osório H, Konstantinidi A, Vakhrushev SY, Magalhães A, Reis CA. Different isolation approaches lead to diverse glycosylated extracellular vesicle populations. *J Extracell Vesicles*. 2019, 8(1):1621131. doi: 10.1080/20013078.2019.1621131.

Maia J, Otake AH, **Poças J**, Carvalho AS, Beck HC, Magalhães A, Matthiesen R, Moraes MCS, Costa-Silva B. Transcriptome Reprogramming od CD11b+ Bone Marrow Cells by Pancreatic Cancer Extracellular Vesicles. *Front. Cell Dev. Biol*., 27 November 2020, Volume 8. https://doi.org/10.3389/fcell.2020.592518.

Scientific manuscript in preparation (included in this thesis):

Poças J, Faria-Ramos I, Santos-Antunes J, Branca RM, Carneiro F, Macedo G, Reis CA, Belting M, Magalhães A. Proteomic profiling of extracellular vesicles along the gastric carcinogenesis cascade. *In preparation*

Patent:

Type: Provisional Patent Application
Reference: 20221000003006
Title: Heparan Sulfate Proteoglycan form of Syndecan-4 as Extracellular Vesicle-associated Biomarker of Poor Survival and Organ Tropism

Authors: Ana Magalhães, **Juliana Poças**, Catarina Marques, Catarina Gomes, Celso A. Reis.

Acknowledgments

What a journey this PhD has been! It was really important to me that during the development of this work I had the opportunity to share this journey with several people. I know I am a lucky girl that had the opportunity to work in three amazing institutions – IPATIMUP/i3S in Porto; Champalimaud Foundation – Centre for the Unknown in Lisbon, and University of Lund in Sweden – where I was taught so much. In each of these instutions I learned, I evolved, I created, I laughed, I cried and I jumped.

I would like to start by thanking my supervisors. Thank you, Ana, for mentoring and guiding me during my PhD (and even before). Thank you for the “pós de prlim pim pim” that you shared together with Sofia and Tiago. Thank you to my co-supervisor Dr. Celso for receiving me in his lab and mentoring me. Mattias, thank you for receiving me in your lab in Lund. It was a great pleasure to know you and your team in Sweden. Your passion for science is truly inspiring. I am grateful for the time I had and how much I learned.

Thank you, Bruno Costa-Silva, for making me feel welcome in your lab in Lisbon, for all the scientific discussions and for being available every time we needed you!

To my family: You are everything to me! Thank you, thank you! I am so grateful to all of you! I will start with my sister. Sigé, you are a rock, my rock, my co-pilot. You are my shield, my support, who I can count for everything! Thank you for never allowing me to give up of this PhD (and there were quite a few times!) and always pushing me forward!

Thank you mommy linda! Without you, none of this journey would have been possible. You are the biggest reference I could ever ask; you are a woman with strength, determination, persistence and truthful to her beliefs. You deserve a bright and beautiful life! Thank you, Fernando, for supporting my supporter.

Margaret, Camila e Luna, my tiny creatures, thank you for existing and making me smile! I really hope that life will smile you back! Looking forward to seeing you all grow. Thank you to my brother, Frederico, obrigada!

To the best uncles I have, thank you for walking side by side with me since I was born. You are the best uncles that exist in this world: you are my second mother and father. It’s how I see you! I am so grateful that you exist in my life, that I can share my life with. Both of you are two pillars in this world, and in my world.

Grandma, thank you for the support and always believing in me. Grandpa, we will continue to play dominoes one day. I love you!

João, I do not know where the future will take us, but I want you to know, that I am deeply thankful that I met you during this journey. You are the kindest man I know. Thank you for

the everyday support, for listening to all my complains and vents, and for walking on my side everyday of this ride.

Oscar, thank you for being here all the time with my sister! Bruno, thank you for being the craziest person.

Claudio, bff, thank you for being here for more years than I can count with my fingers, and for sharing the difficult turnarounds of a PhD.

Ricardo, padrinho, thank you for always being around here for me and for the kind person that you are.

Nuno, I don't know if you are aware the importance of your friendship to me. I am really thankful that we met in Sweden! You were a great support during my time abroad and you still continue to be! A giant thank you for still being around!

Rita Vaz, pulga, thank you for listening and supporting me during all these years since graduation! You are a giant person and I hope you know that!

And since science is not only done on the bench, I would like to thank my lab colleagues, not just for the nerd discussions but also sharing the fun part including the vents, the dinners, the dances, the parties (also the drunk moments), the coffee breaks, and the gateways (☺). Thank you, to each of you, the ones that still are in the group and, as well, the ones which future took them in another path. Thank you so so much! You rock!

Thank you to the awesome team in Lund: Myriam, Valeria, Axel, Hugo, Anna, Sarah, Emilie and Jiaxin. A huge thank you to Kelin for helping me so much in the lab, as well the friendship outside of the lab. Thank you to Maria and Ann-Sofie for all the guidance in the lab, and for the conversations. I am grateful that I met you all.

Thank you to all the team in Champalimaud Foundation for your support and your help. Thank you, Andreia! Your help during my time in Lisbon was crucial for the development of this work. Thank you for your friendship!

Thank you to Hugo Osorio (head of the i3s Proteomics platform) and Rui Fernandes (head of i3s HEMS platform). Your attention and help were crucial for the development (and publication) of this work.

This thesis was written in Castro Daire, Porto, Lisboa, Lund and Geneva!

Table of contents

Figure Index 13

Abstract 15

Resumo 16

List of Abbreviations 17

Chapter I: General Introduction 21

1.1 Gastric cancer 23

1.2 Glycosylation in cancer 27

1.3 Glycosaminoglycans in cancer 30

1.4 Heparan Sulfate Proteoglycans 33

1.4.1 Syndecans 34

1.4.2 SDC structural features and biological functions 36

1.4.2.1 SDC1 36

1.4.2.2 SDC2 37

1.4.2.3 SDC3 37

1.4.2.4 SDC4 38

1.4.3 SDC aberrant expression in cancer 39

1.4.3.1 SDC1 39

1.4.3.2 SDC2 40

1.4.3.3 SDC3 41

1.4.3.4 SDC4 41

1.5 Extracellular Vesicles 42

1.5.1 The biogenesis of EVs 44

1.5.2 EV uptake and cell-cell communication 47

1.5.3 EVs and pre-metastatic niche establishment 48

1.6 PGs and EVs in cancer cell communication 50

1.6.1 Potential as biomarkers and therapeutic targets 50

Chapter II: General aim and specific objectives 53

2.1 Rationale and General aim 54

2.2 Specific objectives 54

Chapter III: Study of the SDC4 functional impact on gastric cancer 59

3.2 Supporting Information 71

3.3 Additional Information 103

Chapter IV: EV isolation methodologies and PG analysis 107

Chapter V: Disclosing EV signature along the gastric carcinogenesis 123
Chapter VI: General Discussion 131
Chapter VII: Conclusion and future perspectives 141
References 145

Figure Index

Chapter I

Figure 1 – The hallmarks of cancer, initially proposed by Hanahan and Weinberg; the later reviewed version also identified tumor-promoting inflammation and genome instability & mutation as enabling factors and emerging hallmarks. 23

Figure 2 - Gastric cancer age standardized incidence in males and females around the world 24

Figure 3 - Gastric cancer intestinal subtype progression accordingly to Pelayo Correa cascade 25

Figure 4 – Graphical depiction of overlapping histological and molecular classifications, with the features associated with each of the four molecular subtypes of gastric cancer highlighted 26

Figure 5 – The aberrant alteration of cancer cells involves molecular modifications affecting the glycosylation patterns 27

Figure 6 – The diverse structural composition of the GAG chains 31

Figure 7 – Schematic representation of the four syndecan members 35

Figure 8 – Cytoplasmic domain of SDC family members 36

Figure 9 – Schematic representation of EV content, including proteins, glycans, lipids, metabolites, and nucleic acids 43

Figure 10 – EV biogenesis occurs through distinct pathways 45

Figure 11 - Schematic representation of the establishment of the pre-metastatic niche 49

Chapter III

Figure 1 – SDC4 is highly expressed in intestinal subtype gastric cancer and associates with patient poor survival 62

Figure 2 – *SDC4* KO impairs gastric cancer cell motility features 63

Figure 3 – SDC4 is carried by gastric cancer cell EVs and affects EV secretion and size 65

Figure 4 – SDC4 impacts EVs proteomic signature 66

Figure 5 – EVs depend on SDC4 for their internalisation and functional activity ... 67

Figure 6 – SDC4 impacts EVs organ distribution 68

3.2 Supporting Information

Fig. S1. Higher magnification of a lymph node metastasis from diffuse gastric cancer 72

Fig. S2. *SDC4* expression associates with worse survival in gastric cancer patients 73
Fig. S3. *SDC4* KO validation by indel sequencing 75
Fig. S4. *SDC4* silencing impairs gastric cancer cell invasion 76
Fig. S5. Assessment of *SDC4* KO impact on key cellular signalling pathways 77
Fig. S6. Ponceau staining of protein lysates from cells and EVs 79
Fig. S7. Data from MS-based proteomic analysis 80
Fig. S8. WB for heparan sulfate (HS) in WT cells and EVs treated with Heparinase III (Hep. III) 81
Fig. S9. Biodistribution of EVs derived from WT and *SDC4* KO cells 82
Fig. S10. Sample gating strategy for FITC positive cells (Exo+), in flow cytometry assays 84
Fig. S11. Determination of EV uptake by NOD SCID mice organs 85
Fig. S12. EV uptake by macrophages 86

3.3 Additional Information

Figure 1 – Gastric cancer cell seeding assay in mice liver upon EV education 103

Chapter IV

Figure 1 – Schematic representation of LC-MS/MS proteomic analysis of EVs isolated from conditioned medium (CM) through ultracentrifugation (UC) plus Optiprep density gradient (ODG) and patient plasma EVs isolated by size exclusion chromatography (SEC) 110

Chapter V

Figure 1 – The amount and size of plasma circulating EVs increases along the gastric carcinogenesis cascade 128

Chapter VII

Figure 1 - Schematic representation of the experimental design from blood collection until LC-MS/MS analysis 142

Abstract

Gastric cancer is a leading cause of cancer-related mortality globally, and effective treatment options are limited. Heparan sulfate proteoglycans (HSPGs) have recently emerged as crucial players in tumor progression and intercellular communication. However, the functional implications of HSPGs in gastric cancer development are not well understood. In this study, we demonstrate that syndecan-4 (SDC4), a transmembrane proteoglycan, is highly expressed in gastric tumors of the intestinal subtype, which correlates with unfavorable patient outcome. Mechanistically, we establish SDC4 as a key regulator of gastric cancer cell motility and invasion. Notably, we observe efficient sorting of SDC4 decorated with heparan sulfate into extracellular vesicles (EVs). Moreover, SDC4 within EVs governs the distribution, uptake, and functional impact of gastric cancer cell-derived EVs in recipient cells. Specifically, our findings reveal that knockout of SDC4 disrupts the tropism of EVs towards common sites of gastric cancer metastasis. Furthermore, our data supports that SDC4-dependent EV education in mice influenced the seeding of gastric cancer cells in the liver. These results shed light on the molecular implications of SDC4 expression in gastric cancer cells and offer broader perspectives for the development of therapeutic strategies targeting the glycan-EV axis to hinder tumor progression.

In this study, we present methodological insights into the analysis of EVs-associated PGs obtained from cell cultures and patient plasma liquid biopsy. Additionally, we advanced knowledge regarding the biological characteristics of EVs along the gastric carcinogenesis, as we observed an increase in the quantity and size of EVs along the conditions associated with disease progression. This finding suggests that the EV cargo is influenced by the evolving events of the disease.

In summary, our findings unveil a novel role of SDC4 in governing the aggressive behavior of gastric cancer cells, with significant implications for patient prognosis. Furthermore, our study offers valuable insights into the glycan code of cancer-derived EVs, elucidating key molecular cues that regulate communication pathways in gastric cancer. These discoveries hold promise for advancing precision oncology and developing targeted interventions to curb tumor progression.

Resumo

O cancro gástrico é uma das principais causas de mortalidade relacionada com cancro, globalmente, e as opções de tratamento eficaz são limitadas. Os proteoglicanos de heparano de sulfato (HSPGs) surgiram recentemente como componentes cruciais na progressão tumoral e comunicação intercelular. No entanto, as implicações funcionais dos HSPGs no desenvolvimento do cancro gástrico não são ainda bem compreendidas. Neste estudo, demonstramos que o syndecan-4 (SDC4), um proteoglicano transmembranar, é altamente expresso em tumores gástricos do subtipo intestinal, e que a sua expressão está associada a um pior prognóstico dos pacientes. Mecanisticamente, estabelecemos o SDC4 como um regulador-chave da motilidade e invasão das células de cancro gástrico. Adicionalmente, observamos uma eficiente incorporação do SDC4 decorado com cadeias de heparano de sulfato em vesículas extracelulares (EVs). De notar, o SDC4 nas EVs coordena a distribuição, internalização e impacto funcional das EVs derivadas de células de cancro gástrico nas células recetoras. Especificamente, os nossos resultados revelam que a eliminação do SDC4 perturba o tropismo das EVs para órgãos comuns de metástase do cancro gástrico. Além disso, os nossos resultados suportam que a educação com EVs com SDC4 em modelos animais influenciou a permanência das células de cancro gástrico no fígado dos ratinhos. Estes resultados revelam as implicações moleculares da expressão do SDC4 nas células de cancro gástrico e oferecem perspetivas mais amplas para o desenvolvimento de estratégias terapêuticas direcionadas ao eixo dos glicanos-EV para inibir a progressão tumoral.

Neste estudo, apresentamos técnicas metodológicas para análise dos PGs associados às EVs isoladas a partir de culturas celulares e de biópsias líquidas de plasma de pacientes. Além disso, por análise das características biológicas das EVs ao longo da carcinogénese gástrica, observamos um aumento na quantidade e tamanho das EVs em diferentes condições associadas à progressão do cancro gástrico. Estes resultados sugerem que o conteúdo das EVs é influenciado pelos eventos moleculares da evolução da doença.

Em resumo, os nossos resultados revelam uma nova função do SDC4 no controlo do comportamento agressivo das células de cancro gástrico, com implicações significativas para o prognóstico dos pacientes. Adicionalmente, o nosso estudo oferece ainda informações sobre o código entre os glicanos e as EVs derivadas do cancro, elucidando mecanismos moleculares que regulam vias de comunicação no cancro gástrico. Estas descobertas possibilitam o avanço da oncologia de precisão e o desenvolvimento de intervenções direcionadas para combater a progressão tumoral.

List of Abbreviations

A

ADAM: A Disintegrin And Metalloproteinase

ADP: Adenosine Diphosphate

Alix: Programmed cell death 6-interacting

ALK: Anaplastic lymphoma kinase

APCs: Antigen-Presenting Cells

ARF: ADP-Ribosylation Factor

ATP: Adenosine Triphosphate

ATPase: Adenosine Triphosphatase

B

BMP: Bone Morphogenetic Protein

BRAF: v-raf murine sarcoma oncogene

BSA: Bovine Serum Albumin

C

c-MET: tyrosine-protein kinase Met

Ca^{2+}: Calcium ions

Cas9: CRISPR-associated protein 9

CD274: Cluster of Differentiation 274

cDNA: complementar DNA

ChT: Chemotherapy

CIN: Chromosomal Instability

CM: Conditioned Medium

COL1A2: Collagen alpha-2 (I)

CRISPR: Clustered Regularly Interspaced Short Palindromic Repeats

CS: Chondroitin Sulfate

CT: Computer Tomography

CXCL: C-X-C Motif Chemokine Ligand

D

DF: Dilution Factor

DFS: Disease Free Survival

DNA: Deoxyribonucleic Acid

DS: Dermatan Sulfate

dsDNA: double stranded DNA

E

EBV: Epstein–Barr Virus

EC: Early Cancer

ECF: Epirubicinecisplatine5-FU

ECM: Extracellular Matrix

EDTA: Ethylenediaminetetraacetic Acid

EGFR: Epidermal Growth Factor Receptor

EMT: Epithelial Mesenchymal Transition

ESCRT: Endosomal-Sorting Complex Required for Transport

EUS: Endoscopic Ultrasonography

EVs: Extracellular Vesicles

F

FACS: Fluorescence-Activated Cell Sorter FBS: Fetal Bovine Serum

FAK: Focal Adhesion Kinase

FGF2: Fibroblast Growth Factor 2

FN: Fibronectin

FOXA2: Forkhead box A2

G

GAGs: Glycosaminoglycans

GAS6: Growth Arrest-Specific 6

GDP: Guanosine Diphosphate

GDPase: Guanosine Diphosphatase

GFP: Green Fluorescent Protein

GIST: Gastrointestinal Stromal Tumors

GlcA: Glucuronic Acid

GPC: Glypican

GPI: Glycosylphosphatidyl-Inositol
gRNA: guide RNA
GS: Genomically Stable
GTP: Guanosine Triphosphate
GTPase: Guanosine Triphosphatase

H

H. pylori: *Helicobacter pylori*
HA: Hyaluronic acid
HDL: High Density Lipoprotein
HepIII: Heparanase III
HER2: Human Epidermal Growth Factor Receptor-type 2
HGD: High Grade Dysplasia
HGF: Hepatocyte Growth Factor
HiRIEF: High Resolution Isoelectric Focusing
HPSE: Heparanase
HS: Heparan Sulfate
HSPGs: Heparan Sulfate Proteoglycans
HUVEC: Human Umbilical Vein Endothelial cells
HYAL: Hyaluronidase

I

I3S: Institute for Research and Innovation in Health
IdoA: Iduronic Acid
ILVs: Intraluminal Vesicles
ITGβ3: Integrin Subunit beta 3
IPO: Instituto Português Oncologia
ISEV: International Society for Extracellular Vesicles

J

JAK: Janus Kinases

K

KD: Knock-Down
KO: Knock-Out
KRAS: Kirsten rat sarcoma viral oncogene homolog
KS: Keratan Sulfate

L

LDL: Low Density Lipoprotein
Le^a: $Lewis^a$
Le^b: $Lewis^b$
Le^x: $Lewis^x$
Le^y: $Lewis^y$
LGD: Low Grade Dysplasia
LMWH: Low Molecular Weight Heparin
LN: Lymph Node
LOX: Lysyl Oxidase
LTβP2: Latent-Transforming Growth Factor beta-binding protein-2

M

MET: Hepatocyte Growth Factor Receptor
Mgat: Alpha-1,3-Mannosyl-Glycoprotein 2-Beta-N-Acetylglucosaminyltransferase
MHC: Major Histocompatibility Complex
MMP: Matrix metalloproteinase
mRNA: Messenger RNA
MS: Mass spectrometry
MSI: Microsatellite instable
MVBs: Multivesicular bodies

N

NaCl: Sodium Chloride
NEUs: Human Sialidases
NIR: Near Infra-Red
NK: Natural Killer

NOD/SCID: Nonobese Diabetic/Severe Combined Immunodeficiency
NTA: Nanoparticle Tracking Analysis
NSCLC: Non-Small Cell Lung Cancer
nSMase2: Neutral Sphingomyelinase 2

O

ORP1L: Oxysterol binding protein related protein 1L
OS: Overall Survival

P

PBS: Phosphate Buffered Saline
PCD1LG2: Programmed Cell Death 1 Ligand 2
PD-1: Programmed Cell Death Protein 1
PD-L1: Programmed Cell Death Protein Ligand 1
PDZ: Postsynaptic density protein, Drosophila disc large tumor suppressor, Zonula occludens-1 protein
PGs: Proteoglycans
PIK3CA: Phosphoinositide 3-Kinases
PIP2: Phosphatidylinositol 4,5-bisphosphate
PKCα: Protein kinase C-alpha
PLD2: Phospholipase D2
PLP: Proteolipid Protein
PS: Phosphatidylserine

R

RAB: Ras-Associated Binding
RhoA: Ras Homolog Family Member A
RT: Room Temperature
RTK: Receptor Tyrosine Kinases

S

SDC: Syndecan
SEC: Size Exclusion Chromatography
Sia: Sialic Acid
siCTRL: Silenced control cells
siRNA: Small interfering RNA
siSDC4: SDC4 silenced cells
sLe^{a}: sialyl Lewis^{a}
sLe^{x}: sialyl Lewis x
SLRPs: Small Leucine-Rich Proteoglycans
SNAREs: Soluble N-Ethylmaleimide-sensitive-factor attachment protein receptor
SPOCK: kazal-like domains proteoglycan
SRGN: Serglycin
ssDNA: single-stranded DNA
ssRNA: single-stranded RNA
STAD: Stomach Adenocarcinoma
ST: Sialyl-T
STn: Sialyl-Tn
STs: Sialyltransferases

T

TBS: Triphosphate Buffered Saline
TCGA: The Cancer Genome Atlas
tCTF: transmembrane C-Terminal Fragment
tDNA: transfer DNA
TEM: Transmission Electron Microscopy
TfR: Transferrin Receptor
TGFβ: Transforming Growth Factor
TGFβ3: Transforming Growth Factor Receptor 3
TKIs: Tyrosine kinase inhibitors
TME: Tumor Microenvironment
TMT: Tandem Mass Tags
TNM: Tumor, Node and Metastasis

TRPM2: Transient Receptor Potential Cation Channel Subfamily M Member 2

TSG101: Tumor Susceptibility Gene 101

TSPNs: Tetraspanins

U

UC: Ultracentrifugation

V

VCAN: Versican

VEGF: Vascular Endothelial Growth Factor

VPS4: Vacuolar Protein Sorting-associated-4

VTE: Venous Thromboembolism

W

WB: Western Blot

Wnt: Wnt signaling pathway

WT: Wild Type

Z

ZNRF3: Zinc and Ring Finger 3

CHAPTER I

General Introduction

1. General Introduction

Cancer is the second leading cause of death at the global level, following cardiovascular disease, with approximately 2.3 million deaths per year. Malignant tumors constitute a global health and socioeconomic problem and there is an increasing number of people worldwide affected by this problem (1). The increasing prevalence of malignant tumors worldwide can be attributed to several factors, including (i) aging population (incidence of cancer tends to increase as populations age); (ii) lifestyle and environmental factors (unhealthy lifestyle choices such as tobacco use, excessive alcohol consumption, poor diet, lack of physical activity, and exposure to environmental carcinogens (e.g., air pollution, radiation)); (iii) improved diagnostic methods (advances in medical technology and improved access to healthcare services have led to early detection and diagnosis of cancer cases that may have gone unnoticed in the past); (iv) increased awareness and screening programs (public awareness campaigns and widespread implementation of cancer screening programs have improved detection rates) and (v) genetic predisposition (certain inherited genetic mutations and familial syndromes can predispose individuals to develop cancer, leading to enhanced detection sensitivity) (1).

The first “Hallmarks of cancer” review, proposed in 2000 by Hanahan and Weinberg, initially envisioned the complementary involvement of six distinct hallmark capabilities acquired by cells on their transformation from normal to malignant (2). Later, in 2011, this number was updated to eight, including sustaining proliferative signaling, evading growth suppressors, resisting cell death, enabling replicative immortality, inducing/accessing vasculature, activating invasion and metastasis, reprogramming cellular metabolism, and avoiding immune destruction (Figure 1) (3).

Despite the large effort of numerous scientific investigations and the advances on novel therapeutic approaches, advances in technology and biological understanding are still required to accelerate early cancer detection and improve cancer survival. Nowadays, the primary prevention strategies encompass a comprehensive range of interventions, which include implementing lifestyle modifications to mitigate cancer risk, occupational and environmental precautions, conducting screening programs to identify early-stage lesions, administering vaccines to prevent infection by cancer-causing agents, genetic counseling and testing, and therapies to disrupt the carcinogenic process (4, 5).

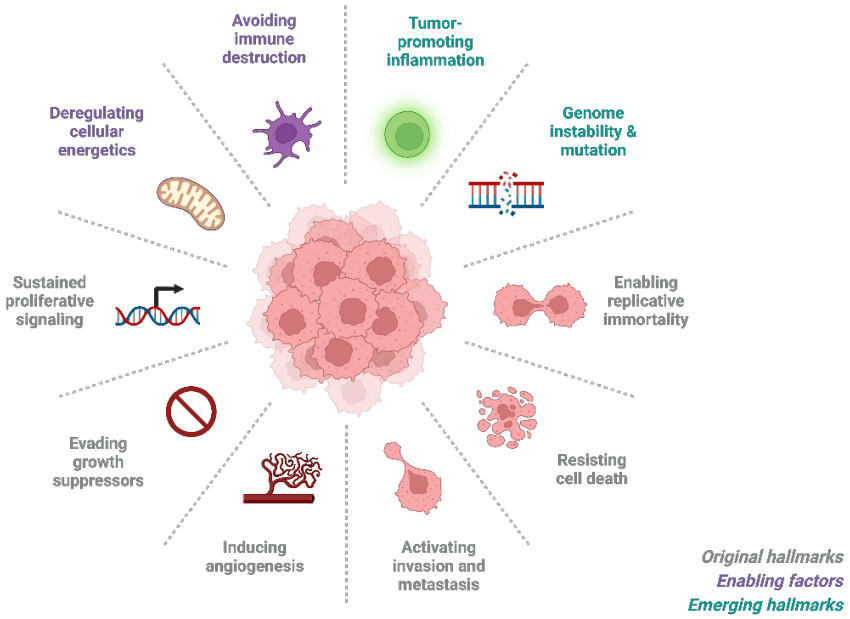


Figure 1 – The hallmarks of cancer, initially proposed by Hanahan and Weinberg (grey); the later reviewed version also identified tumor-promoting inflammation and genome instability & mutation as enabling factors (purple) and emerging hallmarks (green). Adapted from (3).

1.1. Gastric cancer

With over 1 million estimate new cases every year, gastric cancer is a worldwide important disease. This specific type of cancer, in 2020, became ranked as the fifth most diagnosed cancer in the world, and fourth for mortality (with an estimated 769,000 deaths in that year) (1). The incidence and mortality of gastric cancer is heterogeneous in different parts of the world, and it is more frequent in East Asia, South America and Eastern Europe (6, 7), Among the European countries, Portugal presents one of the highest incidence rates (Figure 2) (8).

The increasing development of countries, with improved standards of living, associated with better financial situations have contributed to the declined incidence and mortality rates of gastric cancer. There are several risk factors including older age, low socio-economic status, smoking, alcohol consumption, genetic predisposition, rich salted diet and low intake of fresh fruits and vegetables that promote the prevalence of gastric cancer. However, the major known cause of gastric inflammation and ulcers (and consequently gastric carcinoma) is the infection with the bacteria *Helicobacter pylori (H.pylori)* (1, 6-9).

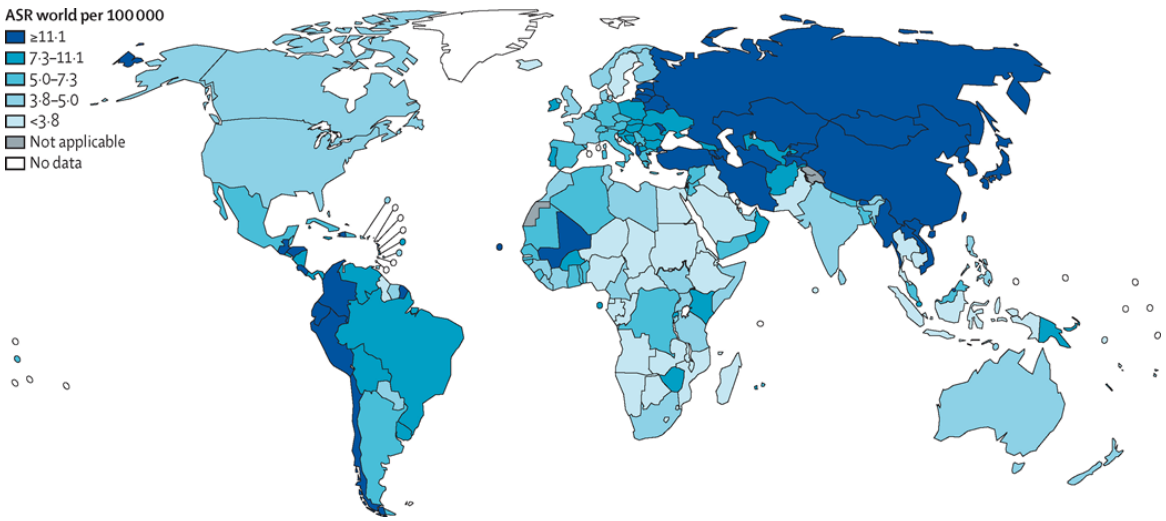


Figure 2 - Gastric cancer age standardized incidence in males and females around the world. From (9).

Gastric adenocarcinoma represents the majority of gastric malignancies. There are several classification systems, however, the Lauren classification is one of the most used. The Lauren classification distinguishes according to histopathological classification, into intestinal, or well-differentiated; diffuse, or poorly differentiated, and mixed subtypes (6, 7, 9). The relative frequencies are approximately 54% for intestinal subtype, 32% for the diffuse subtype and 15% for the remaining subtypes (10, 11). It was previously described that the diffuse subtype of gastric carcinoma is more often in female and young individuals and is associated with endogenous factors, as hereditary conditions; while the intestinal subtype is more frequent in males (mean age of 51 years old) and is caused by exogenous factors, for example intestinal metaplasia and infection with *H. pylori* (12, 13).

In the intestinal subtype, there is a well-established cascade of events that explains the tumor progression model, providing a window for early detection. This cascade is initiated by the transition from normal mucosa to chronic superficial gastritis, then followed by atrophic gastritis and intestinal metaplasia, finally leading to dysplasia and carcinoma (Figure 3) (6, 14, 15).

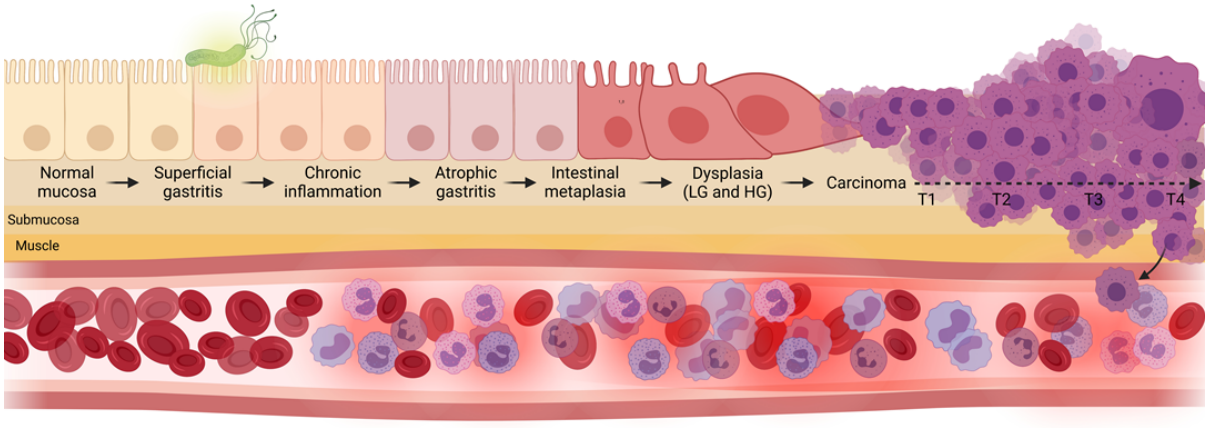


Figure 3 - Gastric cancer intestinal subtype progression accordingly to Pelayo Correa cascade. Many host, bacterial, and environmental factors act in combination to contribute to the precancerous cascade leading to development of gastric cancer. *H. pylori* infection is an established cancer risk factor. The recruitment of inflammatory cells is initiated in the beginning of chronic inflammation.

Based on the molecular profile, gastric cancer is classified into four subtypes, defined by The Cancer Genome Atlas (TCGA), which includes Epstein–Barr virus (EBV) associated, microsatellite instable (MSI), genomically stable (GS), and chromosomal instability (CIN) (Figure 4) (16). The EBV-associated subtype displays recurrently Phosphoinositide 3-kinases (PIK3CA) mutations, DNA hypermethylation, and amplification of Janus kinases (JAK2), cluster of differentiation 274 (CD274) (also known as PD-L1), and Programmed Cell Death 1 Ligand 2 (PCD1LG2) (also known as PD-L2). MSI tumors show elevated mutation rates, including mutations of genes encoding targetable oncogenic signaling proteins. GS tumors are enriched for the diffuse histological variant and display mutations of *RhoA* or fusions involving RHO-family GTPase activating proteins CIN tumors show marked aneuploidy and focal amplification of receptor tyrosine kinases (RTK) (16, 17) (Figure 4).

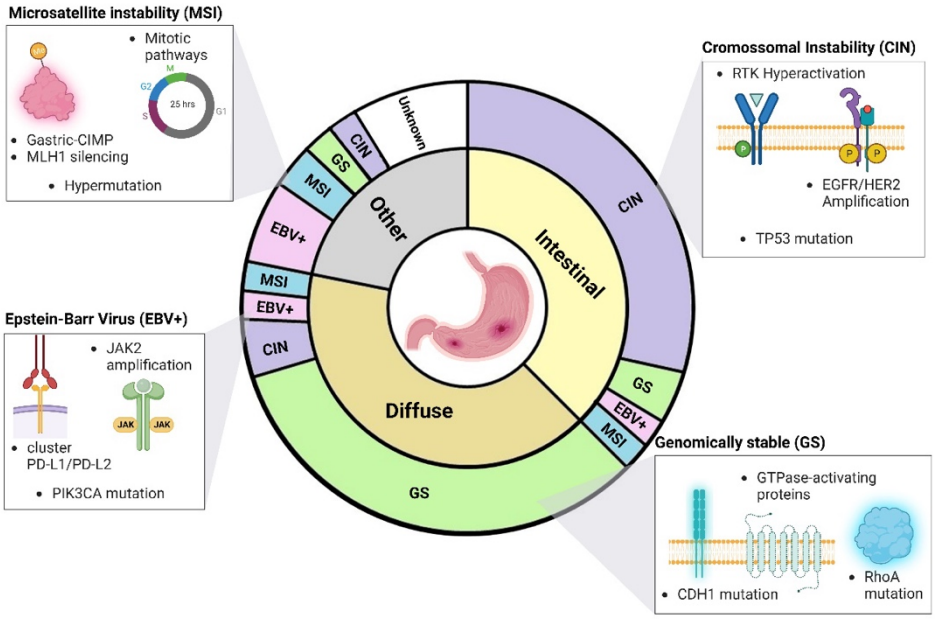


Figure 4 – Graphical depiction of overlapping histological and molecular classifications, with the features associated with each of the four molecular subtypes of gastric cancer highlighted.

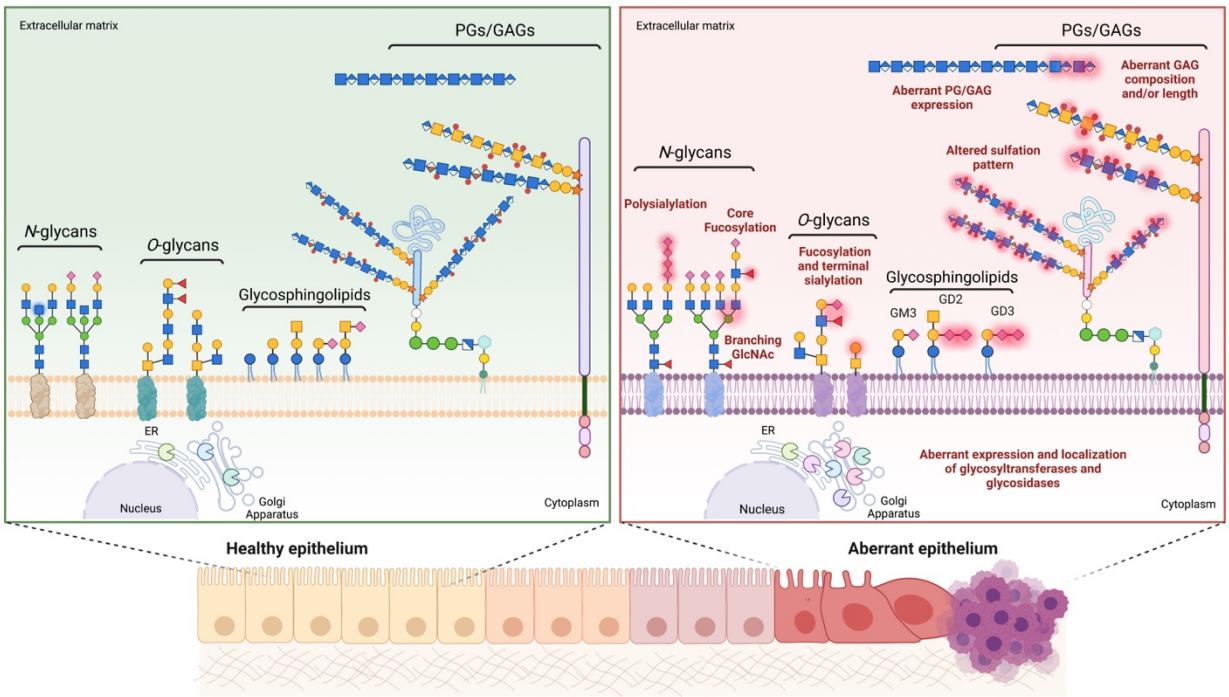
Diagnosis of gastric cancer is frequently done when disease is at a progressive stage since most patients with early-stage gastric cancer are asymptomatic. Normally, the diagnosis of this type of cancer relies on endoscopy and biopsy. Endoscopic Ultrasonography (EUS) and Computer Tomography (CT) of the chest and abdomen; and laparoscopy are strategies for staging advanced gastric cancer and exclude peritoneal metastatic disease, respectively (18-20). Adequate surgical resection is one curative therapeutic option for gastric cancer, however endoscopic resection might be suitable as an alternative to surgery for small well-differentiated early-stage tumors (T1a) (20-23). The extent of surgical resection depends on the tumor location, TNM (classification of malignant tumors: the T refers to the size and extent of the main tumor; the N refers to the number of nearby lymph nodes that have cancer and the M refers to whether the cancer has metastasized) system and histological subtype. Minimally invasive procedures are associated with reduced surgical trauma and immunosuppression compared with conventional open surgery (24, 25). Patients with metastatic gastric cancer typically follow this treatment in combination with chemotherapy (ChT) (26, 27). Other treatments peri-operatives in combination with ChT have been suggested in clinical trials to improve life conditions of patients and in some cases, they have been adopted in Europe and Western countries. For example, in patients with resectable stage II and III gastric cancer treatment with six cycles (three pre- and three post-operative) of epirubicine-cisplatine-5-FU (ECF) compared with surgery alone showed an improvement of patients' 5-year survival. A similar clinical trial showed that a regiment of peri-operative cisplatine-5-FU, instead of anthracyclines led to improved results (28-30).

1.2. Glycosylation in cancer

The surface of mammalian cells is ornamented with a wide range of membrane-bound macromolecules that constitute the glycocalyx. The glycocalyx is arranged with a negatively charged polysaccharide structure and is mainly formed by glycoproteins, glycosaminoglycans (GAGs), glycolipids and fibrous proteins that coat the apical surface of the cells. The content of the glycocalyx is constantly controlled by the cells metabolic turnover allowing the adaptation to change according to the microenvironment, including enzymatic and shear-induced shedding. Dysregulation in ECM deposition alters the cell microenvironment, triggering the onset or the progression of several diseases, including cancer (31-33).

Glycosylation is an enzymatic process, specifically a post-translational modification, that impacts protein trafficking, stability and folding, with consequences in protein biochemical and biophysical properties. Glycoproteins are modified with one or more glycans, covalently attached to the polypeptide backbone, via nitrogen (N-glycans) or oxygen (O-glycans) linkages (31-33).

Aberrant glycosylation in malignant pathologies was first described in 1969, and ever since there has been an increased understanding how changes in the glycosylation patterns of the cell surface and secreted glycoproteins impact cancer biology, disease progression and dissemination (34). In cancer, glycosylation changes are non-random. Glycans can suffer alterations in a variety of forms, including aberrant expression, increased expression of truncated glycans, and rarer, the *de novo* appearance of different glycans (31-33).



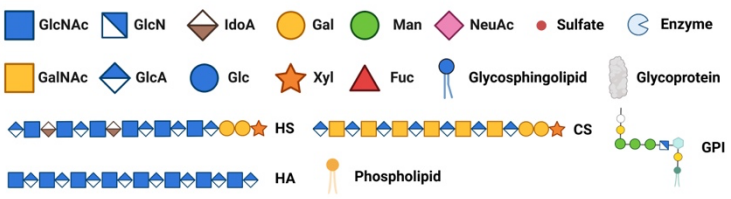


Figure 5 – The aberrant alteration of cancer cells involves molecular modifications affecting the glycosylation patterns. Consequently, tumor cells exhibit aberrant glycosylation profiles, both intracellularly and on their cell surfaces, leading to the modulation of various malignant properties. These altered glycosylation features include an increase in tetra-antennary branched N-glycan chains while bisected structures are reduced. Additionally, there is an upregulation of poly-sialic acid structures, terminal sialylation, and fucosylation, which includes sialylated Lewis antigens. Other features include premature O-glycan truncation and upregulation of sialic acid-containing glycosphingolipids, particularly mono- (e.g., GM3) and di-sialylated (e.g., GD2 and GD3) gangliosides. Furthermore, alterations in the sulfation pattern, composition, and length of proteoglycans (PGs) and/or glycosaminoglycans (GAGs) can occur. Furthermore, glycosyltransferases and glycosidases can be aberrantly expressed and/or mislocated. These glycosylation alterations actively contribute to the malignant characteristics of cancer cells. ER: Endoplasmic Reticulum; HS: Heparan Sulfate; CS: Chondroitin Sulfate; HA: Hyaluronic Acid; GPI: glycosylphosphatidylinositol. Based on (35).

Alterations in glycosylation are a universal feature of cancer cells. These aberrant alterations can arise from various molecular mechanisms contributing to the dysregulation of glycosylation patterns observed in malignant cells (Figure 5). Some potential mechanisms include (i) altered expression of glycosyltransferases and glycosidases: changes in the expression levels or activity of enzymes responsible for adding or removing specific sugar residues can lead to abnormal glycosylation patterns. This can result in the aberrant synthesis or processing of glycan structures on proteins and lipids; (ii) dysregulated expression of glycan biosynthesis-related genes: alterations in the expression of genes involved in glycan biosynthesis pathways can impact the synthesis and composition of glycans. Changes in the expression levels of these genes can disrupt the normal regulation of glycosylation processes; (iii) tumor microenvironment factors: factors such as hypoxia, inflammation, and altered nutrient availability, can impact glycosylation. These conditions can influence the expression and activity of enzymes involved in glycosylation, as well alter the availability of sugar nucleotides, affecting glycan synthesis; and (iv) epigenetic modifications: epigenetic changes, such as DNA methylation and histone modifications can regulate the expression of genes involved in glycosylation (31-33, 36, 37). In normal polarized epithelium, mucins, glycoproteins rich in O-GalNAc glycans, that are expressed in the apical membrane and can be secreted into the lumen, however in

malignant cells, the loss of adhesion junctions and loss of polarization allow mucins to be shed to the extracellular space and can reach the blood (32, 33). Their bulky conformation and the negative charge may repel intercellular interactions, inhibiting adhesion molecules, such as cadherins and integrins, from carrying out their normal functions (38). These glycoproteins may promote displacement of a cell from the primary tumor, contributing to the metastatic process.

A very well-known hallmark of cancer is the expression of incomplete O-glycans, present in mucins and other glycoproteins, such as the Tn and T antigens and their sialylated glycoforms, sialyl-Tn (STn) and sialyl-T (ST). The expression of Tn and STn enhances oncogenic and invasive cellular properties and promote immunosuppression (39). While in healthy tissues is not common the expression of STn, patients with cancer normally display STn in their bloodstream, therefore constituting prognostic markers and therapeutic targets (40, 41).

Another frequent change in glycosylation is the increased sialylation of glycan chains, being recognized as one of the hallmarks of cancer (40). The term sialylation refers to the terminal addition of sialic acid (Sia) to oligosaccharides and glycoproteins (40). Sia belongs to a family of nine-carbon backbone sugars. They are typically found attached to the distal ends of glycans, which make them assembling molecules between cell-cell and cell-ECM (41-44). Sialylation is dynamically regulated by two sets of enzymes, the sialyltransferases (STs) –responsible for sialylation – and sialidases (NEUs) – mediators of desialylation (33, 41, 45, 46). Sia accumulation/upregulation results in an excess of negatively charged Sia on cell surface and may be involved in cancer initiation, progression and immune evasion in diverse malignancies, leading to the ability of metastization (44, 47-49). Sialyltransferase activity has been correlated with different carcinoma types (50-52), mainly epithelial carcinomas, including gastric cancer (52). Increased α2-6Sia on N-glycans, due to ST6Gal1 upregulation in cancer cells, improves integrin-mediation cell motility and protects cells against apoptosis induced by galectins, death receptor ligands and chemotherapeutic drugs (53).

Core fucosylation is another important modification involving oligosaccharides on N-, O-glycans and glycolipids (54, 55). Fucosylation consists of a typical terminal modification of proteins, and GDP-fucose is the only donor of fucose that is synthesized in the cytoplasm. According to the location, fucosylation is characterized in two different categories: (i) core fucosylation (α-1,6-fucosylation) and (ii) terminal fucosylation (α-1,2-fucosylation, α-1,3/4-fucosylation) (33, 56). The participation of fucose is necessary for the formation of Lewis antigen. Lewis oligosaccharides have several structure types, such as Lewis^{a} (Le^{a}); sialyl Lewis^{a} (sLe^{a}); Lewis^{b} (Le^{b}); Lewis^{x} (Le^{x}); sialyl Lewis x (sLe^{x}) and Lewis^{y} (Le^{y}). Fucose

residues and sialylated residues are always involved in the synthesis of the terminal structure of glycans; thus, the transfer of the fucose residue to the glycan marks the end of glycan synthesis (33, 56). Fucosylation participates in the biosynthesis of blood H antigen and Lewis antigen, leucocyte extravasion mediated by selectins, host-microbe interactions, and modification of signaling (55, 57). Protein fucosylation has certainly an important effect on the function of proteins and affects cancer development (58-60).

The branching of asparagine (N)-linked glycans with N-acetylglucosamine by the N-acetylglucosaminyl transferases Mgat1, Mgat2, Mgat4a/b, and Mgat5 sequentially increase production of ligands for the galectin family of sugar-binding proteins (61, 62). At the cell surface, interactions of galectins with branched N-glycans attached to glycoproteins generates a macromolecular framework, thereby they have important roles in protein folding, cell-cell recognition, adhesion, and signaling, all important for cancer development and metastasis (63-65). Although the mechanisms that produce altered glycoconjugates remain poorly understood, there is increased evidence demonstrating that these modifications can occur in various stages of cancer progression, involving genetic mutations, misregulation of glycotransferases and chaperone genes expression, and mislocalization of glycosyltransferases.

In this thesis the focus was given to class of glycoconjugates less explored in cancer, the proteoglycans (PGs) and their GAG chains, as detailed bellow.

1.3. Glycosaminoglycans in cancer

Another class of cell surface glycoconjugates that populate the cell surface and the ECM are the PGs, generally composed by one core protein modified with one or more high molecular weight GAG chains. GAGs are large, linear, negatively charged polysaccharides consisting of repeating disaccharide units that can be sulfated at different positions and to different extents (66). Different combinations of different uronic acids and amino sugars result in five main classes of GAGs including (i) Hyaluronic acid (HA); (ii) Heparan Sulfate (HS)/heparin; (iii) Chondroitin Sulfate (CS); (iv) Keratan sulfate (KS) and (v) Dermatan Sulfate (DS) (Figure 6). Hyaluronic acid is the only GAG that occurs in a form that is not conjugated to a protein, while other GAGs are connected to a core protein. Other characteristic about HA is its nature, simple repetition of the disaccharide units, without sulfation (66).

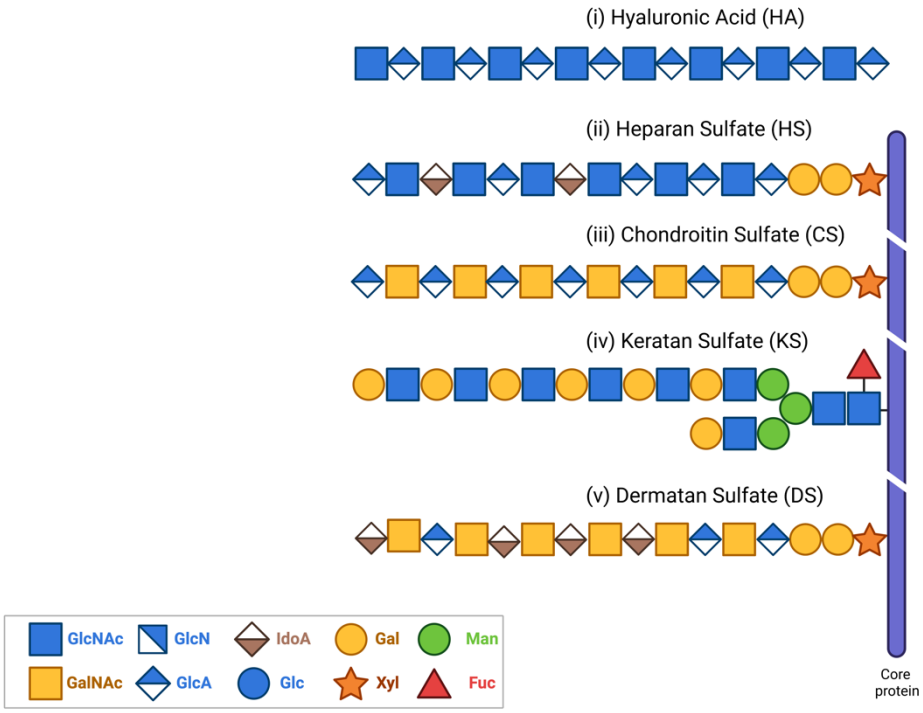


Figure 6 – The diverse structural composition of the GAG chains.

Among the various GAGs that can attach to core proteins to form the PGs, these are divided into four major classes depending on their cellular localization. They can be associated with the cell membrane via a transmembrane core protein, via glycosylphosphatidyl-inositol (GPI) anchor, and can have intracellular or extracellular localizations (66).

PGs have been shown to largely contribute to the acquisition of cancer hallmarks. By binding to several bioactive molecules, including chemokines, cytokines, growth factors, adhesion molecules and matrix components (e.g., collagen, fibronectin, laminin) PGs are major mediators of the cell-cell and cell-ECM interactions (66). Moreover, by binding to heparin-binding sites of ECM components, GAGs collaborate with integrins and are, therefore, essential regulators of cancer progression through modulation of cell differentiation, invasion and metastasis (66). Additionally, GAGs can adjust the biophysical properties of the ECM. Abnormalities in GAGs abundance and structure (e.g., sulfation patterns) are observed in different types of cancer and therefore hold biomarker potential (67).

Changes on GAG-decorated PGs expression levels and on its disaccharide structure has been shown to be directly correlated with malignant transformation. For example, HS-GAGs structural changes have been reported during progression from colon adenoma to carcinoma (68). In addition, HS-GAGs can promote growth factors concentration and

signaling, for example, specific motifs of the HS chains that bind specifically to Fibroblast Growth Factor 2 (FGF2) and its transmembrane receptor (69), promoting the formation of a complex at the cell surface important for modulation of the sulfation patterns, tumor growth and progression (70). Furthermore, CS/DS proteoglycans, have been described as promoters of osteoblast differentiation and ovarian cancer growth, due to its ability to interact with transforming growth factor (TGFβ) (71), bone morphogenetic protein (BMP)-2 and -4 (72, 73) forkhead box A2 (FOXA2) and versican (VCAN) (74). DS formation is regulated by the enzyme DS-epimerase-1, responsible for the conversion of GlcA into IdoA. The upregulation of this enzyme has been associated with several cancers, including esophageal cancer (75).

Cell invasion and metastasis is associated with tumor recurrence, poor survival, and mortality. CS expression is correlated with worse patients´ outcome in breast and prostate cancers (76, 77). Additionally, CS/DS-GAGs of the ECM, facilitate pro-migratory and invasion features of several tumor types, as gastric, ovarian and endometrial carcinomas, melanomas and gliomas (78-82). In further support of CS/DS GAGs role in the metastatic process, removal of CS/DS chains was shown to inhibit invasion of melanoma cells, and highly sulfated CS structures are described as important mediators of dissemination of lung carcinoma and osteosarcoma cells (83-85). Upregulation of enzymes such as Hyaluronidase-1 and -2 (HYAL1 and HYAL2) promotes invasion of human breast cancer associating with tumor progression, while Heparanase (HPSE) has been described with pro-invasive phenotype in pancreatic neuroendocrine tumors and pediatric cancer (86-88). The development of tumors requires the ability of cells to overcome cell-cell adhesion and then invade the surrounding tissue. Increased evidence proposes that glycoconjugate structures can affect tumor cell invasiveness, including the ability to spread and metastasize into distant organs (89). CS/DS/KS-GAGs have been shown to promote metastasis, including in breast, nasopharyngeal and lung carcinomas (90-92). Heparin may regulate tumor metastasis to sites such as the liver, lung and spleen (93, 94). Beyond the defects and abnormal protein expression, HS-GAGs may add another layer of density to tumor cell behavior by binding to the cell-cell and cell-ECM adhesion molecules required for tumor metastasis (94). Thus, targeting of specific sites of the GAGs is a promising approach to interfere with cancer development.

1.4. Heparan Sulfate Proteoglycans

Heparan sulfate proteoglycans (HSPGs) are formed by a core protein to which one or multiple heparan sulfate chains are covalently bound. They are ubiquitously expressed in the cell surface and can be found in the ECM and secretory vesicles (95, 96). The HSPGs can be classified into three major families: the "*full-time*" HSPGs that includes syndecans (SDCs), glypicans (GPCs) and high-molecular weight HSPGs (includes perlecan, agrin and collagen XVIII). This classification is based on similarities in their core-protein structure (66). It is important to note that there are also additional HSPGs, referred to as "*part-time*" HSPGs, such as betaglycan (TGFBR3), epican (HS/CS-carrying form of CD44), testicans (SPOCK1-3), and serglycin (SRGN, carrying heparin/CS) (66, 95, 96).

The localization and function of a HSPG are determined by its core protein, which governs its presence on the cell surface, in the ECM, vesicles, and other cellular compartments. The interaction between the associated GAG chains and specific regions of the cell is facilitated by the HS-protein interactions (95). For example, the transmembrane SDCs and the glycosylphosphatidylinositol (GPI)-anchored GPCs are predominantly located on the cell surface, while the high-molecular weight HSPGs (mentioned above) are mainly secreted by cells and deposited into the ECM and basement membranes (95-97). While the generalizations mentioned regarding the localization of HSPGs are widely accepted, it is crucial to acknowledge that the knowledge of HSPG localization is continuously evolving and expanding.

The HSPGs are typically expressed in abundance and comprehend multiple functionalities including the interaction with other membrane surface proteins to act as a substrate for cellular migration; acting as a binding site for circulating molecules and ligands; to act as a coreceptor that can provide fine tuning of growth factor receptor activity threshold; and to activate intracellular signaling pathways (95-97). Given these key features, HSPGs are widely conserved, and they serve fundamental functions to preserve basic physiological processes. Indeed, they may support specific cellular interactions with growth factors, morphogens, chemokines, ECM components, and microbial pathogens and their secreted virulence factors (95-97).

There are several mechanisms through which HSPGs can be modified in neoplastic conditions, namely, (i) their aberrant expression including upregulation or downregulation, compared to normal cells; (ii) altered enzymatic activity, enzymes involved in HSPG biosynthesis and remodeling, such as glycosyltransferases and sulfotransferases, can be dysregulated in cancer. This can lead to changes in the sulfation pattern and length of HS chains, impacting HSPG function; (iii) enzymatic cleavage: HSPGs can undergo enzymatic cleavage by enzymes such as heparanase and metalloproteinases, resulting in the release

of soluble HSPG/HS fragments. These fragments can have altered functions and contribute to tumor progression and metastasis (iv) changes in sulfation patterns: the sulfation pattern of HS chains, which determines their binding affinity to various ligands, can be modified in cancer. Alterations in sulfation can influence HSPG-ligand interactions and affect signaling pathways involved in tumor growth and metastasis; (v) altered localization and shedding: HSPGs can be redistributed within the tumor microenvironment, with changes in their cellular localization and shedding into the extracellular space. This can impact cell-matrix interactions, cell signaling, and the formation of the ECM; and (vi) genetic alterations: genetic mutations and epigenetic modifications can affect the expression and function of genes involved in HSPG biosynthesis and regulation (67, 98-100). Through these mechanisms, HSPGs can mediate the disruption of cell adhesion, proliferation, migration, and differentiation, and impact the onset, progression, and outcome of pathophysiological processes, such as development, tissue repair, inflammation, infection, and tumorigenesis. Among the different families of HSPGs, the SDC family has gained increased attention in relation on different types of cancer.

1.4.1. Syndecans

SDC family consists of four transmembrane members (SDC 1-4). Each member presents a highly conserved C-terminal cytoplasmic domain, a transmembrane region, and an extracellular N-terminal domain that possesses multiple HS or hybrid HS/CS GAG chains (Figure 7) (96).

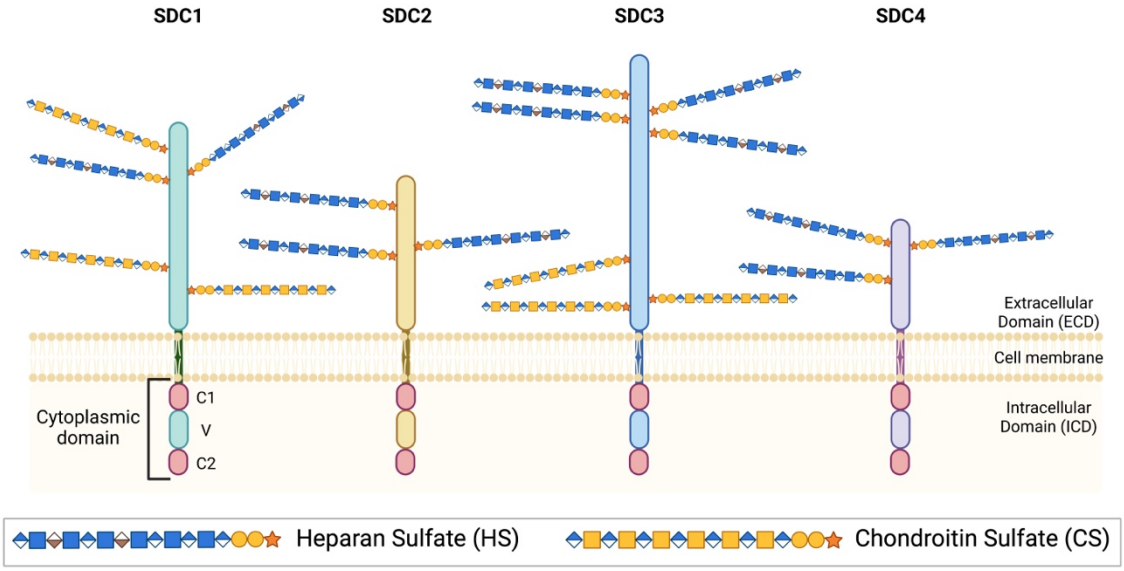


Figure 7 – Schematic representation of the four syndecan members. The core protein extracellular domain can be decorated with heparan sulfate or heparan and chondroitin sulfate chains. Note that under certain circumstances SDC1 only carries CS chains (e.g., cartilage development).

Each of these GAG chains are covalently bound to serine residues of the core protein. The cytoplasmic domain of SDCs is divided in three domains: (i) a highly conserved membrane proximal C1 region, that is implicated in cytoskeleton interactions that induce transduction signals inside the cell upon binding of extracellular ligands; (ii) the highly conserved C2 region located at the C-terminus that contains a hydrophobic motif which interacts with PDZ domains; and (iii) the variable domain that lies between the two C regions (Figure 8). Though these variable regions are different between each member of the SDC family, they are highly conserved between species (96). SDC core proteins can form homodimers, structures promoted by the strong interactions between transmembrane domains. In the outer part of this domain, they have a GXXXG motif, responsible for the assembly of the dimers (101).

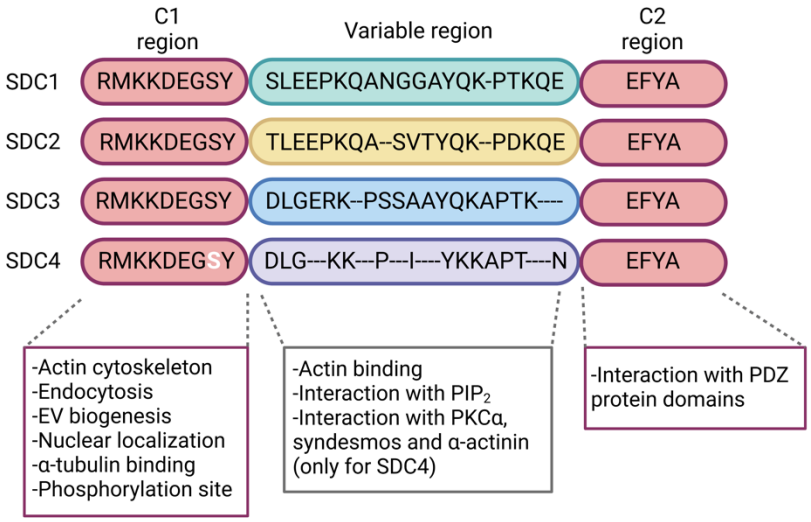


Figure 8 – Cytoplasmic domain of SDC family members. The domain is organized into two conserved (C1 and C2 region) and one variable region. It is shown highlighted interactions partners for each region. Human SDC cytoplasmic domain sequences are shown. The single serine residue of SDC4 that can be phosphorylated is shown in white bold. PIP_2 - phosphatidylinositol bisphosphate. PKCα – protein kinase C alpha. Based on (102, 103).

1.4.2. SDC structural features and biological functions

While each of the four SDC members has a unique sequence and biological purposes, there is some overlap in functionality. Overtime, they have been described as interactors with various growth factors (for example vascular endothelial growth factor (VEGF) and fibroblast growth factor 2 (FGF2), interfering in cell proliferation and tissue healing); adhesion proteins (integrins, which play an essential role in the behavior of healthy and tumorigenic cells); and other ECM proteins (including collagens and fibronectin, thereby helping to anchor cells) (104).

1.4.2.1. SDC1

SDC1, also known as CD138, is expressed predominantly on epithelia and leukocytes. With a length of 288 amino acids, it is the second-largest member of the SDC family (105). SDC1 is one of the most studied members of the family, though more research into its biological functions is still lacking. SDC1 interaction with various growth factors, as well as its propensity for promoting cellular motility, modulating inflammation, and interacting with the ECM have been well described (106-109). SDC1 expression has been studied in different biological contexts. For example, it was described that membrane bound SDC1 in lung

epithelial tissues regulates inflammatory processes in response to influenza infection. In this study, it was reported that SDC1, by promoting c-Met activity leads to a decreasing post-influenza epithelial cell death (110). Moreover, the use of bleomycin, an inducer of acute lung injury, was shown to induce the shedding of SDC1 and to direct the trans-epithelial migration in neutrophils (111). The SDC1 shedding is promoted by the formation of a complex between SDC1 and a C-X-C Motif Chemokine Ligand 1 (CXCL1) into the alveolar space and modulated by matrix metalloproteinase-7 (MMP7), promoting a chemotactic gradient across the alveolar epithelium (111). In another type of anomaly, in acute myocardial infarction, the pre-treatment with recombinant SDC1 lead to a decreased deterioration and cardiomyocyte damage in mouse models (112).

SDC1 has been implicated in facilitating the internalization of lipoproteins into cells, particularly in the context of lipid metabolism. SDC1 has been shown to interact with lipoproteins, such as low-density lipoprotein (LDL) and high-density lipoprotein (HDL), through binding of HS chains to apolipoproteins(113-116).

1.4.2.2. SDC2

SDC2, or CD362 by its antigen name, formed by 201 aminoacids, plays a fundamental role in matrix formation, which is demonstrated by the inability of cells transfected with truncated *SDC2* to assemble fibronectin or laminin into a fibril matrix (105, 117). In addition to matrix formation, SDC2 holds vital roles in neuronal development, by increasing maturation of the dendritic spines, as demonstrated by its expression on the dendritic spines of cultured hippocampal neurons. On immature hippocampal neurons, transfection of *SDC2* cDNA hastens the formation of dendritic spines, while the deletion of SDC2 C-terminal motif limits its ability to promote dendritic spine formation (118).

1.4.2.3. SDC3

SDC3, also known as N-Syndecan, is the largest member of the SDC family. Human SDC3 bears significant homology to SDC1 and contains 442 amino acids (105). Mammalian SDC3 bears four glycosaminoglycan attachment sites at the N-terminal and another three sites closer in proximity to its transmembrane region. Much of what is known about SDC3 is related to SDC3 function in the brain and nervous tissue (119-121). For instance, it has been experimentally shown that mice express SDC3 in hypothalamic regions and it is related to control energy balance. SDC3 levels in these regions were shown to be increased when these mice are food deprived. Additionally, SDC3 null mice have significantly less hyperphagia (abnormally increased appetite for consumption of food frequently associated

with injury to the hypothalamus) when compared with the mice subjected to normal diet (122). *SDC3* null mice have lower adipose tissue. Males lacking *SDC3* expression gained less weight on a high-fat diet due to reductions of food consumption, while females lacking *SDC3* gained less weight due to increase in energy expenditure (123). SDC3, together with SDC4, has chief roles in skeletal stem cell functions. These two HSPGs are normally expressed on quiescent satellite cells in adult skeletal muscle. After activation, these cells continue to express SDC3 and SDC4, suggesting an important function for each of them in regeneration of the muscles. Furthermore, intact myofibers treatment with chlorate, inhibiting the HSPGs sulfation, delays proliferation and alterations in the expression of MyoD, suggestive that these proteoglycans may regulate the activation, proliferation and differentiation of adult skeletal muscle satellite cells (124). Further studies, led to the discovery that when SDC3 is absent there is a delay on S-phase in satellite cells, disclosing SDC3 important features in delaying differentiation and reducing proliferation, as well as increasing cell death (125).

1.4.2.4. SDC4

SDC4, also known as Ryudocan and Amphiglycan, is the smallest (198 aminoacids) and most ubiquitously expressed member of the family (105). One of the most well described functions of SDC4 is its role in inflammation (126). For example, inflammation induced SDC4 shedding causes impairment in macrovascular angiogenesis in diabetic rats (127). The knock down of *SDC4* leads to an increased pro-inflammatory factor in umbilical vein endothelial cells (HUVEC), suggestive of its involvement in inflammatory responses. Additionally, SDC4 shedding, in the context of diabetes mellitus, results in decreased macrovascular angiogenesis (127). Apart of inflammation responses, SDC4 has also been described in wound healing regulation. SDC1 and SDC4 ectodomains are shed into acute human dermal fluids. Enzymatic treatments that led to the degradation of HS and immunodepletion of SDC1 and SDC4 reduced the cathepsin G and elastase proteolytic activities in the fluid, indicating a role for regulation of the proteases in the wound environment through their ectodomains (128). SDC4 has also been implicated in immunosuppression, inhibition of leucocyte migration, development of blood vessels and may act as protector against endotoxic shock (129-132). Importantly, SDC4 has essential roles in governing cellular adhesion and migration, as well as mechanotransduction (133-135). A conformational change of cytoplasmic domain of SDC4 has been previously described in the presence of EC tension. This feature allows the formation of a molecular scaffold involving SDC4, α-actinin, and F-actin, leading to adaptive cell stiffening. In regular conditions, SDC4 is crucially involved in the intracellular Ca^{2+} gradient, while KO of this

syndecan abrogates this gradient, and simultaneously limits centrosome reorientation leading to implications in cellular motility (136, 137). Moreover, while SDC4 shedding may recruit immune cells, the *SDC4* KO in mice hearts potentiates the decreasing expression of immune cell markers. Additionally, depletion of *SDC4* decreases adhesion receptors intracellular adhesion molecule-1 and vascular cell adhesion molecule-1 (138).

SDCs are major's mediators of cellular interactions with the cellular microenvironment, and its expression is cell, tissue and development stage specific. SDCs contribute to critical functions to cell adhesion, cell signaling events and numerous biological processes. The multiple features of SDCs in orchestrating cell behavior and signaling support that aberrant expression of SDCs is key within the tumor microenvironment.

1.4.3. SDC aberrant expression in cancer

Aberrant expression of SDCs in a variety of diseases including cancer and inflammation has stimulated research into their biological functions in disease scenarios (139, 140). It is now clear that in some cases, SDCs can act as drivers of disease progression (141),, and in other cancers SDCs are prognostic indicators (142). Changes in SDC expression can have numerous effects on tumor progression and metastasis influencing patient survival. These findings allude to SDCs potential as prognostic or diagnostic markers or use as a target in forthcoming cancer treatments.

1.4.3.1. SDC1

Though there are a myriad of known functions for SDC1 in health, its role in tumor behavior is unequivocally important from a clinical perspective. Further, while data regarding the therapeutic targeting of SDC proteins is scarce, the available literature does demonstrate promise for their use in cancer treatment. SDC1 expression has been reported as dysregulated in cancer microenvironment. For example, elevated SDC1 expression levels were observed in most patients with non-muscle-invasive bladder cancer (143). On the other hand, high-stage and high-grade bladder cancer were associated with decreased expression of SDC1 in tumor along with a rise of SDC1 levels in serum, yielding evidence that SDC shedding may contribute to the aggressiveness of this cancer (144). Cervical carcinoma cells are mostly (83.5% of the tumors screened) positive for SDC1, and there is an association with better survival rates with high SDC1 expression levels. Similar results were observed for colorectal cancer context where increased levels of shed SDC1 were described (145). Additionally, in the same study, a mechanism of chemotherapy resistance

mediated by interactions between shed SDC1, and epidermal growth factor receptor (EGFR) was described, causing various downstream signaling effects via EGFR phosphorylation. In healthy colonic epithelial cells, SDC1 is expressed at the basolateral borders, while in colorectal adenocarcinoma, the expression of this PG is localized over the cell membrane and cytoplasm (145). Concordantly, elevated SDC1 stromal levels were found in muscle-invasive compared to non-muscle-invasive bladder cancer and control groups. Interestingly, cases in which lymph nodes were positive yielded the highest concentration of SDC1 in the serum (109). Specifically in gastric cancer, loss of epithelial SDC1 expression has been associated with high stromal SDC1 expression, higher tumor grade, poor overall survival, and lymph node metastasis (146, 147). This unique SDC1 expression patterns lends credence to the utility of SDC1 as a biomarker in different types of cancer.

1.4.3.2. SDC2

Increased levels of SDC2 are associated with advanced colorectal cancer (148), as well as SDC2 methylation in stool-derived DNA (149, 150) being useful for cancer detection. High levels of SDC2 have been associated with pancreatic ductal adenocarcinoma, particularly with higher invasive phenotype (151). SDC2 upregulation in colorectal cancer is highly associated with vascular invasion, cancer stage, lymph node and distant metastasis (148). Furthermore, there is an inverse correlation between SDC2 expression and overall patient survival. Knockdown of SDC2 showed to induce apoptosis, in addition to abrogating the ability of colorectal cancer cells to proliferate, migrate, and invade. Of notable importance, SDC2 promotes epithelial-mesenchymal transition (EMT), a process by which epithelial cells transmute toward a mesenchymal cell phenotype, enhancing migratory capabilities, invasive capacity, and an increased ability to generate new ECM constituents. Patients with lung adenocarcinoma demonstrated high expression levels of SDC2 staining, in malignant epithelial cells localized in the core of tumor, while in the tumor-free margins, SDC2 is expressed primarily on macrophages (152). Lung Cancer Tissue MicroArray reveals significant increase in SDC2 staining in lung adenocarcinoma les when compared to control lung. mRNA Levels of *SDC1* were also examined, and no significant differences were found between the lung adenocarcinoma group and the controls, yet *SDC2* mRNA expression levels were increased by 5- to 35-fold in tumors (152).

1.4.3.3. SDC3

Information regarding the role of SDC3 in cancer behavior is sparse. Despite this fact, SDC3 together with Midkine, a protein known to bind to SDC3 as a high-affinity receptor (153), is associated with pro-invasive phenotype in pancreatic cancer (154). Midkine levels were associated with tumor progression, lymph node metastasis and reduced post-operative survival rate, while SDC3 expression was correlated with tumor size. Patients lacking SDC3 expression showed a higher cumulative survival rate, comparing to patients bearing SDC3-positive tumors (154). SDC3 and pleiotrophin were associated with perineural invasion, in human pancreatic cancer cells (155). In this study, pleiotrophin was associated with liver metastasis, large blood ascites and reduced survival time; overall tumor size was correlated with SDC3 expression (155). Another study, shown that combined Transient Receptor Potential Cation Channel Subfamily M Member 2 (TRPM2) and SDC3 were significantly upregulated in ovarian tissues and cells, promoting ovarian cancer development and progression. In this study, the authors described this complex where SDC3 is involved in tumorigenesis and chemotherapy resistance (156). In prostate cancer, SDC3 expression was associated with poorer survival. Additionally, SDC3 overexpression was correlated with decreased recurrence-free survival. In the same study, SDC1 expression was also associated with a more aggressive phenotype and poorer prognosis (157). In renal carcinoma SDC3 was shown to be regulated by circular and micro RNAs, specifically circSCARB1/miR-510-5p axis, functionalizing as an oncogene (158). While much more needs to be done to fully elucidate the function of SDC3 in tumors of different origins, the highlighted studies provide valuable insight on SDC3 expression in a tumor microenvironment.

1.4.3.4. SDC4

There is still lack of clinical information regarding the function of SDC4, nonetheless, similarly to other members of the family, SDC4 is involved in signal transduction processes across the cell membrane. SDC4 mediates several steps of tumor progression, by being a major player in cell proliferation, migration and cell adhesion. It is also involved in cytokinesis, endocytosis and mechanotransduction.

Among the available literature, there is data demonstrating the SDC4 correlation with several cancer types. SDC4 is expressed in most breast carcinomas, and it has been described that its expression is significantly correlated with positive estrogen and progesterone receptor status. SDC1 expression and lack of SDC4 has been associated with high-grade breast carcinomas (159). These findings are in contrary to other study,

which showed that SDC4 expression was correlated with estrogen receptor negativity, grade and size of breast carcinomas (160). In glioblastoma context, elevated levels of SDC4 expression are indicators of patient poor prognosis. This study investigating the use of SDC4 as a predictive biomarker for the transcription factor WT1 peptide vaccine, showed a 1-year survival rates of 18.5% and 64% in the SDC4-high and SDC4-low groups, respectively (161). Similar results were observed in high-grade osteosarcoma, where strong SDC4 expression levels were correlated with disease severity. Of important note, SDC4 and fibronectin expression were increased in high-grade osteosarcomas, and this expression was correlated with occurrence of distant metastasis leading to a shorter overall survival (162). Similarly, SDC4 upregulation is correlated with oncogenic inducement in the early stages of the gastric carcinogenesis (163).

The identification of new cellular constituents that can be used for diagnostic, prognostic, and therapeutic purposes is crucial in improving patient outcomes worldwide. Growing evidence has demonstrated that among the myriad of changes seen in cancer cells, the SDC family of proteins has been observed to undergo drastic alterations in expression. Moreover, SDCs have been associated as crucial managers of Extracellular Vesicles biogenesis, uptake and establishment of the pre-metastatic niche – already described as important machineries for cancer progression.

1.5. Extracellular Vesicles

Extracellular vesicles (EVs) were originally reported in 1946 by Chargaff and West as procoagulant platelet-derived particles in normal plasma (164). Later, in 1967, this observation was termed by “platelet dust” by Wolf (165). The term “exosomes” was used in the first place in 1981, referring to membranous vesicles that are released from glioma cells (166). Two years later, two studies reported that transferrin receptors associated with small vesicles were released from mammalian reticulocytes to the extracellular space during the maturation into erythrocytes (167-169). Following these reports, it was defined the term “exosomes” for these EVs, however on that time it was thought that these EVs were trash cargos of unnecessary components from cells (170-172). Far ahead, in 1996, EV research gained recognition when Raposo and her team reported that exosomes isolated from immune cells were essential activators of the immune system by maturing antigen-presenting cells (APCs) and activating T cells (173, 174). The increase appreciation towards the EV research, lead to the establishment of the International Society for Extracellular Vesicles (ISEV) in 2011, in order to standardize the nomenclature and the methodologies for isolating and analyzing exosomes and other extracellular vesicles (175).

EVs are nanoparticles found in almost all body fluids and are produced and secreted by almost all types of cells, including both eukaryotic and prokaryotic cells (176, 177). They are enclosed within a phospholipid bilayer that envelops their components, protecting them from enzymatic degradation. EVs can carry numerous biomolecules, including proteins, glycans, lipids, and nucleic acids such as DNAs or RNAs (Figure 9) (178, 179). EVs may vary in size, morphology and other properties (178). They can be classified, according to their biogenesis pathway into (i) exosomes, which are small membrane vesicles (30-120 nm); (ii) microvesicles (MVs) or ectosomes, are large membrane vesicles (100-1000 nm); and (iii) apoptotic bodies, a type of large EVs, ranging from 800 to 5000 nm (179). Microvesicles are composed of lipid components of the plasma membrane and are released via shedding from the plasma membrane, whereas apoptotic bodies are formed during cytoskeletal rearrangement, being released by outward blebbing and decomposition of the apoptotic cells' membrane (180-182).

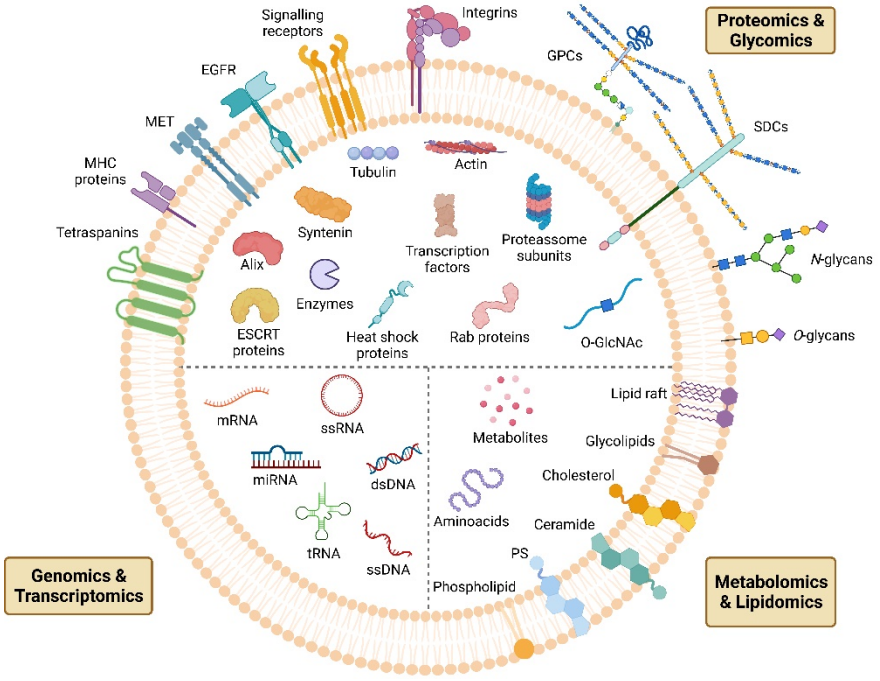


Figure 9 – Schematic representation of EV content, including proteins, glycans, lipids, metabolites, and nucleic acids. Several areas of biology have generated complex proteomics and glycomics, lipidomics and metabolomics, and genomics and transcriptomic data that contribute to the understanding of several biological processes and functions. Major Histocompatibility Complex (MHC). Hepatocyte Growth Factor Receptor (MET). Epidermal Growth Factor Receptor (EGFR). Endosomal-Sorting Complex Required for Transport (ESCRT). Glypicans (GPCs). Syndecans (SDCs). Phosphatidylserine (PS). Note that components of this figure are representative. Based on (183).

1.5.1. The biogenesis of EVs

EV biogenesis begins with the formation of the intraluminal vesicles (ILVs). The inner membrane inward budding of the endosome, limiting membrane and detachment of the bud as a vesicle, into de endosome lumen allows the formation of the ILVs. These intracellular endosomal structures are known as multivesicular bodies (MVBs). During this process, cytosolic proteins, nucleic acids and lipids are sorted into these compartments. After ILVs formation, the late endosomes (or MVBs) can traffic to the plasma membrane where they fuse and release the ILVs to the extracellular milieu in the form of exosomes (184-186). Alternatively, the MVBs can fuse with the lysosome if the content is intended for degradation (185, 186).

This endosomal biogenesis pathway is accompanied with critical proteins responsible to produce the exosomes. EVs can be formed through multiple molecular mechanisms (Figure 10). The ILV pathway budding into MVBs include those regulated by the Endosomal-Sorting Complex Required for Transport (ESCRT) machinery, by programmed cell death 6-interacting protein (Alix), the GTPase ADP-Ribosylation Factor-6 (ARF6), the lipid modifying enzyme phospholipase D2 (PLD2) and the HS glycosidase, Heparanase (187-192). The ESCRT pathway involves a cascade of four main complexes (ESCRT-0 to -III). These complexes interact and assemble in a specific order: (i) ESCRT-0 controls the selection of the cargo; (ii) ESCRT-I and –II manages the intraluminal membrane budding; and (iii) ATPase vacuolar protein sorting-associated protein-4 (VPS4) interacts with ESCRT-III to support completion of ILV formation by promoting membrane scission, resulting in ILVs pinching off into MVBs lumen (189, 191-193). Of note, the EV biogenesis is affected when depletion of multiple ESCRT proteins or VPS4, impacting exosome number, size, and protein cargo (194, 195). Tetraspanins (TSPNs), such as CD63, CD81 and CD9, are transmembrane proteins particularly enriched in EVs, which play a crucial function in exosome formation. TSPNs are mainly implied in sorting specific cargo into ILVs and exosome production (196-198). An alternative to ESCRT pathway, is the syndecan-syntenin-Alix complex pathway. In this pathway there are numerous mediators with a key role in the formation of exosomes and loading of proteins, namely, heparanase, SDC, ARF6, PLD2, and syntenin (187). This pathway is initiated when SDC is internalized through endocytic activity, leaving the cytoplasmic domain free for syntenin and Alix proteins interaction (187, 188). This step is dependent of the availability of HS, SDCs and Alix. After generation of the MVBs by inward budding of their membrane, EVs are secreted through exocytosis process. Alternatively, EVs enriched with TSPN6 are forward for lysosome degradation (199). Heparanase stimulates release of exosomes containing syntenin,

syndecan, CD63 and facilitates endosomal membrane budding and biogenesis of exosomes by enzymatic degradation of HS chains (190). This approach of ILV budding is controlled by ARF6 and PDL2 activities (200). More recently, it was shown that heparanase stimulated the production of exosomes with syntenin-1, syndecan and CD63 (201), but not CD81 or flotillin-1 (190, 201). The underlying mechanism proposed that SDC clustered upon heparanase and protease cleavage, which resulted in enhanced formation of intraluminal vesicles (in multivesicular endosomes), subsequently released as exosomes (188).

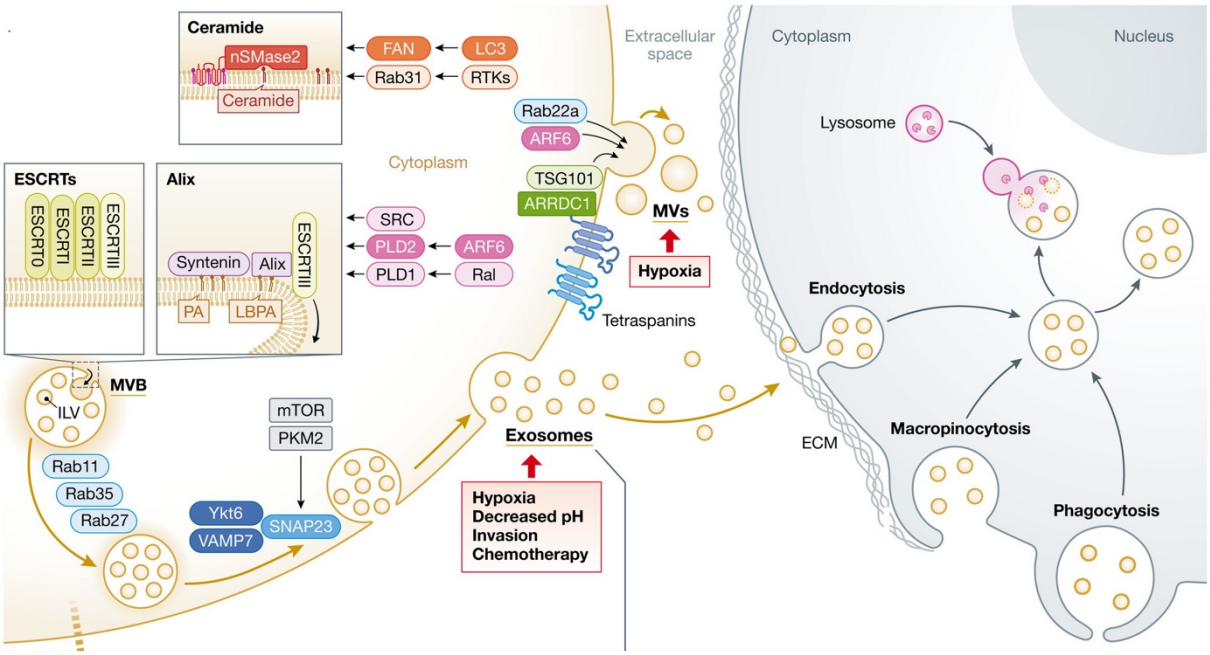


Figure 10 – EV biogenesis occurs through distinct pathways. One takes place in endosomes, giving rise to secreted exosomes, while the other occurs at the plasma membrane, resulting in the generation of microvesicles, also known as ectosomes. In MVB endosomes, invagination of the membrane leads to the formation of nanosized ILVs ranging from 50 to 150 nm, where the complex syndecan-syntenin-Alix has a crucial contribution (although SDC is not represented in this image). The ILV formation is regulated by various molecular processes at the MVB membrane, involving cargo capture and membrane remodeling. These processes are induced by upstream regulators. The trafficking of MVBs is controlled by Rabs and SNARE-complexes, facilitating the secretion of exosomes at the cell surface. On the other hand, MVs/ectosomes range in size from 50 nm to almost 1 µm and bud at plasma membrane microdomains enriched with ESCRT proteins, such as TSG101, recruited by ARRDC1 for MV formation. Additionally, microvesicles biogenesis is stimulated by ARF6. In cancer, various molecular pathways involving RTKs/Rab31, SRC, ARF6/PLD2, Ral/PLD1, and mTOR/PKM2, along with environmental and cellular factors related to hypoxia, pH, invasion, and chemotherapy, can influence exosome biogenesis. Specifically, hypoxia and Rab22a promote

microvesicles formation in cancer cells. The uptake of EVs (mentioned below) by recipient cells involves attachment of EVs to the ECM via adhesion molecules, such as integrins present on EVs. Cellular uptake of EVs occurs through pathways such as endocytosis, macropinocytosis, and phagocytosis. Once internalized, EVs traffic to the perinuclear area of recipient cells, where they may fuse with lysosomes. This intricate process of EV biogenesis and uptake plays a crucial role in intercellular communication, facilitating the exchange of biological information between cells. Extracted from (202).

A lipid driven mechanism has also been described for exosome production (203). Exosome biogenesis may depend on ceramide synthesis, as the inhibition of neutral sphingomyelinase 2 (nSMase2), which is the enzyme that converts sphingomyelin into ceramide at endosomes, has proved to reduce exosome release (204). Exosome secretion is regulated by calcium. Treatment with calcium ionophores resulted in enhanced intracellular calcium levels, which prompt the exosome production (205).

There are other factors that may also affect exosome production, including rearrangements in the actin and microtubule cytoskeleton that contribute to MVBs transport to the plasma membrane (206-208). Recent data suggests that dynamic endoplasmic reticulum may also mediate intercellular communication by affecting late endosomes formation (through oxysterol binding protein related protein 1L (ORP1L)) (209). Apart from this biogenesis machinery, small GTPase proteins, including ARF1 and RhoA, also enable EVs to bud off from the plasma membrane (210, 211). The release of exosomes into the extracellular space is facilitated by the fusion of the MVBs limiting membrane with the plasma membrane. This process may be mediated by several proteins. A few RAB GTPases, including RAB11 and RAB35, are facilitators of the fusion of the MVB with the plasma membrane. The exosomes released via these mediators are enriched in proteins, such as flotillin and other specific proteins, including Wnt, myelin proteolipid protein (PLP), and the transferrin receptor (TfR) (205, 212, 213). The exosomes secreted through RAB27A and RAB27B, are recognized as products of late endosomal activity and secretory compartments that are enriched in late endosomal proteins, including CD63, Alix and TSG101 (214, 215). Interestingly, a different RAB GTPase, RAB7, is involved in the release of exosomes containing Alix and syntenin by cancer cells (187). Although the depletion of this protein, RAB7, does not affect exosome release by different cancer cells (214).

1.5.2. EV uptake and cell-cell communication

EVs can enter and deliver their content into different recipient cells. Owing to their cargo EVs can transfer different molecules to the target cells and change the phenotype of these cells. The destiny of the content of an EV depends on its target destination (216). This uptake is mediated by components on the surface of the EV (216). Moreover, these nanoparticles might undergo multiple cell uptake and release cycles to allow access to several layers of tissues (217). It is unknown whether a different mode of EV uptake by recipient cells results in distinct localization, degradation, and/or functional outcomes of the EV constituents. Moreover, it is possible that the internalized EV cargo depends on the nature of the cargo and the recipient cells metabolic status, which may regulate the uptake of these nanoparticles.

Although the mechanisms of EV uptake by recipient cells remain unclear, EVs can interact with target cells via three different ways: (i) membrane fusion, (ii) receptor (direct) interaction, and (iii) internalization into recipient cell (216). In the first process, (i) the membrane fusion, the membrane of the recipient cell and the membrane of the EV fuse directly to release the intraluminal cargo content of the EV into the cytosol of the recipient cell. In this process, the hemifusion is formed between the hydrophobic lipid bilayers of the EV and the plasma membrane, which then expands to form a single coherent structure. Families of SNAREs and RAB proteins mediate this fusion (218, 219). In the (ii) receptor (direct) interaction, transmembrane proteins on the exosome surface directly bind with proteasomes on the target cell membrane. When this interaction happens, a downstream signaling cascade is activated, and soluble ligands are released (220-222). HSPGs, namely SDCs and GPCs are critical internalizing receptors for EV uptake, determining their functional activity (223, 224). The GAG chains, particularly the 2-*O*- and *N*-sulfation domains, were described to be key mediators of exosome uptake Additionally, it was shown that enzymatic treatment with Heparanase, that trims HS chains, and xylosides, which hinder HS biosynthesis, also resulted in EV uptake inhibition (225). Moreover, integrins have pivots roles in EV uptake. Under hypoxic conditions, the EV uptake is upregulated through a mechanism dependent on HSPGs and lipid raft mediated endocytosis. Thus, the EV content is selectively taken into the cell via permeable intracellular signals. This interaction may mediate immunomodulatory and apoptotic functions (226, 227). EVs can transmit information to acceptor cells by acting at the cell surface, without intracellular delivery of their content (228). For instance, during immune responses, EVs harboring major histocompatibility complex-peptide complexes can activate cognate T cell receptors on T-lymphocytes (173, 226). In (iii) internalization way, the EVs are internalized by the target cell, then fuse with intracellular compartments or endosomal pathways to transfer and

release the cargo. In this method, the common endocytic pathway is applied. Different endocytic pathways can occur, including clathrin-mediated, lipid-raft mediated, or caveolin-mediated endocytosis, phagocytosis and micropinocytosis (Figure 10). These endocytic pathways have been described for different cell types, for example, clatherin-dependent endocytosis or phagocytosis occur in neurons, micropinocytosis by microglia, phagocytosis or receptor-mediated endocytosis by dendritic cells, and caveolin-mediated endocytosis in epithelial cells (229-237). The content of the EVs can be internalized and can be targeted for lysosome degradation or recycled and released in the extracellular space. As an example, the EV recycling within acceptor breast cancer cells enables association of Wnt signaling with internalized fibroblast-derived CD81 positive EVs. The re-release of these particles triggers breast cancer cells motility through Wnt-related signaling (238, 239). The release of EVs has various biological roles, including the disposal of superfluous or harmful cellular contents. EVs emit signals and regulate molecules that can be recognized by, or transferred to, other cells in a selective manner, thereby influencing the phenotype and function of the recipient cells.

1.5.3. EVs and pre-metastatic niche establishment

In 1889, Stephen Paget proposed the “seed and soil” hypothesis. Cancer cells were compared to “seeds” and the site of cancer metastasis to “soil” in his hypothesis (240, 241). The destination of cancer metastasis is not random, but selectively distributed: so, the “seeds”, cancer cells, are able to spread through the body and just will grow in the fertile “soil” (242). Cancer cells are able to metastasize to specific organs, known as “metastatic organotropism”, or “organ-specific metastasis”, and are regulated by several factors (243-245). In this process EVs may act as “fertilizers”, by preparing a favorable microenvironment at future specific metastatic sites (243, 244).

The development of malignant tumors requires the ability of tumor cells to overcome cell-cell adhesion and then invade the surrounding tissue. Certain glycan structures can affect tumor cell invasiveness, including the ability to disseminate through the circulation and metastasize into distant organs (89, 246). The common metastatic organs may vary depending on the cancer type and subtype, for example, in gastric cancer, the most common metastatic sites are the liver, lung and spleen (247); prostate cancer often metastasizes to bone, while pancreatic cancer and melanoma usually form metastasis in the liver (248-250). Additionally, cancer cells can also display a methodical order and hierarchical organ-specific metastatic pattern. For instance, colorectal cancer typically metastasizes primary to the liver and then to the lung (251). Several factors mediate the metastatic organotropism, including the circulatory system pattern, the inner

microenvironment of the tumor, the tissue- or organ-specific microenvironment, host-organ microenvironment and metabolic adaptation mechanisms (252-255).

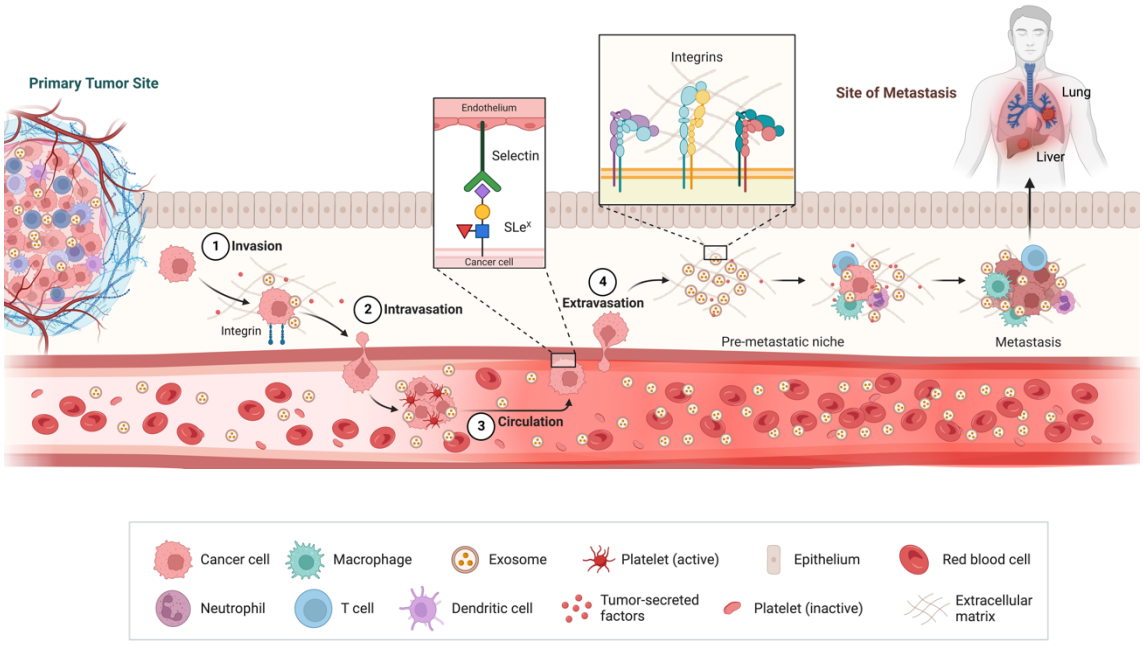


Figure 11 – Schematic representation of the establishment of the pre-metastatic niche. (1) Stromal cells escape from primary tumor (invasion) and (2) penetrate the blood vessels (intravasation). Intravasation involves various cellular and molecular mechanisms, including changes in cell adhesion, degradation of the extracellular matrix, and acquisition of migratory and invasive properties by tumor cells. After (3) cells enter the circulation and survive, previous released immune chemokines initiate expression of selectins which have high affinity for Sialyl Lewis X glycan epitopes. This interaction facilitates (4) endothelial adhesion and movement towards the site of inflammation (extravasation). The recruited EVs, previously released by cancer cells, created a supportive microenvironment through the secretion of additional factors and remodeling of the ECM. Integrins are crucial factors in this step. The establishment of the pre-metastatic niche can involve immune modulation, where the immune response in the target organ is altered to create an immunosuppressive or immune-tolerant environment. This immune modulation can help the metastatic cancer cells evade immune surveillance and establish themselves in the target organ. Once the pre-metastatic niche is established, circulating tumor cells that have detached from the primary tumor can home to the pre-metastatic site. The altered microenvironment and the presence of specific cellular adhesion molecules in the niche promote the extravasation and retention of these metastatic cells.

EVs mediate cell–cell communication locally and systemically and are secreted by most cell types including dendritic cells, macrophages, cancer cells and mesenchymal stem cells (256). EVs can transfer cargo to various cell types with varying degrees of efficiency, and distribution depends on the host cell. For instance, while macrophages are commonly

intermediators in EV uptake, specifically the endothelial cells are the intervenient for EV uptake into the lungs (257-259). This fact supports the notion that EVs constitute communication vehicles between neighboring cells that affect apoptosis, growth, cell cycle, migration, invasion, and differentiation of recipient cells (260, 261). These communication routes of the EVs lead the transference of their cargo into the recipient cell correlating with their metastatic potential, therefore, developing the pre-metastatic niches (Figure 11) (260-262). This process also involves secretory factors that induce vascular leakage, ECM remodeling and immunosuppression (260). Moreover, integrins have been identified as the major players within EVs orchestrating the formation of these pre-metastatic niches at distant sites (263). Additionally, signaling factors mediated by EVs can activate EGRF (and its ligands) signaling to support cancer metastasis (see Figure 11) (264). Furthermore, EVs can remodel the ECM by interacting with fibroblasts, stromal cells, and endothelial cells to degrade protease-associated components such as collagen, laminin, and fibronectin (265, 266). Proteomic expression profile of bone cancer showed an altered integrin pattern, whereby the exosomal integrins α6β4 and α6β1 were correlated with lung metastasis, whereas exosomal integrin αvβ5 was linked to liver metastasis (263). In contrast, the inhibition of exosome exocytosis, via RAB27A KO led to reduced metastasis (267, 268). EVs act as intercellular shuttles, which are crucial for primary tumor growth and metastatic spread. Moreover exosomes/EVs specific signatures make them promising diagnostic biomarkers.

1.6. PGs and EVs in cancer cell communication

1.6.1. Potential as biomarkers and therapeutic targets

There is a great need of identifying novel targets for improving diagnostic and prognostic monitoring of gastric cancer patients. Adding to this equation, the designing of novel cancer therapies has proved to be challenging. Despite decades of research, treatments resulting in a consistent and permanent reversal from an oncogenic cell state have remained elusive, and patient outcome have failed to considerably improve. Although there are a few cases of success where new therapies, including targeted therapies and immunotherapies, have revolutionized the outcome of some patient groups.

Although there are numerous factors contributing to cancer patient outcome, the design of more effective treatment regimens and the identification of effective biomarkers for patients' diagnosis and prognosis are needed. Due to the many emerging roles presented by EVs, their use in clinical treatment sceneries is progressively happening. For example, clinical trials testing EVs for diagnostic tools and therapeutic applications are generating a

remarkable interest from the scientific community (269). Though numerous biomarkers already exist that allow the detection, prognostic evaluation, and treatment of various cancers, the unpredictable nature of many tumors still presents an extraordinary challenge. These findings allude to the possibility of using EVs for prognostic or diagnostic purposes in the future, or potentially as a target in forthcoming cancer treatments. On top of that, liquid biopsies using EVs carry minimal risk and are generally well-tolerated by patients, making them a safer option compared to surgical biopsies, which can pose potential complications. This non-invasive approach is particularly beneficial for patients who cannot undergo or prefer to avoid surgical biopsies (270).

The proteoglycan profile, which has been demonstrated has actively involved in the EV biogenesis, release, sorting and function, is frequently altered in pathological conditions. Therefore, the modulation of glycoconjugate composition of EVs has been considered as an attractive tool in the design of novel therapeutics. Moreover, other applications, as tissue regeneration, gene therapy, cancer, and immune-modulatory treatments are becoming more attractive to open new perspectives in exploiting EVs-proteoglycans and optimizing delivery platforms. Abnormalities in PGs/GAG abundance and structure (e.g., sulfation patterns and molecular weight) are found across various cancer types and show biomarker potential. Targeting PGs/GAGs, as well as their usage or of their mimetics, are promising approaches to interfere with cancer progression. However, phase III clinical trials using prophylactic Low-Molecular-Weight Heparin (LMWH) can reduce the incidence of venous thromboembolism (VTE) events in cancer patients undergoing surgery or chemotherapy, it has been failing to impact the overall survival and progression-free survival in cancer patients (e.g. FRAGMATIC and RASTEN clinical trials) (271-274). In addition, PGs/GAGs can be used as drug and cytokine carriers to induce an antitumor response. Growing evidence has demonstrated that among the myriad of glycosylation changes seen in cancer cells, the SDC family of proteins often undergoes alterations in expression. Glycoconjugate-based mechanisms may offer a promising strategy for advances in EV-based targeted delivery systems, however, understand characterization and heterogenous composition is required.

Glycan motifs, specifically α-2,3- and α-2,6 linked sialic acid, on glioblastoma-derived exosomes were shown to be immunosuppressive (275, 276). Overexpression of high-mannose glycans increased the uptake of EVs by monocyte-derived dendritic cells, resulting in enhanced priming of tumor-specific $CD8^+$ T cells (277). The effect of the glycan structure impacts heterogeneously cellular uptake, depending on the target cells. Removal of surface glycans from exosomes derived from human breast cancer cells stimulated their uptake by human umbilical vein endothelial cells (278). Modification of the glycosylated complexes on the vesicle surface can also affect their distribution. Removal of sialic acid

residues from mouse liver-derived exosomes resulted in a higher uptake and accumulation of EVs in the lung (279). Promising results describes miR-122-5p overexpression or liver-cell-derived exosomal miR-122-5p enhances the human breast cancer cell motility via directly targeting the *SDC1* 3′ UTR. Moreover, exosomes miRNA content increases when hepatoma cells are treated with apoptotic drugs, demonstrating that the presence of this exosomal miRNA affects distant metastasis by downregulating SDC1 expression (280). This possible mechanism is a key for the development of strategic drug therapy for the prevention of distant metastases.

Remarkably, EVs can deliver both synthetic and natural agents. In a recent experiment, exosomes with triptolide were used in the treatment of ovarian cancer. The exosomes showed high encapsulation efficiency and were able to slow tumor growth *in vivo* (281). On the other side, EVs may carry specific proteins and genetic material that can influence drug resistance or enhance drug delivery to tumor cells. For example, it was shown that EVs released by cancer cells could sequester cytostatic drugs, thereby reducing their effectiveness. Additionally, it was observed that EVs could also bind to therapeutic antibodies, such as those directed against HER2, preventing their interaction with cancer cells, and limiting their therapeutic efficacy (282, 283). Similarly, monoclonal antibodies, like trastuzumab and rituximab, target specific receptors or antigens on cancer cells, and while the role of EVs in the action of these therapies is not fully understood, it is hypothesized that EVs might carry antigens or receptors that could affect treatment response or act as potential targets for therapeutic intervention (284, 285). Furthermore, EVs have been shown to modulate the immune response and may potentially influence the efficacy of checkpoint inhibitors by carrying immunomodulatory molecules or antigens (286, 287).

Biomarkers of SDC signaling pathways may be useful for selecting patients that would most likely respond to therapy at the time of diagnosis or for predicting relapse. Although there are several challenges (as their complexity, heterogeneity, detection, and quantification), in their clinical application, EVs are considered valid diagnostic biomarkers and potential therapeutic tools in cancer. Moreover, along with chemical, cellular, and genetic engineering techniques, EV modification strategies may be promising for the development of clinical therapies.

CHAPTER II

General aim and specific objectives

2. General aim and specific objectives

2.1. Rationale and General aim

The gastric carcinogenesis pathway is accompanied by significant cellular glycosylation changes. During gastric cancer initiation and progression there is upregulated expression of specific proteoglycans. Noteworthy, a growing body of evidence reveals that HSPGs regulate several key biological processes of EVs, including biogenesis and uptake, and recipient cell functionalization. EVs are recognized as important mediators of tumor and stromal cells communication during tumor progression. Moreover, several studies have proposed that EVs can contribute to define metastasis organotropism.

Here, the major objective was to understand how SDC4, a major carrier of HS in gastric epithelial cells, regulates gastric cancer cell biomechanical features, such as motility and invasion, as well as SDC4 impact on EV cargo and biodistribution.

2.2. Specific objectives

To accomplish the above-mentioned general aim, the following specific objectives were followed as described:

1) **Evaluate SDC4 expression in gastric cancer and assess the association with patients' clinical features.**

In collaboration with IPO-Porto, we had access to a well characterized human gastric cancer carcinoma cohort. By immunohistochemistry, we evaluated the SDC4 expression profile in this series. We associated this expression signature with histological classification, and when possible, with lymph node (LN) metastasis. Additionally, our findings were validated using online human databases (for example TCGA database) and bioinformatic tools.

2) **Understand the impact of SDC4 in defining gastric cancer motility features and invasion capacity.**

Cell migration is an essential process in development, wound healing, and immune response, but it can also contribute to pathological conditions such as cancer metastasis and autoimmune disorders. The migration of cells is a complex and dynamic process involving multiple steps, including protrusion of the cell membrane, formation of focal adhesions, contraction of the cytoskeleton, and detachment and retraction of the trailing edge. Focal adhesions are prominent macromolecular structures that serve as sites of connection between the ECM and cytoskeleton. These dynamic structures consist of adhesion receptors, such as integrins and SDCs, which recruit a variety of adaptor and

scaffold proteins to reinforce the adhesion (288). In addition, the formation and turnover of focal adhesions in response to the microenvironment is vital for the mesenchymal migration of cells (288).

The gastric cancer cell line MKN74 was used to generate models with a defined repertoire of proteoglycans and specific glycan chain modifications. The glycoengineered cell models were generated via CRISPR/Cas 9 genome editing, using FACS enrichment of nuclease-expressing cells and indel detection by amplicon analysis (289). Cells were transfected with Cas9 endonuclease vector containing GFP and plasmids with the gRNAs. Single cell sorting was used to obtain different clones. Indel detection was performed by amplicon analysis and sequencing. Using the glycoengineered SDC4 KO clones and their parental cells, we evaluated cell migration using different ECM components (namely, uncoated, fibronectin, collagen IV and Poly-D-lysine). In addition, the invasion potential of the glycoengineered cancer cells was evaluated using Matrigel Invasion Chambers.

3) Uncover the signaling pathways that are modulated by SDC4.

Cells depend on adhesion molecules, specifically cell surface glycoproteins, to engage with and react to the ECM. The integrins are the main actors in cell-ECM interaction, although other molecules such as selectins and SDCs can also attach to the ECM. Cell migration involves a complex interplay of signaling pathways that regulate focal adhesion formation, maturation, and turnover. One of the key proteins involved in this process is paxillin, which acts as a scaffold or adaptor protein to recruit kinases and other adaptors to facilitate signaling events (290). SDC4 has been recognized for its role in focal adhesions, functions as a direct interface between the ECM extracellular signaling proteins, as it has the ability to bind fibronectin and α-actinin, an intracellular actin-associated protein, simultaneously. Additionally, it can recruit other proteins to the focal adhesion sites, including the signaling molecule PKCα (291-293). SDC4 plays a critical role in activating FAK and promoting downstream signaling pathways in focal adhesions (294-296).

In order to identify the intracellular signaling pathways activated by SDCs, we resorted to human phospho-RTK (Receptor Tyrosine Kinase) antibody array. Moreover, using Western Blot technique we evaluated the activation of already described intracellular pathways associated with SDC4.

4) Study the impact of SDC4 expression on EV biophysical properties and on their cargo content.

EVs are membrane-bound particles secreted by cells and play a crucial role in cell-cell communication. SDC4 is a transmembrane protein that can be found on EVs and may play a role in the biogenesis of EVs. Using different glycoengineered gastric cell models that we established in the previous task; we used a workflow for EVs isolation. Our group has previously demonstrated the impact of using different isolation methodologies in the populations of EVs that are obtained and its consequences in the glycosylation profile of the isolated populations (297). Accordingly, EVs were isolated, from the cell lines established, using a combination of two different approaches differential ultracentrifugation (UC) plus qEV original size exclusion chromatography (SEC) columns. The content of the purified EVs, and their respective parental cells, was analyzed using advanced Mass Spectrometry (MS).

5) Evaluate if SDC4 affects EVs uptake *in vitro* and *in vivo* organotropism.

To disclose the impact of SDC4 and its glycosylation features in the EV recognition and uptake, EVs isolated from glycoengineered cells displaying different glycosylation profile were labelled and incubated with different cell populations, including epithelial, stromal, and immune cell lineages. The quantification of the internalized EVs was performed by fluorescence quantification using the high-content imaging system IN Cell Analyzer 2000 or Operetta CLS High Content Analysis System.

To evaluate the organ distribution of EV (with defined proteoglycan signatures), labelled EVs with either NIR815 or PKH67 and then inject in 6 – 8 weeks old NOD-SCID mice by retro-orbital route. Mice organs were collected and the quantification of EV uptake by the different organs was monitored using near-infrared detection at Odyssey CLx Imaging System In parallel, mice organs were digested and EVs uptake will be quantified by FACS. Lastly, in order to test the role of EVs displaying specific proteoglycans in pre-metastatic niche education mice were educated with EVs from WT and SDC4 KO cells. At the end of the 21 days, animals were subjected with intrasplenic injection of mCherry-MKN74 cells. The intrasplenic route has been chosen because the principal metastatic site of gastric cancer is the liver, and the spleen. After 24 hours of surgery, mice were sacrificed, and livers were evaluated for mCherry+ cells (298).

6) Evaluation of EV properties along the gastric carcinogenesis pathways resorting to human clinical samples.

Plasma samples were collected from controls (healthy donors) and patients with gastric disease who underwent endoscopic resection (premalignant and early stage), or partial or total gastrectomy. The samples collection was performed at Centro Hospitalar Universitário São João. EVs were isolated from a subset of 50 plasma samples. The selection of the cases was performed based on the patients clinico-pathological information, in order to have representation of all biological groups tested (healthy controls (Ctrl); intestinal metaplasia; low grade dysplasia (LGD); high grade dysplasia (HGD); and early cancer (EC)). Briefly, plasma was recovered from blood samples and EVs isolation was performed using size exclusion chromatography (SEC) (299). EVs were characterized by Nanoparticle Tracking Analysis (towards NanoSight) to determine particle quantification and size, visualized by transmission electron microscopy (TEM) to evaluate morphology and integrity. In order to analyze EV cargo from these biological samples, a MS analysis, using a high-resolution methodology already established (300, 301) was implemented.

CHAPTER II

Study of the SDC4 functional impact on gastric cancer

THIS CHAPTER CONTAINS THE FOLLOWING PUBLICATION:

Poças J, Marques C, Gomes C, Otake AH, Pinto F, Ferreira M, Silva T, Faria-Ramos I, Matos R, Ribeiro AR, Senra E, Cavadas B, Batista S, Maia J, Macedo JA, Lima L, Afonso LP, Ferreira JA, Santos LL, Polónia A, Osório H, Belting M, Reis CA, Costa-Silva B, Magalhães A. Syndecan-4 is a maestro of gastric cancer cell invasion and communication that underscores poor survival. Proc Natl Acad Sci U S A. 2023 May 16;120(20):e2214853120. doi: 10.1073/pnas.2214853120. Epub 2023 May 8. PMID: 37155874; PMCID: PMC10193992.

PNAS RESEARCH ARTICLE | CELL BIOLOGY OPEN ACCESS

Syndecan-4 is a maestro of gastric cancer cell invasion and communication that underscores poor survival

Juliana Poças[a,b,c], Catarina Marques[a,b,c], Catarina Gomes[a,b], Andreia Hanada Otake[d,1], Filipe Pinto[a,b], Mariana Ferreira[a,b], Tiago Silva[a,b], Isabel Faria-Ramos[a,b], Rita Matos[a,b], Ana Raquel Ribeiro[a], Emanuel Senra[a], Bruno Cavadas[a], Sílvia Batista[d], Joana Maia[d], Joana A. Macedo[a,b], Luís Lima[e], Luís Pedro Afonso[e], José Alexandre Ferreira[e], Lúcio Lara Santos[e], António Polónia[a,b], Hugo Osório[a,b,f], Mattias Belting[g,h,i], Celso A. Reis[a,b,c,f], Bruno Costa-Silva[d], and Ana Magalhães[a,b,c,2]

Edited by Gabriel Rabinovich, Universidad de Buenos Aires, Buenos Aires CABA, Argentina; received August 30, 2022; accepted March 22, 2023

Gastric cancer is a dominating cause of cancer-associated mortality with limited therapeutic options. Here, we show that syndecan-4 (SDC4), a transmembrane proteoglycan, is highly expressed in intestinal subtype gastric tumors and that this signature associates with patient poor survival. Further, we mechanistically demonstrate that SDC4 is a master regulator of gastric cancer cell motility and invasion. We also find that SDC4 decorated with heparan sulfate is efficiently sorted in extracellular vesicles (EVs). Interestingly, SDC4 in EVs regulates gastric cancer cell-derived EV organ distribution, uptake, and functional effects in recipient cells. Specifically, we show that *SDC4* knockout disrupts the tropism of EVs for the common gastric cancer metastatic sites. Our findings set the basis for the molecular implications of SDC4 expression in gastric cancer cells and provide broader perspectives on the development of therapeutic strategies targeting the glycan-EV axis to limit tumor progression.

syndecan-4 | heparan sulfate proteoglycans | gastric cancer | extracellular vesicles | cancer cell invasion

Significance

Gastric cancer is a clinically challenging disease with poor prognosis. Heparan sulfate proteoglycans (HSPGs) have emerged as key molecules in tumor progression and communication. However, the functional relevance of HSPGs during gastric cancer development remains poorly known. Here, we demonstrate that Syndecan 4 (SDC4) is highly expressed in intestinal subtype gastric tumors and associates with higher invasion and patient poor survival. We provide evidence that glycosylated-SDC4 is packed on extracellular vesicles (EVs) and impacts EV protein cargo, uptake by recipient cells and, importantly, defines the tropism of cancer EVs to the common metastatic sites of gastric cancer. Thus, our data uncover SDC4 potential as a therapeutic target in precision oncology for limiting gastric cancer invasion and communication routes.

Gastric cancer persists as a global health challenge, as it is the fifth most frequent malignancy with over one million new cases annually, and the fourth leading cause of cancer-related death worldwide (1). The clinical aggressiveness of gastric cancer, which is translated into poor survival of patients, is mainly attributed to the late diagnosis due to silent disease progression and the lack of efficient therapeutic options (2, 3).

Paramount evidence shows that alterations in the cellular glycosylation pathways are drivers of tumor progression (4, 5), as glycans and glycoconjugates are key regulators of the cross talk between cancer cells and the different components of the tumor microenvironment (5, 6). Particularly in gastric cancer, aberrant glycan signatures have been shown to govern important oncogenic processes, including proliferation, cell–cell and cell-extracellular matrix (ECM) adhesion, receptor tyrosine kinase (RTK) signaling, migration, invasion, angiogenesis, and metastatic dissemination (7–9).

Syndecans (SDCs) are a family of four transmembrane heparan sulfate proteoglycans (HSPGs). SDCs act in cooperation with key transmembrane receptors and ECM molecules mediating pleiotropic functions, such as signaling, adhesion, proliferation, migration, apoptosis, and differentiation (10). HSPG expression patterns, and particularly SDC signatures, have been described as aberrant in different cancer models, including tumors of the gastrointestinal tract (11, 12). However, there is a considerable gap of knowledge on the functional mechanisms and relevance of HSPGs and their ECM interactomes during gastric cancer development.

Syndecan-4 (SDC4) is one of the carriers of HS glycosaminoglycan chains in epithelial cells with key roles in the control of focal adhesion formation, migration, invasion, and endocytosis (13–16). SDC4 expression was shown to be up-regulated in response to oncogenic stimulus during the early stages of the gastric carcinogenesis pathway (17, 18).

Remarkably, SDCs are also key regulators of extracellular vesicle (EV) biogenesis (19). EVs are a heterogeneous group of secreted vesicles, which include exosomes and microvesicles, found in all body fluids. EVs are secreted by all cell types, including cancer cells, and hold major roles in tumor cell communication due to their capacity of reprograming recipient cells, and ultimately defining metastasis organ tropism (20, 21). SDCs together with their small intracellular adaptor syntenin and their associated regulators Alix (an accessory component of the endosomal-sorting complex required for transport), the small GTPase ARF6, the lipid modifying enzyme PLD2, and the HS glycosidase heparanase, have been shown to regulate the formation of EVs of endosomal origin and to impact their cargo composition (19, 22, 23). Moreover, the interaction of tetraspanin 6 (TSPN6) with SDC4 was shown to functionally control EV degradation and release (24). On the

This article is a PNAS Direct Submission.

Copyright © 2023 the Author(s). Published by PNAS. This open access article is distributed under Creative Commons Attribution-NonCommercial-NoDerivatives License 4.0 (CC BY-NC-ND).

[1]Present address: Instituto do Cancer do Estado de Sao Paulo, Hospital das Clinicas HCFMUSP, Faculdade de Medicina, Universidade de Sao Paulo, Sao Paulo 01246-000, Brazil.

[2]To whom correspondence may be addressed. Email: amagalhaes@ipatimup.pt.

This article contains supporting information online at https://www.pnas.org/lookup/suppl/doi:10.1073/pnas.2214853120/-/DCSupplemental.

Published May 8, 2023.

Downloaded from https://www.pnas.org by 92.106.253.224 on June 22, 2023 from IP address 92.106.253.224.

recipient cell side, HS chains, including those carried by SDCs, act as critical internalizing receptors of cancer cell-derived EVs with impact on their functional activity (25). Taking together the key roles played by HSPGs in both axes of cancer cell communication, EVs and their recipient cells, it is of utmost relevance to understand how SDC4, a master HSPG, impacts EV-mediated signaling and cancer-derived EV organ tropism.

In this study, we show that SDC4 is highly expressed in intestinal subtype gastric tumors and lymph node (LN) metastasis and associates with poor patient survival. Moreover, we mechanistically demonstrate, using *SDC4* knockout (KO) gastric cancer cells, that SDC4 is a key regulator of gastric cancer aggressive features, such as migration and invasion. On top of modulating gastric cancer cell motility, we reveal that SDC4 conjugated with HS glycosaminoglycans is present in the EV cargo and defines EV organ distribution, uptake, and oncogenic functional effects on recipient cell populations.

Results

SDC4 Expression Is Up-Regulated in Intestinal Subtype Gastric Tumors and Is a Marker of Poor Patient Survival. Aberrant expression of SDC4 has been reported in several cancer models (26–34). We have previously demonstrated that *SDC4* transcription in gastric cells is up-regulated in response to inflammatory stimulus, such as cytokines or bacterial infection. In addition, we showed that SDC4 expression on *Helicobacter pylori*-inflamed gastric mucosa is associated with the virulence of the infecting strain (17, 18). However, the expression profile of SDC4 in gastric tumors remained to be elucidated. Thus, in this study we evaluated SDC4 expression in a retrospective series of 152 stage I–IV gastric carcinomas. *SI Appendix*, Table S1 summarizes the clinicopathological information of this cohort of gastric cancer patients. We observed that SDC4 tissue staining, using the 8G3 antibody which binds to the extracellular domain (ECD) of SDC4 (35), was significantly associated with tumor histological classification ($P = 0.031$), with 71.4% of the intestinal subtype tumors showing SDC4 positivity (Fig. 1 *A* and *C* and *SI Appendix*, Table S1), whereas among diffuse subtype tumors, SDC4 staining was lower in intensity and frequency and near half of the evaluated cases showed no staining (47.6% of positive cases) (Fig. 1 *B* and *C* and *SI Appendix*, Table S1). Interestingly, the SDC4 staining profile was also preserved in the LN metastases, with the majority of cases of intestinal subtype tumors showing SDC4-positive LN metastases (Fig. 1 *A* and *D* and *SI Appendix*, Fig. S1 and Table S1).

Kaplan–Meier analysis of patient prognosis, showed that SDC4 expression was significantly associated with overall poor survival of patients (OS) (80.4 vs. 59.7 mo, $P = 0.025$) (Fig. 1*E* and *SI Appendix*, Table S2). When stratified by clinicopathological variables, this association was also observed in younger (<66 y) ($P = 0.005$), male ($P = 0.028$), patients without metastatic disease, pN0 ($P = 0.016$) and pM0 ($P = 0.044$) and exclusively treated with surgery ($P = 0.026$). Considering the histological classification, the OS association with SDC4 expression was only significant in patients within the intestinal gastric cancer subtype group (88.8 vs. 60.6 mo, $P = 0.018$) (Fig. 1*F* and *SI Appendix*, Table S2), while for diffuse subtype there was no association between SDC4-positivity and survival (Fig. 1*G* and *SI Appendix*, Table S2).

The independent prognostic value of SDC4 expression was assessed via stepwise multivariate Cox regression with backward elimination. The analysis was performed in all patients and then stratified by histological (Lauren) classification, since SDC4 expression was associated with poor prognosis especially in patients with intestinal subtype. Variables such as gender, age, disease stage, and treatment were added to the model, and disease stage was the only covariable retained. In patients with intestinal subtype tumors, the association of SDC4 expression remained significant when adjusted to disease stage (HR = 1.893; 95% CI: [1.033–3.471]; $P = 0.039$), highlighting its value as an independent prognostic factor.

To further validate our observations in an independent gastric cancer patient cohort, we analyzed the *SDC4* transcriptomic profile of gastric cancer samples from The Cancer Genome Atlas Stomach Adenocarcinoma (STAD-TCGA). We observed that *SDC4* high-transcript levels clustered with cancer aggressive features, such as metastasis (M1) and disease recurrence (Fig. 1*H*). Again, *SDC4* expression was clustered with the intestinal subtype (Fig. 1 *H* and *I*). Noteworthy, high *SDC4* transcription levels also clustered with the CIN molecular subtype and with low MSI/high aneuploidy scores (Fig. 1*H*). In this STAD-TCGA cohort, *SDC4* expression showed a trend toward higher expression in higher disease grades (Fig. 1*J*). Kaplan–Meier analysis of *SDC4* mRNA levels and gastric cancer patient OS and DFS was performed in two additional independent cohorts: the STAD-TCGA cohort (Fig. 1 *K* and *L* and *SI Appendix*, Fig. S2 *A* and *B*) and in the cohort from the Kaplan–Meier Plotter (KM plotter) database (*SI Appendix*, Fig. S2 *C* and *D*). These analyses validated a significant association between *SDC4* expression and patient worse prognosis (DFS) for all patients and in intestinal subtype in STAD-TCGA dataset (Fig. 1*L* and *SI Appendix*, Fig. S2*B*). A significant association between *SDC4* and OS and DFS was also confirmed in KM plotter cohort for intestinal subtype (*SI Appendix*, Fig. S2 *C* and *D*).

A multivariate Cox regression with backward elimination was performed to assess the independent prognostic value of *SDC4* expression in all gastric cancer patients and then in the intestinal subtype patients, within the STAD-TCGA database. The clinicopathological parameters gender, Lauren classification, age, and disease stage were used as covariables for OS and DFS. Of note, the expression data from all patients from this dataset were collected before treatment. We found that the covariables disease stage and age (≥67 y) were associated with OS. However, *SDC4* was not associated with OS (HR = 1.782; 95%CI: [0.747 – 4.258]; $P = 0.187$). When the multivariate analysis was performed for DFS, we found that the clinical parameter grade was the only covariable retained only for the intestinal subtype. Importantly, this analysis validated the independent prognostic value of *SDC4* for DFS, when adjusted to disease stage in all gastric cancer patients (HR = 4.004; 95%CI: [1.080 – 14.837]; $P = 0.038$) and when subclassified by intestinal subtype (HR = 3.912; 95%CI: [0.109–12.872]; $P = 0.017$).

SDC4 Promotes Promigratory and Invasive Phenotypes in Gastric Cancer Cells. Taking into consideration the high expression of SDC4 in gastric tumors and its clinical association with patient poor outcome, we sought to determine the functional role of SDC4 in cancer cell features. SDC transcription analysis in four gastric cancer cell lines showed that SDC4 is highly expressed, SDC1 and SDC3 were detected in lower levels, whereas SDC2 was not detected in all cells (Fig. 2*A*). Next, we evaluated the SDC4 protein expression and cellular distribution in gastric cancer cells (Fig. 2 *B* and *C*). The WB analysis revealed a high MW smear corresponding to the fully glycosylated forms of SDC4, tetrameric (70 kDa), dimeric (35 kDa), and monomeric (17 kDa) forms. Confocal microscopy showed that SDC4 was predominantly expressed in the plasma membrane of most gastric cancer cells, with AGS cells displaying also punctuated cytoplasmic staining (Fig. 2*C*).

To determine the functional impact of SDC4, its expression was KO in the MKN74 intestinal subtype gastric cancer cell line

Downloaded from https://www.pnas.org by 92.106.253.224 on June 22, 2023 from IP address 92.106.253.224.

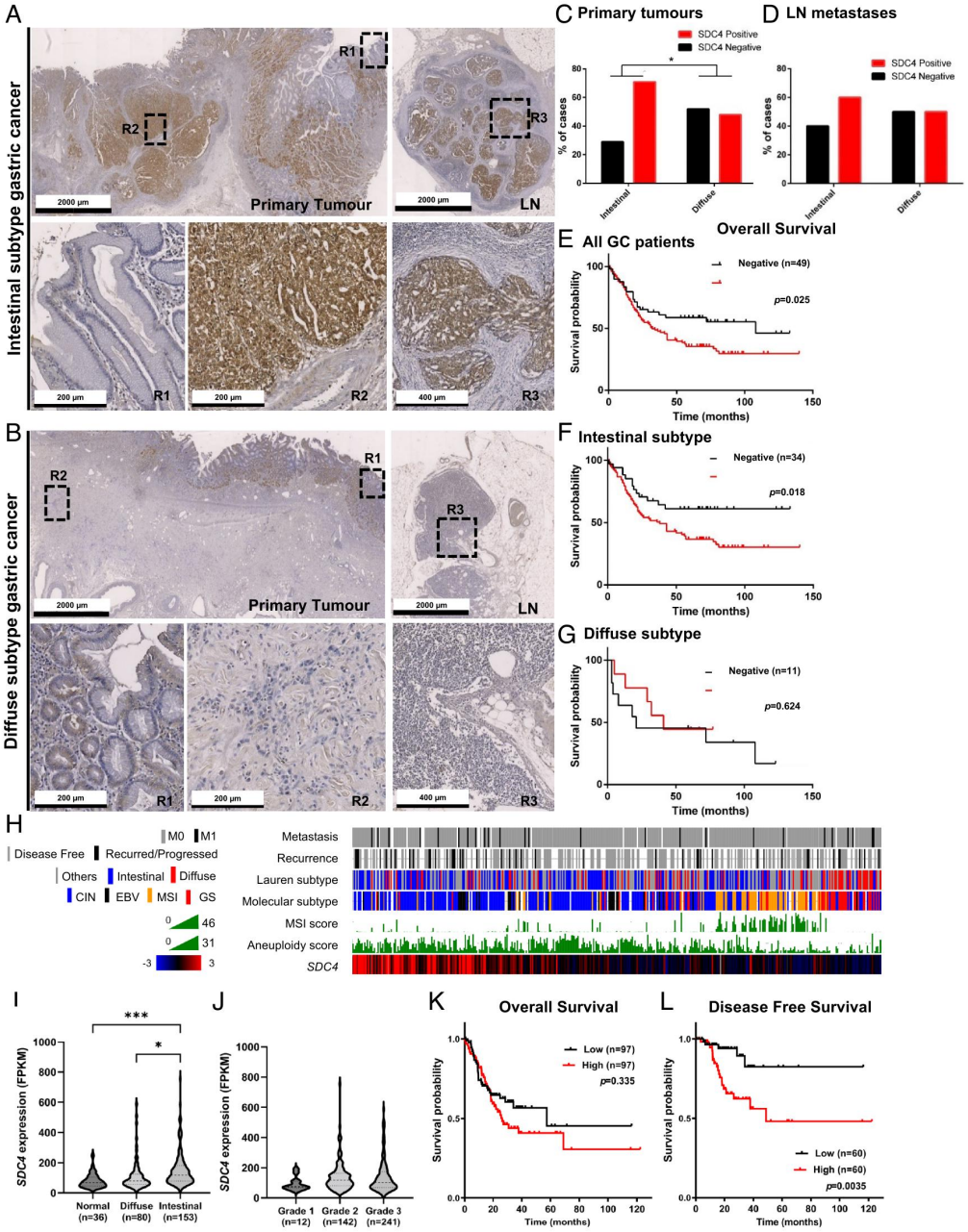


Fig. 1. SDC4 is highly expressed in intestinal subtype gastric cancer and associates with patient poor survival. (*A* and *B*) Representative images of SDC4 immunohistochemistry (IHC) analysis of (*A*) intestinal and (*B*) diffuse subtypes of primary gastric tumor tissue samples paired with respective LN metastases. Three regions (R1-3) were selected: R1-adjacent mucosa; R2-primary tumor; R3-LN metastasis. (*C* and *D*) Bar graphs show the percentage of (*C*) primary tumor cases or (*D*) LN metastasis positive (red bar) or negative (black bar) for SDC4, for intestinal and diffuse gastric cancer subtypes. The chi-square test was performed and * represents $P < 0.005$. (*E*–*G*) Kaplan–Meier (KM) analysis of SDC4 tissue expression levels and gastric cancer patients overall survival (OS) for (*E*) all gastric cancer, (*F*) intestinal subtype and (*G*) diffuse subtype patients, the categorization of these clinical samples was assigned into SDC4 IHC positive (red lines) or SDC4 IHC negative (black lines). Comparison between curves in KM plots was performed using the log-rank test. (*H*) SDC4 expression signature in gastric cancer (STAD-TCGA cohort) was clustered using the heatmap CbioPortal algorithm (1, 2) and correlated with clinicopathological data, including metastasis, recurrence, Lauren subtype, TCGA molecular subtype [chromosomal instability (CIN); Epstein–Barr virus (EBV); microsatellite instability (MSI); genomically stable (GS)], MSI and aneuploid scores. (*I* and *J*) Distribution of *SDC4* mRNA expression levels in the STAD-TCGA cohort by (*I*) Lauren classification and by (*J*) tumor grade. Samples classified as undetermined gastric cancer NOS (Not otherwise specified) in this dataset were excluded from the analysis. RNA sequencing of *SDC4* expression is represented as fragments per kilobase million. (*K* and *L*) KM analysis of *SDC4* mRNA levels and gastric cancer (*K*) OS or (*L*) disease-free survival (DFS) (STAD-TCGA cohort). The categorization of patient samples was divided into low (lowest 25%, black lines) and high (highest 25%, red lines) subgroups according to the levels of *SDC4* mRNA expression. Comparison between curves in KM plots was performed using the log-rank test. **References:** 1. E. Cerami E, Gao J, Dogrusoz U, Gross BE, Sumer SO, Aksoy BA, et al. The cBio cancer genomics portal: an open platform for exploring multidimensional cancer genomics data. Cancer Discov. 2012;2(5):401-4. 2. Gao J, Aksoy BA, Dogrusoz U, Dresdner G, Gross B, Sumer SO, et al. Integrative analysis of complex cancer genomics and clinical profiles using the cBioPortal. Sci Signal. 2013;6(269):pl1.

Downloaded from https://www.pnas.org by 92.106.253.224 on June 22, 2023 from IP address 92.106.253.224.

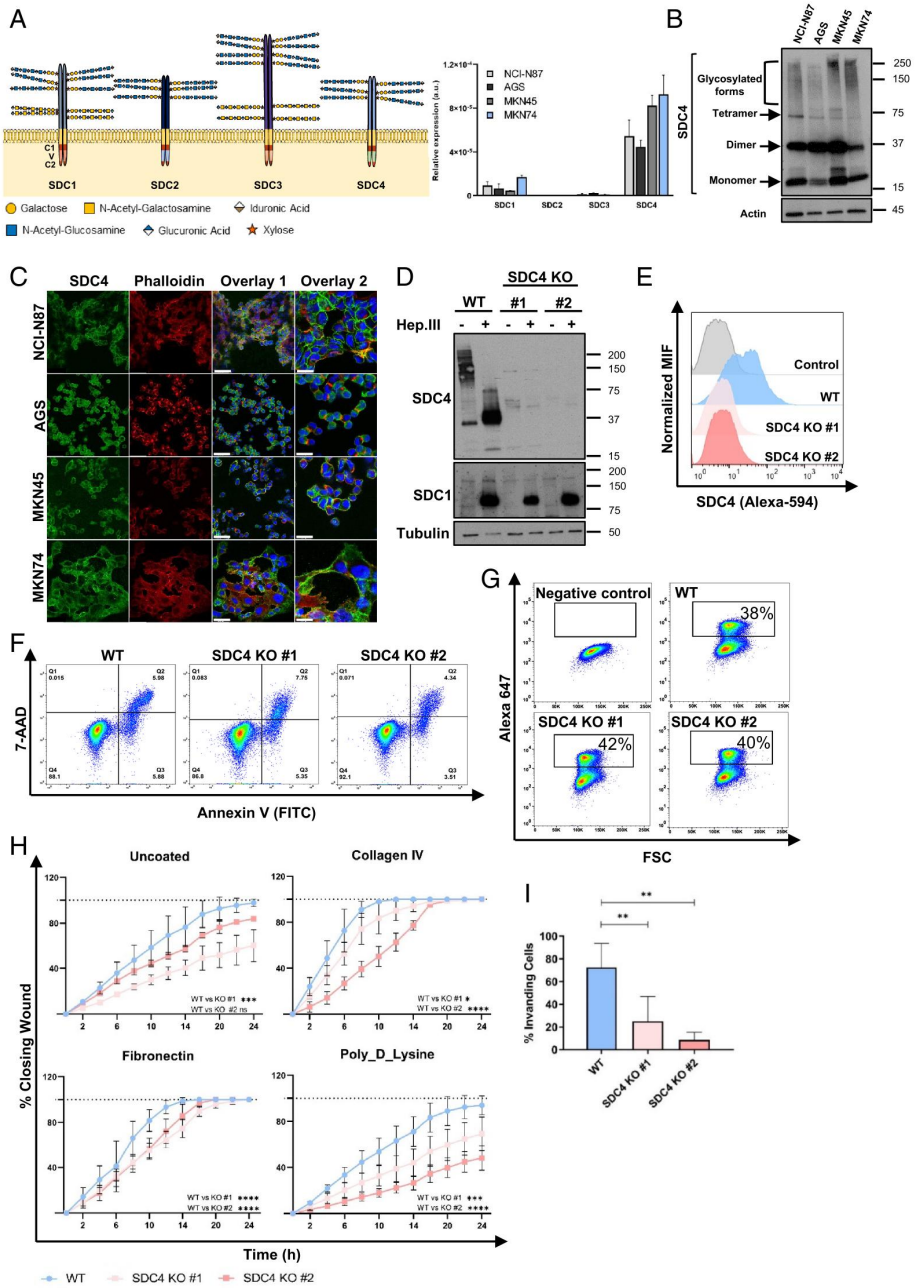


Fig. 2. *SDC4* KO impairs gastric cancer cell motility features. (*A*) Schematic representation of SDC family, showing the cytoplasmic domain with two highly conserved regions (C1 and C2) and the SDC-specific variable (V) region, and the ECD that may be decorated with heparan sulfate (HS) and chondroitin sulfate (CS) chains; Bar graph displays the qRT-PCR analysis of *SDC1-4* mRNA levels in four gastric cancer cell lines (NCI-N87, AGS, MKN45, MKN74). (*B*) WB analysis of SDC4 protein expression showing high-MW heterogeneous bands corresponding to the glycosylated forms of SDC4, tetramer, dimer, and monomer; Actin was used as loading control. (*C*) Confocal imaging of SDC4 (8G3) (green), phalloidin (red), and DAPI (blue) staining in gastric cancer cell lines. Scale bar corresponds to 50 µm (Overlay 1) and 20 µm (Overlay 2). (*D*) WB analysis of SDC4 and SDC1 in *SDC4* KO models and parental cells with (+) and without (−) Heparinase III (Hep. III) digestion. Tubulin was used as loading control. (*E*) FACS analysis of SDC4 (8G3 clone) cell surface expression on KO models and parental cells. MFI-mean fluorescence intensity. (*F*) Cell viability analysis by 7-AAD/ Annexin V-FITC cell labeling. Dot plots show the percentages of (Q1) cells in necrosis, (Q2) cells in late apoptosis, (Q3) cells in early apoptosis, and (Q4) viable cells. Representative dot plot of two independent biological replicates. (*G*) Evaluation of cell proliferation by EdU incorporation assessed by flow cytometry. Dot plots show the percentage of proliferating cells as EdU-Alexa647-positive cells, highlighted in the black box. A representative dot plot of a negative control (without EdU) is shown. Data from one representative assay of two independent biological replicates. (*H*) Migration capacity of parental and KO cells by wound healing migration assays in different coatings. Graphs represent the percentage of closing rate of the wound. Uncoated and poly-D-Lysine data from two independent biological replicates (each n = 6); Collagen IV data from three independent biological replicates (each n = 6), Fibronectin data from six independent biological replicates (each n = 6). Statistical significance was calculated by two-way ANOVA, with error bars representing SD. (*I*) Invasion capacity of parental and KO cells was evaluated by Matrigel invasion assays. Bar graphs show the mean of the percentage of invading cells ± SD. A total of at least n = 6 from four independent experiments is shown. Statistical significance was determined using Student's *t* test with Welch's correction. ns-nonsignificant; *$P \leq 0.05$, **$P < 0.01$, ***$P < 0.001$, ****$P < 0.0001$.

Downloaded from https://www.pnas.org by 92.106.253.224 on June 22, 2023 from IP address 92.106.253.224.

using the CRISPR/Cas9 system. Two independent clones (*SDC4* KO #1 and *SDC4* KO #2) were selected (*SI Appendix*, Fig. S3). We validated the complete abrogation of SDC4 expression at the protein level by WB (Fig. 2*D*) and flow cytometry (Fig. 2*E*). Concerning WB analysis, the hindrance effect of HS chains in antibody binding was discarded by treating the protein extracts with the Heparinase III (Hep.III) enzyme that digests HS chains and confirmed the abrogation of SDC4 (Fig. 2*D*). As a control of Hep.III-digestion efficiency, we evaluated SDC1 expression using the SDC1 B-A38 clone antibody that only binds to the SDC1 core protein upon HS chains removal.

We then evaluated the impact of SDC4 KO in cellular features. We did not find any statistically significant difference either in cellular viability (Fig. 2*F*) or proliferation (Fig. 2*G*). However, we could show that WT gastric cancer cells presented a higher migration rate comparing to *SDC4* KO models in all coatings tested (Fig. 2*H*). Furthermore, we found that the lack of SDC4 expression remarkably decreased the invasion capacity of gastric cancer cells (Fig. 2*I*). The impact of SDC4 in cancer cell invasion was also validated by siRNA strategy in MKN74 and AGS cell models (*SI Appendix*, Fig. S4). It was confirmed that SDC4 was specifically targeted and silenced in more than 75% (*SI Appendix*, Fig. S4).

In order to identify molecular cues underlying the deficient motility of *SDC4* KO cells, we performed a screening of RTK activation status. This analysis showed that the total phosphorylated forms of ephrin type A receptor 4 (EphA4), fibroblast growth factor receptor 3 (FGFR3), and epidermal growth factor receptor (EGFR) were up-regulated in *SDC4* KO cells (*SI Appendix*, Fig. S5 *A* and *B*). However, WB analysis of specific p-Tyr sites in EphA4 (Tyr602) and EGFR (Tyr1068) failed to confirm this increase (*SI Appendix*, Fig. S5*C*). In addition, based on the key role of SDC4 in focal adhesion processes (36–38), we evaluated the effect of *SDC4* KO on the expression of several focal adhesion components. Protein expression levels were evaluated by WB for pFAK (Tyr397)/FAK levels, and total forms of PKCα, paxillin and β1-integrin, in cells cultured in complete (FBS+) or FBS-depleted medium. No major differences were observed regarding FAK activation, PKCα and β1-integrin expression (*SI Appendix*, Fig. S5 *D* and *E*). However, paxillin showed a trend toward lower expression when SDC4 was depleted, which was only significant in one of the KO clones for FBS+ condition (*SI Appendix*, Fig. S5*E*).

Glycosylated SDC4 Is Sorted in EVs and Impacts Their Features. As the evaluated cellular partners of SDC4 did not reveal any major alteration and taking into account the SDCs' role in EV-mediated extracellular communication (19, 22–25), we addressed the impact of *SDC4* KO on gastric cancer cells' EV secretion and biological activity. WB analysis showed that SDC4 was detected in EVs isolated from WT cells (Fig. 3*A*). Ponceau staining (*SI Appendix*, Fig. S6*A*) is shown as a control of sample loading. Remarkably, when SDC4 abundance in the WT EVs was compared with the abundance in the WT cells, there was an enrichment of high MW glycosylated forms, as well as of the monomeric form (17 kDa), while the dimeric conformation was not detected in the EVs (Fig. 3*A*). Gold-immunolabeling methodology validated the presence of SDC4 in WT EVs (Fig. 3*B*). Additionally, MS-based proteomic analysis identified five SDC4 peptides in WT EVs: three located in the ECD, demonstrating that SDC4 ECD is part of EV cargo, and two in the intracellular domain (ICD), one of these in the variable region and the other in the conserved portion (Fig. 3*C* and *SI Appendix*, Table S3). MS analysis further confirmed the enrichment of SDC4 abundance in EVs when compared with cells (*SI Appendix*, Table S3).

Regarding EV size analysis, both WT and *SDC4* KO populations presented size between 50 and 300 nm (Fig. 3 *D* and *E*) with the peak fraction between 70 and 150 nm. Analysis of overall EV abundance, measured by NTA, revealed that the quantity of EVs secreted by *SDC4* KO cells was higher (median 2.4×10^{12} particles/mL) and displayed smaller size (86 nm), when compared to EVs from WT cells (median concentration: 0.7×10^{12} particles/mL and size: 102.1 nm) (Fig. 3 *F* and *G*). These results were confirmed by negative staining analysis by TEM (Fig. 3*H*). Interestingly, the ratio protein/particle was significantly higher in WT EVs compared to *SDC4* KO EVs (Fig. 3*I*). Importantly, WB confirmed the expression of a panel of EV-markers, including Alix, HSP70, syntenin-1, CD9, and CD81 in both WT and *SDC4* KO EVs (Fig. 3*J*). Cytochrome-c and α-tubulin were used as cell lysate controls. Ponceau staining (*SI Appendix*, Fig. S6*B*) is shown as a control of samples loading.

SDC4 KO Leads to a Different Proteomic Profile in the EVs' Cargo. In view of the differences observed between WT and *SDC4* KO EVs, we proceeded to evaluate the protein cargo of the two EV populations (Fig. 4 *A* and *B*). A total of 2,431 proteins were identified by MS analysis of gastric cancer cells-derived EVs. The identified proteins were compared with the ones present in the open EV-database Vesiclepedia (Fig. 4*A*). Of note, 2,289 of the identified proteins were also present in this database, and 142 proteins were identified only in this study (Fig. 4*A*). Next, the comparison of the identified proteins with the top 100 EV proteins reported in Vesiclepedia showed that most of the proteins detected in our study overlap with the top 100 proteins from Vesiclepedia (Fig. 4*B*).

The combined MS analysis of WT and *SDC4* KO EVs and cells identified 4,659 proteins (Fig. 4*C*). The segregation of the different biological conditions was confirmed by the principal component analysis of the MS data (*SI Appendix*, Fig. S7*A*). Gastric cancer cells showed a higher amount of identified proteins (4,189 proteins) when compared with EVs (2,431 proteins). Considering only the cell populations (WT and KO), the Venn diagram revealed that most of the identified proteins were common (1,739 proteins, 37.3%) (Fig. 4*C*). Moreover, we observed that 26.3% of the proteins overlapped in all populations examined (cells and EVs) (Fig. 4*C*). Noteworthy, EV-markers (Alix, syntenin-1, CD9 and CD81), that were previously identified by WB (Fig. 3*J*), were present in this group of overlapping proteins (Fig. 4*C* and *SI Appendix*, Table S4). Syntenin-1 abundance was higher in WT cells comparing with KO. Both Syntenin-1 and Alix were highly enriched in the EV populations (*SI Appendix*, Table S4).

Interestingly, *SDC4* KO population (cells and EVs) presented a higher amount of unique identified proteins (4,318 proteins), compared to the WT population (4,133 proteins).

In addition to SDC4, the cancer-associated molecules transforming growth factor beta-1 protein (TGFβ1) and growth arrest-specific protein 6 (GAS6) were exclusively present in the cargo of EVs secreted from WT cells (Fig. 4*C*). This observation was validated in two independent EV preparations. Furthermore, volcano plots (Fig. 4 *D* and *E*), highlighting the significantly different protein content of each population, show that *SDC4* KO significantly changed the proteome of both cells and secreted EVs. The EV proteomic data demonstrated that SDC1 abundance is higher in KO EVs. Interestingly, this effect is specific of EV cargo and not observed in the parental cell lines (*SI Appendix*, Table S4). Network analysis for GO biological process terms for SDC4-exclusive proteins in WT EVs showed an enrichment in several relevant categories, including *protein phosphorylation, cell migration, and axon guidance* (Fig. 4*F*). In contrast, the exclusive proteome of KO EVs displayed enriched

Downloaded from https://www.pnas.org by 92.106.253.224 on June 22, 2023 from IP address 92.106.253.224.

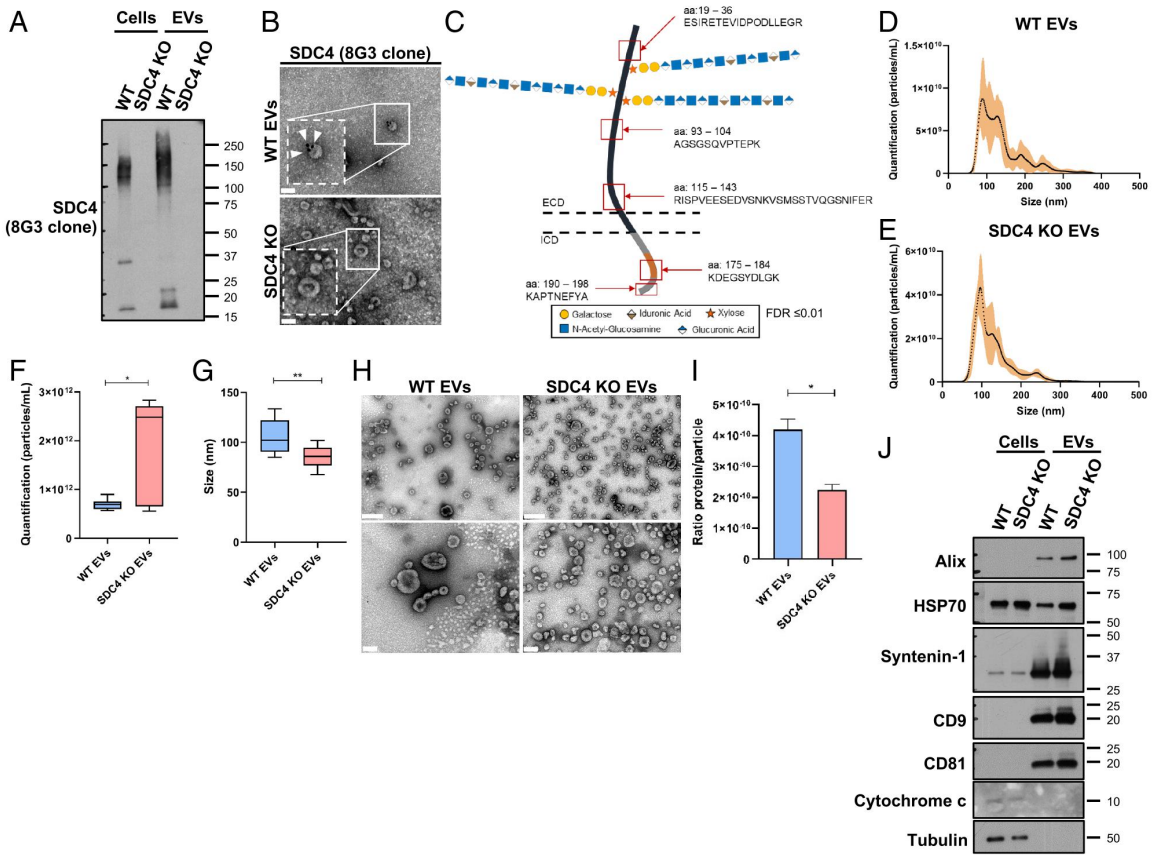


Fig. 3. SDC4 is carried by gastric cancer cell EVs and affects EV secretion and size. (*A*) WB of SDC4 (8G3) in WT and KO cells and EVs. (*B*) Gold-immunolabeling of SDC4 (8G3) in EVs isolated from WT and KO cells. Scale bar corresponds to 100 nm and white arrowheads point the labeling. (*C*) Schematic representation of SDC4 showing the sequenced peptides (red squares) in ECD and ICD (variable region in orange and conserved region in grey) by mass spectrometry (MS) analysis. (*D* and *E*) Concentration and size distribution analysis using NTA of EVs isolated from (*D*) WT and (*E*) KO cells. (*F* and *G*) Quantification of the (*F*) concentration and (*G*) size of the WT and KO EVs. Bar graphs show the median of the concentration and the median of the size of EVs ± SD. Data from two independent biological replicates. (*H*) Representative images of negative staining in TEM of the WT and KO EVs. On the *Top* panel, the scale bar corresponds to 200 nm and below to 100 nm. (*I*) Bar graphs show the average of the ratio protein per particle ± SD. Data from two independent biological replicates. (*J*) WB analysis of EV-markers [Programmed cell death 6-interacting protein (Alix), Heat shock 70 (HSP70), syntenin-1, CD9 antigen (CD9), CD81 antigen (CD81)] using WT and KO, cells and EVs. Cytochrome c was used as control for EV fraction isolation and α-tubulin as loading control. Statistical significance was assessed using Student's *t* test with Welch's correction. $*P \leq 0.05$, $**P < 0.01$.

signal transduction, apoptotic process, and cell–cell adhesion biological processes (Fig. 4*F*). Analysis of GO molecular function revealed enrichment in categories such as *calcium ion binding* on WT and *ubiquitin protein ligase binding* in KO EVs (*SI Appendix*, Fig. S7*B*). Protein–protein interaction analysis revealed a high degree of connectivity between of SDC4, TGFβ1, and GAS6 in WT EVs (Fig. 4*G*). Analysis of KO EVs interconnected several proteins involved in the Wnt pathway, such as Frizzled (FZD) receptors and E3 Ubiquitin-Protein Ligase (ZNRF3) (*SI Appendix*, Fig. S7*C*). In addition, we evaluated whether the exclusive proteomic signature of WT and KO EVs would associate with patient clinical prognosis. Remarkably, the WT EV signature significantly associated with patient poor OS and DFS, based on the STAD-TCGA database (Fig. 4 *H* and *I*).

SDC4 in EVs Is Critical for EV Uptake and Functional Effects on Recipient Cells. Since EVs are crucial regulators of intercellular communication, we next sought to investigate the impact of SDC4 on EV uptake and functional signaling on recipient cells. We evaluated WT and *SDC4* KO EVs uptake by two macrophage cell lines (RAW and Kupffer) and MKN74 gastric cancer cells. The results showed a significant decrease in the uptake of *SDC4* KO EVs by all recipient cells, as illustrated in Fig. 5 (Fig. 5 *A*–*C*). Moreover, treatment of the WT EVs with Hep. III resulted in more than 70% uptake inhibition (Fig. 5*C*). EV uptake was reduced by 17% when performed in the presence of heparin and by 72% when EVs where preincubated with an HS-blocking antibody (Fig. 5*C*). The efficient Hep. III digestion of HS chains in EVs was confirmed by HS detection in WB (*SI Appendix*, Fig. S8).

To further assess whether EV internalization would modulate cancer cells' malignant features, we treated the WT and *SDC4* KO gastric cancer cells with both WT and *SDC4* KO EVs and evaluated cell invasion (Fig. 5*D*). Remarkably, when *SDC4* KO cells were treated with WT EVs, their invasion capacity was restored to values similar to the WT. On the other hand, when KO cells were treated with KO EVs, the invasion capacity was not affected (Fig. 5*D*). Comparative analysis of the cellular proteome of KO cells treated with WT EVs with the KO cells (without EV treatment) revealed that SDC4 was present in the EV-treated cell population (Fig. 5*E*).

The Gastric Cancer Cell EV Tropism to the Liver and Lung Is Disrupted by SDC4 KO. Following the in vitro functional

Downloaded from https://www.pnas.org by 92.106.253.224 on June 22, 2023 from IP address 92.106.253.224.

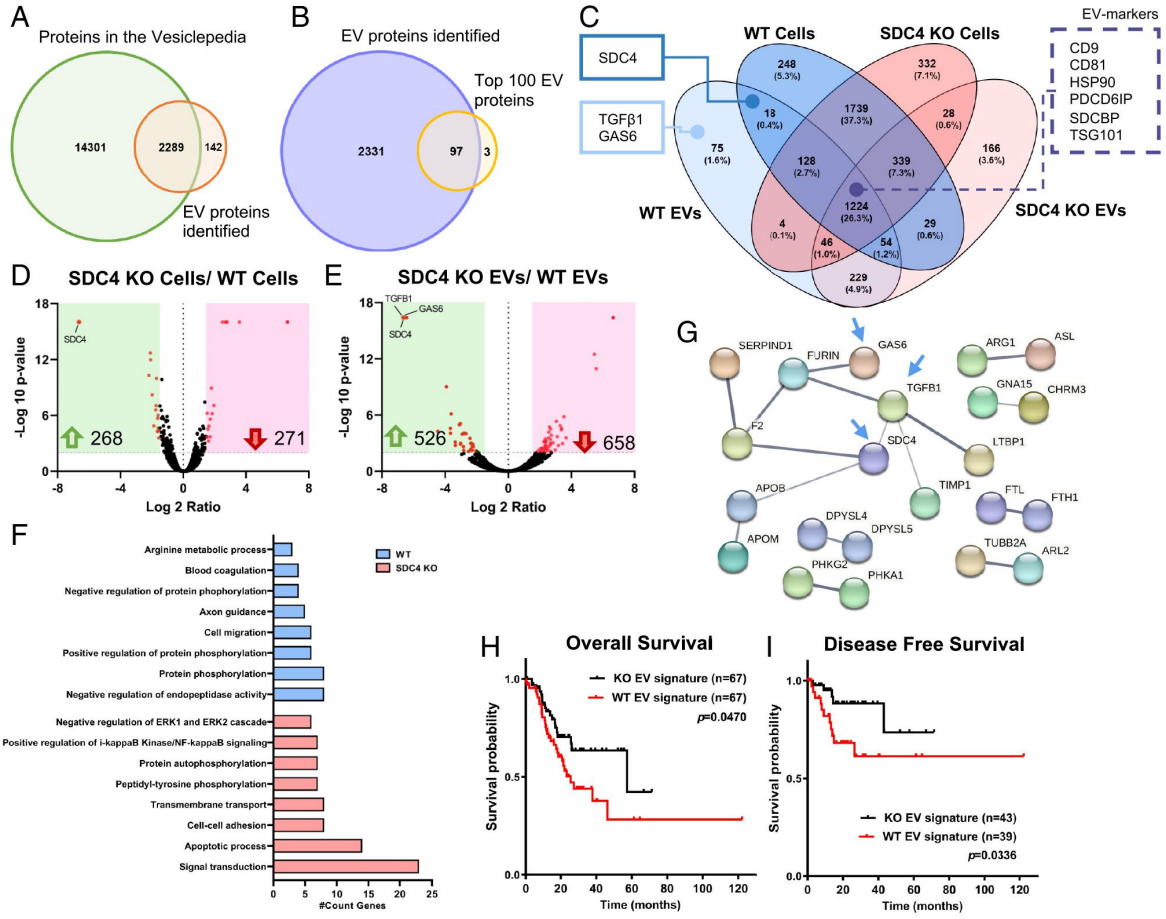


Fig. 4. SDC4 impacts EVs proteomic signature. Protein identification was evaluated by LC-MS/MS proteomic analysis. (*A*) Venn diagram displays the number of unique and overlapping proteins identified in this study for WT and KO EVs, comparing to all proteins deposited in the Vesiclepedia database (1). (*B*) Venn diagram shows comparative analysis between the EV proteins detected in this study and the Top100 EV proteins described in the Vesiclepedia. (*C*) Venn diagram illustrates the number (and percentage) of the unique and overlapping proteins from WT and KO cell and EV populations. Two key cancer-related proteins and SDC4 are highlighted in full line box, as well, EV-markers are highlighted in dashed line box. (*D* and *E*) Volcano plot analysis displaying differentially expressed proteins (red dots) when comparing the protein cargo of (*D*) KO vs. WT cells and (*E*) KO vs. WT EVs. Each protein is represented as a dot and is mapped according to its fold change on the *x* axis, and the *P*-value on the *y* axis. Red dots indicate proteins exhibiting significantly altered expression [−Log10 (*p*-value) > 2 and Log 2 ratio < −1.5 or >1.5], and black dots indicate proteins whose expression did not vary significantly. The number of proteins up-regulated (green arrow) and down-regulated (red arrow) are highlighted. (*F*) Functionally grouped network of gene ontology (GO) biological process terms for the exclusive proteome in WT and KO EVs (Benjamini $P < 0.01$). (*G*) Protein–protein interaction for the SDC4-specific proteome in WT EVs. Blue arrows point to SDC4, GAS6 and TGFβ1. (*H* and *I*) In silico analysis of the prognostic value of WT and KO EV signatures. Analysis of (*H*) OS and (*I*) DFS was assessed using the STAD-TCGA database. **Reference:** 1. Kalra H, Simpson RJ, Ji H, Aikawa E, Altevogt P, Askenase P, et al. Vesiclepedia: A Compendium for Extracellular Vesicles with Continuous Community Annotation. PLOS Biology. 2012;10(12):e1001450.

characterization, we tested whether the presence of SDC4 in EVs influences their organ distribution in NOD SCID mice (Fig. 6*A*). First, we confirmed that WT and KO EVs were equally labeled with the near-infrared fluorescent dye NIR815 (*SI Appendix*, Fig. S9*A*). Organ NIR fluorescence analysis revealed that the three organs with higher intensity signal upon EV treatment were the liver, spleen, and lung (Fig. 6 *B–E* and *SI Appendix*, Fig. S9 *B–E*). Among these, the liver was the organ that presented the highest intensity, followed by the spleen (Fig. 6 *B–D*). The comparative analysis of WT and KO EVs showed a significantly lower uptake of KO EVs in the liver (Fig. 6 *B* and *C*), spleen (Fig. 6 *B* and *D*), and lung (Fig. 6 *B* and *E*), while no differences were observed between both EV populations when analyzing brain, bone, kidney, and pancreas (*SI Appendix*, Fig. S9 *B–E*). Flow cytometry analysis further confirmed the lower uptake of KO EVs by the liver cells (Fig. 6*F* and *SI Appendix*, Fig. S10*A*), and a tendency for decreased uptake of KO EVs was observed in spleen and lung (*SI Appendix*, Fig. S11 *A–C*). The use of complementary labeling and gating strategies (*SI Appendix*, Fig. S10*B*) showed that a decreased uptake of KO EVs was occurring specifically by the liver Kupffer macrophages (CD45+, CD11b+, F4/80+ /Tim4+) (Fig. 6*G*). No significant differences were noticed on EV uptake by Tim4- macrophages (CD45+, CD11b+, F4/80+) in the bone marrow, spleen, and lung (*SI Appendix*, Fig. S12).

Discussion

In the present era of precision oncology, glycans and glycoconjugates are emerging as major players in cancer initiation and progression with strong potential both as biomarkers and as therapeutic targets (4, 5, 7, 12). In this study, we reveal that the HS proteoglycan SDC4 is highly expressed in intestinal subtype

Downloaded from https://www.pnas.org by 92.106.253.224 on June 22, 2023 from IP address 92.106.253.224.

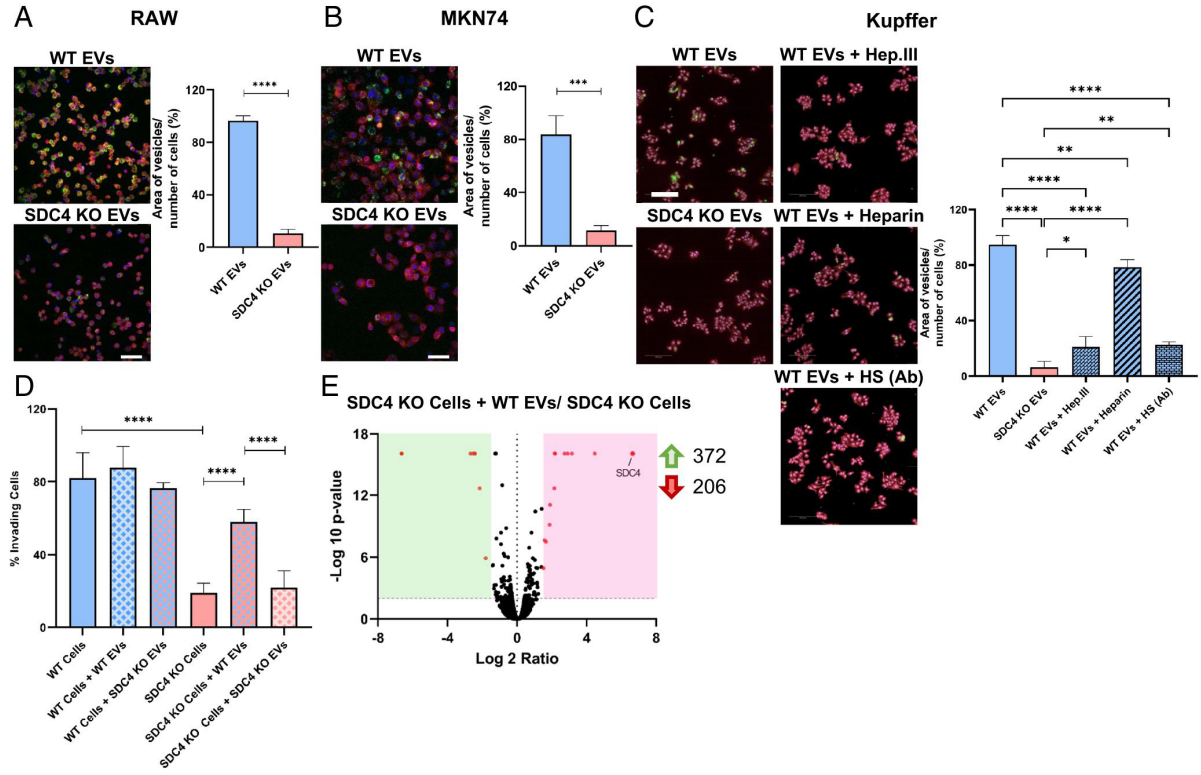


Fig. 5. EVs depend on SDC4 for their internalization and functional activity. (*A* and *B*) WT and KO EV uptake was evaluated in (*A*) RAW and (*B*) MKN74. (*C*) EV uptake on Kupffer cells was evaluated including WT and KO EVs, WT EVs pretreated with Heparinase III (WT EVs + Hep. III), EVs blocked with heparan sulfate (HS)-antibody (WT EVs + HS Ab), and coincubation with WT EVs and heparin (WT EVs + Heparin). EVs were labeled with PKH67 (green), cells with HCS CellMask (red) and nuclei with Hoechst (blue). Bar graphs show the average of EV area per number of cells (%) ± SD. A representative image of each condition is shown. Data from 3 (RAW), 1 (MKN74) and 2 (Kupffer) independent biological replicates (each n = 2 and 25 field captures). (Scale bar corresponds to 20 μm). (*D*) Invasion assay of WT and KO cells upon treatment with WT and KO EVs. Bar graphs show the mean of the invading cells percentage ± SD. Data from at least two independent biological replicates (each n = 3). (*E*) Volcano plot displaying the differentially expressed proteins (red dots) when comparing the protein cargo of KO cells treated with WT EVs vs. KO cells without treatment. Statistical significance was assessed using Student's *t* test for two conditions or one-way ANOVA when comparing more than two conditions. **P* ≤ 0.05, ***P* < 0.01, ****P* < 0.001, *****P* < 0.0001.

gastric tumors and that this glycosylation profile correlates with cancer aggressiveness features and poorer prognosis. We addressed SDC4 functional implications in gastric cancer cell biology and demonstrated that SDC4 promotes a promigratory phenotype with higher invasion capacity, which was abrogated by *SDC4* KO. Interestingly, we further demonstrate that glycosylated SDC4 is sorted in EVs secreted by gastric cancer cells and showed that *SDC4* KO impacted EV secretion and proteomic profile. Moreover, our results disclose that *SDC4* KO impacts EV uptake by recipient cells and disrupts the tropism of gastric cancer cell-derived EVs.

The aberrant expression of HS proteoglycans has been described in different tumor models (12). In particular, SDC4 was previously shown to be up-regulated in glioma, melanoma, osteosarcoma, papillary thyroid carcinoma, breast, liver, kidney, and bladder carcinomas (27–34). In our series of gastric cancer patients, we demonstrate that SDC4 protein expression is associated with intestinal subtype and patient poor OS. Of note, we observed a significant worse OS in male patients with SDC4 expression, which was not observed in women. This observation aligns with previous reports on hormonal regulation of HSPGs during cancer progression (39). Among patients presenting metastatic disease, SDC4 expression was not associated with OS, yet it should be noticed that the number of individuals in this category, in the IPO-Porto cohort, is relatively small. Moreover, in STAD-TCGA dataset, *SDC4* high-transcript levels clustered with metastasis and disease recurrence. When considering the stratification of patients by treatment regiment, SDC4 expression only associated with poor OS in the subgroup that exclusively received surgical treatment. Multivariate analysis demonstrated the independent prognostic value of SDC4 expression in intestinal subtype gastric cancer.

In breast and liver carcinoma cells, SDC4 has been associated with higher migration and invasion (40, 41). In line with these observations, *SDC4* KO has been shown to result in decreased invasion capacity of glioblastoma cells (42). Moreover, shedding of the *N*-terminal portion of the ectodomain of SDC4 by members of the ADAMTS protease family was shown to enhance the migration of cancer cells (43). In this work, we show that *SDC4* has a role in intestinal subtype gastric cancer cell migration and invasion, independently of the presence of different matrix components. Noteworthy, it was possible to restore the invasive capacity of *SDC4* KO cells by coculturing them with EVs secreted by WT cells with proinvasive phenotype. MS analysis of KO cells with restored invasion capacity demonstrated de novo incorporation of SDC4, further supporting the important role of EVs cargo in the SDC4-associated malignant phenotype.

Several seminal studies have comprehensively addressed the EV cargo, including nucleic acids, proteins, lipids, and metabolites (44–46). However, the glycans and glycoconjugates carried

Downloaded from https://www.pnas.org by 92.106.253.224 on June 22, 2023 from IP address 92.106.253.224.

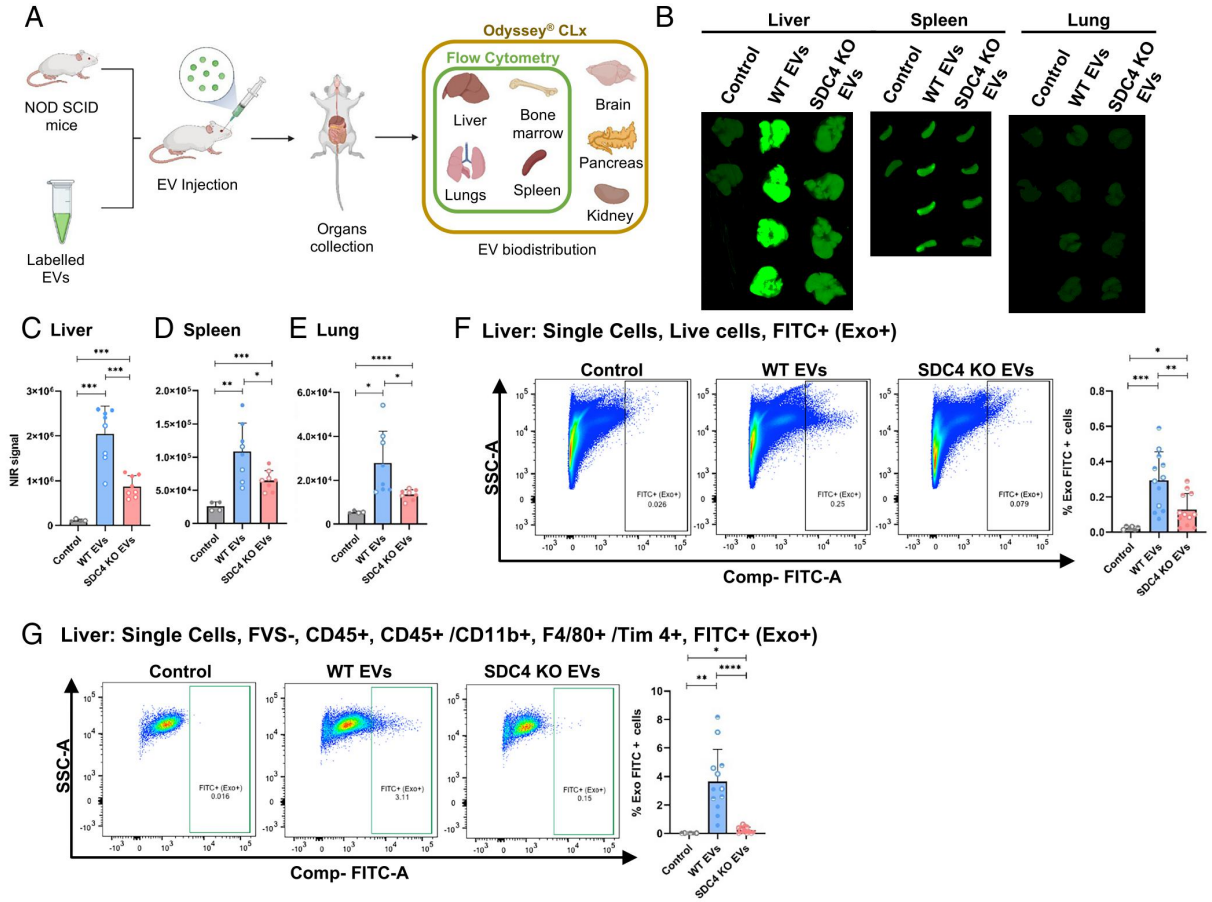


Fig. 6. SDC4 impacts EVs organ distribution. (*A*) Schematic representation of the experimental design. (*B*) EV organ distribution in NOD SCID mice by measurement of NIR fluorescence. Quantification of NIR signaling in (*C*) liver, (*D*) spleen and (*E*) lung. Bar graphs represent the average of fluorescence quantification ± SD. Data from two independent biological replicates for WT and KO EVs (each n = 4, per condition group), and for control (n = 2). (*F* and *G*) FACS analysis of liver cells collected from mice injected with PKH67-labeled WT and KO EVs: (*F*) all live FITC+ (Exo+) cells and (*G*) all CD45+/CD11b+, F4/80+ Tim4+, FITC+ (Exo+) cells. Bar graphs represent the average of the percentage of cells that incorporated EVs. Data from three independent biological replicates for WT and KO EVs (each n = 4, per condition group), and for control (each n = 2). Statistical significance was assessed using Student's *t* test. **P* ≤ 0.05; ***P* < 0.01; ****P* < 0.001; *****P* < 0.0001.

by EVs remain poorly characterized. Of note, HS-rich proteoglycans, namely SDCs, together with syntenin and Alix have been shown to play important roles in EV biogenesis (19, 24, 47). Furthermore, heparanase, the enzyme responsible for HS remodeling, can stimulate intraluminal budding of SDC–syntenin–Alix complex promoting EV secretion (23, 48, 49). Our data revealed an enrichment of highly glycosylated SDC4 forms in EVs when compared to the parental cells. Specifically, MS analysis identified three peptides, corresponding to the ECD of SDC4, that were exclusively sequenced in EVs. Of notice, *SDC4* KO impacted EV biogenesis with KO cells producing higher amounts of vesicles with smaller size and decreased protein/particle ratio. *SDC4* KO EVs presented higher SDC1 levels, supporting a compensatory effect for the lack of SDC4. The HSPG SDC1 has been previously reported to control the biogenesis of intraluminal vesicles and exosomes (EVs) (19).

Interestingly, proteomic analysis revealed that TGFβ1 and GAS6 were exclusively identified on WT EVs. In addition, network analysis of SDC4-exclusive proteins in WT EVs, clustered together SDC4, GAS6, and TGFβ1, showing an enrichment in biological processes involved in *protein phosphorylation, cell migration, and axon guidance*. This proteomic signature is associated with the proinvasive phenotype induced by these EVs. TGFβ1 is a key regulator of migration, invasion, and epithelial–mesenchymal transition in gastric carcinogenesis (50, 51) and GAS6 was described as involved in the recruitment and polarization of macrophages (52, 53), therefore supporting EV contribution for cancer cell invasion and tumor progression. Protein network analysis of the KO EV proteome revealed several proteins of the Wnt pathway, including ZNRF3 that acts as a negative feedback regulator of Wnt signaling (54), therefore, corroborating the less aggressive phenotype of KO EVs. In line with these observations, the SDC4-specific signature of WT EVs was significantly associated with gastric cancer patient poor overall and DFS.

The functional effects of EVs are dependent on an efficient uptake by recipient cells, and the different pattern of surface components on EVs, e.g., integrins, cytokines, and glycoconjugates, has been shown to dictate EV uptake (21, 55, 56). Furthermore, from the recipient cell side HSPGs have been described as regulators of EV internalization and functional activity (57). The glycosaminoglycan chains that decorate HSPGs, particularly the 2-*O*- and *N*-sulfation domains, were demonstrated to be key for exosome uptake (25). Additionally, it was shown that enzymatic treatment with heparanase, that

Downloaded from https://www.pnas.org by 92.106.253.224 on June 22, 2023 from IP address 92.106.253.224.

trims HS chains, and xylosides, which hinder HS biosynthesis, also resulted in EV uptake inhibition (25). Here, we provide evidence that SDC4 plays a crucial role on EV uptake, as KO of this specific proteoglycan impacts the EV cellular internalization and organ distribution. Our data further support that HS glycosaminoglycans in EVs are mechanistically involved in the EV internalization process, since enzymatic digestion of EV HS-chains or EV blocking with HS-antibody significantly impaired EV uptake. However, we cannot exclude the possibility of SDC4-independent alternative uptake pathways since *SDC4* KO did not completely abolished EV uptake. Interestingly, we observed a significant decrease in *SDC4* KO EV uptake by the liver, lung and spleen, which are common metastatic sites of gastric primary tumor (58). These results highlight the specific tropism of the gastric cancer EVs to these organs. Furthermore, our data provide evidence that Kupffer cells are major players in gastric cancer-derived EV uptake in the liver. The uptake of gastric cancer-derived EVs by macrophages, with consequences on macrophage differentiation and tumor dissemination, has been previously reported (59). Moreover, Kupffer cells have been demonstrated as a key cell subpopulation in the uptake of pancreatic cancer exosomes, having a functional contribution for the establishment of a liver premetastatic niche (60, 61).

The understanding of the functional implications of proteoglycans glycosylation in EV cellular recognition and uptake holds great potential for the therapeutic inhibition of EV-mediated tumor progression (62). This knowledge is particularly relevant in gastric cancer where the identification of molecular targets to design personalized therapeutic strategies is of utmost need. Moreover, proteoglycans carried by EVs have been already recognized as biomarkers for minimally invasive cancer diagnosis: Glypican-1 in pancreatic cancer (63) and SDC1 in glioma (62). Therefore, the identification of SDC4 in gastric cancer cell-derived EVs holds biomarker potential.

The role of SDC4 in the definition of EV tropism to common metastatic sites of gastric cancer is of utmost relevance within the emerging concept that EVs prime a premetastatic niche. This knowledge prompts future research on the impact of glycosylated-SDC4 in EVs for gastric cancer dissemination. However, the current challenge is the lack of good experimental models that mimic the human gastric cancer metastasis features. Therefore, the foreseeable study of EV education using gastric cancer orthotopic patient-derived xenograft models has particular pertinence. Moreover, it would be important to decipher the TGFβ1, GAS6, and SDC4 molecular interplay and the role of these partners in EV-mediated immune regulation, namely on macrophage polarization, within the tumor microenvironment.

Collectively, our findings reveal a previously unappreciated role of SDC4 in determining gastric cancer cell aggressiveness with implications in patient clinical outcome and further uncover the potential of this HSPG as a therapeutic target. Furthermore, our data contribute to decipher the glycan code of cancer-derived EVs and for the identification of key molecular cues that determine gastric cancer communication routes.

Materials and Methods

Detailed description of reagents, immunohistochemistry, in silico analyses, cell culture, CRISPR/Cas9 KO methodology, qPCR, western blot, flow cytometry, immunofluorescence, enzymatic digestion, viability and proliferation assays, RTK phosphorylation analysis, EV isolation, NTA, EV protein quantification, TEM, gold-immunolabeling microscopy, LC-MS/MS analysis, EV uptake, and biodistribution experiments are provided in *SI Appendix*.

Ethic Statements. All procedures concerning the inclusion of patients were approved by the institutional Ethics Committee (Comissão de ética para a saúde–CES-IPOFG-EPE 87/2017) after patients' informed consent. Additional details regarding this cohort are provided in *SI Appendix, Materials and Methods*.

All animal procedures were conducted in accordance with National Animal Experimentation Guidelines (DGAV) on the use and care of experimental animals, and approved by the Champalimaud Foundation Ethics Committee (0421/000/000/2018).

In Silico Analysis of SDC4 Expression and Prognostic Impact. *SDC4* transcript levels were investigated in STAD-TCGA and the KM plotter database (64), as described in *SI Appendix, Materials and Methods*.

SDC4 KO by CRISPR/Cas9. The *SDC4* KO was performed in MKN74 cell line using CRISPR/Cas9 genome editing and validated, as previously described (65, 66). Additional information is provided in *SI Appendix, Materials and Methods*.

Isolation of EVs. The EV isolation and characterization were performed according to the International Society for Extracellular Vesicles (ISEV) (67) guidelines and are described in *SI Appendix, Materials and Methods*.

Statistical Analysis. Prism software (GraphPad, v8.0) and IBM® SPSS® Statistics v.22 were used for statistical analysis, as detailed in *SI Appendix, Materials and Methods*.

Data, Materials, and Software Availability. All relevant data from EV experiments were submitted to the EV-TRACK knowledgebase (EV-TRACK ID: EV210302) (68). The MS-based proteomic data have been deposited to the ProteomeXchange Consortium via the PRIDE (69) partner repository with the dataset identifier PXD035679 and 10.6019/PXD035679 (70). All study data are included in the article and/or *SI Appendix*.

ACKNOWLEDGMENTS. We thank all patients and clinicians for their participation in this study. we would like to acknowledge Guido David for providing the 8G3 antibody, Henrik Clausen for providing GFP-Cas9 and David Lyden for the RAW and Kupffer cells. We would like to thank Henrique O. Duarte for manuscript proof reading. We acknowledge the support of the i3S Scientific Platforms: Proteomics, Bioinformatics, Translation Cytometry, Advanced Light Microscopy, BioSciences Screening, Bioimaging, and Histology and Electron Microscopy, members of the PPBI (PPBI-POCI-01-0145-FEDER-022122). This work was funded by FEDER funds through the Operational Programme for Competitiveness Factors-COMPETE (POCI-01-0145-FEDER-028489; POCI-01-0145-FEDER-029780) and National funds through the Foundation for Science and Technology (FCT), under the projects PTDC/MED-ONC/28489/2017 (to A.M.); PTDC/MED-QUI/29780/2017 and PTDC/MED-QUI/2335/2021 (C.G.), EXPL/BTM-ORG/1450/2021 (F.P.) and PTDC/MEDOUT/2512/2021 (J.A.F.); and the project Norte-01-0145-FEDER-000051-"Cancer Research on Therapy Resistance: From Basic Mechanisms to Novel Targets," and "P.CCC.: Porto Comprehensive Cancer Center Raquel Seruca" - NORTE-01-0145-FEDER-072678 both supported by NORTE 2020, under the PORTUGAL 2020 Partnership Agreement, through the European Regional Development Fund; and COST Action CA18103 INNOGLY: INNOvation with Glycans: new frontiers from synthesis to new biological targets. This work was also financed by the Portuguese Mass Spectrometry Network, integrated in the National Roadmap of Research Infrastructures of Strategic Relevance (ROTEIRO/0028/2013; LISBOA-01-0145-FEDER-022125). J.P. and C.M. acknowledge FCT PhD scholarships SFRH/BD/137319/2018 and 2020.06412.BD, respectively. F.P. acknowledges the SFRH/BPD/115730/2016 FCT fellowship. A.H.O. acknowledges the FAPESP 19/00740-0 fellowship. B.C. is supported by a JUNIOR_RESEARCHER/CEEC_INST21/IBMC/2802/2022. J.A.F. acknowledges FCT position CEECIND/03186/2017.

Author affiliations: [a]I3S - Instituto de Investigação e Inovação em Saúde, Universidade do Porto, Porto 4200-135, Portugal; [b]IPATIMUP - Instituto de Patologia e Imunologia Molecular da Universidade do Porto, Porto 4200-465, Portugal; [c]ICBAS - Instituto de Ciências Biomédicas Abel Salazar, Universidade do Porto, Porto 4050-313, Portugal; [d]Champalimaud Physiology and Cancer Programme, Champalimaud Foundation, Lisbon 1400-038, Portugal; [e]Experimental Pathology and Therapeutics Group, Research Center of IPO Porto (CI-IPOP)/RISE@CI-IPOP (Health Research Network), Portuguese Oncology

Downloaded from https://www.pnas.org by 92.106.253.224 on June 22, 2023 from IP address 92.106.253.224.

Institute of Porto (IPO Porto), 4200-072 Porto, Portugal; [f]FMUP - Faculdade de Medicina da Universidade do Porto, Porto 4200-319, Portugal; [g]Department of Clinical Sciences, Section of Oncology, Lund University, 221 84 Lund, Sweden; [h]Department of Immunology, Genetics and Pathology, Science for Life Laboratory, Uppsala University, 751 85 Uppsala, Sweden; and [i]Skåne University Hospital, 221 85 Lund, Sweden

Author contributions: J.P., B.C.-S., and A.M. designed research; J.P., C.M., C.G., A.H.O., F.P., M.F., T.S., I.F.-R., R.M., A.R.R., E.S., S.B., J.M., J.A.M., L.P.A., A.P., and H.O. performed research; F.P. and B.C. performed bioinformatic analysis; C.G., C.A.R., B.C.-S., and A.M. contributed new reagents/analytic tools; J.P., A.R.R., E.S., B.C., L.L., J.A.F., L.L.S., A.P., H.O., M.B., C.A.R., B.C.-S., and A.M. analyzed data; and J.P. and A.M. wrote the paper.

Competing interest statement: J.P., C.M., C.G., C.A.R., and A.M. have submitted a provisional patent application (reference: 20221000003006) related to the exploitation of SDC4 as a biomarker of poor survival and organ tropism. The remaining authors declare no competing interests.

1. H. Sung *et al.*, Global cancer statistics 2020: GLOBOCAN estimates of incidence and mortality worldwide for 36 cancers in 185 countries. *CA Cancer J. Clin.* **71**, 209–249 (2021).
2. H. O. Duarte, J. Gomes, J. C. Machado, C. A. Reis, Gastric cancer: Basic aspects. *Helicobacter* **23**, e12523 (2018).
3. E. Van Cutsem, X. Sagaert, B. Topal, K. Haustermans, H. Prenen, Gastric cancer. *Lancet* **388**, 2654–2664 (2016).
4. S. Mereiter, M. Balmaña, D. Campos, J. Gomes, C. A. Reis, Glycosylation in the era of cancer-targeted therapy: Where are we heading? *Cancer Cell* **36**, 6–16 (2019).
5. S. S. Pinho, C. A. Reis, Glycosylation in cancer: Mechanisms and clinical implications. *Nat. Rev. Cancer* **15**, 540–555 (2015).
6. A. Magalhães, H. O. Duarte, C. A. Reis, The role of O-glycosylation in human disease. *Mol. Aspects Med.* **79**, 100964 (2021).
7. J. A. Ferreira *et al.*, Protein glycosylation in gastric and colorectal cancers: Toward cancer detection and targeted therapeutics. *Cancer Lett.* **387**, 32–45 (2017).
8. C. Gomes *et al.*, Expression of ST3GAL4 leads to SLe(x) expression and induces c-Met activation and an invasive phenotype in gastric carcinoma cells. *PLoS One* **8**, e66737 (2013).
9. D. Freitas *et al.*, O-glycans truncation modulates gastric cancer cell signaling and transcription leading to a more aggressive phenotype. *EBioMedicine* **40**, 349–362 (2019).
10. J. R. Couchman, H. Multhaupt, R. D. Sanderson, Recent insights into cell surface heparan sulphate proteoglycans and cancer. *F1000 Res.* **5,** 1541 (2016).
11. I. Faria-Ramos *et al.*, Heparan sulfate glycosaminoglycans: (Un)expected allies in cancer clinical management. *Biomolecules* **11**, 136 (2021).
12. S. Bratulic *et al.*, Noninvasive detection of any-stage cancer using free glycosaminoglycans. *Proc. Natl. Acad. Sci. U.S.A.* **119**, e2115328119 (2022).
13. S. Gopal *et al.*, Heparan sulfate chain valency controls syndecan-4 function in cell adhesion. *J. Biol. Chem.* **285**, 14247–14258 (2010).
14. M. D. Bass *et al.*, Syndecan-4-dependent Rac1 regulation determines directional migration in response to the extracellular matrix. *J. Cell Biol.* **177**, 527–538 (2007).
15. F. Echtermeyer *et al.*, Delayed wound repair and impaired angiogenesis in mice lacking syndecan-4. *J. Clin. Invest.* **107**, R9–R14 (2001).
16. R. L. Longley *et al.*, Control of morphology, cytoskeleton and migration by syndecan-4. *J. Cell Sci.* **112**, 3421–3431 (1999).
17. A. Magalhaes *et al.*, Helicobacter pylori cag pathogenicity island-positive strains induce syndecan-4 expression in gastric epithelial cells. *FEMS Immunol. Med. Microbiol.* **56**, 223–232 (2009).
18. N. T. Marcos *et al.*, Helicobacter pylori induces β3GnT5 in human gastric cell lines, modulating expression of the SabA ligand sialyl–Lewis x. *The J. Clin. Invest.* **118**, 2325–2336 (2008).
19. M. F. Baietti *et al.*, Syndecan–syntenin–ALIX regulates the biogenesis of exosomes. *Nat. Cell Biol.* **14**, 677–685 (2012).
20. M. Mathieu, L. Martin-Jaular, G. Lavieu, C. Théry, Specificities of secretion and uptake of exosomes and other extracellular vesicles for cell-to-cell communication. *Nat. Cell Biol.* **21**, 9–17 (2019).
21. H. Peinado *et al.*, Pre-metastatic niches: Organ-specific homes for metastases. *Nat. Rev. Cancer* **17**, 302–317 (2017).
22. V. Friand, G. David, P. Zimmermann, Syntenin and syndecan in the biogenesis of exosomes. *Biol. Cell* **107**, 331–341 (2015).
23. B. Roucourt, S. Meeussen, J. Bao, P. Zimmermann, G. David, Heparanase activates the syndecan-syntenin-ALIX exosome pathway. *Cell Res.* **25**, 412–428 (2015).
24. R. Ghossoub *et al.*, Tetraspanin-6 negatively regulates exosome production. *Proc. Natl. Acad. Sci. U.S.A.* **117**, 5913 (2020).
25. H. C. Christianson, K. J. Svensson, T. H. van Kuppevelt, J.-P. Li, M. Belting, Cancer cell exosomes depend on cell-surface heparan sulfate proteoglycans for their internalization and functional activity. *Proc. Natl. Acad. Sci. U.S.A.* **110**, 17380 (2013).
26. J. O. S. Onyeisi, C. C. Lopes, M. Götte, Syndecan-4 as a pathogenesis factor and therapeutic target in cancer. *Biomolecules* **11**, 503 (2021).
27. A. Watanabe *et al.*, Expression of syndecans, a heparan sulfate proteoglycan, in malignant gliomas: Participation of nuclear factor-κB in upregulation of syndecan-1 expression. *J. Neuro. Oncol.* **77**, 25–32 (2006).
28. F. Baba *et al.*, Syndecan-1 and syndecan-4 are overexpressed in an estrogen receptor-negative, highly proliferative breast carcinoma subtype. *Breast Cancer Res. Treat.* **98**, 91–98 (2006).
29. T. Roskams, R. De Vos, G. David, B. Van Damme, V. Desmet, Heparan sulphate proteoglycan expression in human primary liver tumours. *J. Pathol.* **185**, 290–297 (1998).
30. M. P. O'Connell *et al.*, Heparan sulfate proteoglycan modulation of Wnt5A signal transduction in metastatic melanoma cells. *J. Biol. Chem.* **284**, 28704–28712 (2009).
31. K. Y. Na, P. Bacchini, F. Bertoni, Y. W. Kim, Y. K. Park, Syndecan-4 and fibronectin in osteosarcoma. *Pathology* **44**, 325–330 (2012).
32. M. Erdem *et al.*, Up-regulation of TGM2 with ITGB1 and SDC4 is important in the development and metastasis of renal cell carcinoma. *Urol. Oncol.* **32**, e13-20 (2014).
33. L. L. Chen *et al.*, SDC4 gene silencing favors human papillary thyroid carcinoma cell apoptosis and inhibits epithelial mesenchymal transition via Wnt/β-catenin pathway. *Mol. Cells* **41**, 853–867 (2018).
34. D. Marzioni *et al.*, Expression of basic fibroblast growth factor, its receptors and syndecans in bladder cancer. *Int. J. Immunopathol. Pharmacol.* **22**, 627–638 (2009).
35. G. David, B. van der Schueren, P. Marynen, J. J. Cassiman, H. van den Berghe, Molecular cloning of amphiglycan, a novel integral membrane heparan sulfate proteoglycan expressed by epithelial and fibroblastic cells. *J. Cell Biol.* **118**, 961–969 (1992).
36. S. Gopal, H. A. B. Multhaupt, R. Pocock, J. R. Couchman, Cell-extracellular matrix and cell-cell adhesion are linked by syndecan-4. *Matrix Biol.* **60–61**, 57–69 (2017).
37. H. C. Lim, H. A. Multhaupt, J. R. Couchman, Cell surface heparan sulfate proteoglycans control adhesion and invasion of breast carcinoma cells. *Mol. Cancer* **14**, 15 (2015).
38. F. Denhez *et al.*, Syndesmos, a syndecan-4 cytoplasmic domain interactor, binds to the focal adhesion adaptor proteins paxillin and Hic-5. *J. Biol. Chem.* **277**, 12270–12274 (2002).
39. A. I. Tsonis *et al.*, Evaluation of the coordinated actions of estrogen receptors with epidermal growth factor receptor and insulin-like growth factor receptor in the expression of cell surface heparan sulfate proteoglycans and cell motility in breast cancer cells. *FEBS J.* **280**, 2248–2259 (2013).
40. C. Habes, G. Weber, C. Goupille, Sulfated glycoaminoglycans and proteoglycan syndecan-4 are involved in membrane fixation of LL-37 and its pro-migratory effect in breast cancer cells. *Biomolecules* **9**, 481 (2019).
41. F. Charni *et al.*, Syndecan-1 and syndecan-4 are involved in RANTES/CCL5-induced migration and invasion of human hepatoma cells. *Biochim. Biophys. Acta* **1790**, 1314–1326 (2009).
42. J. Ochieng *et al.*, Extracellular histones are the ligands for the uptake of exosomes and hydroxyapatite-nanoparticles by tumor cells via syndecan-4. *FEBS Lett.* **592**, 3274–3285 (2018).
43. J. C. Rodríguez-Manzaneque *et al.*, Cleavage of syndecan-4 by ADAMTS1 provokes defects in adhesion. *Int. J. Biochem. Cell Biol.* **41**, 800–810 (2009).
44. E. N. M. Nolte-'t Hoen *et al.*, Deep sequencing of RNA from immune cell-derived vesicles uncovers the selective incorporation of small non-coding RNA biotypes with potential regulatory functions. *Nucleic Acids Res.* **40**, 9272–9285 (2012).
45. L. Martin-Jaular *et al.*, Unbiased proteomic profiling of host cell extracellular vesicle composition and dynamics upon HIV-1 infection. *EMbo J.* **40**, e105492 (2021).
46. R. A. Haraszti *et al.*, High-resolution proteomic and lipidomic analysis of exosomes and microvesicles from different cell sources. *J. Extracell. Vesicles* **5**, 32570 (2016).
47. R. Kashyap *et al.*, Syntenin-knock out reduces exosome turnover and viral transduction. *Sci. Rep.* **11**, 4083 (2021).
48. R. D. Sanderson, M. Elkin, A. C. Rapraeger, N. Ilan, I. Vlodavsky, Heparanase regulation of cancer, autophagy and inflammation: New mechanisms and targets for therapy. *FEBS J.* **284**, 42–55 (2017).
49. G. David, P. Zimmermann, Heparanase involvement in exosome formation. *Adv. Exp. Med. Biol.* **1221**, 285–307 (2020).
50. T. Li *et al.*, TGF-β1-SOX9 axis-inducible COL10A1 promotes invasion and metastasis in gastric cancer via epithelial-to-mesenchymal transition. *Cell Death Dis.* **9**, 849 (2018).
51. L. Zhang, K. W. Peng, B. Wang, X. F. Yang, Z. M. Zhang, EDIL3 regulates gastric cancer cell migration, invasion and epithelial-mesenchymal transition via TGF-β1/XIST/miR-137 feedback loop. *Transl. Cancer Res.* **9**, 6313–6330 (2020).
52. F. Yang *et al.*, Interaction with CD68 and regulation of GAS6 expression by endosialin in fibroblasts drives recruitment and polarization of macrophages in hepatocellular carcinoma. *Cancer Res.* **80**, 3892–3905 (2020).
53. D. Zdżalik-Bielecka *et al.*, The GAS6-AXL signaling pathway triggers actin remodeling that drives membrane ruffling, macropinocytosis, and cancer-cell invasion. *Proc. Natl. Acad. Sci. U.S.A.* **118**, e2024596118 (2021).
54. Z. A. Zhong, M. N. Michalski, P. D. Stevens, E. A. Sall, B. O. Williams, Regulation of Wnt receptor activity: Implications for therapeutic development in colon cancer. *J. Biol. Chem.* **296**, 100782 (2021).
55. L. G. Lima *et al.*, Tumor microenvironmental cytokines bound to cancer exosomes determine uptake by cytokine receptor-expressing cells and biodistribution. *Nat. Commun.* **12**, 3543 (2021).
56. C. Williams *et al.*, Assessing the role of surface glycans of extracellular vesicles on cellular uptake. *Sci. Rep.* **9**, 11920 (2019).
57. M. Cerezo-Magaña, A. Bång-Rudenstam, M. Belting, The pleiotropic role of proteoglycans in extracellular vesicle mediated communication in the tumor microenvironment. *Semin. Cancer Biol.* **62**, 99–107 (2020).
58. W. Li, J. M. Ng, C. C. Wong, E. K. W. Ng, J. Yu, Molecular alterations of cancer cell and tumour microenvironment in metastatic gastric cancer. *Oncogene* **37**, 4903–4920 (2018).
59. A. Ito *et al.*, Extracellular vesicles shed from gastric cancer mediate protumor macrophage differentiation. *BMC Cancer* **21**, 102 (2021).
60. A. Hoshino *et al.*, Tumour exosome integrins determine organotropic metastasis. *Nature* **527**, 329–335 (2015).
61. B. Costa-Silva *et al.*, Pancreatic cancer exosomes initiate pre-metastatic niche formation in the liver. *Nat. Cell Biol.* **17**, 816–826 (2015).
62. V. Indira Chandran *et al.*, Ultrasensitive immunoprofiling of plasma extracellular vesicles identifies syndecan-1 as a potential tool for minimally invasive diagnosis of glioma. *Clin. Cancer Res.* **25**, 3115–3127 (2019).
63. S. A. Melo *et al.*, Glypican-1 identifies cancer exosomes and detects early pancreatic cancer. *Nature* **523**, 177–182 (2015).
64. A. M. Szász *et al.*, Cross-validation of survival associated biomarkers in gastric cancer using transcriptomic data of 1,065 patients. *Oncotarget* **7**, 49322–49333 (2016).
65. L. A. Lonowski *et al.*, Genome editing using FACS enrichment of nuclease-expressing cells and indel detection by amplicon analysis. *Nat. Protocols* **12**, 581–603 (2017).
66. Y.-H. Chen *et al.*, The GAGOme: A cell-based library of displayed glycosaminoglycans. *Nat. Methods* **15**, 881–888 (2018).
67. C. Théry *et al.*, Minimal information for studies of extracellular vesicles 2018 (MISEV2018): A position statement of the International Society for Extracellular Vesicles and update of the MISEV2014 guidelines. *J. Extracell. Vesicles* **7**, 1535750 (2018).
68. J. Van Deun *et al.*, EV-TRACK: Transparent reporting and centralizing knowledge in extracellular vesicle research. *Nat. Methods* **14**, 228–232 (2017).
69. Y. Perez-Riverol *et al.*, The PRIDE database resources in 2022: A hub for mass spectrometry-based proteomics evidences. *Nucleic Acids Res.* **50**, D543–D552 (2022).
70. J. Poças, H. Osório, A. Magalhães, Identification and quantification of proteins from MKN74 WT and SDC4 KO cells and EVs. The PRoteomics IDEntifications (PRIDE) database. www.ebi.ac.uk/pride/archive/projects/PXD035679. Deposited 1 August 2022.

Downloaded from https://www.pnas.org by 92.106.253.224 on June 22, 2023 from IP address 92.106.253.224.

3.2. Supporting Information

PNAS

Supporting Information for

Syndecan-4 is a maestro of gastric cancer cell invasion and communication that underscores poor survival

Juliana Poças[1,2,3], Catarina Marques[1,2,3], Catarina Gomes[1,2], Andreia Hanada Otake[4,♦], Filipe Pinto[1,2], Mariana Ferreira[1,2], Tiago Silva[1,2], Isabel Faria-Ramos[1,2], Rita Matos[1,2], Ana Raquel Ribeiro[1], Emanuel Senra[1], Bruno Cavadas[1], Sílvia Batista[4], Joana Maia[4], Joana A. Macedo[1,2], Luís Lima[5], Luís Pedro Afonso[5], José Alexandre Ferreira[5], Lúcio Lara Santos[5], António Polónia[1,2], Hugo Osório[1,2,6], Mattias Belting[7,8,9], Celso A. Reis[1,2,3,6], Bruno Costa-Silva[4], Ana Magalhães[1,2,3*]

[1] i3S - Instituto de Investigação e Inovação em Saúde, Universidade do Porto, 4200-135 Porto, Portugal.
[2] IPATIMUP - Instituto de Patologia e Imunologia Molecular da Universidade do Porto, 4200-465 Porto, Portugal.
[3] ICBAS - Instituto de Ciências Biomédicas Abel Salazar, Universidade do Porto, 4050-313 Porto, Portugal.
[4] Champalimaud Physiology and Cancer Programme, Champalimaud Foundation, 1400-038 Lisbon, Portugal.
[5] Experimental Pathology and Therapeutics Group, Research Center of IPO Porto (CI-IPOP)/RISE@CI-IPOP (Health Research Network), Portuguese Oncology Institute of Porto (IPO Porto)/Porto Comprehensive Cancer Centre (Porto.CCC), Porto, Portugal.
[6] FMUP - Faculdade de Medicina da Universidade do Porto, 4200-319 Porto, Portugal.
[7] Department of Clinical Sciences, Section of Oncology, Lund University, Lund, Sweden.
[8] Department of Immunology, Genetics and Pathology, Science for Life Laboratory, Uppsala University, Uppsala, Sweden.
[9] Skåne University Hospital, Lund, Sweden.
♦current address: Instituto do Cancer do Estado de Sao Paulo, Hospital das Clinicas HCFMUSP, Faculdade de Medicina, Universidade de Sao Paulo, 01246-000, Sao Paulo, Brazil.

***To whom correspondence may be addressed. Email:** amagalhaes@ipatimup.pt

This PDF file includes:

Figures S1 to S12
Tables S1 to S4
SI Material and Methods

SI also includes Excel file: SI_EV signature risk.xlsx

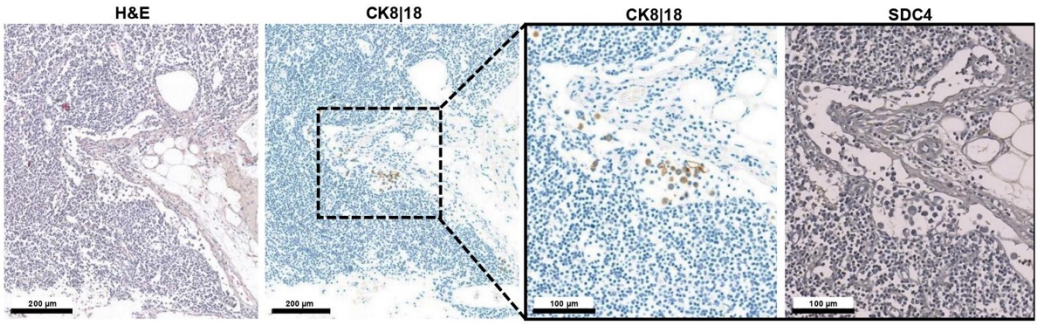
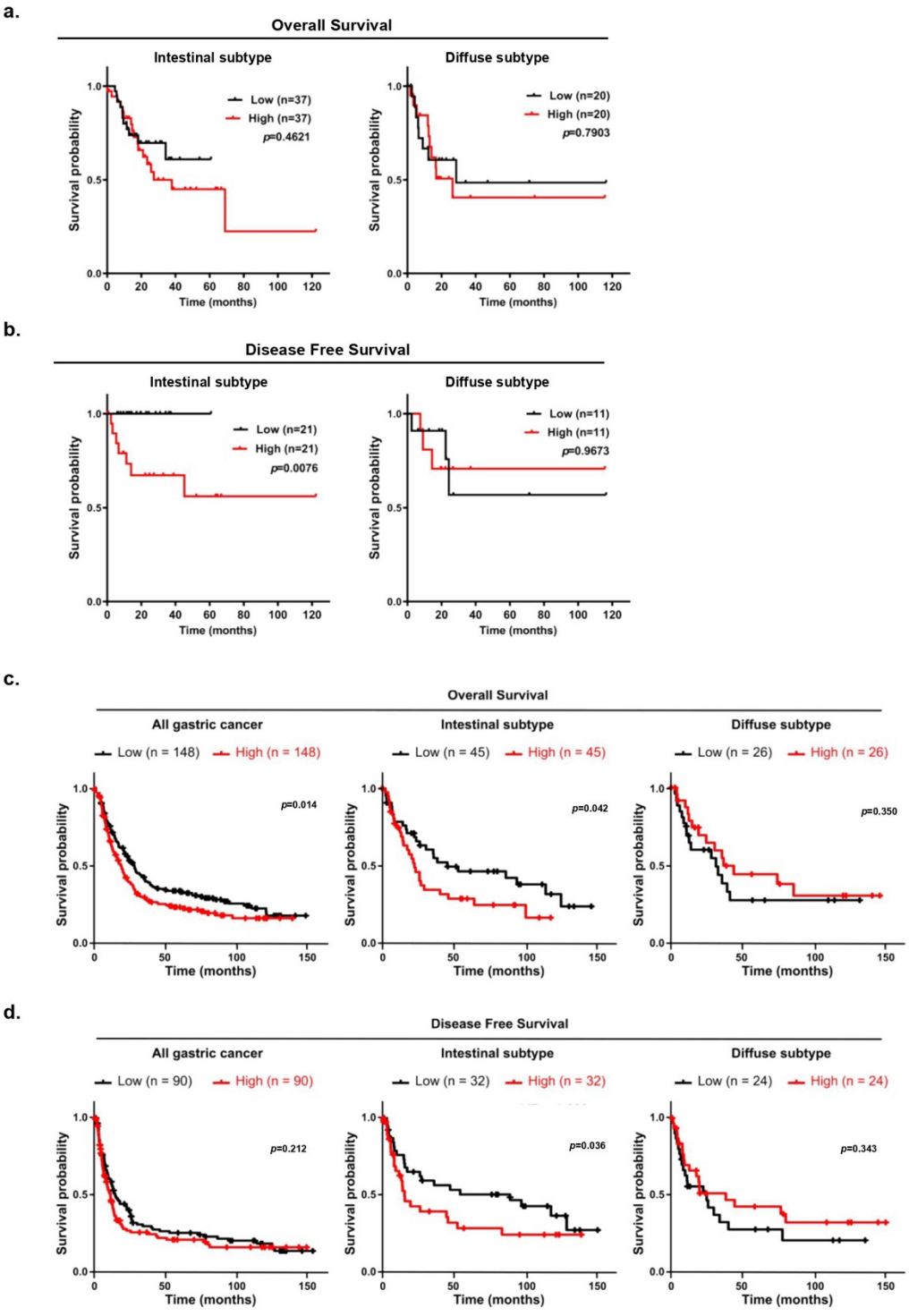


Fig. S1. Higher magnification of a lymph node metastasis from diffuse gastric cancer. Magnification images of the R3 area shown in Figure 1b. Hematoxylin-eosin (H&E) staining and cytokeratin 8 and 18 (CK8/18) allow the identification of the tumour epithelial cells and higher magnification of SDC4 staining confirms that these tumour cells are negative for SDC4 expression.

2


a.
Overall Survival
Intestinal subtype
Low (n=37)
High (n=37)
p=0.4621
Diffuse subtype
Low (n=20)
High (n=20)
p=0.7903
Survival probability
Time (months)
b.
Disease Free Survival
Intestinal subtype
Low (n=21)
High (n=21)
p=0.0076
Diffuse subtype
Low (n=11)
High (n=11)
p=0.9673
c.
Overall Survival
All gastric cancer
Low (n = 148)
High (n = 148)
p=0.014
Intestinal subtype
Low (n = 45)
High (n = 45)
p=0.042
Diffuse subtype
Low (n = 26)
High (n = 26)
p=0.350
d.
Disease Free Survival
All gastric cancer
Low (n = 90)
High (n = 90)
p=0.212
Intestinal subtype
Low (n = 32)
High (n = 32)
p=0.036
Diffuse subtype
Low (n = 24)
High (n = 24)
p=0.343

3

Fig. S2. *SDC4* expression associates with worse survival in gastric cancer patients. Kaplan-Meier (KM) analysis between *SDC4* mRNA levels and gastric cancer **(a, c)** overall survival (OS) or **(b, d)** disease-free survival (DFS). **(a, b)** Refer to TCGA database and **(c, d)** to GEO cohort extracted from KM Plotter database. The categorization of patients' samples was divided into low (lowest 25%, black lines) and high (highest 25%, red lines) subgroups according to *SDC4* mRNA expression levels. Comparison between curves in KM plots was performed using log-rank test.

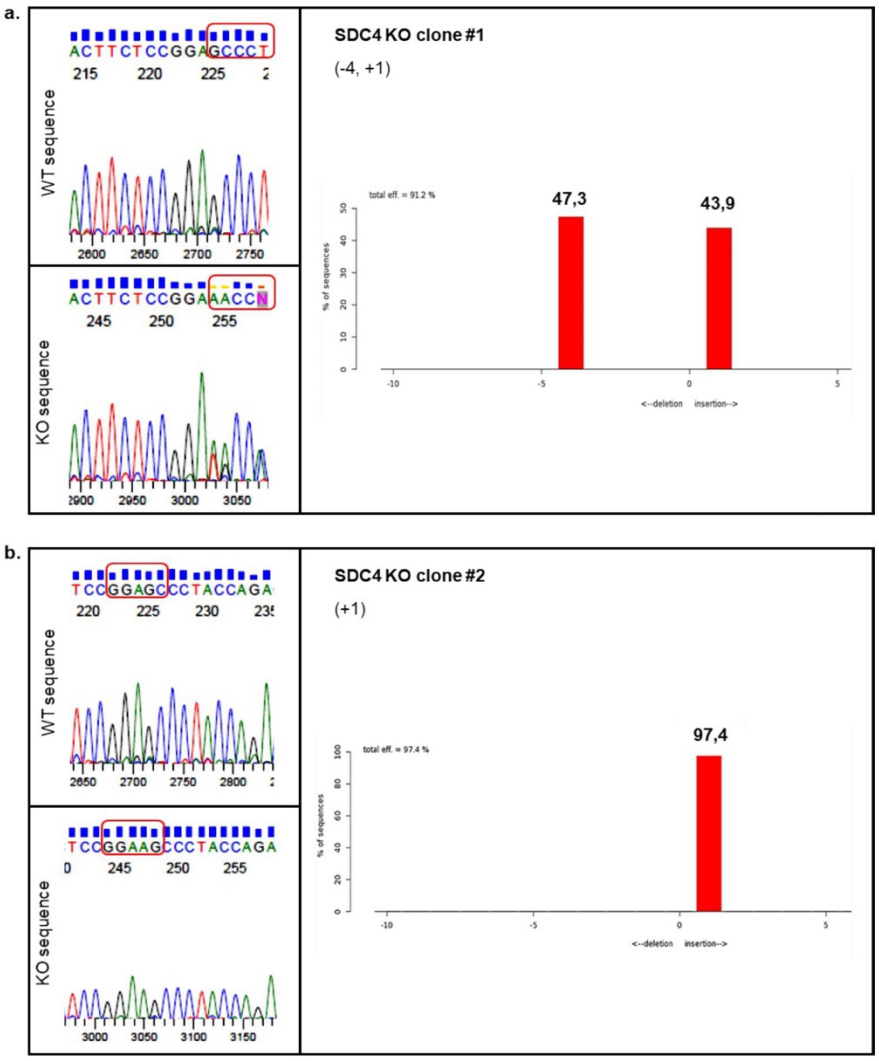


Fig. S3. *SDC4* KO validation by indel sequencing. *SDC4* KO validation through Sanger sequencing for **(a)** *SDC4* KO #1 and **(b)** *SDC4* KO #2 clones, from MKN74 WT cell line (Control). Indel sequencing was validated through Tracking of Indels by Decomposition (TIDE) analysis.

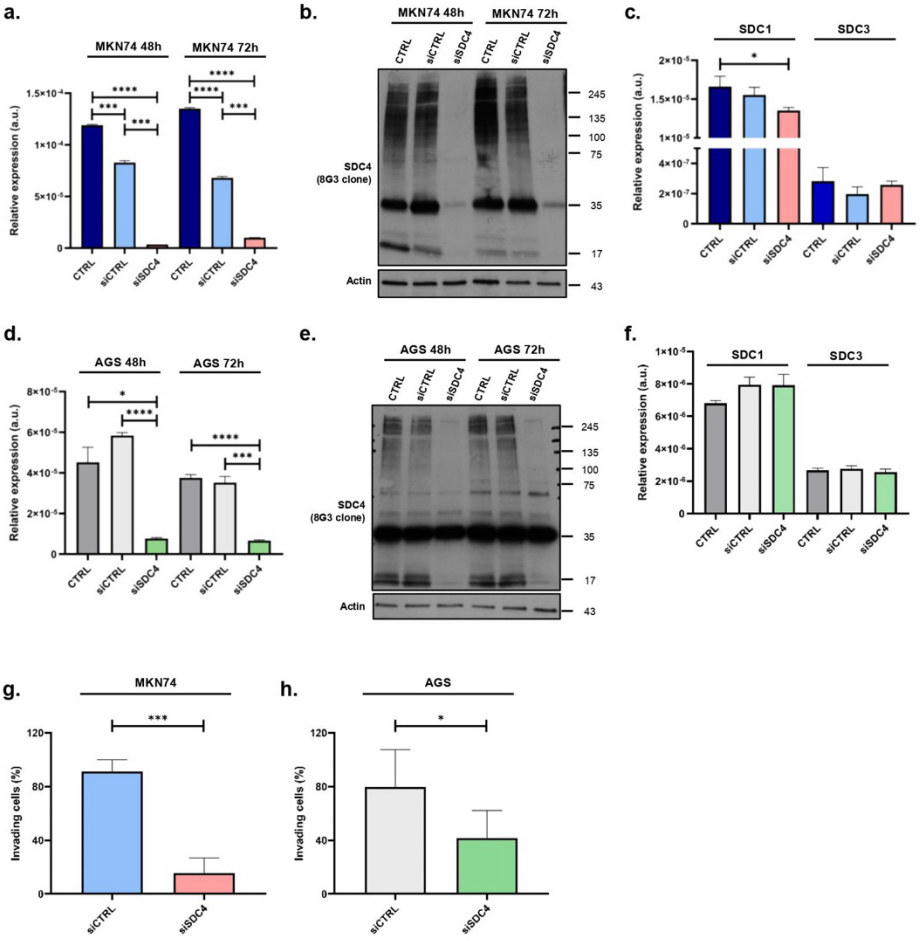


Fig. S4. *SDC4* silencing impairs gastric cancer cell invasion. (a, d) Bar graphs display *SDC4* mRNA levels in **(a)** MKN74 and **(d)** AGS cell lines: CTRL (Lipofectamine), siCTRL(scramble) and si*SDC4*, 48h and 72h after transfection. **(b, e)** WB analysis of SDC4 on **(b)** MKN74 and **(e)** AGS cell lines. Actin was used as loading control. **(c, f)** Bar graphs display *SDC1* and *SDC3* mRNA levels in **(c)** MKN74 and **(f)** AGS cell lines: CTRL (Lipofectamine), siCTRL(scramble) and si*SDC4*, 72h after transfection. **(g, h)** Invasion capacity of siCTRL (scramble) and si*SDC4* was evaluated on **(g)** MKN74 and **(h)** AGS cells. Bar graphs show the average of the percentage of invading cells + SD. A total of n= 6 from 3 independent experiments is shown. Statistical significance was determined using student's t-test with Welch's correction. *p≤0.05, ***p<0.001, ****p<0.0001.

6

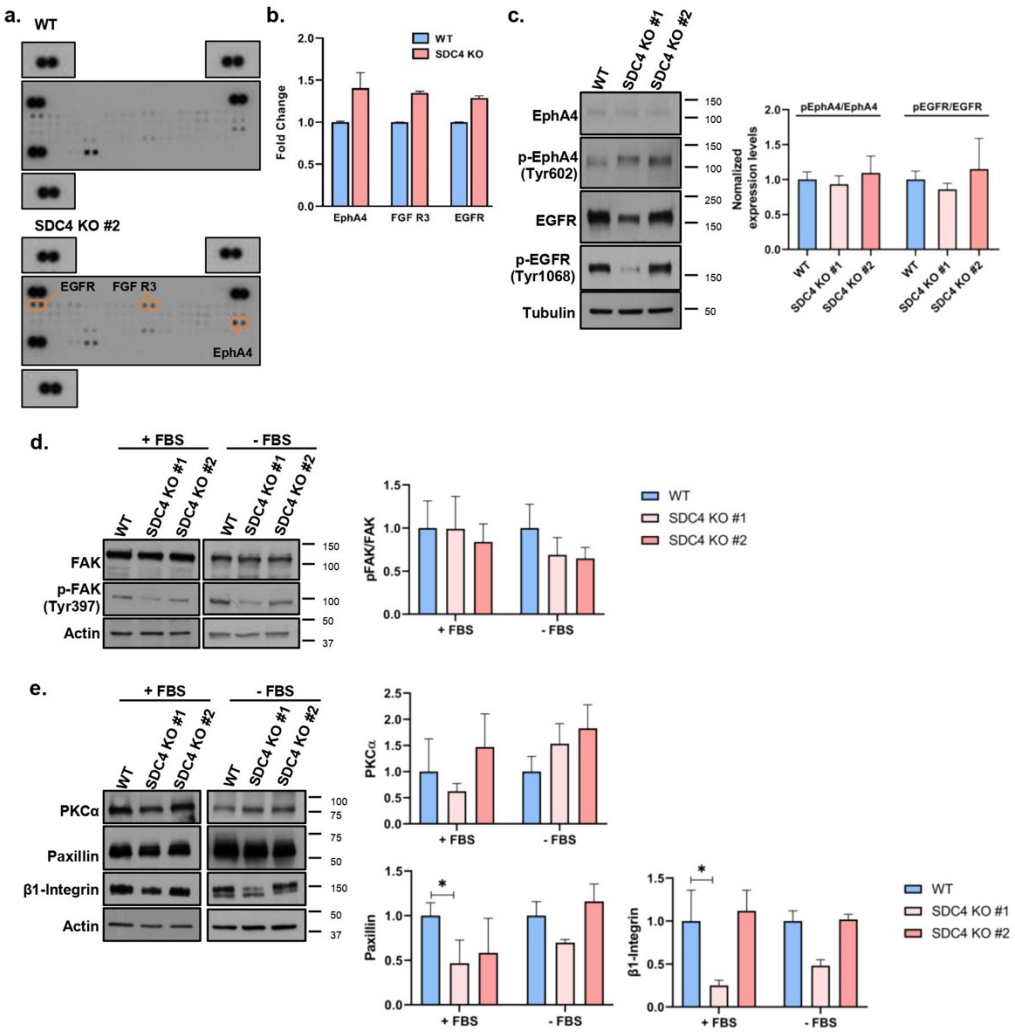


Fig. S5. Assessment of *SDC4* KO impact on key cellular signalling pathways. (a) Evaluation of the phosphorylation state of 50 Receptor Tyrosine Kinases (RTKs) in WT and *SDC4* KO cells using the Proteome Profiler Human p-RTK array. Each couple of dots represents one p-RTK. Reference spots are shown. The RTKs that presented a fold change ≥ 0.15 when comparing *SDC4* KO and WT cells are highlighted **(b)** Bar graphs show relative phosphorylation levels of *SDC4* KO cells normalized to WT values for the RTKs highlighted in (a). **(c)** The activation of EphA4 and EGFR in WT and *SDC4* KO cell clones was measured by WB analysis. α-tubulin was

used as loading control. Band density values of pEphA4 and pEGFR were normalized to the levels of the total receptor. Bar graph shows the mean values of the normalized phosphorylated receptor + SD. Data from 3 independent biological replicates. **(d)** The activation of FAK in WT and *SDC4* KO cell clones was measured by WB in protein extracts collected from cells grown in complete medium (+FBS) and simple medium (-FBS). Bar graph shows the mean values of the normalized phosphorylated receptor (pFAK/FAK) and normalized total form to β-actin. Data from 4 (+FBS) and 3 (-FBS) independent biological replicates **(e)** Evaluation of the expression levels of PKCα, paxillin and β1-Integrin in protein extracts collected from cells grown in complete medium (+FBS) and simple medium (-FBS). β-actin was used as loading control. Bar graphs show the mean values normalized to β-actin + SD. Data from 4 (+FBS) and 3 (-FBS) independent biological replicates, and 4 (+FBS) and 2 (-FBS) for β1-Integrin. One representative image from each experiment is shown. Statistical significance was determined using one-way ANOVA. *p≤0.05.

8

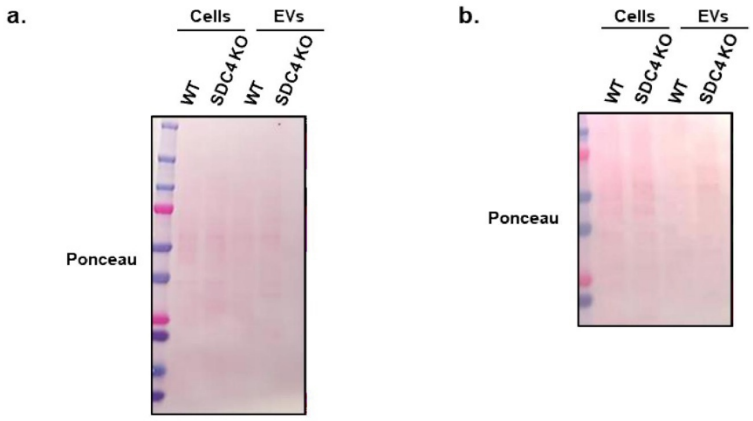


Fig. S6. Ponceau staining of protein lysates from cells and EVs. (a) Ponceau staining of the membrane used to evaluate SDC4 expression (relatively to Fig. 3a). **(b)** Ponceau staining of the membrane used to evaluate classical EV-markers (relatively to Fig. 3j).

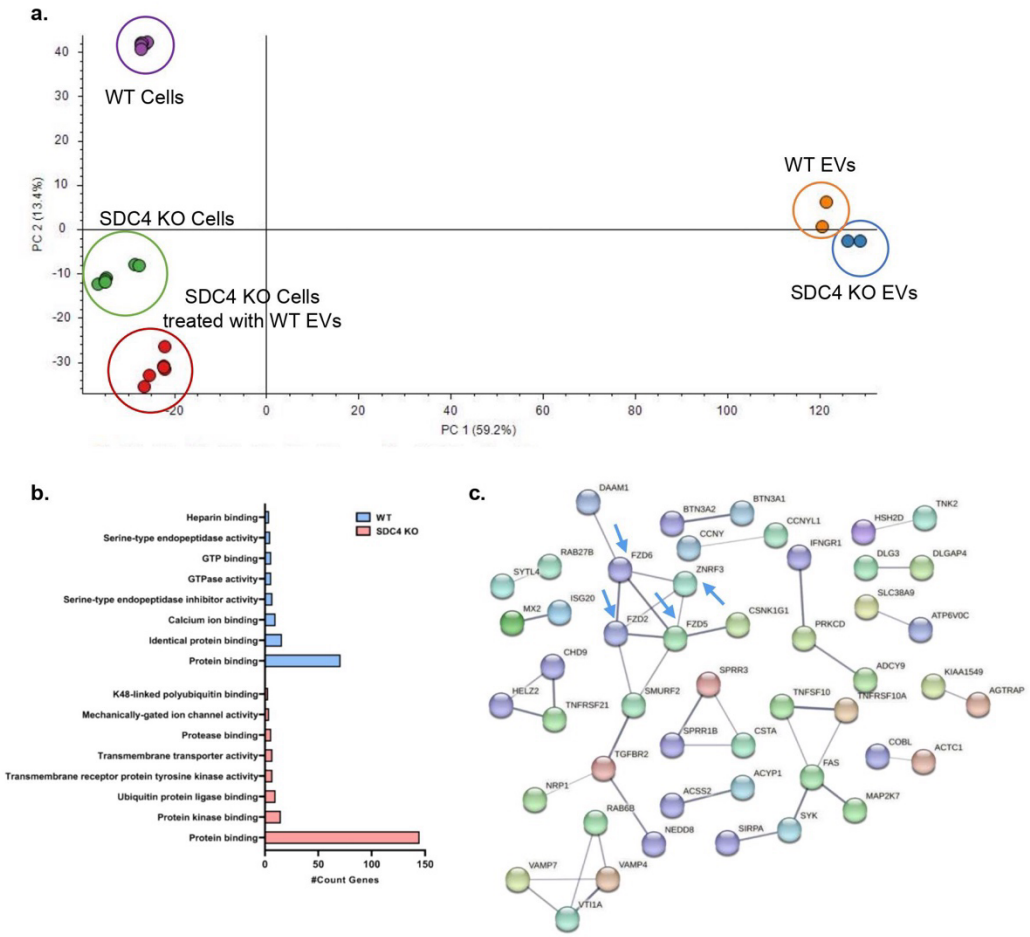


Fig. S7. Data from MS-based proteomic analysis. (a) Principal Component Analysis (PCA) based normalized abundance. **(b)** Functionally grouped network of gene ontology (GO) molecular function terms for the SDC4-specific proteome in WT EVs and exclusive proteins in KO EVs (Benjamini $p<0.01$). **(c)** Protein-protein interaction for the exclusive KO EVs proteome. Blue arrows highlight Frizzled receptors (FDZ2, FDZ5, and FDZ6) and E3 Ubiquitin-Protein Ligase (ZNRF3).

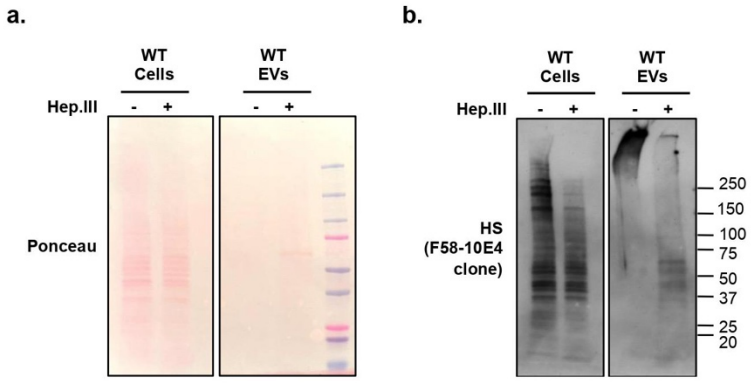


Fig. S8. WB for heparan sulfate (HS) in WT cells and EVs treated with Heparinase III (Hep. III). (a) Ponceau staining of the membrane used to evaluate HS in WT cells and EVs, with (+) and without (-) Hep.III digestion. **(b)** WB analysis of HS in WT cells and EVs, with (+) and without (-) Hep.III digestion.

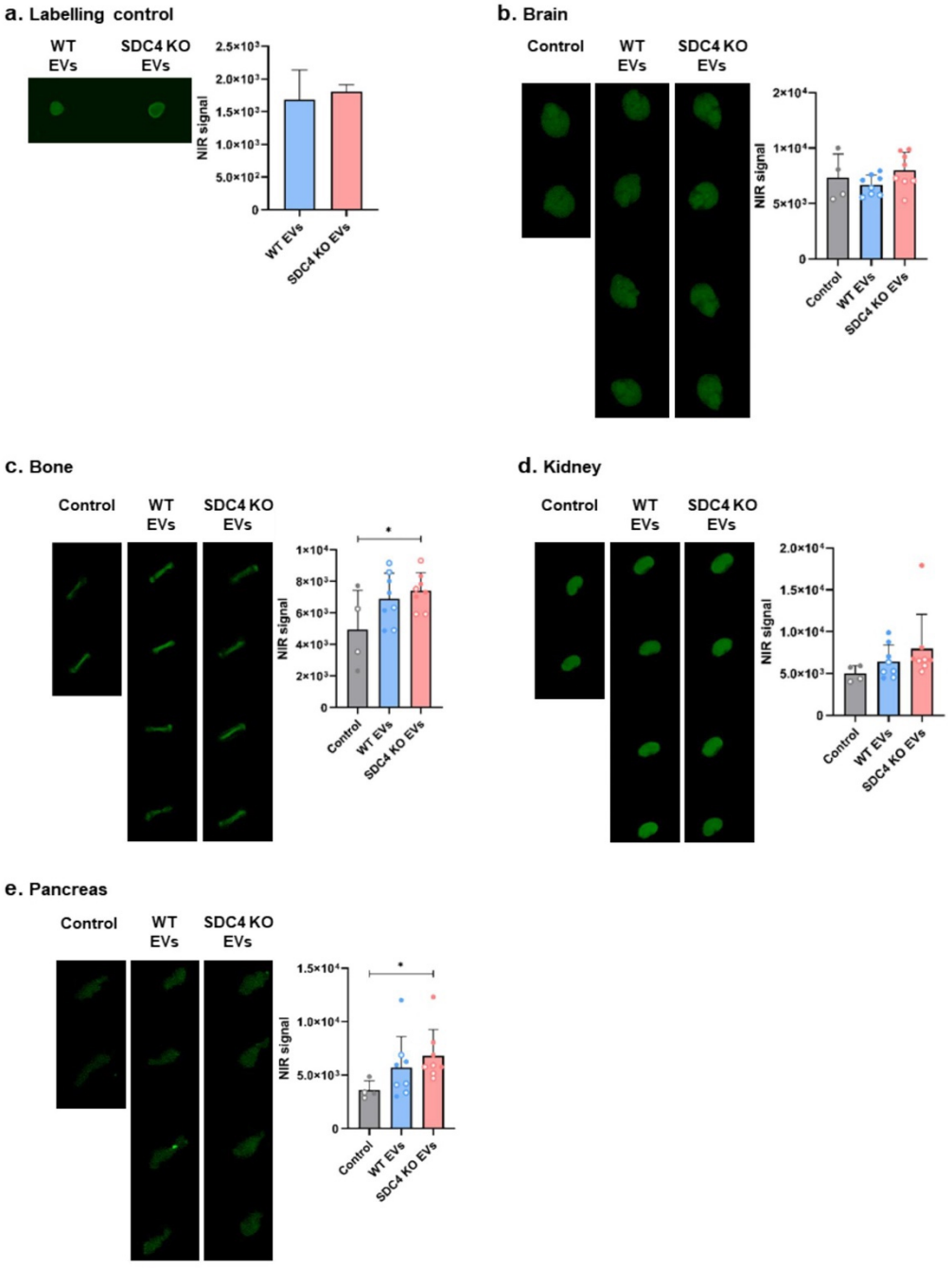


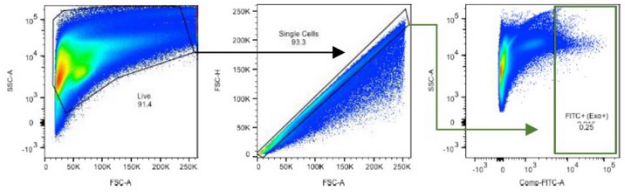
Fig. S9. Biodistribution of EVs derived from WT and *SDC4* KO cells. (a) Labelling control of WT and *SDC4* KO EVs was performed with Odyssey® CLx Imaging System (Licor) by fluorescence quantification. Bar graphs represents the average of NIR fluorescence signal

12

quantification + SD. It is shown n=2 from 2 independent experiments. Statistical significance was assessed using student's t-test. One representative image is shown. EVs biodistribution was assed using immunodeficient NOD SCID mice by measurement of fluorescence intensity of the collected organs **(b)** brain, **(c)** bone, **(d)** kidney and **(e)** pancreas. The NIR fluorescence quantification was assessed using Odyssey® CLx Imaging System. Bar graphs represent the average of fluorescence quantification of the organs + SD. Data from 2 independent biological replicates for WT and *SDC4* KO (each n=4, per condition group), and for control (each n=2). Statistical significance was assessed using student's t-test.*$p \leq 0.05$; ** $p < 0.01$; ***$p < 0.001$.

13

a. Sample gating strategy for Exo FITC positive cells (same for all organs tested)



b. Sample gating strategy for Exo FITC positive cells (all organs tested → Tim-4+ cells were considered just for liver)

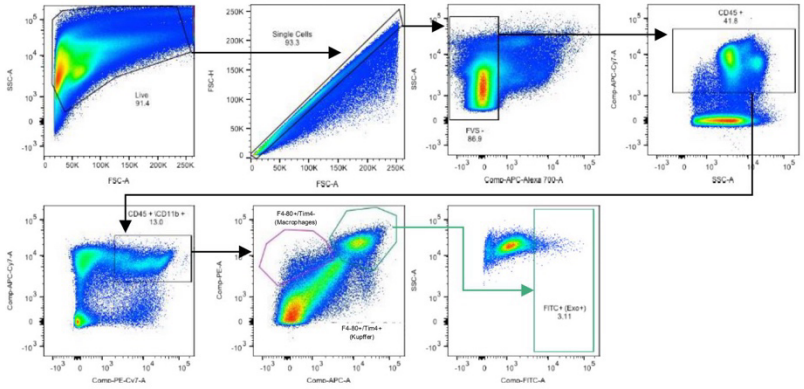


Fig. S10. Sample gating strategy for FITC positive cells (Exo+), in flow cytometry assays. (a) Direct gating strategy to evaluate all the live cells that are FITC positive (incorporated PKH67-labelled EVs) Single Cells, Live cells, FITC+ (Exo+). **(b)** Gating strategy used to evaluate Tim4- macrophages cell population that is FITC positive (incorporated PKH67-labelled EVs) - Single cells, FVS-, CD45+, CD45+ /CD11b+, F4/80+ /Tim4-, FITC+ (Exo+) and Kupffer cell population that is FITC positive (incorporated PKH67-labelled EVs) - Single cells, FVS-, CD45+, CD45+ /CD11b+, F4/80+ /Tim4+, FITC+ (Exo+).

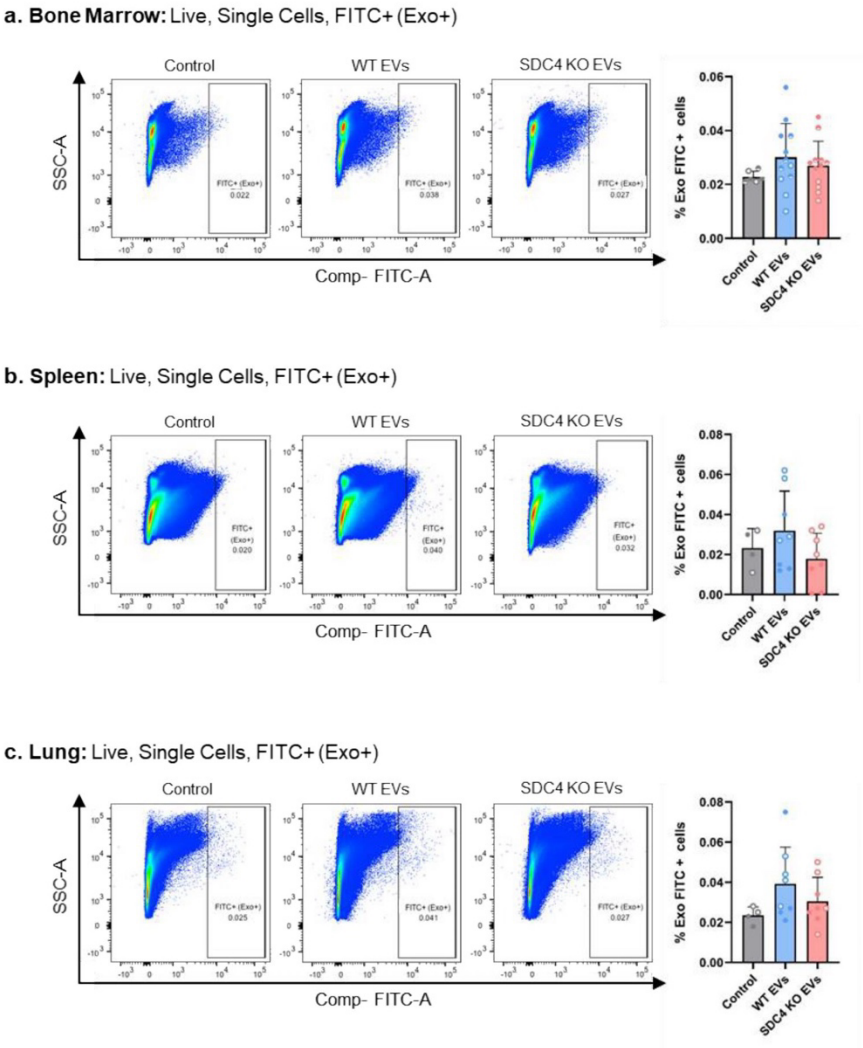


Fig. S11. Determination of EV uptake by NOD SCID mice organs. FACS analysis of **(a)** bone marrow, **(b)** spleen and **(b)** lung cells from mice injected with PKH67-labelled EVs isolated from either WT or *SDC4* KO cells. Cells were analyzed using the following gating strategy: Single Cells, Live cells, FITC+ (Exo+) cells. Bar graphs represent the average of the percentage of cells that incorporated EVs (FITC+ cells). Data for bone marrow from 3 independent biological replicates for WT and KO EVs (each n=4, per condition group) and for control (each n=2). Data for spleen and lung from 2 independent biological replicates for WT and KO EVs (each n=4, per condition group) and for control (each n=2). Statistical significance was assessed using student's t-test.

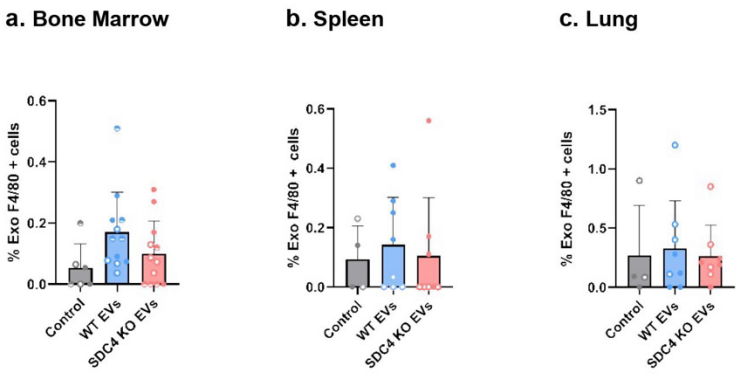


Fig. S12. EV uptake by macrophages. FACS analysis of **(a)** bone marrow, **(b)** spleen and **(c)** lung cells from mice injected with PKH67-labelled WT and KO EVs. Cells were analyzed using the following gating strategy: Single cells, FVS-, CD45+, CD45+ /CD11b+, F4/80+ /Tim4-, FITC+ (Exo+). Bar graphs represent the average of the percentage of cells that incorporated EVs (FITC+ cells). Data for bone marrow from 3 independent biological replicates for WT and KO EVs (each n=4, per condition group) and for control (each n=2). Data for spleen and lung from 2 independent biological replicates for WT and KO EVs (each n=4, per condition group) and for control (each n=2). Statistical significance was assessed using student's t-test with Welch's correction.

Table S1. Association of SDC4 expression with clinicopathological variables in gastric cancer patients.

Clinicopathological variable	Total	SDC4 (8G3)				
		Negative		Positive		
		n	%	n	%	*p*-value*
Age (median, 35-89)						
<66	68	27	39.7	41	60.3	0.085
≥66	83	22	26.5	61	73.5	
Gender						
Male	82	28	34.1	54	65.9	0.586
Female	70	21	30.0	49	70.0	
Stage						
IA-IB	17	9	52.9	8	47.1	0.225
II	55	17	30.9	38	69.1	
IIIA-IIIB	57	15	26.3	42	73.7	
IV	23	8	34.8	15	65.2	
Primary tumour						
T1	11	6	54.5	5	45.5	0.178
T2	17	7	41.2	10	58.8	
T3	100	27	27.0	73	73.0	
T4	20	8	40.0	12	60.0	
Regional lymph nodes						
pN0	44	18	40.9	26	59.1	0.083
pN1	37	14	37.8	23	62.2	
pN2	25	3	12.0	22	88.0	
pN3	41	13	31.7	28	68.3	
Metastasis						
pM0	114	41	36.0	73	64.0	0.914
pM1	23	8	34.8	15	65.2	
Lauren classification						
Intestinal (primary tumour)	119	34	28.6	85	71.4	**0.031**
Diffuse (primary tumour)	21	11	52.4	10	47.6	
Intestinal (LN metastasis)	10	4	40	6	60	1.000
Diffuse (LN metastasis)	2	1	50	1	50	
Treatment						
Surgery alone	105	33	31.4	72	68.6	0.750
Surgery plus other tx	47	16	34.0	31	66.0	

*Pearson Chi-Square

Table S2. Kaplan-Meier analysis for overall survival stratified for subgroups of gastric cancer patients (represented values correspond to the mean).

		Overall survival (95% CI)		
Subgroup	**Total**	**SDC4 (8G3)**		
		SDC4-negative	**SDC4-positive**	**p-value***
All patients	67.0 (57.4-76.6)	80.4 (64.2-96.7)	59.7 (48.7-70.8)	**0.025**
Age				
<66	64.0 (50.6-77.5)	89.0 (67.6-110.4)	42.1 (31.2-53.0)	**0.005**
≥66	68.4 (55.5-81.2)	66.3 (44.3-88.2)	66.4 (55.5-81.2)	0.672
Gender				
Male	59.6 (48.8-70.4)	78.7 (59.5-97.8)	49.7 (38.0-61.3)	**0.028**
Female	70.6 (56.2-85.1)	76.9 (51.7-102.1)	66.5 (49.6-83.4)	0.378
Stage				
IA-IB	-	-	-	0.480
II	81.9 (68.8-94.9)	100.6 (81.2-120.1)	69.3 (54.7-83.8)	0.073
IIIA-IIIB	42.8 (31.1-54.5)	52.1 (26.2-78.0)	34.9 (25.7-44.0)	0.464
IV	17.09 (10.9-23.3)	18.0 (7.08-28.9)	16.6 (8.76-24.4)	0.618
Primary tumour				
T1	-	-	-	0.273
T2	87.1 (64.4-109.6)	111.4 (83.2-139.7)	60.7 (43.6-77.7)	0.129
T3	57.9 (47.3-68.5)	74.8 (53.5-96.1)	47.8 (37.6-58.0)	0.071
T4	56.2 (32.5-79.8)	41.1 (7.8-74.4)	52.6 (30.9-74.3)	0.302
Regional lymph nodes				
pN0	94.1 (79.8-108.3)	115.8 (101.1-130.4)	74.6 (57.1-92.1)	**0.016**
pN1	87.3 (67.6-106.9)	57.2 (39.2-75.1)	87.1 (62.2-112.1)	0.967
pN2	46.4 (30.3-62.5)	46.7 (0-106.9)	42.6 (28.9-56.3)	0.867
pN3	31.8 (20.4-43.2)	43.3 (15.0-71.6)	24.9 (17.2-32.6)	0.469
Metastasis				
pM0	76.4 (66.0-86.8)	90.9 (74.0-107.8)	62.9 (52.0-73.7)	**0.044**
pM1	17.1 (10.9-23.3)	18.0 (7.08-28.9)	16.6 (8.76-24.4)	0.618
Lauren classification				
Intestinal	69.3 (58.4-80.1)	88.8 (69.8-107.7)	60.6 (48.5-72.8)	**0.018**
Diffuse	56.9 (35.2-78.6)	52.7 (23.1-82.3)	47.6 (29.2-65.9)	0.624
Treatment				
Surgery alone	19.8 (18.3-21.2)	20.5 (17.9-23.1)	19.4 (17.7-21.2)	**0.026**
Surgery plus other tx	18.3 (16.4-20.3)	18.8 (15.6-22.0)	18.1 (15.6-20.5)	0.371

*log-rank (Mantel-Cox)

Table S3. SDC4 abundance through proteomic analysis in WT and *SDC4* KO #2 cells and respective EVs (WT and KO); and in *SDC4* KO #2 cells treated with WT EVs.

Identification	Condition	Abundance (Normalized)	Abundance Average	Position and Peptide Sequence
EVs_WT1	WT EVs_1	3,43E+08	2,45E+08	[19-36]: A.ESIREREVIDPQDLLEGR.Y [23-36]: R.ETEVIDPQDLLEGR.Y [93-104]: R.AGSGSQVPTEPK.K [115-128]: K.RISPVEESEDVSNK.V [116-128]: K.ISPVEESEDVSNK.V [129-143]: K.VSMSSTVQGSNIFER.T [132-143]: M.SSTVQGSNIFER.T [175-184]: K.KDEGSYDLGK.K [176-184]: K.DEGSYDLGK.K [190-198]: K.KAPTNEFYA.-
EVs_WT2	WT EVs_2	1,47E+08		
EVs_KO1	SDC4 KO EVs_1	Not Found	n.a.	
EVs_KO2	SDC4 KO EVs_2	Not Found		
WT1	WT Cells_1_TR1	1,67E+07	1,67E+07	[19-36]: A.ESIREREVIDPQDLLEGR.Y [23-36]: R.ETEVIDPQDLLEGR.Y [115-128]: K.RISPVEESEDVSNK.V [116-128]: K.ISPVEESEDVSNK.V [176-184]: K.DEGSYDLGK.K [190-198]: K.KAPTNEFYA.-
WT1	WT Cells_1_TR2	1,70E+07		
WT2	WT Cells_2_TR1	1,76E+07		
WT2	WT Cells_2_TR2	1,78E+07		
WT3	WT Cells_3_TR1	1,52E+07		
WT3	WT Cells_3_TR2	1,52E+07		
KO1	SDC4 KO Cells_1_TR1	Not Found	n.a.	
KO1	SDC4 KO Cells_1_TR2	Not Found		
KO2	SDC4 KO Cells_2_TR1	Not Found		
KO2	SDC4 KO Cells_2_TR2	Not Found		
KO3	SDC4 KO Cells_3_TR1	Not Found		
KO3	SDC4 KO Cells_3_TR2	Not Found		
KO_WT1	SDC4 KO Cells + WT EVs_1_TR1	1,40E+06	1,17E+06	[93-104]: R.AGSGSQVPTEPK.K [176-184]: K.DEGSYDLGK.K
KO_WT1	SDC4 KO Cells + WT EVs_1_TR2	8,84E+05		
KO_WT2	SDC4 KO Cells + WT EVs_2_TR1	1,01E+06		
KO_WT2	SDC4 KO Cells + WT EVs_2_TR2	1,30E+06		
KO_WT3	SDC4 KO Cells + WT EVs_3_TR1	1,08E+06		
KO_WT3	SDC4 KO Cells + WT EVs_3_TR2	1,34E+06		

Table S4. Syntenin-1, Alix and SDC1 abundance through proteomic analysis in WT and *SDC4* KO #2 cells and respective EVs (WT and KO); and in *SDC4* KO #2 cells treated with WT EVs.

		Syntenin-1		ALIX		SDC1	
Identification	**Condition**	**Abundance (Normalized)**	**Abundance Average**	**Abundance (Normalized)**	**Abundance Average**	**Abundance (Normalized)**	**Abundance Average**
EVs_WT1	**WT EVs_1**	1,54E+10	1,54E+10	6,23E+09	6,22E+09	2,31E+07	3,58E+07
EVs_WT2	**WT EVs_2**	1,54E+10		6,20E+09		4,85E+07	
EVs_KO1	**SDC4 KO EVs_1**	1,75E+10	1,75E+10	7,93E+09	8,46E+09	1,15E+08	1,19E+08
EVs_KO2	**SDC4 KO EVs_2**	1,75E+10		8,99E+09		1,24E+08	
WT1	**WT Cells_1_TR1**	1,10E+10	1,93E+09	5,35E+08	5,59E+08	1,18E+07	1,35E+07
WT1	**WT Cells_1_TR2**	1,09E+08		5,60E+08		1,27E+07	
WT2	**WT Cells_2_TR1**	1,11E+08		5,52E+08		1,21E+07	
WT2	**WT Cells_2_TR2**	1,15E+08		5,54E+08		1,27E+07	
WT3	**WT Cells_3_TR1**	1,12E+08		5,68E+08		1,54E+07	
WT3	**WT Cells_3_TR2**	1,15E+08		5,84E+08		1,59E+07	
KO1	**SDC4 KO Cells_1_TR1**	1,12E+08	1,14E+08	6,20E+08	6,40E+08	1,13E+07	1,15E+07
KO1	**SDC4 KO Cells_1_TR2**	1,14E+08		6,30E+08		1,12E+07	
KO2	**SDC4 KO Cells_2_TR1**	1,18E+08		6,52E+08		1,05E+07	
KO2	**SDC4 KO Cells_2_TR2**	1,19E+08		6,53E+08		1,12E+07	
KO3	**SDC4 KO Cells_3_TR1**	1,09E+08		6,36E+08		1,22E+07	
KO3	**SDC4 KO Cells_3_TR2**	1,12E+08		6,48E+08		1,24E+07	
KO_WT1	**SDC4 KO Cells + WT EVs_1_TR1**	1,30E+08	1,26E+08	5,46E+08	5,48E+08	1,07E+07	1,06E+07
KO_WT1	**SDC4 KO Cells + WT EVs_1_TR2**	1,35E+08		5,28E+08		8,31E+06	
KO_WT2	**SDC4 KO Cells + WT EVs_2_TR1**	1,29E+08		5,25E+08		8,89E+06	
KO_WT2	**SDC4 KO Cells + WT EVs_2_TR2**	1,23E+08		5,78E+08		1,25E+07	
KO_WT3	**SDC4 KO Cells + WT EVs_3_TR1**	1,17E+08		5,45E+08		1,00E+07	
KO_WT3	**SDC4 KO Cells + WT EVs_3_TR2**	1,20E+08		5,66E+08		1,31E+07	

SI Materials and Methods

Gastric cancer tissue samples. This study was performed retrospectively in a series of 152 formalin-fixed paraffin-embedded (FFPE) gastric tumour tissues obtained from archived blocks at the Portuguese Institute of Oncology-Porto (IPO-Porto), Portugal. Clinicopathological information was obtained from patients' clinical records, upon IPO ethics committee approval (reference 87/17 approved on 23 March 2017). All procedures were carried out following the rules of the Declaration of Helsinki of 1975, revised in 2013.The gastric tumours obtained from IPO-Porto were surgically removed from 82 men and 70 women, ranging from 39 to 89 years of age with a mean age of 64.2 ± 12.1 (median 66 years), admitted and treated at the IPO-Porto between 2004 and 2009 (Supplementary Table 1). Approximately 70% of the patients were treated only with surgery, 17% performed chemotherapy in palliative setting, 10% as adjuvant treatment and only 3% were treated with neoadjuvant chemotherapy and/or radiotherapy prior to the surgery. For analysis purposes we dichotomized treatment variable into "surgery alone" and "surgery plus other tx". Overall survival (OS) was defined as the period between the date of surgery and the date of patient death by cancer or last follow-up.

Mice. Male and female NOD SCID mice were purchased from the Charles River Laboratories (Barcelona, Spain) and used at 6-8 weeks of age. NOD SCID mice were bred and maintained at the Champalimaud Foundation animal facility.

Immunohistochemistry. Expression of SDC4 was assessed in 152 cases of human gastric carcinoma and 12 lymph node metastases. Tissue slides were dewaxed and rehydrated. Treatment with 3% H_2O_2 in methanol for 20min was performed to block endogenous peroxidase. After blocking, tissues were incubated with the primary antibody anti-SDC4 8G3 clone (1)in 5% bovine serum albumin (BSA) in phosphate-buffered saline (PBS). Sections were then incubated with 1:200 biotin-labelled secondary rabbit anti-mouse antibody (Dako) in PBS with 5% BSA for 30min and with ABC kit (Vector Labs) for 30min. Sections were stained for 0.05% 3,3'-diaminobenzidinetetrahydrochloride (DAB) containing 0.01% H_2O_2 and counterstained with Mayers' haematoxylin solution, dehydrated and mounted. SDC4 expression was viewed and

assessed by two sample-blind pathologists and classified as either negative or positive (whenever at least 1% of the cells were positive). Slides scanning was performed using D-Sight F 2.0 (Menarini Diagnostics).

***In silico* analysis of *SDC4* expression in gastric cancer tissues.** mRNA *SDC4* transcript data was downloaded from the Cancer Genome Atlas (TCGA; https://gdc.cancer.gov/; data release 36), comprised a total of 412 stomach adenocarcinoma samples and 36 normal gastric tissues.

RNA sequencing data was quantified as FPKM (fragments per kilobase million) by STAR. *SDC4* transcript levels were correlated with the available clinicopathological data, including Lauren classification and TCGA molecular subtype, presence of metastasis, recurrence, MSI and aneuploid status.

***In silico* analysis of the prognostic impact of *SDC4* in gastric cancer.** To determine the clinical relevance of *SDC4* expression in gastric cancer we used the TCGA-STAD dataset. Patients were stratified in two groups with high or low expression. The top 25% of patient samples with highest expression were considered as high *SDC4* expression group. The bottom 25% of patients with the lowest expression values were considered as low *SDC4* expression group. Survival information was extracted from clinical files and information on recurrence was downloaded from the cBioPortal. Kaplan–Meier analysis was used to calculate the survival rate of stratified patients and plot the survival curve. For overall survival (OS) analysis, only individuals with survival information and follow-up information above to zero were keep (n= 387). In disease-free survival (DFS) plots, deceased individuals without information on recurrence were removed from the analysis (n= 240). Multivariate Cox regression with backward elimination was performed to assess the independent prognostic value (OS and DFS) of *SDC4* expression in all GC patients and in the intestinal subtype tumour patients. The clinicopathological parameters such as Lauren classification, gender, age and disease stage were used as covariables. The prognostic value of SDC4 expression was further validated in the KM plotter database (2), with expression data for 740 patients and survival data for 592 patients (GSE14210, GSE15459, GSE22377, GSE29272

and GSE51105). Patients were stratified in two groups with high or low expression, as described above. OS and disease-free survival (DFS) were analysed for all gastric cancer patients and then divided according to the Lauren subtype classification (intestinal n=179, diffuse n=106).

***In silico* analysis of the prognostic impact of EV signatures.** Survival analysis of signature genes was assessed for the WT (93 genes) and *SDC4* KO (194 genes) signature sets using the STAD-TCGA database. Each signature was used to construct the predictive component by Cox proportion hazard regression (3). The risk scores were calculated by a linear combination of the mean normalized gene expression values for the selected genes, weighted by their estimated Cox regression coefficients. Kaplan-Meier survival analyses for OS and DFS was carried for the samples classified into “high” and “low” risk groups according to the upper and lower risk score quartiles of all samples. All analyses were implemented in R (v4.1.2) using the “survival” and “survminer” packages.

Cell culture. The cell lines AGS and MKN45 were obtained from the Japanese Collection of Research Bioresources (JCRB); NCI-N87, MKN74 and RAW 264.7 were obtained from the American Type Culture Collection (ATCC); Kupffer cells (HUKCCS) were obtained from Life Technologies. All cells lines were grown in RPMI 1640 Medium (Thermofisher Scientific), supplemented with 10% FBS (Invitrogen) and maintained at 37ºC in an atmosphere of 5% CO_2. Cultures were routinely screened for mycoplasma. Cell line identity validation was performed by short tandem repeat (STR) profiling using the PowerPlex® 16 HS System kit (Promega).

***SDC4* KO by CRISPR/Cas9.** Briefly, 3 different gRNA targeting exon1 of *SDC4* were design, using DESKGEN platform, and gRNA (5’-CGGAGCCCTACCAGACGATG-3’) was validated. Then, cells were transfected with a plasmid containing Cas9 endonuclease + GFP and a plasmid containing the validated gRNA. Fluorescence-activated cell sorting was used to obtain GFP-positive single cell clones. Indel detection was performed by Restriction Fragment Length Polymorphism (RFLP) analysis by tri primer PCR (SDC4fw_ext: AGCTGACCGGCAGCAAAAAAGGACACGCGGTGAGTTAG; SDC4rv: AGTCTCAAGGCATGGTCACC; Famfw: 6-FAM-AGCTGACCGGCAGCAAAATTG) (4), and indels

of the selected clones were validated by Sanger sequencing and Tracking of Indels by Decomposition (TIDE) analysis.

siRNAs transfection. Cells were transfected with siRNA triplets targeting *SDC4*: siRNAA (5'-AGAAACUAGAGGAG- AAUGAG GUUAT-3'), siRNAB (5'-CUAUUCUAGAGAACUAAACUGGCTT-3') and siRNAC (5'-GGAUUGGAUCACUUCUUAAACUUCC-3') (SR304301, OriGene Technologies) or siScramble (5'-CGUUAAUCGCGUAUAAUACGCGUAT-3') (SR30004, OriGene Technologies), using Lipofectamine 2000 reagent (Invitrogen) according to the manufacturer's instructions. Cells were analyzed 48h and 72h after transfection.

RNA extraction and quantification. RNA extraction was performed using TRI Reagent® (T9424, Sigma-Aldrich®) according to manufacturer's instructions. RNA quantification was done using NanoDrop ND-1000® UV-Vis spectrophotometer (NanoDrop Technologies).

Reverse Transcriptase PCR (RT-PCR) and Real Time PCR (qPCR). The syndecan members were amplified using the primer sequences SDC1 (fw: 5'-ATGGCTCTGGGGATGACTCT-3'; rv: 5'-GTGGGAATAGCCGTCAGGAG-3'), SDC2 (fw: 5'-TCAGACAAAGTCACCTGAAGA-3'; rv: 5'-AACTCCACCAGCAATGAC-3'), SDC3 (fw: 5'-TGACATCCCTGAGAGGAGCA-3'; rv: 5'-GCTACCACCTCATTGGCTGT-3') and SDC4 (fw: 5'-CCGGAGCCCTACCAGACGAT-3'; rv: 5'-AGGCACCAAGGGATGGACAA-3'). The 18S gene was used as control (fw: 5′-CGCCGCTAGAGGTGAAATTC-3′; rv: 5′-CATTCTTGGCAAATGCTTTCG-3′). 1 µg of RNA from each cell condition was converted into cDNA via reverse transcription by incubation with random hexamers/primers, using the SuperScript™ IV Reverse Transcriptase Kit (Invitrogen). After RNA to cDNA conversion, real-time PCR was performed using for each condition: 4 µL of cDNA diluted 1:10 in ultrapure water, 0.6 µL of each primer at 10 mM (Table 1), 10 µL of PowerUp™ SYBR™ Green Master Mix (Thermo Fischer Scientific) and ultrapure water up to a final volume of 20 µL. The real-time PCR run was performed using a 7500 Fast Real-Time PCR System (Applied

Biosystems). RQ values were determined for each gene and 18S ribosomal RNA was used as a housekeeping gene to normalize relative gene expression.

Western Blotting (WB). Protein extracts were prepared from EVs and cells grown in complete medium (+ FBS) or grown in simple medium for 48h (-FBS). Briefly, cells were washed and scraped on ice in lysis buffer 17 (R&D Systems) supplemented with PhosSTOP and Complete Phosphatase/Protease inhibitor cocktails (Roche Diagnostics GmbH). The whole lysate was centrifuged at 16000g for 15min and stored at -80°C. Protein concentration was determined using the BCA protein kit (Pierce, Thermo Fisher Scientific). Protein lysates were separated by gradient (4-15%) (BioRad) gel electrophoresis. After electrophoresis mediated separation, proteins were blotted to nitrocellulose membranes, which were blocked with 5% Milk or BSA (diluted in PBS-Tween 0.1%) for 1h and incubated overnight at 4°C with the following primary antibodies: anti-SDC4 mouse (8G3 clone) (1); anti-EphA4 (1:250) (Invitrogen); anti-phosphorylated EphA4 – Tyr602 (1:1000) (ECM Biosciences); anti-EGFR rabbit (1:1000); anti-phosphorylated EGFR – Tyr1068 (1:1000); anti-FAK rabbit (1:1000); anti-phosphorylated FAK rabbit – Tyr397 (1:1000); anti-Alix mouse (1:1000) (Cell Signalling); anti-β1-Integrin mouse (1:10000) (Biosciences 610468); anti-Paxillin (1:600) (Merck Millipore); anti-syntenin-1 (1:200); anti-Cytochrome-c (1:200); anti-PKCα (1:1000) (Santa Cruz Biotechnology); anti-HSP70 (1:1000); anti-CD9 (1:1000); anti-CD81 (1:1000) (System Biosciences),anti-SDC1 (1:125) (Abcam) and anti-HS (1:600) (Amsbio) primary antibodies. As loading control, membranes were incubated with anti-β-Actin (1:2000) (Santa Cruz Biotechnology) or anti-α-Tubulin (1:10000) (Sigma-Aldrich). After incubation overnight, membranes were washed three times and incubated 1h with either anti-mouse IgG (1:5000), anti-mouse IgG1 (1:10000) or anti-rabbit IgG (1:25000) secondary antibodies (all from Jackson ImmunoResearch Laboratories). Immunodetection of proteins was performed using ECL Western Blotting Detection Reagents (GE Healthcare Life Sciences). WB analysis was performed using Quantity One 1-D Analysis Software (Bio-Rad). The phospho-protein band quantification was normalized for the respective total protein amount.

Flow cytometry. Cell pellets were suspended in 5% BSA/PBS and incubated with SDC4 antibody 8G3 clone (1:200) for 45min at room temperature (RT). Incubation with rabbit anti-mouse FITC (Dako) (1:50) for 45min was carried out on RT. Negative control was performed using only the secondary antibody. Washing steps were performed with 2% BSA/PBS. The stained cells were analysed on a FACS (Fluorescence-Activated Cell Sorting) Calibur flow cytometer and data processed by using CellQuest Pro v8.0 (Becton Dickinson) and FlowJo v10.0 software.

Immunofluorescence. Cells were fixed with 4% paraformaldehyde (PFA) (Alfa Aesar) for 20min. After the blocking procedure, with goat anti-mouse serum (1:250) (Dako), permeabilization of cell membranes was performed using 0.2% triton X-100 in PBS for 10 min. PBS-Tween 0.01% was used for washing steps. The cells were stained with SDC4 8G3 clone antibody (1:200) overnight at 4ºC. Primary antibodies were diluted in 5% BSA/PBS solution. Goat anti-mouse Alexa 488 (Thermo Fisher Scientific) was used as secondary antibody, for 1h at RT. Phalloidin 568 (Invitrogen) was used to stain actin filaments and nuclei were stained with DAPI (Sigma-Aldrich). Cells were visualized using a Zeiss Imager Z.1 microscope (Zeiss).

Enzymatic digestions. HS enzymatic digestion was performed in WT and *SDC4* KO protein extracts and EVs. Protein extracts were treated with calcium acetate and Hep.III (0.005 mU/µL). After incubation overnight at 37°C with agitation, samples were stored at -80°C.

Annexin V viability assay. Cell viability was evaluated by the Annexin V-FITC staining assay. $1.5x10^5$ cells were seeded per well on 6-well plates (Corning Incorporated Costar). 48h following cell seeding, cells were enzymatically detached with trypsin (Biowest), resuspended in their culture medium and centrifuged at 100g for 5min. The supernatant was rejected, and the cell pellet was resuspended in fresh medium. Cells were washed twice in PBS, followed by another two sets of washes with Annexin V Binding Buffer (BioLegend). Each wash was followed by centrifugation at 100g for 5min. The resulting cell pellet was resuspended and incubated with Annexin V-FITC (BioLegend), diluted in a ratio of 1:40 in Annexin V Binding Buffer, for 15min at

RT. Cells were filtered and data was acquired via FACS Canto II cytometer (Becton, Dickinson and Company) and analysed with the FlowJo Software v10.0.

Proliferation assay. Cell proliferation was determined using Click-iT™ Plus EdU Alexa Fluor™ 647 Flow Cytometry Assay Kit (Molecular Probes), following manufacturer's instructions. Briefly, at day one $2.5x10^5$ cells/mL were seeded in a T25 flask in RPMI supplemented with 10% FBS and left to grow at 37ºC with 5% CO_2. In parallel, cells were also grown in simple media (without FBS). After 48h, 10µM of EdU was added to cells for a period of 1h30min prior to harvesting. EdU non-treated cells served as control while cells in simple media served as a cell arrest control. Detection of EdU incorporation into the DNA was performed according to the manufacturer's instructions. Briefly, harvested cells were washed in 1% BSA/PBS and fixed in 100 µL Click-iT1 fixative. After a 15min incubation step at RT in the dark, cells were washed again in 1% BSA/PBS and then resuspended in 100 µL saponin-based permeabilization and wash reagent. Click-iT1 EdU reaction cocktail was prepared according to the manufacturer's instructions and added. Samples were incubated for 30min at RT in the dark and washed with saponin-based permeabilization and wash reagent. Cell pellet was resuspended in 300µL saponin-based permeabilization and wash reagent and acquired using FACS Canto II cytometer, and further analysed using FlowJo software v10.0.

***In vitro* migration assay.** Migration assays were performed using the Ibidi culture-inserts family. ibidi µ-Slide 8 well with different coatings, ibiTreat surface (polymer) (Cat. No 80826), collagen IV (Cat. No 80822), fibronectin (Cat. No 80823) and poly-D-lysine (Cat. No 80824) were used with culture-inserts for self-insertion (Cat. No 80209). WT and SDC4 KO cells were seeded at a density of $2x10^4$ cells/insert with RPMI supplemented with 10% FBS. Cells were monitored during 18h for wound healing. The percentage of free area was calculated by measuring the free area at each time-point and normalizing for the initial free area measured using Image J software. The statistical analysis was performed using GraphPad Prism (version 8.0). Results are shown as average ± SD. Two-way ANOVA was used as statistical test.

***In vitro* invasion assay.** Invasion assays were performed in BD Biocoat Matrigel (Corning) invasion chambers with 8µm of diameter pore size, in 24-well plate. WT and SDC4 KOcells were seeded at a density of $7x10^4$ cells/insert with RPMI medium, using RPMI medium supplemented with 10% FBS as chemo-attractive in the lower part of the insert, for 18h. After incubation, non-invading cells were carefully removed from the upper part of the insert. The inserts were washed and fixed with cold methanol for 10min on ice. The membranes were mounted on slides with Vectashield with DAPI (Vector Laboratories). Assay with EV pre-treatment was performed as described above with a previous 24h co-culture of the cells with with $8x10^8$ particles/mL WT or *SDC4* KO #2 EVs. The total number of invasive nuclei was counted using a Leica DM2000 microscope under 200x magnification (Leica). Results are shown as average ± SD. T-student test was used for statistical analysis performed on GraphPad version 8.0.

RTK phosphorylation array. The activation state of important RTKs was determined by using the Proteome Profiler Human Phospho-RTK Array Kits (R&D Systems #ARY001B) following the manufacturer's instructions. Cells proteome was isolated from confluent cells (1x107 cells/mL) as described above. The RTK array membranes were incubated with the Array Buffer 1 for 1h at RT with continuous shaking. 300µg of whole cell lysates were diluted in Array buffer 1 to a final volume of 1.5mL and incubated on the RTK array membranes overnight at 4°C with continuous shaking. Membranes were then washed thrice with 1x Wash Buffer, 10min each wash, followed by incubation with 1:5000 Anti-Phospho Tyrosine-HRP detection antibody diluted in Array buffer 2, for 2h at RT with continuous shaking. Membranes were washed again thrice with 1x Wash Buffer and finally were developed and visualized with ECL chemiluminescent detection reagent. For signal quantification, densitometry was evaluated and the phosphorylation fold change of each RTK was calculated for KO cell model by comparison with the RTK phosphorylation values determined for the WT sample.

Isolation of EVs by ultracentrifugation and size exclusion chromatography. EV isolation and purification was performed by Ultracentrifugation (UC), followed by Size Exclusion Chromatography (SEC). Specifically, conditioned medium was collected from WT and *SDC4* KO

#2 cells (cells seeded at a concentration of $2x10^6$ cells/ 150 cm^2 plate) grown without FBS for 48h. Conditioned medium was submitted to two initial centrifugations, at 500g for 10min and 3000 g for 20min (at 10ºC) to remove cell debris. The supernatant was then filtered using 0.22µm filtration system (Corning). Media was ultracentrifuged for 2h20min at 100000 g (at 10ºC) and supernatant was discarded. For EV-tracking experiments, EVs were fluorescently labelled using either PKH67 membrane dye (PKH67GL-1KT, Sigma-Aldrich), or NIR815 membrane dye (CellVue® NIR815, Licor). A washing with saline solution (0.9% of NaCl) was performed for 2h at 100000 g (at 10ºC), after 2h at 4ºC to "auto-resuspend". Pellets were pooled together and resuspended in saline solution. All ultracentrifugations were performed with 45Ti fixed angle rotor (Beckman-Coulter) and washing steps with 70Ti fixed angle rotor. After a "auto-resuspension" step, during 2h at 4ºC, SEC was performed according to manufacturer's instructions of the qEV column (iZon). Briefly, 500µL of resuspended pellet in saline solution was overlaid on top of the qEV column. Fractions from 6 to 12 were collected and pooled together. After, samples were concentrated by ultrafiltration with 10K Amicon Ultra-15 centrifugal filter units (EMD Milipore).

Nanoparticle Tracking Analysis (NTA). All EV samples were analysed for particle concentration (particles per millilitre) and size distribution using a NanoSight NS300 system (Malvern Technologies). The NanoSight NS300 system was configured with a Red laser (638 nm) and a high sensitivity scientific sCMOS camera. For NTA analysis of the EVs, saline solution (0.9% of NaCl) as diluent and a syringe pump with constant flow injection were used. Five to nine videos of 30s using a camera level of 16 and a threshold between 5 and 7 were captured per sample. The videos were recorded and analysed by NTA software version 3.4.

EV protein concentration quantification by Bicinchoninic Acid (BCA). Protein quantification of the EV preparations was assessed by BCA assay (PierceTM BCA Protein Assay kit, Thermo Fisher Scientific) following manufacturer's instructions. Absorbance was measured at the wavelength of 562nm.

Negative-staining Transmission Electron Microscopy (TEM). EVs were visualized by TEM using negative staining. For this, 10µL of undiluted sample was mounted on Formvar/carbon film-

coated mesh nickel grids (Electron Microscopy Sciences). After 20min settling, the liquid excess was removed with filter paper and 10µL of 1% uranyl acetate was added onto the grids. Visualization was carried out on a JEOL JEM 1400 TEM at 120 kV (Tokyo, Japan). Images were digitally recorded using a CCD digital camera (Orious 1100W Tokyo, Japan).

Gold-immunolabeling microscopy. WT and *SDC4* KO #2 EVs were deposited on Formvar/carbon film-coated mesh nickel grids (Electron Microscopy Sciences, Hatfield, PA, SA) and let to settle for 20min. EVs were fixed with 2% PFA/PBS for 20min at RT. After, EVs were incubated with 50mM glycine/PBS (4x 4 min), and then with 10% BSA/PBS for 10 min. After 2h of anti-SDC4 (8G3 clone) primary antibody incubation, EVs were washed with 0.5% BSA/PBS (6x 3 min). EVs were incubated with anti-mouse Gold-conjugated secondary antibody (BBI Solutions, EM.GMHL15) in 5% BSA/PBS for 1h and then washed with 0.5% BSA/PBS (6x 3 min). Next, 10µL of 1% uranyl acetate was added onto the grids for 10sec. Visualization was carried out on a JEOL JEM 1400 TEM at 120 kV (Tokyo, Japan). Images were digitally recorded using a CCD digital camera.

Protein identification using LC-MS/MS. Proteins were solubilized with 100 mM Tris pH 8.5, 1% sodium deoxycholate, 10 mM tris(2-carboxyethyl)phosphine (TCEP) and 40 mM chloroacetamide for 10 minutes at 95ºC at 1000 rpm (Thermomixer, Eppendorf). Each sample was processed for proteomic analysis following the solid-phase-enhanced sample-preparation (SP3) protocol as described in (5). Enzymatic digestion was performed with Trypsin/LysC overnight at 37ºC at 1000 rpm. Protein identification and quantitation was performed by nanoLC-MS/MS. This equipment is composed by an Ultimate 3000 liquid chromatography system coupled to a Q-Exactive Hybrid Quadrupole-Orbitrap mass spectrometer (Thermo Scientific, Bremen, Germany). Samples were loaded onto a trapping cartridge (Acclaim PepMap C18 100Å, 5 mm x 300 µm i.d., 160454, Thermo Scientific) in a mobile phase of 2% ACN, 0.1% FA at 10 µL/min. After 3 min loading, the trap column was switched in-line to a 50 cm by 75µm inner diameter EASY-Spray column (ES803, PepMap RSLC, C18, 2 µm, Thermo Scientific) at 250 nL/min. Separation was generated by mixing A: 0.1% FA, and B: 80% ACN, with the following gradient: 5 min (2.5% B to 10% B),

120 min (10% B to 30% B), 20 min (30% B to 50% B), 5 min (50% B to 99% B) and 10 min (hold 99% B). Subsequently, the column was equilibrated with 2.5% B for 17 min. Data acquisition was controlled by Xcalibur 4.0 and Tune 2.11 software (Thermo Scientific). The mass spectrometer was operated in data-dependent (dd) positive acquisition mode alternating between a full scan (m/z 380-1580) and subsequent HCD MS/MS of the 10 most intense peaks from full scan (normalized collision energy of 27%). ESI spray voltage was 1.9 kV. Global settings: use lock masses best (m/z 445.12003), lock mass injection Full MS, chrom. peak width (FWHM) 15s. Full scan settings: 70k resolution (m/z 200), AGC target 3e6, maximum injection time 120 ms. dd settings: minimum AGC target 8e3, intensity threshold 7.3e4, charge exclusion: unassigned, 1, 8, >8, peptide match preferred, exclude isotopes on, dynamic exclusion 45s. MS2 settings: microscans 1, resolution 35k (m/z 200), AGC target $2x10^5$, maximum injection time 110 ms, isolation window 2.0 m/z, isolation offset 0.0 m/z, spectrum data type profile. The raw data was processed using Proteome Discoverer 2.5.0.400 software (Thermo Scientific) and searched against the UniProt database for the Homo sapiens reviewed Proteome 2021_03 with 20371 entries and the NIST human spectral library. A common protein contaminant list from MaxQuant was also considered. The MSPepSearch and Sequest HT search engines were used to identify tryptic peptides. The ion mass tolerance was 10 ppm for precursor ions and 0.02 Da for fragment ions for both software. Maximum allowed missing cleavage sites was set 2. Cysteine carbamidomethylation was defined as constant modification. Methionine oxidation, deamidation of glutamine and asparagine, peptide terminus glutamine to pyroglutamate, and protein N-terminus acetylation, Met-loss and Met-loss+acetyl were defined as variable modifications. Peptide confidence was set to high. The processing node Percolator was enabled with the following settings: maximum delta Cn 0.05; decoy database search target FDR 1%, validation based on q-value. Protein label free quantitation was performed with the Minora feature detector node at the processing step. Precursor ions quantification was performing at the processing step with the following parameters: Peptides to use all peptides, precursor abundance based on intensity, and normalization based on total peptide amount. For data analysis the following filters

References to SI Materials and Methods

1. G. David, B. van der Schueren, P. Marynen, J. J. Cassiman, H. van den Berghe, Molecular cloning of amphiglycan, a novel integral membrane heparan sulfate proteoglycan expressed by epithelial and fibroblastic cells. *J Cell Biol* **118**, 961-969 (1992).
2. A. M. Szász *et al.*, Cross-validation of survival associated biomarkers in gastric cancer using transcriptomic data of 1,065 patients. *Oncotarget* **7**, 49322-49333 (2016).
3. H. Li, J. Gui, Partial Cox regression analysis for high-dimensional microarray gene expression data. *Bioinformatics* **20 Suppl 1**, i208-215 (2004).
4. Y.-H. Chen *et al.*, The GAGOme: a cell-based library of displayed glycosaminoglycans. *Nature Methods* **15**, 881-888 (2018).
5. C. S. Hughes *et al.*, Single-pot, solid-phase-enhanced sample preparation for proteomics experiments. *Nat Protoc* **14**, 68-85 (2019).
6. P. Bardou, J. Mariette, F. Escudié, C. Djemiel, C. Klopp, jvenn: an interactive Venn diagram viewer. *BMC Bioinformatics* **15**, 293 (2014).

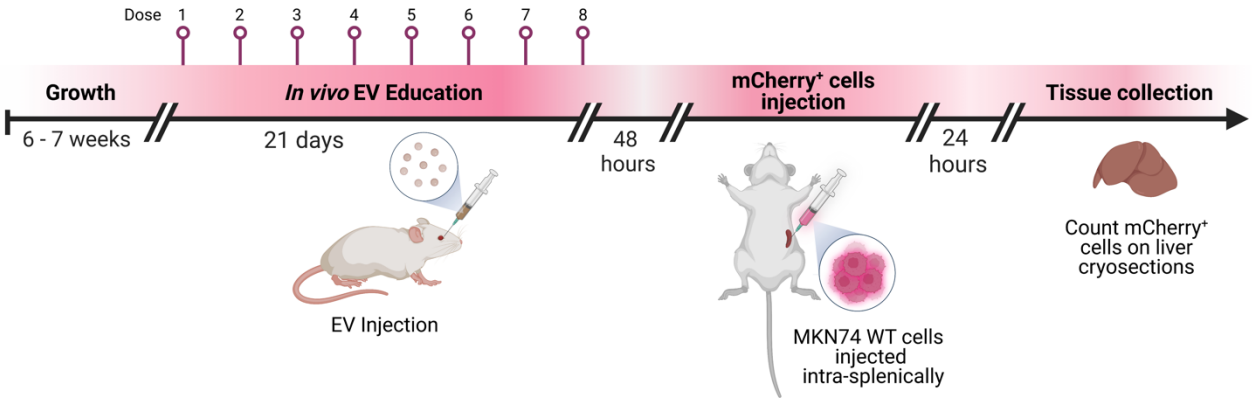
3.3 Additional Information

Gastric cancer cell seeding assay in mice liver upon EV education.

We have performed an *in vivo* experiment to address whether education with WT or SDC4 KO EVs would have an impact in the seeding of gastric cancer cells to the liver of mice (schematic representation of the EV Education experiment is showed in Figure 1a). We have started the experiment with 5 animals per experimental condition (conditions included PBS (control), WT EVs and SDC4 KO EVs), however, due to the severity of the experiment, at the day of the surgery, several animals passed a few hours after intrasplenic injection of mCherry+ gastric cancer cells. Even so, we have collected all the livers, and in the limited mice that survived (n=2 for WT and n=3 for SDC4 KO), we have performed the sucrose cryosection of the tissues. Then we analyzed and screened tissues cryosections to count mCherry+ cells. The obtained data is suggestive of higher accumulation of mCherry+ cancer cells in the vessels of the mice pre-educated with WT EVs (Figure 1b and c).

Results

a.



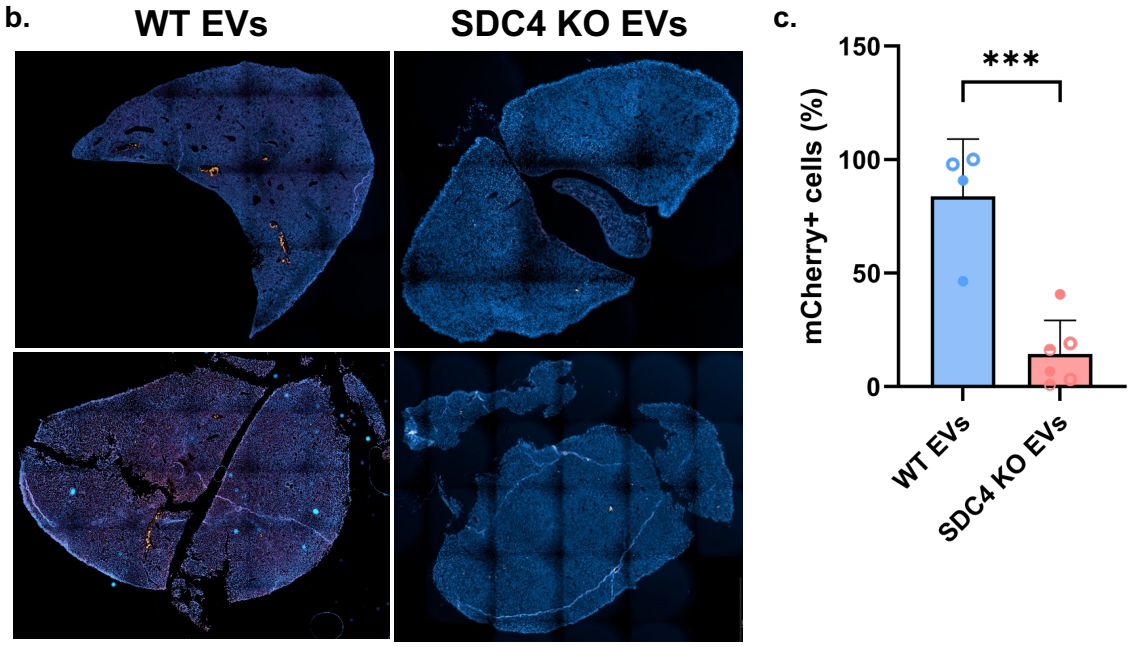


Figure 1 – Gastric cancer cell seeding assay in mice liver upon EV education. (a) Schematic representation of the experimental design. NOD SCID mice with 6-7 weeks old were retro orbital injected 3 times a week, during 21 days with Ctrl (PBS) (n=5), WT (n=5) or KO EVs (n=5). 48h after the last dose of EV injection, mice were subjected to surgery, to intra-splenically inject MKN74 WT-mCherry-labelled cells. After 24 hours, mice were sacrificed, and livers were collected for mCherry+ cells evaluation of by tissue fluorescence screening. **(b)** Panel with 2 representative photos of liver cryosections from mice educated with WT and KO EVs and injected with MKN74 WT mCherry-labelled cells. **(c)** Quantification of MKN74 mCherry+ cells. Bar graphs represent the ratio of mCherry+ cells per Hoechst+ cells + SD. Data from a single biological experiment with duplicates for mice educated with WT (n=2) and KO (n=3) EVs. Statistical significance was determined using student's t-test with Welch's correction. ***p<0.001.

Materials and Methods

mCherry transfection cells. Lentiviral particles were produced by transfecting HEK293T cells (cultured with DMEM supplemented with 10% FBS), using the Lipofectamine™ 2000 transfection reagent (Invitrogen, USA), according to the manufacturer's instructions. Briefly, HEK293T subconfluent cultures were transfected with three distinct plasmid vectors: 2,5 µg of an mCherry-coding plasmid (Addgene #72269), 2 µg of psPAX2 plasmid envelop (Addgene #12260), and 1 µg of pVSV-G plasmid packaging (Addgene #138479). 6h after transfection, the medium was changed to packaging medium (Opti-MEM plus 5% FBS and 1 mM pyruvate (Gibco, USA). The viral supernatant was collected by centrifugation and filtered with 0.45 µm pore filters (VWR, USA), 48h and 72h after transfection. The viral supernatant was added to MKN74 subconfluent cultures in a 1:3 ratio. 48h after transduction, mCherry expression was assessed using a Zoe fluorescence microscope (Bio-Rad, USA). mCherry-positive cells were selected with 10 µg/mL of puromycin (InvivoGen, USA).

EV education studies. 6-7 weeks old female mice pre-educated for 21 days, 3-times a week, with PBS (Ctrl), WT and KO EVs were injected intra-splenically with $2x10^6$ MKN74 mCherry-labelled cells suspended in 30µL matrigel (Corning). 24h after surgery, mice were sacrificed, and livers were collected.

Tissue processing and nuclei staining. For histological analysis, the dissected tissues were fixed in a mix of 2% PFA and 20% sucrose solution. After overnight fixation, tissues were washed 3-times in PBS and embedded in 30% sucrose solution. After incubation, tissues were transferred to a new plate and embedded in a mix of 30% sucrose with Tissue-tek O.C.T. (Electron Microscopy Sciences) and left overnight. Blocks were frozen in a dry ice using the embedding solution of inclusion media (OCT) and sucrose 20%. Liver sections were then stained with Hoechst for nuclear staining and histological evaluation and analyzed for mCherry-positive cells using Operetta CLS High Content Analysis System (PerkinElmer). Quantification of MKN74 mCherry+ cells was performed by calculating the ratio of mCherry+ cells per Hoechst+ cells in two tissue sections from each analyzed animal.

CHAPTER IV

EV isolation methodologies and PG analysis

THIS CHAPTER CONTAINS THE FOLLOWING PUBLICATION:

Poças J and Belting M. Analysis of Extracellular Vesicle-Associated Proteoglycans. In: Karamanos, N.K. (eds) Proteoglycans. Methods in Molecular Biology. 2023, vol 2619. Humana, New York, NY. https://doi.org/10.1007/978-1-0716-2946-8_10.



Chapter 10

Analysis of Extracellular Vesicle-Associated Proteoglycans

Juliana Poças and Mattias Belting

Abstract

Extracellular vesicles (EVs) have emerged as a central mechanism of intercellular communication in physiology and disease. EVs participate in paracrine exchange of nucleic acids as well as lipids, proteins, and glycans to elicit a complex biological response in target cells. Proteoglycans (PGs) are widely expressed in EV-producing cells and are sorted to the membrane of secreted EVs to participate in some of the key processes in EV-mediated signaling. Most notably, PGs mainly of the heparan sulfate (HS) type are involved in EV biogenesis and cellular uptake of EVs through endocytic processes. EV-associated PGs may serve as short- and long-range chaperones of signaling molecules with potential implications for intercellular information exchange, most importantly in cancer development. This motivates the development of approaches targeting EV-HSPG interactions as a strategy in cancer treatment. Moreover, the importance of PG remodeling and alterations in their expression in cancer, together with the fact that EVs mimic their cell or tissue of origin, point at an important role of EV-associated PGs as disease biomarkers. Here, we provide methodological insights into the analysis of EV-PGs isolated from cell cultures as well as patient plasma liquid biopsy.

Key words Proteoglycans, Extracellular vesicles, Cancer, Proteomics, Biomarker

1 Introduction

Glycoconjugates and particularly proteoglycans (PGs) emerge as important players in the modulation of the tumor microenvironment, with critical roles in extracellular matrix (ECM) structuring and cancer cell communication [1, 2]. PGs are complex macromolecules constituted by a core protein decorated with linear glycosaminoglycan (GAG) chains including alternating glucuronic acid and N-acetylglucosamine or N-acetylgalactosamine residues, giving rise to heparan sulfate PGs (HSPGs) and chondroitin sulfate PGs (CSPGs), respectively. The polysaccharide chains are further modified by epimerization of glucuronic acid into iduronic acid and by sulfation. The specific sulfation together with the carboxyl groups

Nikos K. Karamanos (ed.), *Proteoglycans: Methods and Protocols*,
Methods in Molecular Biology, vol. 2619, https://doi.org/10.1007/978-1-0716-2946-8_10,
© The Author(s), under exclusive license to Springer Science+Business Media, LLC, part of Springer Nature 2023

lead to a polyanionic structure. PGs are thus prone to interactions with domains of basic amino acids present in a wide variety of protein ligands, including pro-tumorigenic growth factors and cytokines.

More recently, a growing body of evidence establishes that cell surface PGs are regulators of extracellular vesicle (EV) biogenesis [3] and can serve as internalizing receptors of cancer cell-derived EVs [2, 4]. HSPGs have been shown to internalize and co-traffic with a wide variety of protein ligands and particle structures [5, 6], including EVs that mainly include microvesicles, 100–1000 nm in diameter, and exosomes, 30–50 nm in diameter. EVs are actively produced by cancer cells and exert major roles in defining, e.g., metastasis organ tropism [7]. EV surface PGs, in analogy with cell surface PGs, may constitute binding platforms for growth factors, enzymes, and cytokines, thus protecting them from proteolytic degradation, which together with relatively high dissociation rates allows dynamic exchange of interacting ligands with signalling receptors on target cells.

EVs can be isolated from biological fluids and cell cultures for monitoring of specific pathophysiological processes. Of note, elevated levels of EVs have been found in the circulation of patients with cancer, which may be related to the increased proliferative activity as well as the leaky tumor vasculature allowing escape of EVs to the circulation. EVs have evoked considerable interest as biomarkers for the diagnosis and monitoring of cancer. This is particularly attractive when tumor tissue is relatively inaccessible for biopsy, most importantly in brain tumor patients [8, 9]. Thus, the identification of a defined PG profile in EVs secreted into body fluids can constitute a valuable biomarker for noninvasive liquid biopsy-based diagnosis of brain tumors but also of other cancers.

Here, we present a step-by-step strategy to improve the characterization of PGs associated with EVs, derived either from in vitro conditions (cell conditioned medium) or from patient plasma liquid biopsies (*see* Fig. 1). We describe the use of ultracentrifugation (UC) and size exclusion chromatography (SEC) for EV isolation and proteomic characterization. Metabolic labeling of PGs through incubation of EV donor cells with [^{35}S]-sulfate and downstream purification by anion-exchange chromatography using DEAE-cellulose is described. The [^{35}S]-radioactivity can be used for PG analysis by autoradiography following gel electrophoresis and enzymatic digestion of specific GAG chains as a sensitive tool to quantify relative amounts of PGs in EVs from different models systems and conditions.

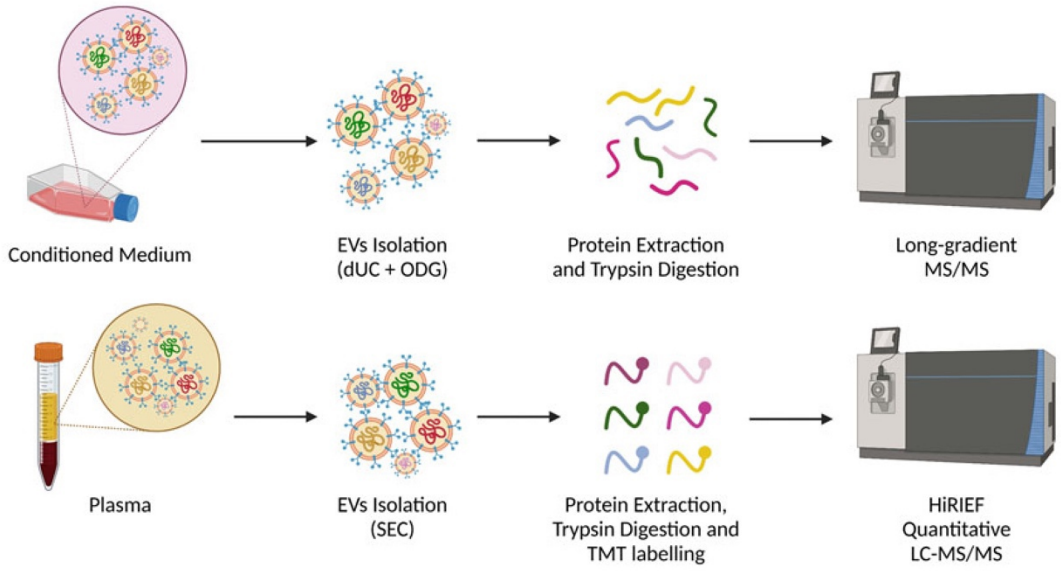


Fig. 1 Schematic representation of LC-MS/MS proteomic analysis of EVs isolated from conditioned medium (CM) through ultracentrifugation (UC) plus Optiprep density gradient (ODG) and patient plasma EVs isolated by size exclusion chromatography (SEC). EVs isolated by both UC and SEC are submitted to protein extraction and trypsin digestion. Specifically, peptides from plasma EVs are labeled with tandem mass tags (TMT), allowing a precise peptide quantification by HiRIEF high-resolution LC-MS/MS

2 Materials

2.1 EV Isolation

1. Sucrose solution: Weigh 0.25 M of sucrose, add 10 mM Tris–HCl in Milli-Q water until 1 L and check the pH (pH = 7.5).
2. OptiPrep™ 60% (w/v) aqueous iodixanol solution.
3. 0.22 μm polyethersulfone (PES) filters, Corning.
4. Ultraclear tubes for ultracentrifugation (UC), Beckman.
5. qEV columns, iZon.
6. 10 kDa Amicon Ultra-15 centrifugal filter units, Merck.
7. Eppendorf low binding protein tube, Axygen.
8. BCA Protein Assay Kit, Pierce™, Thermo Fisher.

2.2 Sample Preparation for MS/MS Analysis

1. Dithiothreitol (DTT).
2. Iodoacetamide (IAA).
3. Ammonium bicarbonate (Ambic).
4. Sequencing grade trypsin, Promega.
5. Trifluoroacetic acid (TFA).
6. Mass spectrometry water (MS water).

7. C18 membrane and peptide desalting.
8. Acetonitrile (AcN).
9. Nanodrop.

High-Resolution Isoelectric Focusing (HiRIEF) Quantitative LC-MS/MS

10. *Lysis buffer (LB) – 4% SDS, 50 mM HEPES pH 7.6, 1 mM DTT.*
11. *Chloroacetamide (CAM).*
12. *Sera-Mag Speed Beads (SP3 beads), GE Healthcare.*
13. *LysC buffer: 1 M urea, 50 mM HEPES, Milli-Q water to make up volume.*
14. *Trypsin buffer: 50 mM HEPES solution.*

2.3 Glycosaminoglycan Digestion

1. Dulbecco's Modified Eagle Medium (DMEM) or other cell medium, as appropriate for the chosen cell type, with and without 10% fetal bovine serum (FBS).
2. Cell type of choice from commercial vendor (e.g., ATCC) or primary cell cultures grown in medium with 10% FBS supplemented with glutamine and penicillin/streptomycin.
3. Phosphate-buffered saline (PBS): 137 mM NaCl, 2.7 mM KCl, 10 mM Na2HPO4, 1.8 mM KH_2PO_4, pH 7.4.
4. Heparinase III (E.C. 4.2.2.8, Sigma-Aldrich) (*see* **Note 1**).
5. Chondroitinase ABC (E.C. 4.2.2.4, Sigma-Aldrich). Store at −20 °C (*see* **Note 2**).
6. Heparinase buffer: 50 mM NaOAc, 150 mM NaCl, 5 mM $CaCl_2$, 50 mM HEPES-HCl, pH 6.5, 0.5× complete protease inhibitor w/o EDTA.
7. ABC'ase buffer: 40 mM NaAc, 40 mM Tris–HCl, pH 7.8, 0.5× complete protease inhibitor w/o EDTA.

2.4 [^{35}S]-Sulfate PG Labeling, DEAE Anion-Exchange Chromatography, and Gel Electrophoresis

1. Modified Eagle Medium (MEM) w/o $MgSO_4$, Invitrogen.
2. [^{35}S]-SO_4, PerkinElmer.
3. Two % Tx-buffer: 0.15 M NaCl, 10 mM KH_2PO_4, 10 mM EDTA, 5 μg/mL ovalbumin (OVA), pH 7.5, 2% Triton X-100, 1× Complete Protease Inhibitor, Roche.
4. DE52 pre-swollen DEAE-cellulose matrix, Sigma-Aldrich (*see* **Note 3**).
5. Poly-Prep chromatography columns, Bio-Rad.
6. PD-10 desalting column, Sigma-Aldrich.
7. Equilibration (eq.) buffer: 7 M urea, 10 mM Tris–HCl, pH 8.0, 0.1% Triton X-100 (*see* **Note 4**).
8. Urea-B buffer: 6 M urea, 0.5 M HAc, 5 μg/mL OVA, pH 5.8, 0.1% Triton X-100.

9. Urea-C buffer: 6 M urea, 10 mM Tris–HCl, 5 μg/mL OVA, pH 8.0, 0.1% Triton X-100.
10. Tris-buffer: 0.05 M Tris–HCl, pH 7.5.
11. Four M Gu-buffer: 4 M Gu–HCl, 50 mM HAc, 5 μg/ml OVA, pH 5.8, 0.2% Triton X-100 (*see* **Note 5**).
12. Dextran, Sigma-Aldrich.
13. Dextran-sulfate, Sigma-Aldrich.
14. Resuspension buffer: 1 M NaCl, 10 mM Tris–HCl, pH 7.5, 0.05% Triton X-100.
15. Four × LDS NuPAGE sample buffer, Invitrogen.
16. Four to twelve % NuPAGE Bis–Tris gel, Invitrogen.
17. Glycerol solution: 30% ethanol, 5% acetic acid, and 2.5% glycerol.

2.5 Immunoblot Analysis of HSPG Core Protein Profile

1. Tris-buffered saline (TBS): 25 mM Tris–HCl, 150 mM NaCl, 2 mM KCl, pH 7.4.
2. TTBS, TBS supplemented with 0.5% Tween-20, Sigma-Aldrich.
3. Dry milk powder, Sigma-Aldrich.
4. Mouse monoclonal 3G10 anti-ΔHS antibody, Seikagaku.
5. HRP-conjugated sheep anti-mouse, Thermo Fisher Scientific.

3 Methods

3.1 EV Isolation from Conditioned Medium

3.1.1 Differential Ultracentrifugation (dUC)

1. Filter conditioned medium (CM) with 0.22 μm polyethersulfone (PES) filter.
2. Fill tubes for ultracentrifugation (UC). Tubes must be filled the maximum possible. To adjust volume, add saline solution (mass difference should be less than ±0.02 g) (*see* **Note 6**).
3. Ultracentrifuge the supernatant at 100.000 g, overnight at 10 °C (*see* also **Note 7**).
4. Discard the upper part of the supernatant. Leave 3 mL of supernatant and resuspend the pellet.
5. Fill the tube with saline solution and scale tubes. To adjust volume, add saline solution (difference should be less than ±0.02 g).
6. Ultracentrifuge at 100.000 g, for 2 h at 10 °C.
7. Discard the supernatant. Leave 500 μL of supernatant and resuspend the pellet. Keep at 4 °C until next isolation step.

3.1.2 Optiprep Density Gradient (ODG)

1. Prepare the gradient solutions the day before use according to table: Gradient 40% (3 mL), 20% (3 mL), 10% (3 mL), 5% (2.5 mL), and then saline solution, plus sample volume (5.5 mL).

Gradient	Optiprep	Sucrose
40%	26.6 mL	13.4 mL
20%	13.3 mL	26.7 mL
10%	6.6 mL	33.4 mL
5%	3.3 mL	36.7 mL

2. From dUC method (3.1.1.7), the sample diluted in 500 μL at 4 °C is further diluted in 3 mL saline.
3. Tilt the tube in nearly horizontal position and let the solution fall drop by drop without touching the wall of the tube.
4. Tilt the tube in vertical position and allow the "menisc" to form (to retrieve also the drops on tube wall). Add an additional 2 mL saline to "clean" the tube.
5. In the end, add 500 μL of sample (total 5.5 mL).
6. Scale the tubes.
7. Ultracentrifuge overnight at 100.000 g, at 10 °C.

3.1.3 Fraction Collection

1. Collect fractions with the micropipette from the upper surface level, gently. The first 5 mL can be discarded.
2. Separate fractions of 1 mL. Usually EVs are present in fractions 6 and 7. Each of the 12 fractions should be weighed for density assessment.
3. Transfer the fractions of interest to 10 kDa Amicon Ultra-15 centrifugal filter units.
4. Add saline solution until reaching maximum volume of 4 mL.
5. Centrifuge, at 16.000 g, for 30 min, at room temperature (RT).
6. Transfer the concentrated sample to a new Eppendorf tube.
7. Separate an aliquot to perform BCA protein quantification.
8. Proceed directly for proteomic analysis or keep samples at −80 °C.

3.2 EV Isolation from Plasma

3.2.1 Size Exclusion Chromatography (SEC) Using qEV Columns

1. Remove the lower luer-slip cap and rinse the column (*see* **Note 8**) with at least 10 mL of PBS with 2 mM of EDTA (*see* **Notes 9**, **10**, and **11**). See also **Note 12** for selection of qEV column.
2. With the bottom luer-slip cap on, pipette out the buffer above the top filter. Load 500 μL of sample. Immediately remove the bottom cap.

3. Immediately start collecting 0.5 mL fractions.
4. Add PBS with 2 mM of EDTA (up to 2 mL each time).
5. Fractions from 1 to 6 (± 3 mL) constitute the void volume, which contains particles larger than EVs.
6. Collect the fractions from 7 to 11 (± 2.5 mL) containing the EVs (*see* **Note 13**).
7. The column can be extensively washed with PBS with 2 mM of EDTA (approximately 45 mL) for repeat use, until a maximum of five times.
8. Concentrate the collected fractions by centrifugation in 10 kDa Amicon Ultra-15 centrifugal filter units. Centrifugation at maximum speed, for 30 min at RT.
9. Separate an aliquot to perform protein quantification.
10. Proceed for proteomic analysis or keep samples at −80 °C.

3.2.2 Sample Preparation for MS/MS Analysis

1. Resuspend protein solution in 5× sample volume of 6 M Urea, vortex, and keep at RT for 60 min.
2. Reduce the samples with DTT (stock solution of 0.5 M) until a concentration of 10 mM. Vortex 2 s to mix, and incubate for 1 h at 56 °C with gentle shaking.
3. Alkylate with 50 mM (final concentration) IAA at RT for 30 min in dark.
4. After alkylation, dilute the sample with 50 mM ammonium bicarbonate (Ambic) (pH 8).
5. Trypsinize the samples with sequencing grade trypsin (concentration at 0.4 μg/μl in AmBic), overnight at 37 °C with gentle shaking.
6. Stop trypsinization by adding 2% TFA (1:10 v/v).
7. Concentrate the samples by speed vacuum.
8. At this stage, store the samples at −20 °C or resuspend the pellet in 100 μL of 0.1% TFA in MS water for C18 membrane purification and concentration.
9. C18 membrane purification:
   (a) Prepare solutions:
      (i) Column calibration: 0.1%TFA in AcN (acetonitrile).
      (ii) Wash solution/solvent: 0.1% TFA in MS water.
      (iii) Elution solution: 50% AcN, 0.1% TFA in MS water.
   (b) Resuspend sample in 100 μL solvent solution.
   (c) Prepare C18 column (capacity 3–30 μg).
   (d) Add 100 μL column calibration buffer.
   (e) Centrifuge at 100 g for 1 min.

(f) Wash 2× with 100 µL wash solution.
(g) Centrifuge 100 g, 1 min each.
(h) Add peptide sample to the column. Change for new low binding protein tubes.
(i) Centrifuge 100 g for 1 min.
(j) Wash 2× with 100 µL wash solution.
(k) Centrifuge at 200 g, 1 min each.
(l) Elute samples with 50 µL elution solution into a new low binding protein tube.
(m) Centrifuge at 200 g, 1 min.

10. Speed-vacuum dry. At this point, proceed with the protocol or keep samples at −80 °C.
11. Resuspend the peptide sample in 2% AcN, 0.1% TFA.
12. Centrifuge at 14,000 g for 10 min, to remove any particles.
13. Measure the peptide concentration with Nanodrop (absorbance 215 nm), dilute the sample to the right concentration in 2% AcN, 0.1% TFA, without touching the bottom of the tube (*see* **Note 14**).

3.2.3 Proteomic Profile: Long Gradient, Tandem Mass Tag (TMT), and HiRIEF Quantitative LC-MS/MS [10] or Other MS/MS Method of Choice

1. Thawed samples on ice and at 4 °C. Concentrate the samples using 10 kDa filters and centrifuge at 3,000 g for 30 min.
2. Add LB to each sample; the LB volume should be equal to the concentrated sample volume.
3. Heat at 95 °C for 10 min.
4. Measure protein concentration.
5. Proceed with defined protein concentration.
6. Spin down. Sonicate for 30 s.
7. Let samples cool down for 15 min at RT.
8. Add chloroacetamide (CAM) to a final concentration of 5 mM. Incubate samples at RT for 10 min.
9. Proceed to "SP3-beads based protein extraction" step.

SP3-Bead-Based Protein Extraction

1. *Add 20 µL beads to each sample. Mix gently.*
2. *Add 1 mL of acetonitrile (100% AcN) to each sample.*
3. *Mix for 30 min on rotator.*
4. *Shake vials properly so that all beads attached to walls come into solution.*
5. *Place tubes on magnetic stand. The beads will immediately come out of solution and get attached to the tube walls. Gently discard the supernatant.*

6. *Wash twice with 70% ethanol (EtOH) and discard the supernatant.*
7. *Wash once with AcN (100%) and discard the supernatant.*
8. *Proceed immediately to the "Protein Digestion" step and do not let the beads dry.*

Protein Digestion

1. *Remove the tubes from magnetic stand and add 100 μL Lys-C solution to each sample. Incubate for 3 h at 37 °C on shaker.*
2. *Add 100 μL trypsin solution to each sample. Incubate overnight at 37 °C on shaker.*
3. *Place tubes on magnetic stand. Collect the peptides in fresh tubes.*
4. *Measure peptide concentration. Prepare aliquots of 25 μg peptide/sample for TMT labeling. Speed vacuum the samples and freeze at −20°C.*

TMT Labeling

1. *Add 50 μL of 100 mM TEAB to each sample. Resuspend the pellet into solution properly.*
2. *Add 20 μL of TMT label per sample. Place TMT-labeled samples on shaker at RT for 1 h.*
3. *Use 1 μL of each labeled sample for label check using LC-MS.*
4. *Here, >98% of peptides for all samples normally carry the label, if successful.*
5. *After label check, the samples of each TMT set can be pooled together.*
6. *Speed vacuum the four TMT set vials* (see ***Note 15***).

Strong Cation Exchange (SCX) Column-Based Cleaning of TMT-Labeled Peptide Pool

1. *Dissolve each TMT set peptide pool in 500 μL of 50 mM HEPES.*
2. *Acidify the sample solution using 10% formic acid.*
3. *Wash columns with 600 μL of 100% methanol.*
4. *Equilibrate column with 100 μL water.*
5. *Add sample to SCX column.*
6. *Wash with 600 μL wash solution.*
7. *Elute peptides with 600 μL elute solution.*

HiRIEF-Based Peptide Fractionation

1. *Dissolve each TMT set peptide pool in 250 μL of 8 M urea.*
2. *Add 2.5 μL of pharmalyte [3–10 pH].*

3. *Add a touch of bromophenol blue dye to each sample.*
4. *Vortex the sample vial and spin down.*
5. *Load the samples in gel strip [3–10 pH] and leave for adsorption overnight.*
6. *The gel strip is first focused, followed by peptide extraction from the gel into 72 contiguous fractions (Milli-Q water/35% AcN/35% AcN, 0.1% TFA) collected in a 96-well plate (V-bottom) using an IPG extractor robot.*
7. *Speed vacuum the plates and submit for TMT16-plex specific LC-MS/MS analysis.*

3.3 Bioinformatics Tools for Posterior Analysis

1. The GlycoGene DataBase (GGDB, http://acgg.asia/ggdb2/) includes identified genes related to glycan synthesis.
2. MatrixDB (http://matrixdb.univ-lyon1.fr/) is focused on extracellular interactions.

3.4 [^{35}S]-Sulfate PG Labeling, DEAE Purification, and Autoradiographic Visualization of EV-Associated PGs

1. Seed cells of choice in 75-cm2 flasks and allow the cells to grow for 24 h (to approximately 80% confluence).
2. Rinse the cell layer with 15 mL PBS.
3. Starve cells for 1 h at 37 °C in sulfate-free medium (MEM).
4. Aspirate medium, add 10 mL sulfate-free medium supplemented with 100 μCi/mL [^{35}S]-sulfate, and incubate overnight.
5. Wash cells twice with PBS, add 10 mL of serum-free medium, and incubate cells for 48 h.
6. Aspirate the medium and collect EVs as described under Subheading 3.1.
7. Lyse EV in 1.5 mL 2% Tx-buffer for 20 min on a shaker at RT.
8. Spin the lysate at 4,500 g for 10 min and keep the supernatant.
9. Add one volume Eq.-buffer to the supernatant.
10. Purify PGs on an equilibrated DEAE-cellulose column as follows:
    (a) Load 0.5 mL of DE-52-matrix (*see* **Note 15**).
    (b) Equilibrate column with 5 mL Eq.-buffer.
    (c) Add 50 μg dextran and 50 μg dextran-sulfate to the sample as carrier.
    (d) Add the sample to the column. Discard the flow-through.
    (e) When the sample has passed through the column, wash the column with 5 mL Urea-B.
    (f) Wash column with 5 mL Urea-C.
    (g) Wash with 5 mL Tris-buffer.

(h) Elute the PGs by sequential addition of 5 × 0.5 mL Gu-buffer. Allow all liquid from each buffer addition to flow-through, before adding the next volume.

11. Add 50 μg dextran to the sample and take off 1/50 volume (50 μL, for DPM measurement).
12. Precipitate the sample with 4.5 volumes of −20 °C pre-cooled 95% ethanol. Make sure the solution is well mixed and keep overnight at −20 °C.
13. Spin sample at 4,500 g for 10 min and discard the supernatant.
14. Wash once with ice-cold 95% ethanol and air-dry.
15. Suspend pellet in 2.5 mL resuspension buffer. Make sure the pellet is dissolved completely (*see* **Note 16**).
16. Desalt sample with PD-10 at 4 °C. Equilibrate the column in water and elute with 3.5 mL water.
17. Take off 1/50 volume of the eluate (for DPM measurement).
18. Divide sample into three fractions (see **Note 17**).
19. Put samples in −80 °C freezer.
20. Speed-vacuum-dry samples.
21. Dissolve two fractions in 100 μL HS'ase buffer (one sample as nondigested control) and one fraction in 100 μL ABC'ase buffer.
22. Add 0.6 mIU heparinase III to the HS'ase sample and 40 mU chondroitinase ABC to the ABC'ase sample. Add no enzyme to the nondigested control sample in HS'ase buffer.
23. Incubate for 3 h at 37 °C.
24. Repeat enzyme additions and incubate at 37 °C, overnight. Also, keep the nondigested sample in HS'ase buffer at 37 °C.
25. Add one-third volume of 4× LDS to all samples (*see* **Note 18**).
26. Load at least 5,000–10,000 DPM (as determined at **step 17**) of each sample on a 4–12% NuPAGE Bis–Tris gel and separate proteins for approximately 1 h at 200 V.
27. Fix and equilibrate gel in glycerol solution for 30 min.
28. Dry gel to a pre-wetted filter paper on a gel-dryer, for 2 h at 80 °C or until completely dry.
29. Visualize intact and digested PGs using autoradiographic film or [^{35}S]-sensitive autoradiographic plate after overnight exposure.

3.5 Immunoblot Analysis of EV-Associated HSPG Core Protein Profile

In order to characterize which HSPG core proteins that are associated with EVs, an appropriate first step is to characterize the HSPG core protein composition. This can be done using the anti-ΔHS antibody 3G10, Amsbio.

1. Isolate EV-PGs from at least two 75-cm^2 flasks, according to the method described under Subheading 3.4, **steps 1–16** (metabolic labeling can be omitted in order to purify nonradioactive PGs).
2. Divide the desalted purified PGs into two fractions.
3. Put samples in −80 °C freezer.
4. Freeze-dry samples.
5. Dissolve the two fractions in 50 μL HS'ase buffer (one digested sample and one nondigested control).
6. Add both 0.6 mIU heparinase III and 40 mU chondroitinase ABC to the sample to be digested (*see* **Note 19**).
7. Incubate for 3 h at 37 °C.
8. Repeat enzyme additions and incubate at 37 °C, overnight. Also, keep the nondigested sample in HS'ase buffer at 37 °C.
9. Add one-third volume of 4× LDS to all samples.
10. Load, at least, a sample amount corresponding to the material from 4-cm^2 of cells per lane on a 4–12% NuPAGE Bis–Tris gel and separate proteins.
11. Transfer proteins to a PVDF membrane.
12. Block the PVDF membrane for 30 min with 5% dry milk in TTBS.
13. Probe the membrane with anti-ΔHS (3G10) antibody (1:1000 in 5% dry milk in TTBS) overnight at 4 °C.
14. Wash membrane 3 × 5 min in TTBS.
15. Probe membrane with appropriate HRP-conjugated secondary antibody.
16. Visualize protein bands using standard ECL substrate and chemiluminescence detection system (*see* **Note 20**).

4 Notes

1. Powder can be reconstituted in 20 mM Tris–HCl (pH 7.5) containing 0.1 mg/mL BSA and 4 mM $CaCl_2$. The enzyme preparation is stable for 1 week at −20 °C.
2. Lyophilized powder should be reconstituted in distilled water containing 0.01% BSA. Further dilutions can be made with a buffer containing 50 mM Tris (pH 8.0), 60 mM sodium acetate, and 0.02% BSA. Solutions should be prepared fresh.
3. Reconstitute the dry DEAE-cellulose in water to approximately 50% matrix suspension or slurry (v/v).

4. Urea in solution is in equilibrium with ammonium cyanate that can react covalently with proteins. Therefore, dissolve urea in water and prepare buffer immediately after complete dissolution. Do not heat the solution. Alternatively, a dissolved urea stock solution can be stored at 4 °C and purified by anion-exchange chromatography prior to preparation of buffers.
5. The use of practical grade Gu–HCl requires removal of impurities by activated charcoal. Dissolve practical grade of Gu–HCl in water. Purify the solution by the addition of approximately 10 g/L of activated charcoal. Stir overnight at 4 °C and clear solution by filtration two times over two layers of filter paper. Add remaining buffer constituents and adjust pH.
6. The typical yield of EVs is 30 ug per subconfluent (80%) 75-cm^2 culture flask but varies greatly between cell lines and time for collection of EVs, which typically is 24–72 h. For increased cell viability, BSA or EV-depleted serum can be added, thereby reducing contamination with debris from dead cells.
7. Optimal settings for ultracentrifuge: Acceleration and deceleration on maximum; confirm the compatible tubes for each rotor in use. The type of tubes will depend on rotor in use. For UC, normally ultraclear tubes (Beckman) for large volumes must be used; for ODG, ultraclear thinner tubes (Beckman) must be used.
8. Use a column holder, making sure that the column is vertical.
9. Columns are stored at 4 °C, with ≤0.05% w/v sodium azide (toxic in large quantities).
10. Elution buffer should be filtered (0.2 μm) to avoid introducing particulate contamination.
11. Do not allow the column to run dry.
12. There are different qEV columns. Depending on sample volume, consider using columns for 500 μL (qEV original) or 1 mL (qEV1). There are two types: 35 nm and 70 nm, and selection should be based on the different EV size recovery ranges (35–350 nm and 70–1000 nm, respectively).
13. Collect the fractions from 7 to 11 (± 2.5 mL) containing the EVs. Typically, EVs start to elute in fraction 6 (start counting fractions after sample loading on column); however, this can vary depending on EVs from CM or plasma. Consider to collect other fractions depending on the aimed final volume, EV yield, and purity (without contaminants by, e.g., protein aggregates).

14. The concentration of peptides to inject may be dependent of the MS instrument. Typically, 1 μg is the concentration advised.
15. Label check is a quick LC-MS run of 30 min with simple database search to determine how many peptides (or peptide-spectrum matches [PSMs]) carry the TMT label and how many are label free.
16. De-gas the DE-52 slurry for several minutes before packing the columns. Resuspend the slurry with an automatic pipette and be careful not to introduce air-bubbles. Pack columns by the addition of approximately two times the intended column matrix volume.
17. In order to obtain complete enzymatic digestion in subsequent steps, it is important to remove as much guanidine as possible. Resuspension of the precipitated pellet in a buffer containing 1 M NaCl competes off most guanidine counter-ions bound to GAGs. Also, make sure the pellet is completely dissolved, as there otherwise will be substantial sample loss.
18. As the EV-associated PGs of most cell types are either HS or CS substituted, the intact PG after heparinase and chondroitinase digestion is primarily CS and HSPG, respectively. If the enzyme digestions are complete, the reduction in [^{35}S]-sulfate radioactivity in the high-molecular weight region after heparinase digestion should correspond roughly to the remaining signal intensity after chondroitinase digestion. This signal represents the HSPG pool of the total cell-associated PG and vice versa for the CSPG pool.
19. If additional analyses are to be performed on the purified PG, the sample can be frozen at −80 °C before the addition of 4× LDS-buffer, which may interfere and make subsequent assays impossible.
20. Certain syndecan HSPGs can, in addition to being HS substituted, also bear CS chains. In order to obtain gel bands at positions reflecting the size of the core protein, it is critical that all GAG chains are degraded. Thus, samples must be both heparinase and chondroitinase treated.
21. HSPG core protein bands appear specifically in GAG lyase-treated samples. In initial experiments, it is advised to include a lane with no PG, containing only GAG lyases. This is in order to exclude that bands appearing in digested lanes are the result of unspecific detection of constituents of the enzyme preparations.
22. This antibody recognizes a neoepitope produced by heparinase III digestion ("HS-stub"). The antibody can thus be used to detect all HSPG core proteins on an immunoblot. Ideally, the identities of the detected bands are confirmed by either core

protein-specific antibodies or by siRNA-mediated core protein knock down. However, conclusions can be drawn directly from the molecular weight of the detected bands as the different syndecans have different masses. In contrast, all glypicans are approximately 60 kDa.

References

1. Couchman JR, Multhaupt H, Sanderson RD (2016) Recent insights into cell surface Heparan Sulphate proteoglycans and cancer. F1000Res 5:5
2. Belting M (2014) Glycosaminoglycans in cancer treatment. Thromb Res 133:S95–S101
3. Baietti MF et al (2012) Syndecan–syntenin–ALIX regulates the biogenesis of exosomes. Nat Cell Biol 14(7):677–685
4. Christianson HC et al (2013) Cancer cell exosomes depend on cell-surface heparan sulfate proteoglycans for their internalization and functional activity. Proc Natl Acad Sci 110(43):17380
5. Mani K et al (2003) Prion, amyloid beta-derived cu(II) ions, or free Zn(II) ions support S-nitroso-dependent autocleavage of glypican-1 heparan sulfate. J Biol Chem 278(40): 38956–38965
6. Wittrup A et al (2007) Identification of proteins released by mammalian cells that mediate DNA internalization through proteoglycan-dependent macropinocytosis. J Biol Chem 282(38):27897–27904
7. Peinado H et al (2017) Pre-metastatic niches: organ-specific homes for metastases. Nat Rev Cancer 17(5):302–317
8. Indira Chandran V et al (2019) Ultrasensitive Immunoprofiling of plasma extracellular vesicles identifies Syndecan-1 as a potential tool for minimally invasive diagnosis of glioma. Clin Cancer Res 25(10):3115–3127
9. Papiewska-Pająk I et al (2020) Glypican-1 level is elevated in extracellular vesicles released from MC38 colon adenocarcinoma cells overexpressing snail. Cell 9(7)
10. Panizza E et al (2017) Isoelectric point-based fractionation by HiRIEF coupled to LC-MS allows for in-depth quantitative analysis of the phosphoproteome. Sci Rep 7(1):4513–4513

CHAPTER V

Disclosing EV signature along the gastric carcinogenesis

THIS CHAPTER CONTAINS THE FOLLOWING MANUSCRIPT IN PREPARATION:

Poças J, Faria-Ramos I, Santos-Antunes J, Branca RM, Carneiro F, Macedo G, Reis CA, Belting M, Magalhães A. Proteomic profiling of extracellular vesicles along the gastric carcinogenesis cascade. *In preparation*

Proteomic profiling of extracellular vesicles along the gastric carcinogenesis cascade

Juliana Poças[1,2,3], Isabel Faria-Ramos[1], João Santos-Antunes[1,4,5,6], Rui M. Branca[7], Fátima Carneiro[1,5,6], Guilherme Macedo[4], Celso A. Reis[1,2,3,5], Mattias Belting[8,9,10], Ana Magalhães[1,2,3]*

[1]i3S - Instituto de Investigação e Inovação em Saúde, Universidade do Porto, 4200-135 Porto, Portugal.

[2]IPATIMUP - Instituto de Patologia e Imunologia Molecular da Universidade do Porto, 4200-465 Porto, Portugal.

[3]ICBAS - Instituto de Ciências Biomédicas Abel Salazar, Universidade do Porto, 4050-313 Porto, Portugal.

[4]Gastroenterology and Hepatology Department, Centro Hospitalar Universitário de São João, Alameda Prof. Hernâni Monteiro, 4200-319 Porto, Portugal.

[5]Faculty of Medicine, University of Porto (FMUP), 4200-319 Porto, Portugal.

[6]Department of Pathology, Centro Hospitalar Universitário de São João (CHUSJ), Porto.

[7]Science for Life Laboratory, Department of Oncology-Pathology, Karolinska Institutet, 171 21, Solna, Sweden.

[8]Department of Clinical Sciences, Section of Oncology, Lund University, Lund, Sweden.

[9]Department of Immunology, Genetics and Pathology, Science for Life Laboratory, Uppsala University, Uppsala, Sweden.

[10]Skåne University Hospital, Lund, Sweden.

Introduction

Gastric cancer is still among the most prevalent cancers worldwide, being the fifth most frequent malignancy, and the fourth prominent cause of cancer-related deaths (7, 17). There is a higher incidence and mortality of gastric cancer in East Asia, South America and Eastern Europe, including Portugal (6, 7). Several risk factors are associated with the prevalence of gastric cancer, including smoking, alcohol consumption and poor diet (17, 20). However, the main reason that leads to gastric inflammation is the infection with the bacteria *Helicobacter pylori* (14, 15, 163). The Lauren classification distinguishes gastric cancer accordingly to the histopathological classification, into intestinal and diffuse subtypes. In the intestinal subtype, the most prevalent gastric cancer subtype, there is a multistep progression model comprising the gastric carcinogenesis (10, 11, 17). This cascade is initiated with *H. pylori* infection related chronic gastritis, leading to gastric atrophy and intestinal metaplasia, followed by dysplasia, divided in low- and high-grade dysplasia (302). The gastric carcinoma, the last stage of the cascade, is divided in different grades: the T1 grade, when cells start to growth divide uncontrolled; the T2 grade when submucosa is invaded, or the muscle (T3 grade); and T4 grade, when eventually cells start to migrate

and invade other tissues reaching blood circulation (302). All these events may give insights that may have practical consequences for therapeutic recommendations (303).

Liquid biopsies have been proposed as an appealing alternative to the invasive tissue biopsies, due to its capacity for early cancer detection, treatment stratification, exposure of residual disease and recurrence monitoring (304-307). While the clinically utility of minimum invasive measures techniques have been investigated, extracellular vesicles offer a great platform with translational potential (308, 309).

Extracellular vesicles (EVs) are nanoparticles released upon fusion of multivesicular bodies and the plasma membrane. EVs are secreted by mammalian cells and body fluids, including blood. Derived from their originating cells, EVs are surrounded with a lipid bilayer and can harbor a diverse of functional molecules, including proteins, glycans, lipids and nucleic acids. They can carry endosomal markers such as Syndecan-Alix-Syntenin-1 complex or Tumor Susceptibility Gene 101 (TSG101) (187, 188, 200). Cancerous EVs play crucial roles in cancer progression and metastasis. Diverse studies have shown that cancer derived-EVs can promote metastasis by remodeling the tumor microenvironment and alter the extracellular matrix to facilitate the spread and colonization of metastatic cancer cells. Plasma proteome contains secreted proteins originating from multiple organs and tissues, making it a favorable matrix for comprehensive biomarker discovery. Using high resolution mass spectrometry, the proteomic analysis between diffuse and intestinal subtypes of gastric cancer identified a different proteomic signature (310). Moreover, some of these proteins identified were previously linked in other types of tumor progression and metastasis. Tumor progression can be promoted through ECM remodeling, by activating receptors and cellular processes. Specific proteins identified in intestinal subtype of gastric cancer, namely, collagen alpha-2 (I) chain (COL1A2), lysyl oxidase (LOX) and latent-transforming growth factor beta-binding protein 2 (LTBP2) are correlated with high tumor stage, having impact on patient overall survival (311). It was previously described that diffuse gastric cancer patients may be classified into different subtypes based on the altered proteome profile (312).

The gastric cancer intestinal subtype progression is well known, however the role of EVs during this cascade of events is poorly understood. To address this gap in knowledge, we sought to define EV biological signatures that distinguish gastric early cancer-associated lesions from healthy individuals. We also conceived that plasma derived-EV proteins could be promising resources for screening of biomarkers and therapeutic targets.

Materials and Methods

Blood collection and plasma isolation. The blood samples from healthy donors, intestinal metaplasia, low grade dysplasia, high grade dysplasia and early gastric cancer patients were collected directly for Vacuette® Tube 9 ml K3 EDTA tubes (lavender cap-black ring and non-ridged) and processed within 2h of phlebotomy (collection of blood). Plasmapheresis (plasma isolation) was performed from donated blood by two serial centrifugations, the first at 500g for 10min, followed by another spin at 3000g for 20 min, both at RT. Plasma aliquots were executed in low binding protein Eppendorf's, and kept at -80°C until further analysis. This study was conducted under approval from the ethical committee of the Centro Hospitalar Universitário São João (Ethical approval document number 159/19) in a collaboration protocol already established with i3S. All human subject research samples were collected after patients written informed consents (Directive 2004/23/EC). Patient data was anonymized in an electronic database.

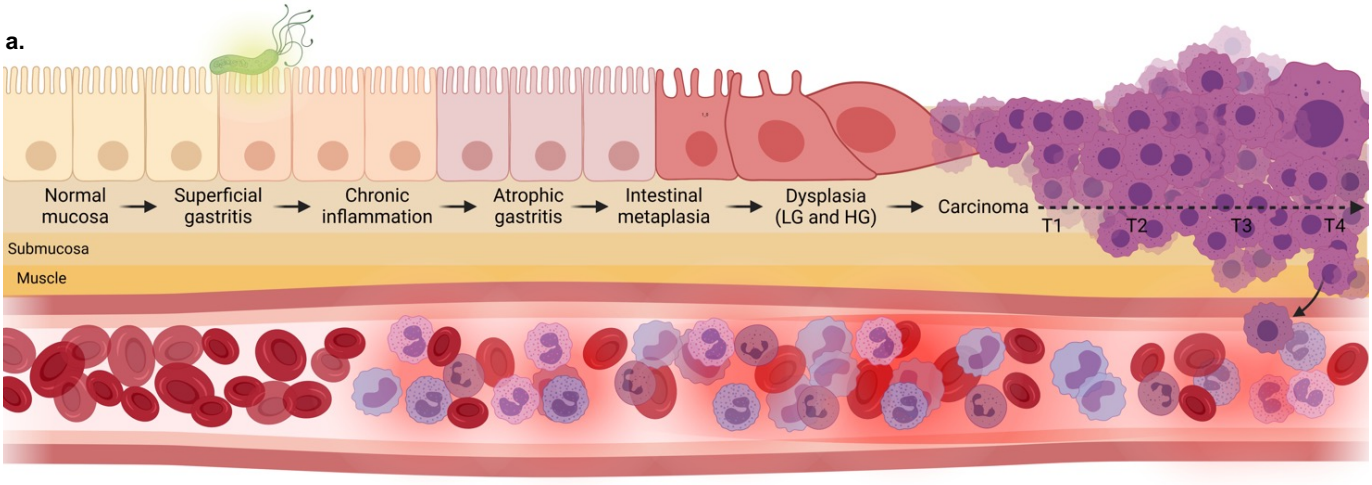
Isolation of EVs by size exclusion chromatography. The EV isolation, purification and characterization methodology were performed according to the guidelines provided by the International Society for Extracellular Vesicles (ISEV) (175). Isolation and purification were performed by Size Exclusion Chromatography (SEC). Specifically, the diluent PBS with 2mM of EDTA was filtered using 0.22µm filtration system (Corning) and SEC was performed according to manufacturer's instructions of the qEV column (iZon). Briefly, 500µL of plasma was overlaid on top of the qEV column after equilibrating the column with PBS/EDTA. Fractions from 7 to 11 were collected and pooled together. After, samples were concentrated by ultrafiltration with 10K Amicon Ultra-15 centrifugal filter units (EMD Milipore) (299).

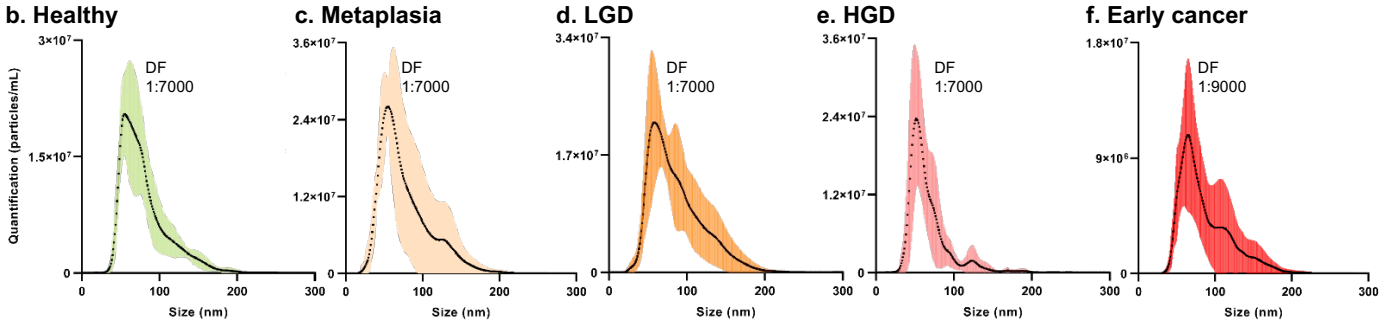
Nanoparticle Tracking Analysis (NTA). Particle size (nm) and quantification (particles per milliliter) were measured using NTA with a NanoSight NS300 system (Malvern Technologies). Samples were diluted in filtered saline solution (0.9% NaCl) and dispensed at a constant flow rate using a syringe pump. Five videos of 30s using a camera level of 16 and a threshold between 5 to 7 were captured per sample. The videos were recorded and analyzed by NTA software version 3.4. For each condition evaluated, three random samples were selected and analyzed.

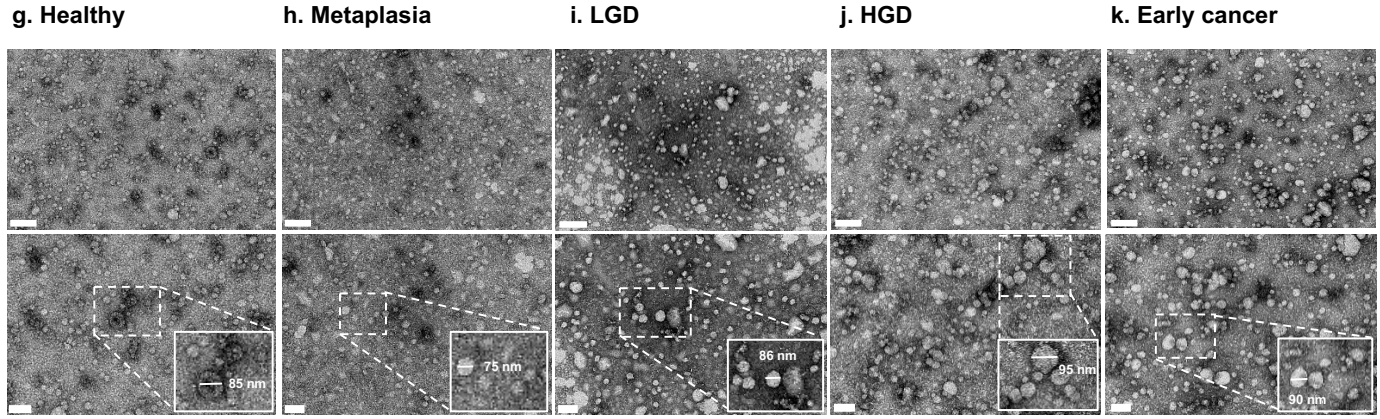
Negative-staining Transmission Electron Microscopy (TEM). EVs were visualized by TEM using negative staining. For this, 10µL of diluted (dilution factor referred) sample was mounted on Formvar/carbon film-coated mesh nickel grids (Electron Microscopy Sciences). After 30sec settling, the liquid excess was removed with filter paper

and fixation was performed with 10µL of 1% uranyl acetate onto the grids. Visualization was carried out on a microscope JEOL JEM 1400 TEM at 120 kV (Tokyo, Japan). Images were digitally recorded using a CCD digital camera (Orious 1100W Tokyo, Japan).

Results


a.
Normal mucosa
Superficial gastritis
Chronic inflammation
Atrophic gastritis
Intestinal metaplasia
Dysplasia (LG and HG)
Carcinoma
T1
T2
T3
T4
Submucosa
Muscle


b. Healthy
c. Metaplasia
d. LGD
e. HGD
f. Early cancer
DF 1:7000
DF 1:7000
DF 1:7000
DF 1:7000
DF 1:9000
Quantification (particles/mL)
Size (nm)


g. Healthy
h. Metaplasia
i. LGD
j. HGD
k. Early cancer
85 nm
75 nm
86 nm
95 nm
90 nm

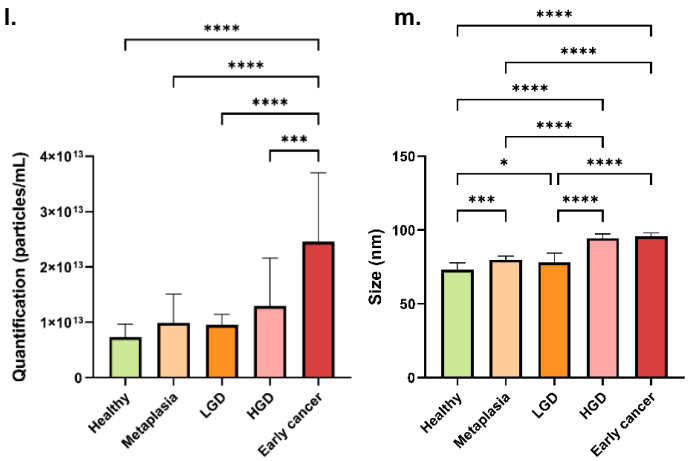

l.
m.
Quantification (particles/mL)
Size (nm)
Healthy
Metaplasia
LGD
HGD
Early cancer

Figure 1 – **The amount and size of plasma circulating EVs increases along the gastric carcinogenesis cascade. (A)** Schematic representation of the gastric cancer intestinal subtype cascade of events. **(B-F)** Concentration and size distribution analysis using NTA of EVs isolated from **(B)** healthy donors, patients with **(C)** intestinal metaplasia, **(D)** low grade dysplasia (LGD), **(F)** high grade dysplasia (HGD) and **(f)** early cancer, DF – Dilution Factor. **(G-K)** Representative images of the negative staining in TEM of the EVs isolated from **(G)** healthy donors, patients with **(H)** intestinal metaplasia, **(I)** LGD, **(J)** HGD and **(K)** early gastric cancer. On the top panel the scale bar corresponds to 200 nm and below to 100 nm. Sample diluted 1:50. **(L, M)** Quantification of the **(L)** concentration (corrected for the sample DF) and **(M)** size of the EVs isolated from plasma samples. Bar graphs shows the mean of the concentration and the size of EVs + SD. Data from 3 independent biological clinical samples, for each condition. Statistical significance was assessed using one-way ANOVA with Tukey's correction. *$p \leq 0.05$, ***$p < 0.001$, ****$p < 0.0001$.

The amount and size of plasma circulating EVs increases along the gastric carcinogenesis cascade.

We have isolated plasma-EVs from normal (healthy), intestinal metaplasia, low grade dysplasia (LGD), high grade dysplasia (HGD) and early cancer patients (schematic representation of cascade of events in gastric cancer intestinal subtype is summarized in Fig.1A). Size exclusion chromatography (SEC) was used to isolate EVs from 50 patient samples. EV populations were characterized in terms of range and morphology via nanoparticle tracking analysis (NTA) (Fig. 1B-F) and transmission electron microscopy (TEM) (Fig. 1G-K). Heterogenous population was analyzed into nanoparticles that range from 50 to 300 nm, with peak fraction between 70-150 nm. Analysis comparing all EV populations showed that the quantity of EVs secreted increases according to the evolution of events until early gastric cancer (Fig. 1L), except in the LGD condition. The average of the quantity of EVs was $7.3x10^{12}$ particles/mL (healthy donors), $9.9x10^{12}$ particles/mL (intestinal metaplasia), $9.5x10^{12}$ particles/mL (LGD), $1.3x10^{13}$ particles/mL (HGD) and $2.5x10^{13}$ particles/mL (early cancer). Regarding the size, these EVs presented similar results, as their size also increase during progression of events (Fig. 1M) (except in the LGD condition), namely, 73.1 nm (healthy donors), 79.9 nm (intestinal metaplasia), 77.9 nm (LGD), 94.4 nm (HGD) and 95.7 nm (early cancer).

The augmented generation of EVs during the progression of gastric tumor may be linked to various functional implications. These results give us a preliminary insight that the production of EVs during gastric carcinogenesis is linked to the severity of the disease. However, gaining understandings into the mechanisms that drive the enhanced production of EVs during tumor progression is crucial for comprehending the intricate interactions between cancer cells and their microenvironment.

CHAPTER VI

General Discussion

6. General Discussion

Aberrant cellular glycosylation represents a hallmark of cancer and abnormal glycan expression at the cell surface constitutes an important source of biomarkers and/or therapeutic targets. The heavily glycosylated proteins, the HSPGs, have been extensively described as key mediators in diverse cellular mechanisms. They are critical maestros of cancer cell interaction with ECM and regulate cancer cell communication, modulating tumor microenvironment and progression. Using CRISPR/Cas9 genome editing, we have established glycoengineering gastric cancer cells with altered expression of a transmembrane proteoglycan, SDC4. This modification impacted gastric cancer cell migration and invasion.

Herein, we show SDC4 is highly expressed in intestinal subtype gastric cancer through screening on clinical gastric cancer samples from IPO-Porto cohort. This profile is associated with patient poor prognosis. A significant worse overall survival was assessed in male patients with SDC4 expression, opposite when comparing to women. As mentioned in Chapter I in this thesis, intestinal subtype gastric cancer has been previously associated with higher frequency in males (mean age of 51 years old), and this factor may be explained due to hormonal regulation of HSPGs during cancer progression (12, 13, 313). Other explanation for this factor is that men have higher rates of exposure to risk factors such as smoking, alcohol consumption, and dietary habits that increase the likelihood of developing gastric cancer. In addition, hormonal factors may also play a role, as studies have shown that estrogen may have a protective effect against gastric cancer development in women (314). These hormonal differences between males and females may influence tumor biology and response to treatment, which can ultimately impact prognostic outcomes (315). It is possible that SDC4 interacts with hormonal pathways or is regulated differently in male and female gastric cancers, leading to different prognostic effects. There are known differences in the immune response between males and females, including variations in immune cell populations, cytokine production, and immune signaling pathways (316). SDC4 may modulate the immune system in a gender-specific manner, shaping the tumor microenvironment and affecting disease progression and prognosis. However, further research is needed to fully understand the underlying reasons for the gender disparity and specifically the role of SDC4 in gastric cancer incidence and prognosis.

Other interesting feature observed was the fact that SDC4 expression was kept in lymph node metastasis, however, this expression was not significantly associated with overall survival between patients presenting metastasis. This observation may be attributed to the limited sample size within this category. When considering the STAD-TCGA cohort, where

higher numbers of individuals were assessed, SDC4 expression was associated with metastasis and disease recurrence. When examining the classification of patients based on their treatment regimen, our findings reveal that SDC4 expression is solely correlated with unfavorable overall survival outcomes in the subset of individuals who underwent surgical intervention. Our multivariate analysis further indicates that the prognostic value of SDC4 expression is independent, when considering cases of intestinal subtype of gastric cancer. Furthermore, our study aimed to investigate the functional implications of SDC4 in the context of gastric cancer. Our findings demonstrate that SDC4 plays a significant role in promoting cellular migration and invasion in intestinal subtype gastric cancer cells. Furthermore, we observed a notable reduction in these pro-migratory and pro-invasive features when using glycoengineered cells that lack SDC4.

SDC4 expression has been correlated with increased migratory and invasive capabilities of cancer cells in various types of tumors (317, 318). SDC4 acts as a direct mediator between the ECM and intracellular signaling proteins, as it has the ability to bind both fibronectin and the intracellular actin-associated protein α-actinin. Additionally, SDC4 can recruit other proteins to the sites of focal adhesions, with protein kinase C α (PKCα) being a key example (291). PKCα is vital for adhesion-mediated signal transduction, and the interaction between the SDC4 cytoplasmic domain and phosphatidylinositol 4,5-bisphosphate facilitates the recruitment and activation of PKCα to the sites of focal adhesions through its catalytic domain (292). This interaction also plays a critical role in determining the location and stability of PKCα (293). Moreover, the proteolytic cleavage of the ectodomain of SDCs by secretases, such as members of the ADAM (disintegrin and metalloproteinase) family and MMPs, has been described in its involvement in various pathophysiological processes, such as inflammation and tissue regeneration (319-322). The proteolytic shedding of SDCs results in the liberation of the soluble N-terminal ectodomain from the transmembrane C-terminal fragment (tCTF). *In vitro* studies examining wound scratch assays have demonstrated that the tCTF of SDC4 increases cell migration in SDC1-deficient A459 cells to a similar extent as the SDC1 tCTF. Moreover, the presence of the SDC1 tCTF alone is adequate for the formation of lung metastasis *in vivo* (323). Our study demonstrates the involvement of SDC4 in the migration and invasion of gastric cancer cells, regardless of the presence of diverse matrix components.

In our investigation on the impact of SDC4 in intercellular signaling, we have observed that glycosylated SDC4 is sorted into EVs released by gastric cancer cells, and that the KO of SDC4 interferes both EV secretion and the composition of its cargo. Remarkably, the invasive potential of SDC4 KO cells was restored through their co-culture with EVs secreted by WT cells with a pro-invasive phenotype. MS analysis corroborated the presence of newly incorporated SDC4, providing additional evidence for the critical role of EV cargo in the

SDC4-mediated malignant phenotype. Several molecules previously demonstrated to promote directional cell motility have been identified as sorted into exosomes and/or involved in regulating their cargo content (187). Recent studies have shown that SDCs not only control exosome biogenesis (together with syntenin and Alix) (187, 199, 324) but also direct migration independently (325). Similarly, Wnt molecules are significant EV components and together with SDC4, they modulate directional cell motility *in vivo* (238). Based on these observations, it was previously proposed that several molecules involved in regulating directional cell motility may control EV biogenesis or cargo content, or function as biological cargoes of EV (326). Additionally, SDC4 has been shown to promote the release of EVs from cells, possibly through its interactions with cytoskeletal proteins and the plasma membrane (199). This suggests that SDC4 may play a crucial role in the regulation of EV secretion and cargo, and in turn, impact cellular communication and signaling in both physiological and pathological contexts.

It has been demonstrated that Heparanase, the enzyme that modulates HS, can induce the budding of the SDC-syntenin-Alix complex, promoting the EV secretion. Our findings indicate a significant enrichment of highly glycosylated forms of SDC4 in EVs compared to the corresponding parental cells. MS analysis corroborated the results observed by the SDC4 WB, as three peptides from the ectodomain of SDC4, which were exclusively identified in the EVs.

Notably, the KO of SDC4 had a significant impact on EV biogenesis, as evidenced by an increase in the number of vesicles produced by KO cells with smaller size and decreased protein/particle ratio. Moreover, the EVs derived from SDC4 KO cells exhibited higher levels of SDC1, suggesting a compensatory effect for the absence of SDC4. SDC1 has previously been demonstrated to regulate the biogenesis of intraluminal vesicles and exosomes (EVs) (187) and has been described as a regulator of the mRNA profile within secreted exosomes (327). In the context of the tumor microenvironment, the action of heparinase is known to promote the cleavage of HSPGs, thereby increasing the availability of various secretory factors. This, in turn, drives tumor angiogenesis and facilitates cell migration and invasion (328-330). Notably, perlecan and SDC1 are among the HSPGs that can be degraded by heparinase to promote tumor cell growth and invasion (331). Interestingly, heparinase has also been found to play a critical role in facilitating the invasion of natural killer (NK) cells through the dense ECM of tumors. This underscores the fact that the ECM represents a barrier to both tumor cells and immune cells in the context of cancer (332). Elevated levels of heparinase have been observed in several types of cancer, including head and neck squamous cell carcinoma, breast cancer, and gastric cancer, and have been linked to an unfavorable prognosis in affected patients (333-335). Given this information, it would be of

significant scientific interest and clinical relevance to assess the expression of Heparanase in our cohort.

Notably, MS analysis revealed that EVs derived from WT cells showed the presence of transforming growth factor beta-1 protein (TGFβ1) and growth arrest-specific protein 6 (GAS6). Furthermore, a network analysis of the proteins exclusively identified in WT EVs and associated with SDC4 revealed a clustering of SDC4, GAS6, and TGFβ1. This clustering was found to be enriched in biological processes involved in *protein phosphorylation*, *cell migration*, and *axon guidance*. Interestingly, both proteins signature is indicative of EVs pro-invasive phenotype induction. TGFβ1 is a cytokine that plays a critical role in regulating cell growth and differentiation, as well as in immune response and inflammation. In gastric cancer, TGFβ1 has been shown to promote cell migration and invasion, as well as to induce epithelial-mesenchymal transition (EMT), which is a process that enhances the invasive potential of cancer cells. TGFβ1 has also been implicated in the regulation of the tumor microenvironment, promoting angiogenesis and immune suppression (336, 337). GAS6 is a growth factor that belongs to the family of vitamin K-dependent proteins. It is involved in the regulation of cell growth, survival, and differentiation, and has been shown to be overexpressed in gastric cancer. GAS6 promotes tumor growth, invasion, and metastasis. It has also been implicated in the regulation of the immune response and in the maintenance of the tumor microenvironment (338, 339). Based on the protein-protein network results in WT EVs, Furin is another protein that deserves our attention. Furin is a proprotein convertase that plays a critical role in the post-translational processing of various protein precursors, including growth factors, receptors, enzymes, and ECM proteins (340). In gastric cancer, Furin has been shown to promote tumor progression and metastasis through its ability to activate pro-tumorigenic factors and to cleave components of the ECM, thereby facilitating cancer cell invasion and migration (341). Thus, targeting Furin may represent a promising strategy for gastric cancer management.

Protein network analysis of EV proteome derived from SDC4 KO cells showed the presence of several proteins related to the Wnt signaling pathway, including ZNRF3, a negative feedback regulator of Wnt signaling. These results are suggestive of a less aggressive phenotype of the KO EVs and are according to our results. Furthermore, analysis from TCGA cohort showed the signature of SDC4-specific proteins identified in EVs derived from WT cells was significantly associated with poor overall and disease-free survival in patients with gastric cancer.

The biological activity of EVs largely depends on their efficient internalization by recipient cells, which is modulated by various surface components such as integrins, cytokines, and glycoconjugates (260, 342, 343). Interestingly, genetic-based evidence suggests that cell

surface HSPGs are crucial receptors for internalization and functional activity of exosomes derived from cancer cells. This finding highlights the potential therapeutic value of targeting SDC expression as a strategy to hinder the delivery of exosome cargo and organotrophic metastasis (224). Studies have shown that specific glycosaminoglycan chains, especially those with 2-O- and N-sulfation domains, play a crucial role in the process of exosome internalization through HSPGs (225). Moreover, it has been demonstrated that enzymatic cleavage of HS chains by Heparanase, and inhibition of HS biosynthesis by xylosides, both lead to the inhibition of EV uptake (225). This study presents compelling evidence that SDC4 plays a vital role in the uptake of EVs. We demonstrate that the KO of this particular proteoglycan has a significant impact on the cellular internalization and organ distribution of EVs. Our data also indicates that the HS-GAGs present in EVs are crucially involved in the internalization process. This is demonstrated by the fact that enzymatic digestion of EV HS-chains or blocking EVs with HS-antibodies significantly impairs EV uptake. However, it is important to note that alternative uptake pathways, independent of SDC4, cannot be ruled out as the complete abolition of EV uptake was not achieved through SDC4 KO alone. Furthermore, it should be acknowledged that the partners of SDC4, as integrins, which have been previously described as significant mediators of EV uptake, may contribute to alternative uptake pathways (263, 344). Collectively, the involvement of these partners highlights the complex and multifaceted nature of EV uptake mechanisms. The *in vivo* experiments lead us to observe a significant reduction in the uptake of SDC4 KO EVs by the frequent sites of metastasis for gastric primary tumors, as the liver, lung, and spleen (247). EVs released by cancer cells or microorganisms have the potential to contribute to disease progression by delivering bioactive molecules, such as proteins and miRNAs, to recipient cells. Modulating the uptake of EVs secreted by recipient cells represents a potential therapeutic strategy for certain illnesses. For instance, *Helicobacter pylori*-derived EVs have been shown to accumulate preferentially in the stomach, where they induce inflammatory responses that ultimately lead to stomach cancer (345). Therefore, it would be interesting inhibit or reduce the uptake of *H. pylori* EVs by recipient cells to potentially prevent progression to gastric cancer. Our findings emphasize the distinct tropism of EVs derived from gastric cancer towards the above organs mentioned. Additionally, our data provides evidence that Kupffer cells play a significant role in the uptake of gastric cancer-derived EVs within the liver. Kupffer cells, which are resident macrophages of the liver, have been shown to play a crucial role in the uptake of cancer-derived EVs, for example in pancreatic cancer, they are crucial for contribution of the establishment of a liver pre-metastatic niche (263, 298). Kupffer cells also express integrins, such as αvβ3 and αvβ5, which interact with specific ligands on the surface of EVs to promote their uptake (263, 346). Moreover, the inhibition of αvβ3 integrin decreases CD63 expression in cancer cells,

suggestive an effect on EV content (344). ITGβ3 is an EV surface integrin that promotes EV uptake, and peptide-mediated blocking of ITGβ3 could potentially inhibit EV uptake and control metastasis (347). Targeting the α6β4 and αvβ5 integrins present on the EV surface using integrin-blocking decoy peptides has been shown to reduce exosome uptake (263). Through these mechanisms, Kupffer cells may contribute to the formation of a pre-metastatic niche in the liver, facilitating the subsequent colonization of this organ by cancer cells. The internalization of gastric cancer-derived EVs by macrophages, and the subsequent impact on macrophage differentiation and tumor dissemination, has been previously documented in the literature (348). EVs function as vehicles for intercellular communication by delivering their molecular components, including lipids, proteins, or nucleic acids, to neighboring or distant cells. Distant metastasis accounts for more than 90% of cancer-related mortality (349). Tumors from various origins exhibit distinct patterns of dissemination, with a predilection for the colonization of specific organs. Although the organotropism of cancer cells can be partly explained by the anatomical proximity between organs (e.g., the liver collects the venous drainage of the colon system via the portal vein), it has been described research providing compelling evidence for the existence of cellular and molecular programs that guide tumor cells to specific organs. The pre-metastatic niche suggests that cells at the primary tumor sites produce soluble factors and EVs that modify the microenvironment of distant organs in diverse ways, thereby promoting the survival and growth of disseminated cancer cells (298, 350-352). Our results based on a preliminary study, showed that education with WT or SDC4 KO EVs had an impact in the seeding of gastric cancer cells to the liver of mice. The obtained data is suggestive of higher accumulation of mCherry+ cancer cells in the vessels of the mice pre-educated with WT EVs. Nonetheless, is important to mention that the data analyzed includes a low number of animals, therefore validation in an independent assay with higher number of animals is required.

The study of gastric cancer metastasis is hindered by the limited availability of suitable experimental animal models. Existing literature includes only a few studies that have successfully replicated liver and lung metastasis observed in clinical settings using gastric cancer cell lines in mice (353, 354). Additionally, these studies often rely on non-commercial gastric cancer cell lines and involve lengthy experimental procedures. To overcome this challenge, it would be interesting to use orthotopic patient-derived xenograft (PDX) models as a potential solution. However, implementing this strategy is in its early stages and requires considerable time and optimization to incorporate EV education into this model, but holds a great potential.

The comprehension of the functional implications of proteoglycan glycosylation in EV cellular recognition, uptake and content transfer presents significant potential for the

therapeutic intervention of EV-mediated tumor progression (301). A subset of the several isoforms of D-glucosaminyl 3-O-sulfotransferase is capable of creating binding sites on either the surface of recipient cells or EVs (355). In the context of gastric cancer, the identification of molecular targets for the development of personalized therapeutic strategies is crucial. Understanding the role of proteoglycans in EV cellular recognition and uptake is of great significance in this regard. EV-carried proteoglycans such as Glypican-1 in pancreatic cancer and SDC1 in glioma (301, 356) have already been recognized as biomarkers for minimally-invasive cancer diagnosis. Accordingly, the identification of SDC4 in EVs derived from gastric cancer cells presents the potential for biomarker development.

It is worth to note that there is currently no gold standard method accepted for the isolation of EVs, which can potentially hinder the reproducibility of research findings in the field of EV research. The choice of isolation technique can significantly affect the efficiency of isolation in terms of yield, purity, and EV composition, which, in turn, may affect downstream analyses such as molecular profiling of cargo (297, 357-359). This fact led us to the writing of the paper included in Chapter IV of this thesis, where we present two different isolation methodologies to provide insights into the EV analysis from cell cultures, as well, as patient plasma liquid biopsies, with focus on PGs analysis (299).

By understanding EV biological features, as their quantity, size, and cargo content, may lead to provide new biomarkers and/or therapeutic targets for improving clinical management of various diseases, including gastric cancer. For instance, it has been demonstrated the transportation of gastric cancer cell-derived exosomal EGFR to the liver, where it can be incorporated into the plasma membrane of hepatic stromal cells (360). Moreover, in this study, exosomal EGFR derived from gastric cancer cells can activate hepatocyte growth factor (HGF) in hepatic stromal cells by reducing the levels of miR-26a/b. This, in turn, results in the secretion of paracrine HGF, which interacts with the c-MET receptor on migrated cancer cells, establishing a microenvironment that is conducive for the proliferation of metastatic cancer cells in the liver (360). As cancer cells undergo malignant transformation and acquire aggressive phenotypes, they often exhibit enhanced release of EVs into the extracellular space. Some studies describe that EV production may increase during cell activation, oxidative stress, tissue hypoxia, and in various disease conditions (361, 362). In Chapter V of this thesis is included a preliminary study where we observed that quantity and size of EVs from different conditions of the gastric carcinogenesis – healthy donors, intestinal metaplasia, LGD, HGD and early cancer - changes according to the evolution of the events of the disease, namely, the quantity of EVs secreted increases, as well, as their size. The increased production of EVs during tumor progression is associated with several functional implications. Firstly, EVs can transfer bioactive molecules, including growth factors, cytokines, and oncogenic proteins, to neighboring or distant cells (363-365).

This transfer of molecules can promote proliferation, angiogenesis, and invasion, thereby facilitating tumor growth and metastasis. Furthermore, EVs derived from tumor cells can remodel the tumor microenvironment by influencing the behavior of stromal cells, such as fibroblasts, endothelial cells, and immune cells (363-365). These EV-mediated interactions can create a supportive environment for tumor progression, including angiogenic switch, immune evasion, and remodeling of the ECM. Understanding the mechanisms underlying the increased production of EVs during tumor progression is important for unraveling the complex interplay between cancer cells and their microenvironment. Moreover, exploring the cargo composition and functional consequences of these EVs holds promise for the development of novel diagnostic tools, therapeutic strategies, and biomarkers for cancer detection, prognosis, and treatment monitoring (363-365). It is worth noting that the specific mechanisms and functional implications of EV production can vary among different types of cancer. Hence, it is imperative to explore different cancer types to gain in-depth understanding of the involvement of EVs in the progression of tumors.

CHAPTER VII

Conclusion and future perspectives

7. Conclusion and future perspectives

Taken together, our results demonstrate a previously unexplored function of SDC4 in regulating the aggressiveness of gastric cancer cells, thereby having clinical implications in patient prognosis, and highlight the therapeutic potential of targeting this particular HSPG. Additionally, our findings shed light on the glycan code of EVs derived from cancer cells, providing crucial information for identifying essential molecular signals that dictate gastric cancer communication routes.

Potential future perspectives in gastric cancer research may involve a deeper investigation of the glycosylation molecular mechanisms involved in the development and progression of gastric cancer. This could include the identification of novel molecular targets and the development of more effective diagnostic and therapeutic strategies. Furthermore, a better understanding of the interplay between the tumor microenvironment and gastric cancer cells could help improve treatment outcomes for patients with this disease.

Alterations in glycosylation are a well-established hallmark of cancer and have been linked to diagnosis but need further studies to better understand its underlying mechanisms. The impact of HSPGs glycosylation role in cancer communication and metastasis formation aims to provide new therapeutic targets for improving gastric cancer clinical management. To identify a unique gastric tumour-associated proteoglycan profile and provide a novel biomarker for early diagnosis of gastric cancer, using a high-resolution methodology already established (300, 301) and included in this thesis on Chapter III, could be implemented (see Figure 1).

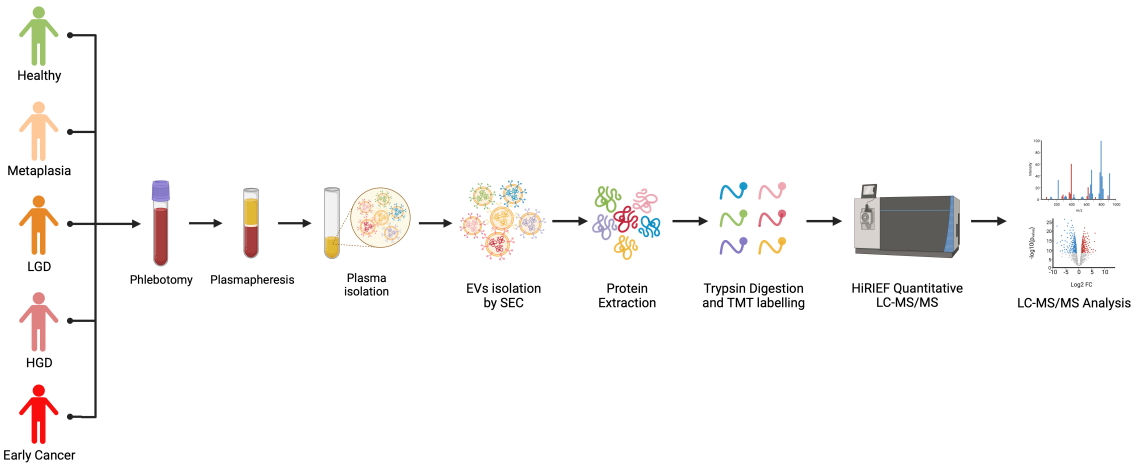


Figure 1 - Schematic representation of the experimental design from blood collection until LC-MS/MS analysis.

The detection of circulating GAGs in body fluids has emerged as a promising approach for noninvasive cancer diagnosis (366). However, several challenges remain in this field of research. There is a need for elucidation the key enzymatic regulatory events underlying aberrant GAG expression in tumors. Elucidating the key enzymatic events underlying aberrant GAG expression in tumors is crucial for understanding the molecular mechanisms driving tumor progression. It can also provide opportunities for the development of targeted therapeutic strategies aimed at modulating GAG synthesis, modification, or interactions to disrupt tumor-promoting processes.

Other important challenge is to understand the molecular mechanisms by which aberrant GAG expression modulates tumor cell signaling and disease progression. For this specific challenge, it would be interesting to discern the contributions of the core protein and GAG moieties and obtain detailed structural information on cancer-associated site-specific GAG epitopes, particularly regarding sulfation patterns. In tumors, the dysregulation expression of the GAGs can result in changes in their composition, sulfation patterns, and chain length, which can have significant functional implications for tumor development and progression.

Targeting PGs/GAGs requires a thorough understanding of the molecular interactions and signaling pathways involved. Some ideas on how PGs/GAGs could be targeted include using small molecule inhibitors, for example HPSE inhibitors (small molecule inhibitors targeting HPSE); glycosyltransferases inhibitors (inhibiting specific glycosyltransferases could modulate the composition and structure of GAGs, potentially affecting tumor cell behavior and tumor microenvironment) and HS mimetics (mimetics could compete with native HS for binding sites on proteins, interfering with various signaling pathways involved in tumor) (100). Other ideas is to exploit SDC and GPC antagonists (molecule antagonists could be designed to interfere with the interactions of SDCs and GPCs with ligands and receptors, disrupting downstream signaling pathways); disrupt the modulation of GAG epitope expression (in order to regulate the expression of specific GAG epitopes on PGs - this modulation might alter PG interactions with growth factors, cytokines, and other signaling molecules) and using a system of delivery of small molecule inhibitors via EVs (facilitating their targeted delivery to tumor cells and the tumor microenvironment). The development of monoclonal antibodies against PGs/GAGs to specifically target SDCs and/or GPCs, or HS and CS chains, that could interfere with the interactions of PGs with ligands and receptors, modulating downstream signaling pathway is another possible strategy.

In the future, the idea of targeting PGs/GAGs in the clinic environment would be most valuable in the early stages of disease development or as part of an adjuvant therapy after the primary tumor has been treated. The rationale behind this approach is that targeting

PGs/GAGs at an early stage may prevent or delay tumor progression and metastasis, leading to better long-term outcomes for patients with minimal potential side effects.
As other questions also arise, it is important to understand, in the specific case of SDC4 in gastric cancer, if SDC4 carry a specific subset of HS chains when compared to other SDCs (or even GPCs). These differences in HS chain composition (or length) and subsequent interactions with ligands and proteins can play a crucial role in various cellular processes and pathological conditions. Understanding these differences is essential for exploring the unique functions of SDC4 and other PGs in cancer biology and for developing targeted therapies that take advantage of these specific features.
Overall, gaining a deeper understanding of the regulatory events that contribute to aberrant GAG expression in tumors is essential. This knowledge can potentially lead to the identification of novel diagnostic markers and therapeutic targets.

Although this PhD thesis primarily focuses on basic research, these findings carry significant clinical implications and lay the foundation for more targeted investigations with potential translational applications in clinical settings. This underscores the vital role of basic research in generating knowledge that can be translated into clinical practice. It highlights the essential synergy between basic and clinical research, facilitating the transfer of bench-derived knowledge to patient care, thereby promoting clinical efficacy, and ultimately improving patient outcomes, which remains the ultimate objective in advancing medical science.

References

1. H. Sung *et al.*, Global Cancer Statistics 2020: GLOBOCAN Estimates of Incidence and Mortality Worldwide for 36 Cancers in 185 Countries. *CA Cancer J Clin* **71**, 209-249 (2021).
2. D. Hanahan, R. A. Weinberg, The Hallmarks of Cancer. *Cell* **100**, 57-70 (2000).
3. D. Hanahan, Robert A. Weinberg, Hallmarks of Cancer: The Next Generation. *Cell* **144**, 646-674 (2011).
4. M. N. Krstic, D. D. Mijac, D. D. Popovic, A. Pavlovic Markovic, T. Milosavljević, General Aspects of Primary Cancer Prevention. *Dig Dis* **37**, 406-415 (2019).
5. A. M. Lewandowska, T. Lewandowski, M. Rudzki, S. Rudzki, B. Laskowska, Cancer prevention – review paper. *Ann Agric Environ Med.* **28**, 11-19 (2021).
6. P. Sipponen, B. J. Marshall, Gastritis and gastric cancer. Western countries. *Gastroenterol Clin North Am* **29**, 579-592, v-vi (2000).
7. P. Correa, Gastric cancer: overview. *Gastroenterol Clin North Am* **42**, 211-217 (2013).
8. S. Morais *et al.*, Trends in gastric cancer mortality and in the prevalence of Helicobacter pylori infection in Portugal. *Eur J Cancer Prev* **25**, 275-281 (2016).
9. E. C. Smyth, M. Nilsson, H. I. Grabsch, N. C. van Grieken, F. Lordick, Gastric cancer. *Lancet* **396**, 635-648 (2020).
10. B. Hu *et al.*, Gastric cancer: Classification, histology and application of molecular pathology. *J Gastrointest Oncol* **3**, 251-261 (2012).
11. W. Polkowski *et al.*, Prognostic value of Laurén classification and c-erbB-2 oncogene overexpression in adenocarcinoma of the esophagus and gastroesophageal junction. *Ann Surg Oncol* **6**, 290-297 (1999).
12. W. F. Anderson *et al.*, Age-specific trends in incidence of noncardia gastric cancer in US adults. *Jama* **303**, 1723-1728 (2010).
13. P. Correa *et al.*, Chemoprevention of Gastric Dysplasia: Randomized Trial of Antioxidant Supplements and Anti-Helicobacter pylori Therapy. *JNCI: Journal of the National Cancer Institute* **92**, 1881-1888 (2000).
14. P. Correa, J. Houghton, Carcinogenesis of Helicobacter pylori. *Gastroenterology* **133**, 659-672 (2007).
15. S. Ishaq, L. Nunn, Helicobacter pylori and gastric cancer: a state of the art review. *Gastroenterol Hepatol Bed Bench* **8**, S6-s14 (2015).
16. Anonymous, Comprehensive molecular characterization of gastric adenocarcinoma. *Nature* **513**, 202-209 (2014).

17. E. Van Cutsem, X. Sagaert, B. Topal, K. Haustermans, H. Prenen, Gastric cancer. *Lancet* **388**, 2654-2664 (2016).
18. I. Gullo *et al.*, Minimum biopsy set for HER2 evaluation in gastric and gastro-esophageal junction cancer. *Endosc Int Open* **3**, E165-170 (2015).
19. N. Tominaga *et al.*, Five biopsy specimens from the proximal part of the tumor reliably determine HER2 protein expression status in gastric cancer. *Gastric Cancer* **19**, 553-560 (2016).
20. T. Waddell *et al.*, Gastric cancer: ESMO-ESSO-ESTRO Clinical Practice Guidelines for diagnosis, treatment and follow-up. *Ann Oncol* **24 Suppl 6**, vi57-63 (2013).
21. K. Hamada *et al.*, Examination of Endoscopic Ultrasonographic Diagnosis for the Depth of Early Gastric Cancer. *J Clin Med Res* **13**, 222-229 (2021).
22. M. Moehler *et al.*, International comparison of the German evidence-based S3-guidelines on the diagnosis and multimodal treatment of early and locally advanced gastric cancer, including adenocarcinoma of the lower esophagus. *Gastric Cancer* **18**, 550-563 (2015).
23. H. Ono *et al.*, Guidelines for endoscopic submucosal dissection and endoscopic mucosal resection for early gastric cancer (second edition). *Dig Endosc* **33**, 4-20 (2021).
24. M. P. Lutz *et al.*, Highlights of the EORTC St. Gallen International Expert Consensus on the primary therapy of gastric, gastroesophageal and oesophageal cancer - differential treatment strategies for subtypes of early gastroesophageal cancer. *Eur J Cancer* **48**, 2941-2953 (2012).
25. E. Van Cutsem *et al.*, The diagnosis and management of gastric cancer: expert discussion and recommendations from the 12th ESMO/World Congress on Gastrointestinal Cancer, Barcelona, 2010. *Ann Oncol* **22 Suppl 5**, v1-9 (2011).
26. Y. J. Bang *et al.*, Trastuzumab in combination with chemotherapy versus chemotherapy alone for treatment of HER2-positive advanced gastric or gastro-oesophageal junction cancer (ToGA): a phase 3, open-label, randomised controlled trial. *Lancet* **376**, 687-697 (2010).
27. Y. Y. Janjigian *et al.*, First-line nivolumab plus chemotherapy versus chemotherapy alone for advanced gastric, gastro-oesophageal junction, and oesophageal adenocarcinoma (CheckMate 649): a randomised, open-label, phase 3 trial. *Lancet* **398**, 27-40 (2021).
28. D. Cunningham *et al.*, Perioperative chemotherapy versus surgery alone for resectable gastroesophageal cancer. *N Engl J Med* **355**, 11-20 (2006).
29. F. Lordick *et al.*, Gastric cancer: ESMO Clinical Practice Guideline for diagnosis, treatment and follow-up. *Ann Oncol* **33**, 1005-1020 (2022).

30. M. Ychou *et al.*, Perioperative chemotherapy compared with surgery alone for resectable gastroesophageal adenocarcinoma: an FNCLCC and FFCD multicenter phase III trial. *J Clin Oncol* **29**, 1715-1721 (2011).
31. A. Magalhães, H. O. Duarte, C. A. Reis, The role of O-glycosylation in human disease. *Mol Aspects Med* **79**, 100964 (2021).
32. S. Mereiter, M. Balmaña, D. Campos, J. Gomes, C. A. Reis, Glycosylation in the Era of Cancer-Targeted Therapy: Where Are We Heading? *Cancer Cell* **36**, 6-16 (2019).
33. S. S. Pinho, C. A. Reis, Glycosylation in cancer: mechanisms and clinical implications. *Nat Rev Cancer* **15**, 540-555 (2015).
34. E. Meezan, H. C. Wu, P. H. Black, P. W. Robbins, Comparative studies on the carbohydrate-containing membrane components of normal and virus-transformed mouse fibroblasts. II. Separation of glycoproteins and glycopeptides by sephadex chromatography. *Biochemistry* **8**, 2518-2524 (1969).
35. A. Magalhães, H. O. Duarte, C. A. Reis, "Glycans and Cancer" in Encyclopedia of Cell Biology (Second Edition)*,* R. A. Bradshaw, G. W. Hart, P. D. Stahl, Eds. (Academic Press, Oxford, 2023), https://doi.org/10.1016/B978-0-12-821618-7.00019-5, pp. 373-384.
36. D. Thomas, A. K. Rathinavel, P. Radhakrishnan, Altered glycosylation in cancer: A promising target for biomarkers and therapeutics. *Biochim Biophys Acta Rev Cancer* **1875**, 188464 (2021).
37. A. Silsirivanit, Glycosylation markers in cancer. *Adv Clin Chem* **89**, 189-213 (2019).
38. G. F. Weber, M. A. Bjerke, D. W. DeSimone, Integrins and cadherins join forces to form adhesive networks. *J Cell Sci* **124**, 1183-1193 (2011).
39. T. Ju *et al.*, Tn and sialyl-Tn antigens, aberrant O-glycomics as human disease markers. *Proteomics Clin Appl* **7**, 618-631 (2013).
40. K. Okamoto, T. Goto, Glycosidation of sialic acid. *Tetrahedron* **46**, 5835-5857 (1990).
41. S. Ghosh, Sialic acid and biology of life: An introduction. *Sialic Acids and Sialoglycoconjugates in the Biology of Life, Health and Disease* doi: 10.1016/B978-0-12-816126-5.00001-9. (2020).
42. T. Angata, A. Varki, Chemical diversity in the sialic acids and related alpha-keto acids: an evolutionary perspective. *Chem Rev* **102**, 439-469 (2002).
43. X. Chen, A. Varki, Advances in the biology and chemistry of sialic acids. *ACS Chem Biol* **5**, 163-176 (2010).
44. O. M. Pearce, H. Läubli, Sialic acids in cancer biology and immunity. *Glycobiology* **26**, 111-128 (2016).

45. H. Rachel, L. Chang-Chun, "Chapter 5 - Recent advances toward the development of inhibitors to attenuate tumor metastasis via the interruption of lectin–ligand interactions" in Advances in Carbohydrate Chemistry and Biochemistry, D. Horton, Ed. (Academic Press, 2013), vol. 69, pp. 125-207.
46. R. Wen, H. Zhao, D. Zhang, C. L. Chiu, J. D. Brooks, Sialylated glycoproteins as biomarkers and drivers of progression in prostate cancer. *Carbohydr Res* **519**, 108598 (2022).
47. C. Büll, M. A. Stoel, M. H. den Brok, G. J. Adema, Sialic acids sweeten a tumor's life. *Cancer Res* **74**, 3199-3204 (2014).
48. E. RodrÍguez, S. T. T. Schetters, Y. van Kooyk, The tumour glyco-code as a novel immune checkpoint for immunotherapy. *Nat Rev Immunol* **18**, 204-211 (2018).
49. F. Li, J. Ding, Sialylation is involved in cell fate decision during development, reprogramming and cancer progression. *Protein Cell* **10**, 550-565 (2019).
50. T. Okajima *et al.*, Molecular cloning of a novel alpha2,3-sialyltransferase (ST3Gal VI) that sialylates type II lactosamine structures on glycoproteins and glycolipids. *J Biol Chem* **274**, 11479-11486 (1999).
51. J. C. Paulson, J. I. Rearick, R. L. Hill, Enzymatic properties of beta-D-galactoside alpha2 leads to 6 sialytransferase from bovine colostrum. *Journal of Biological Chemistry* **252**, 2363-2371 (1977).
52. J. Yeh, R. D. Cummings, Differential recognition of glycoprotein acceptors by terminal glycosyltransferases. *Glycobiology* **7**, 241-251 (1997).
53. R. Sackstein *et al.*, "Glycans in Acquired Human Diseases" in Essentials of Glycobiology, A. Varki *et al.*, Eds. (Cold Spring Harbor Laboratory Press

Copyright © 2022 The Consortium of Glycobiology Editors, La Jolla, California; published by Cold Spring Harbor Laboratory Press; doi:10.1101/glycobiology.4e.46. All rights reserved., Cold Spring Harbor (NY), 2022), 10.1101/glycobiology.4e.46, pp. 615-630.

54. E. Miyoshi, K. Moriwaki, T. Nakagawa, Biological function of fucosylation in cancer biology. *J Biochem* **143**, 725-729 (2008).
55. E. Miyoshi *et al.*, Fucosylation is a promising target for cancer diagnosis and therapy. *Biomolecules* **2**, 34-45 (2012).
56. D. J. Becker, J. B. Lowe, Fucose: biosynthesis and biological function in mammals. *Glycobiology* **13**, 41r-53r (2003).
57. M. A. Carrascal *et al.*, Inhibition of fucosylation in human invasive ductal carcinoma reduces E-selectin ligand expression, cell proliferation, and ERK1/2 and p38 MAPK activation. *Mol Oncol* **12**, 579-593 (2018).

58. M. N. Christiansen *et al.*, Cell surface protein glycosylation in cancer. *Proteomics* **14**, 525-546 (2014).
59. A. Magalhães, H. O. Duarte, C. A. Reis, Aberrant Glycosylation in Cancer: A Novel Molecular Mechanism Controlling Metastasis. *Cancer Cell* **31**, 733-735 (2017).
60. Y. P. Zhao *et al.*, Decreased core-fucosylation contributes to malignancy in gastric cancer. *PLoS One* **9**, e94536 (2014).
61. J. W. Dennis, I. R. Nabi, M. Demetriou, Metabolism, cell surface organization, and disease. *Cell* **139**, 1229-1241 (2009).
62. A. Grigorian, S. Torossian, M. Demetriou, T-cell growth, cell surface organization, and the galectin-glycoprotein lattice. *Immunol Rev* **230**, 232-246 (2009).
63. I. J. Chen, H. L. Chen, M. Demetriou, Lateral compartmentalization of T cell receptor versus CD45 by galectin-N-glycan binding and microfilaments coordinate basal and activation signaling. *J Biol Chem* **282**, 35361-35372 (2007).
64. K. S. Lau *et al.*, Complex N-glycan number and degree of branching cooperate to regulate cell proliferation and differentiation. *Cell* **129**, 123-134 (2007).
65. S. U. Lee *et al.*, N-glycan processing deficiency promotes spontaneous inflammatory demyelination and neurodegeneration. *J Biol Chem* **282**, 33725-33734 (2007).
66. U. L. Catherine L.R. Merry, John Couchman, and Jeffrey D. Esko. (2022) Chapter 17-Proteoglycans and Sulfated Glycosaminoglycans. in *Essentials of Glycobiology.* , ed C. R. In: Varki A, Esko JD, et al., editors. (Cold Spring Harbor Laboratory Press;, Cold Spring Harbor (NY)).
67. I. Faria-Ramos *et al.*, Heparan Sulfate Glycosaminoglycans: (Un)Expected Allies in Cancer Clinical Management. *Biomolecules* **11** (2021).
68. G. C. Jayson *et al.*, Heparan sulfate undergoes specific structural changes during the progression from human colon adenoma to carcinoma in vitro. *J Biol Chem* **273**, 51-57 (1998).
69. J. Li, N. W. Shworak, M. Simons, Increased responsiveness of hypoxic endothelial cells to FGF2 is mediated by HIF-1alpha-dependent regulation of enzymes involved in synthesis of heparan sulfate FGF2-binding sites. *J Cell Sci* **115**, 1951-1959 (2002).
70. J. Kreuger, M. Salmivirta, L. Sturiale, G. Giménez-Gallego, U. Lindahl, Sequence analysis of heparan sulfate epitopes with graded affinities for fibroblast growth factors 1 and 2. *J Biol Chem* **276**, 30744-30752 (2001).
71. A. Hildebrand *et al.*, Interaction of the small interstitial proteoglycans biglycan, decorin and fibromodulin with transforming growth factor beta. *Biochem J* **302 (Pt 2)**, 527-534 (1994).

72. X. D. Chen, L. W. Fisher, P. G. Robey, M. F. Young, The small leucine-rich proteoglycan biglycan modulates BMP-4-induced osteoblast differentiation. *Faseb j* **18**, 948-958 (2004).
73. Y. Mochida, D. Parisuthiman, M. Yamauchi, Biglycan is a positive modulator of BMP-2 induced osteoblast differentiation. *Adv Exp Med Biol* **585**, 101-113 (2006).
74. M. Salem *et al.*, miR-590-3p Promotes Ovarian Cancer Growth and Metastasis via a Novel FOXA2-Versican Pathway. *Cancer Res* **78**, 4175-4190 (2018).
75. M. A. Thelin *et al.*, Dermatan sulfate is involved in the tumorigenic properties of esophagus squamous cell carcinoma. *Cancer Res* **72**, 1943-1952 (2012).
76. C. Ricciardelli *et al.*, Elevated stromal chondroitin sulfate glycosaminoglycan predicts progression in early-stage prostate cancer. *Clin Cancer Res* **3**, 983-992 (1997).
77. K. J. Svensson *et al.*, Chondroitin sulfate expression predicts poor outcome in breast cancer. *Int J Oncol* **39**, 1421-1428 (2011).
78. H. Andrlová *et al.*, Biglycan expression in the melanoma microenvironment promotes invasiveness via increased tissue stiffness inducing integrin-β1 expression. *Oncotarget* **8**, 42901-42916 (2017).
79. L. Hu *et al.*, Biglycan enhances gastric cancer invasion by activating FAK signaling pathway. *Oncotarget* **5**, 1885-1896 (2014).
80. H. Sun *et al.*, Biglycan enhances the ability of migration and invasion in endometrial cancer. *Arch Gynecol Obstet* **293**, 429-438 (2016).
81. M. S. Viapiano, W. L. Bi, J. Piepmeier, S. Hockfield, R. T. Matthews, Novel tumor-specific isoforms of BEHAB/brevican identified in human malignant gliomas. *Cancer Res* **65**, 6726-6733 (2005).
82. T. L. Yeung *et al.*, TGF-β modulates ovarian cancer invasion by upregulating CAF-derived versican in the tumor microenvironment. *Cancer Res* **73**, 5016-5028 (2013).
83. Basappa *et al.*, Involvement of chondroitin sulfate E in the liver tumor focal formation of murine osteosarcoma cells. *Glycobiology* **19**, 735-742 (2009).
84. E. M. Denholm, Y. Q. Lin, P. J. Silver, Anti-tumor activities of chondroitinase AC and chondroitinase B: inhibition of angiogenesis, proliferation and invasion. *Eur J Pharmacol* **416**, 213-221 (2001).
85. F. Li *et al.*, Involvement of highly sulfated chondroitin sulfate in the metastasis of the Lewis lung carcinoma cells. *J Biol Chem* **283**, 34294-34304 (2008).
86. A. Kadenhe-Chiweshe *et al.*, Sustained VEGF blockade results in microenvironmental sequestration of VEGF by tumors and persistent VEGF receptor-2 activation. *Mol Cancer Res* **6**, 1-9 (2008).

87. J. X. Tan *et al.*, HYAL1 overexpression is correlated with the malignant behavior of human breast cancer. *Int J Cancer* **128**, 1303-1315 (2011).
88. L. Udabage, G. R. Brownlee, S. K. Nilsson, T. J. Brown, The over-expression of HAS2, Hyal-2 and CD44 is implicated in the invasiveness of breast cancer. *Exp Cell Res* **310**, 205-217 (2005).
89. J. Munkley, D. J. Elliott, Hallmarks of glycosylation in cancer. *Oncotarget* **7**, 35478-35489 (2016).
90. K. C. Hsiao, P. Y. Chu, G. C. Chang, K. J. Liu, Elevated Expression of Lumican in Lung Cancer Cells Promotes Bone Metastasis through an Autocrine Regulatory Mechanism. *Cancers (Basel)* **12** (2020).
91. X. J. Li *et al.*, Serglycin is a theranostic target in nasopharyngeal carcinoma that promotes metastasis. *Cancer Res* **71**, 3162-3172 (2011).
92. Y. Zhang *et al.*, Enhanced PAPSS2/VCAN sulfation axis is essential for Snail-mediated breast cancer cell migration and metastasis. *Cell Death & Differentiation* **26**, 565-579 (2019).
93. S. M. Smorenburg, C. J. Van Noorden, The complex effects of heparins on cancer progression and metastasis in experimental studies. *Pharmacol Rev* **53**, 93-105 (2001).
94. N. M. Varki, A. Varki, Heparin inhibition of selectin-mediated interactions during the hematogenous phase of carcinoma metastasis: rationale for clinical studies in humans. *Semin Thromb Hemost* **28**, 53-66 (2002).
95. S. Sarrazin, W. C. Lamanna, J. D. Esko, Heparan sulfate proteoglycans. *Cold Spring Harb Perspect Biol* **3** (2011).
96. R. V. Iozzo, L. Schaefer, Proteoglycan form and function: A comprehensive nomenclature of proteoglycans. *Matrix Biol* **42**, 11-55 (2015).
97. J. R. Couchman, C. A. Pataki, An introduction to proteoglycans and their localization. *J Histochem Cytochem* **60**, 885-897 (2012).
98. V. De Pasquale, L. M. Pavone, Heparan Sulfate Proteoglycan Signaling in Tumor Microenvironment. *Int J Mol Sci* **21** (2020).
99. N. Hassan, B. Greve, N. A. Espinoza-Sánchez, M. Götte, Cell-surface heparan sulfate proteoglycans as multifunctional integrators of signaling in cancer. *Cell Signal* **77**, 109822 (2021).
100. C. Marques, C. A. Reis, R. R. Vivès, A. Magalhães, Heparan Sulfate Biosynthesis and Sulfation Profiles as Modulators of Cancer Signalling and Progression. *Front Oncol* **11**, 778752 (2021).
101. I. C. Dews, K. R. MacKenzie, Transmembrane domains of the syndecan family of growth factor coreceptors display a hierarchy of homotypic and heterotypic

interactions. *Proceedings of the National Academy of Sciences* **104**, 20782-20787 (2007).

102. J. R. Couchman, Syndecans: proteoglycan regulators of cell-surface microdomains? *Nature Reviews Molecular Cell Biology* **4**, 926-938 (2003).
103. M. R. Morgan, M. J. Humphries, M. D. Bass, Synergistic control of cell adhesion by integrins and syndecans. *Nat Rev Mol Cell Biol* **8**, 957-969 (2007).
104. M. J. Kwon, B. Jang, J. Y. Yi, I. O. Han, E. S. Oh, Syndecans play dual roles as cell adhesion receptors and docking receptors. *FEBS Lett* **586**, 2207-2211 (2012).
105. F. Gondelaud, S. Ricard-Blum, Structures and interactions of syndecans. *Febs j* **286**, 2994-3007 (2019).
106. M. S. Filla, P. Dam, A. C. Rapraeger, The cell surface proteoglycan syndecan-1 mediates fibroblast growth factor-2 binding and activity. *J Cell Physiol* **174**, 310-321 (1998).
107. A. C. Rapraeger *et al.*, Vascular endothelial-cadherin stimulates syndecan-1-coupled insulin-like growth factor-1 receptor and cross-talk between αVβ3 integrin and vascular endothelial growth factor receptor 2 at the onset of endothelial cell dissemination during angiogenesis. *Febs j* **280**, 2194-2206 (2013).
108. T. Szatmári, K. Dobra, The role of syndecan-1 in cellular signaling and its effects on heparan sulfate biosynthesis in mesenchymal tumors. *Front Oncol* **3**, 310 (2013).
109. M. R. Akl *et al.*, Molecular and clinical profiles of syndecan-1 in solid and hematological cancer for prognosis and precision medicine. *Oncotarget* **6**, 28693-28715 (2015).
110. R. Brauer *et al.*, Syndecan-1 Attenuates Lung Injury during Influenza Infection by Potentiating c-Met Signaling to Suppress Epithelial Apoptosis. *Am J Respir Crit Care Med* **194**, 333-344 (2016).
111. Q. Li, P. W. Park, C. L. Wilson, W. C. Parks, Matrilysin shedding of syndecan-1 regulates chemokine mobilization and transepithelial efflux of neutrophils in acute lung injury. *Cell* **111**, 635-646 (2002).
112. C. Vahldieck *et al.*, Endothelial Glycocalyx and Cardiomyocyte Damage Is Prevented by Recombinant Syndecan-1 in Acute Myocardial Infarction. *Am J Pathol* **193**, 474-492 (2023).
113. K. Shimada, P. J. Gill, J. E. Silbert, W. H. Douglas, B. L. Fanburg, Involvement of cell surface heparin sulfate in the binding of lipoprotein lipase to cultured bovine endothelial cells. *J Clin Invest* **68**, 995-1002 (1981).
114. K. I. Stanford *et al.*, Syndecan-1 is the primary heparan sulfate proteoglycan mediating hepatic clearance of triglyceride-rich lipoproteins in mice. *J Clin Invest* **119**, 3236-3245 (2009).

115. J. A. Menard *et al.*, Metastasis Stimulation by Hypoxia and Acidosis-Induced Extracellular Lipid Uptake Is Mediated by Proteoglycan-Dependent Endocytosis. *Cancer Res* **76**, 4828-4840 (2016).
116. L. C. Wilsie, A. M. Gonzales, R. A. Orlando, Syndecan-1 mediates internalization of apoE-VLDL through a low density lipoprotein receptor-related protein (LRP)-independent, non-clathrin-mediated pathway. *Lipids Health Dis* **5**, 23 (2006).
117. C. M. Klass, J. R. Couchman, A. Woods, Control of extracellular matrix assembly by syndecan-2 proteoglycan. *J Cell Sci* **113 (Pt 3)**, 493-506 (2000).
118. I. M. Ethell, Y. Yamaguchi, Cell surface heparan sulfate proteoglycan syndecan-2 induces the maturation of dendritic spines in rat hippocampal neurons. *J Cell Biol* **144**, 575-586 (1999).
119. A. Hienola, S. Tumova, E. Kulesskiy, H. Rauvala, N-syndecan deficiency impairs neural migration in brain. *J Cell Biol* **174**, 569-580 (2006).
120. M. Kaksonen *et al.*, Syndecan-3-deficient mice exhibit enhanced LTP and impaired hippocampus-dependent memory. *Mol Cell Neurosci* **21**, 158-172 (2002).
121. O. Reizes, D. J. Clegg, A. D. Strader, S. C. Benoit, A role for syndecan-3 in the melanocortin regulation of energy balance. *Peptides* **27**, 274-280 (2006).
122. O. Reizes *et al.*, Transgenic expression of syndecan-1 uncovers a physiological control of feeding behavior by syndecan-3. *Cell* **106**, 105-116 (2001).
123. A. D. Strader, O. Reizes, S. C. Woods, S. C. Benoit, R. J. Seeley, Mice lacking the syndecan-3 gene are resistant to diet-induced obesity. *J Clin Invest* **114**, 1354-1360 (2004).
124. D. D. Cornelison, M. S. Filla, H. M. Stanley, A. C. Rapraeger, B. B. Olwin, Syndecan-3 and syndecan-4 specifically mark skeletal muscle satellite cells and are implicated in satellite cell maintenance and muscle regeneration. *Dev Biol* **239**, 79-94 (2001).
125. A. Pisconti, D. D. Cornelison, H. C. Olguín, T. L. Antwine, B. B. Olwin, Syndecan-3 and Notch cooperate in regulating adult myogenesis. *J Cell Biol* **190**, 427-441 (2010).
126. S. Gopal, Syndecans in Inflammation at a Glance. *Front Immunol* **11**, 227 (2020).
127. R. Li *et al.*, Syndecan-4 shedding impairs macrovascular angiogenesis in diabetes mellitus. *Biochem Biophys Res Commun* **474**, 15-21 (2016).
128. V. Kainulainen, H. Wang, C. Schick, M. Bernfield, Syndecans, heparan sulfate proteoglycans, maintain the proteolytic balance of acute wound fluids. *J Biol Chem* **273**, 11563-11569 (1998).
129. J. S. Chung *et al.*, The DC-HIL ligand syndecan-4 is a negative regulator of T-cell allo-reactivity responsible for graft-versus-host disease. *Immunology* **138**, 173-182 (2013).

130. K. Ishiguro *et al.*, Syndecan-4 deficiency leads to high mortality of lipopolysaccharide-injected mice. *J Biol Chem* **276**, 47483-47488 (2001).
131. N. C. Kaneider, C. M. Reinisch, S. Dunzendorfer, J. Römisch, C. J. Wiedermann, Syndecan-4 on human peripheral blood lymphocytes and monocytes mediates effects of antithrombin on chemotaxis.
132. C. Partovian, R. Ju, Z. W. Zhuang, K. A. Martin, M. Simons, Syndecan-4 regulates subcellular localization of mTOR Complex2 and Akt activation in a PKCalpha-dependent manner in endothelial cells. *Mol Cell* **32**, 140-149 (2008).
133. R. M. Bellin *et al.*, Defining the role of syndecan-4 in mechanotransduction using surface-modification approaches. *Proceedings of the National Academy of Sciences* **106**, 22102-22107 (2009).
134. E. Okina, A. Grossi, S. Gopal, H. A. Multhaupt, J. R. Couchman, Alpha-actinin interactions with syndecan-4 are integral to fibroblast-matrix adhesion and regulate cytoskeletal architecture. *Int J Biochem Cell Biol* **44**, 2161-2174 (2012).
135. E. Tkachenko, A. Elfenbein, D. Tirziu, M. Simons, Syndecan-4 clustering induces cell migration in a PDZ-dependent manner. *Circ Res* **98**, 1398-1404 (2006).
136. D. Becsky *et al.*, Syndecan-4 Modulates Cell Polarity and Migration by Influencing Centrosome Positioning and Intracellular Calcium Distribution. *Front Cell Dev Biol* **8**, 575227 (2020).
137. A. Chronopoulos *et al.*, Syndecan-4 tunes cell mechanics by activating the kindlin-integrin-RhoA pathway. *Nat Mater* **19**, 669-678 (2020).
138. M. E. Strand *et al.*, Shedding of syndecan-4 promotes immune cell recruitment and mitigates cardiac dysfunction after lipopolysaccharide challenge in mice. *J Mol Cell Cardiol* **88**, 133-144 (2015).
139. J. R. Couchman, S. Gopal, H. C. Lim, S. Nørgaard, H. A. Multhaupt, Fell-Muir Lecture: Syndecans: from peripheral coreceptors to mainstream regulators of cell behaviour. *Int J Exp Pathol* **96**, 1-10 (2015).
140. X. Xian, S. Gopal, J. R. Couchman, Syndecans as receptors and organizers of the extracellular matrix. *Cell Tissue Res* **339**, 31-46 (2010).
141. D. M. Beauvais, O. Jung, Y. Yang, R. D. Sanderson, A. C. Rapraeger, Syndecan-1 (CD138) Suppresses Apoptosis in Multiple Myeloma by Activating IGF1 Receptor: Prevention by SynstatinIGF1R Inhibits Tumor Growth. *Cancer Res* **76**, 4981-4993 (2016).
142. A. D. Theocharis *et al.*, Insights into the key roles of proteoglycans in breast cancer biology and translational medicine. *Biochim Biophys Acta* **1855**, 276-300 (2015).

143. J. H. Kim, J. Park, Prognostic significance of heme oxygenase-1, S100 calcium-binding protein A4, and syndecan-1 expression in primary non-muscle-invasive bladder cancer. *Hum Pathol* **45**, 1830-1838 (2014).
144. T. Szarvas *et al.*, Enhanced stromal syndecan-1 expression is an independent risk factor for poor survival in bladder cancer. *Hum Pathol* **45**, 674-682 (2014).
145. X. Wang *et al.*, Shed Syndecan-1 is involved in chemotherapy resistance via the EGFR pathway in colorectal cancer. *British Journal of Cancer* **111**, 1965-1976 (2014).
146. J. P. Wiksten, J. Lundin, S. Nordling, A. Kokkola, C. Haglund, Comparison of the prognostic value of a panel of tissue tumor markers and established clinicopathological factors in patients with gastric cancer. *Anticancer Res* **28**, 2279-2287 (2008).
147. J. P. Wiksten *et al.*, Epithelial and stromal syndecan-1 expression as predictor of outcome in patients with gastric cancer. *Int J Cancer* **95**, 1-6 (2001).
148. R. Hua *et al.*, Syndecan-2 in colorectal cancer plays oncogenic role via epithelial-mesenchymal transition and MAPK pathway. *Biomedicine & Pharmacotherapy* **121**, 109630 (2020).
149. Y. D. Han *et al.*, Early detection of colorectal cancer based on presence of methylated syndecan-2 (SDC2) in stool DNA. *Clinical Epigenetics* **11**, 51 (2019).
150. F. Niu *et al.*, Stool DNA Test of Methylated Syndecan-2 for the Early Detection of Colorectal Neoplasia. *Cancer Epidemiol Biomarkers Prev* **26**, 1411-1419 (2017).
151. D. Hrabar *et al.*, Epithelial and stromal expression of syndecan-2 in pancreatic carcinoma. *Anticancer Res* **30**, 2749-2753 (2010).
152. K. Tsoyi *et al.*, Lung Adenocarcinoma Syndecan-2 Potentiates Cell Invasiveness. *Am J Respir Cell Mol Biol* **60**, 659-666 (2019).
153. A. Kinnunen *et al.*, N-syndecan and HB-GAM (heparin-binding growth-associated molecule) associate with early axonal tracts in the rat brain. *Eur J Neurosci* **10**, 635-648 (1998).
154. J. Yao, W. Y. Li, S. G. Li, X. S. Feng, S. G. Gao, Midkine promotes perineural invasion in human pancreatic cancer. *World J Gastroenterol* **20**, 3018-3024 (2014).
155. J. Yao, L. L. Zhang, X. M. Huang, W. Y. Li, S. G. Gao, Pleiotrophin and N-syndecan promote perineural invasion and tumor progression in an orthotopic mouse model of pancreatic cancer. *World J Gastroenterol* **23**, 3907-3914 (2017).
156. Y. Ding *et al.*, LncRNA TRPM2-AS promotes ovarian cancer progression and cisplatin resistance by sponging miR-138-5p to release SDC3 mRNA. *Aging (Albany NY)* **13**, 6832-6848 (2021).

157. N. J. Santos *et al.*, Syndecan Family Gene and Protein Expression and Their Prognostic Values for Prostate Cancer. *Int J Mol Sci* **22** (2021).
158. J. Sun, S. Pan, H. Cui, H. Li, CircRNA SCARB1 Promotes Renal Cell Carcinoma Progression Via Mir- 510-5p/SDC3 Axis. *Curr Cancer Drug Targets* **20**, 461-470 (2020).
159. M. E. Lendorf, T. Manon-Jensen, P. Kronqvist, H. A. Multhaupt, J. R. Couchman, Syndecan-1 and syndecan-4 are independent indicators in breast carcinoma. *J Histochem Cytochem* **59**, 615-629 (2011).
160. F. Baba *et al.*, Syndecan-1 and syndecan-4 are overexpressed in an estrogen receptor-negative, highly proliferative breast carcinoma subtype. *Breast Cancer Res Treat* **98**, 91-98 (2006).
161. S. Takashima *et al.*, Syndecan-4 as a biomarker to predict clinical outcome for glioblastoma multiforme treated with WT1 peptide vaccine. *Future Sci OA* **2**, Fso96 (2016).
162. K. Y. Na, P. Bacchini, F. Bertoni, Y. W. Kim, Y. K. Park, Syndecan-4 and fibronectin in osteosarcoma. *Pathology* **44**, 325-330 (2012).
163. A. Magalhães *et al.*, Helicobacter pylori cag pathogenicity island-positive strains induce syndecan-4 expression in gastric epithelial cells. *FEMS Immunol Med Microbiol* **56**, 223-232 (2009).
164. E. Chargaff, R. West, The biological significance of the thromboplastic protein of blood. *J Biol Chem* **166**, 189-197 (1946).
165. P. Wolf, The nature and significance of platelet products in human plasma. *Br J Haematol* **13**, 269-288 (1967).
166. E. G. Trams, C. J. Lauter, N. Salem, Jr., U. Heine, Exfoliation of membrane ecto-enzymes in the form of micro-vesicles. *Biochim Biophys Acta* **645**, 63-70 (1981).
167. C. Harding, J. Heuser, P. Stahl, Receptor-mediated endocytosis of transferrin and recycling of the transferrin receptor in rat reticulocytes. *J Cell Biol* **97**, 329-339 (1983).
168. C. Harding, P. Stahl, Transferrin recycling in reticulocytes: pH and iron are important determinants of ligand binding and processing. *Biochem Biophys Res Commun* **113**, 650-658 (1983).
169. B. T. Pan, K. Teng, C. Wu, M. Adam, R. M. Johnstone, Electron microscopic evidence for externalization of the transferrin receptor in vesicular form in sheep reticulocytes. *J Cell Biol* **101**, 942-948 (1985).
170. R. M. Johnstone, M. Adam, J. R. Hammond, L. Orr, C. Turbide, Vesicle formation during reticulocyte maturation. Association of plasma membrane activities with released vesicles (exosomes). *J Biol Chem* **262**, 9412-9420 (1987).

171. R. M. Johnstone, A. Bianchini, K. Teng, Reticulocyte Maturation and Exosome Release: Transferrin Receptor Containing Exosomes Shows Multiple Plasma Membrane Functions. *Blood* **74**, 1844-1851 (1989).
172. C. Théry, Exosomes: secreted vesicles and intercellular communications. *F1000 Biol Rep* **3**, 15 (2011).
173. G. Raposo *et al.*, B lymphocytes secrete antigen-presenting vesicles. *J Exp Med* **183**, 1161-1172 (1996).
174. L. Zitvogel *et al.*, Eradication of established murine tumors using a novel cell-free vaccine: dendritic cell-derived exosomes. *Nat Med* **4**, 594-600 (1998).
175. C. Théry *et al.*, Minimal information for studies of extracellular vesicles 2018 (MISEV2018): a position statement of the International Society for Extracellular Vesicles and update of the MISEV2014 guidelines. *J Extracell Vesicles* **7**, 1535750 (2018).
176. J. Liu *et al.*, Extracellular membrane vesicles and nanotubes in Archaea. *Microlife* **2**, uqab007 (2021).
177. Y. J. Yoon, O. Y. Kim, Y. S. Gho, Extracellular vesicles as emerging intercellular communicasomes. *BMB Rep* **47**, 531-539 (2014).
178. E. R. Abels, X. O. Breakefield, Introduction to Extracellular Vesicles: Biogenesis, RNA Cargo Selection, Content, Release, and Uptake. *Cell Mol Neurobiol* **36**, 301-312 (2016).
179. J. Kowal *et al.*, Proteomic comparison defines novel markers to characterize heterogeneous populations of extracellular vesicle subtypes. *Proc Natl Acad Sci U S A* **113**, E968-977 (2016).
180. E. Cocucci, J. Meldolesi, Ectosomes and exosomes: shedding the confusion between extracellular vesicles. *Trends Cell Biol* **25**, 364-372 (2015).
181. T. Yamamoto, N. Kosaka, T. Ochiya, Latest advances in extracellular vesicles: from bench to bedside. *Sci Technol Adv Mater* **20**, 746-757 (2019).
182. M. Yáñez-Mó *et al.*, Biological properties of extracellular vesicles and their physiological functions. *J Extracell Vesicles* **4**, 27066 (2015).
183. L. Chitoiu, A. Dobranici, M. Gherghiceanu, S. Dinescu, M. Costache, Multi-Omics Data Integration in Extracellular Vesicle Biology-Utopia or Future Reality? *Int J Mol Sci* **21** (2020).
184. N. P. Hessvik, A. Llorente, Current knowledge on exosome biogenesis and release. *Cell Mol Life Sci* **75**, 193-208 (2018).
185. M. Mathieu, L. Martin-Jaular, G. Lavieu, C. Théry, Specificities of secretion and uptake of exosomes and other extracellular vesicles for cell-to-cell communication. *Nat Cell Biol* **21**, 9-17 (2019).

186. G. van Niel, G. D'Angelo, G. Raposo, Shedding light on the cell biology of extracellular vesicles. *Nat Rev Mol Cell Biol* **19**, 213-228 (2018).
187. M. F. Baietti *et al.*, Syndecan-syntenin-ALIX regulates the biogenesis of exosomes. *Nat Cell Biol* **14**, 677-685 (2012).
188. V. Friand, G. David, P. Zimmermann, Syntenin and syndecan in the biogenesis of exosomes. *Biol Cell* **107**, 331-341 (2015).
189. P. I. Hanson, A. Cashikar, Multivesicular body morphogenesis. *Annu Rev Cell Dev Biol* **28**, 337-362 (2012).
190. B. Roucourt, S. Meeussen, J. Bao, P. Zimmermann, G. David, Heparanase activates the syndecan-syntenin-ALIX exosome pathway. *Cell Res* **25**, 412-428 (2015).
191. J. H. Hurley, G. Odorizzi, Get on the exosome bus with ALIX. *Nat Cell Biol* **14**, 654-655 (2012).
192. M. Colombo *et al.*, Analysis of ESCRT functions in exosome biogenesis, composition and secretion highlights the heterogeneity of extracellular vesicles. *J Cell Sci* **126**, 5553-5565 (2013).
193. S. Bänfer *et al.*, Molecular mechanism to recruit galectin-3 into multivesicular bodies for polarized exosomal secretion. *Proc Natl Acad Sci U S A* **115**, E4396-e4405 (2018).
194. C. E. Jackson, B. S. Scruggs, J. E. Schaffer, P. I. Hanson, Effects of Inhibiting VPS4 Support a General Role for ESCRTs in Extracellular Vesicle Biogenesis. *Biophys J* **113**, 1342-1352 (2017).
195. S. Stuffers, C. Sem Wegner, H. Stenmark, A. Brech, Multivesicular endosome biogenesis in the absence of ESCRTs. *Traffic* **10**, 925-937 (2009).
196. D. Perez-Hernandez *et al.*, The intracellular interactome of tetraspanin-enriched microdomains reveals their function as sorting machineries toward exosomes. *J Biol Chem* **288**, 11649-11661 (2013).
197. G. van Niel *et al.*, The tetraspanin CD63 regulates ESCRT-independent and -dependent endosomal sorting during melanogenesis. *Dev Cell* **21**, 708-721 (2011).
198. I. Nazarenko *et al.*, Cell surface tetraspanin Tspan8 contributes to molecular pathways of exosome-induced endothelial cell activation. *Cancer Res* **70**, 1668-1678 (2010).
199. R. Ghossoub *et al.*, Tetraspanin-6 negatively regulates exosome production. *Proc Natl Acad Sci U S A* **117**, 5913-5922 (2020).
200. R. Ghossoub *et al.*, Syntenin-ALIX exosome biogenesis and budding into multivesicular bodies are controlled by ARF6 and PLD2. *Nature Communications* **5**, 3477 (2014).

201. G. David, P. Zimmermann, Heparanase tailors syndecan for exosome production. *Mol Cell Oncol* **3**, e1047556 (2016).
202. S. Lucotti, C. M. Kenific, H. Zhang, D. Lyden, Extracellular vesicles and particles impact the systemic landscape of cancer. *The EMBO Journal* **41**, e109288 (2022).
203. B. Brügger, V. A. Bankaitis, Lipids and vesicular transport. *Biochim Biophys Acta* **1821**, 1039 (2012).
204. K. Trajkovic *et al.*, Ceramide triggers budding of exosome vesicles into multivesicular endosomes. *Science* **319**, 1244-1247 (2008).
205. A. Savina, M. Furlán, M. Vidal, M. I. Colombo, Exosome release is regulated by a calcium-dependent mechanism in K562 cells. *J Biol Chem* **278**, 20083-20090 (2003).
206. D. Hoshino *et al.*, Exosome secretion is enhanced by invadopodia and drives invasive behavior. *Cell Rep* **5**, 1159-1168 (2013).
207. S. Sinha *et al.*, Cortactin promotes exosome secretion by controlling branched actin dynamics. *J Cell Biol* **214**, 197-213 (2016).
208. E. Granger, G. McNee, V. Allan, P. Woodman, The role of the cytoskeleton and molecular motors in endosomal dynamics. *Semin Cell Dev Biol* **31**, 20-29 (2014).
209. F. J. Verweij *et al.*, ER membrane contact sites support endosomal small GTPase conversion for exosome secretion. *J Cell Biol* **221** (2022).
210. M. A. Antonyak, K. F. Wilson, R. A. Cerione, R(h)oads to microvesicles. *Small GTPases* **3**, 219-224 (2012).
211. S. Schlienger, S. Campbell, A. Claing, ARF1 regulates the Rho/MLC pathway to control EGF-dependent breast cancer cell invasion. *Mol Biol Cell* **25**, 17-29 (2014).
212. C. Hsu *et al.*, Regulation of exosome secretion by Rab35 and its GTPase-activating proteins TBC1D10A-C. *J Cell Biol* **189**, 223-232 (2010).
213. K. Laulagnier *et al.*, PLD2 is enriched on exosomes and its activity is correlated to the release of exosomes. *FEBS Lett* **572**, 11-14 (2004).
214. M. Ostrowski *et al.*, Rab27a and Rab27b control different steps of the exosome secretion pathway. *Nat Cell Biol* **12**, 19-30; sup pp 11-13 (2010).
215. H. Stenmark, Rab GTPases as coordinators of vesicle traffic. *Nature Reviews Molecular Cell Biology* **10**, 513-525 (2009).
216. L. A. Mulcahy, R. C. Pink, D. R. Carter, Routes and mechanisms of extracellular vesicle uptake. *J Extracell Vesicles* **3** (2014).
217. S. Lakhal, M. J. Wood, Exosome nanotechnology: an emerging paradigm shift in drug delivery: exploitation of exosome nanovesicles for systemic in vivo delivery of RNAi heralds new horizons for drug delivery across biological barriers. *Bioessays* **33**, 737-741 (2011).

218. L. V. Chernomordik, G. B. Melikyan, Y. A. Chizmadzhev, Biomembrane fusion: a new concept derived from model studies using two interacting planar lipid bilayers. *Biochim Biophys Acta* **906**, 309-352 (1987).
219. R. Jahn, T. C. Südhof, Membrane fusion and exocytosis. *Annu Rev Biochem* **68**, 863-911 (1999).
220. B. S. Joshi, M. A. de Beer, B. N. G. Giepmans, I. S. Zuhorn, Endocytosis of Extracellular Vesicles and Release of Their Cargo from Endosomes. *ACS Nano* **14**, 4444-4455 (2020).
221. T. Tian, Y. Wang, H. Wang, Z. Zhu, Z. Xiao, Visualizing of the cellular uptake and intracellular trafficking of exosomes by live-cell microscopy. *J Cell Biochem* **111**, 488-496 (2010).
222. T. Tian *et al.*, Dynamics of exosome internalization and trafficking. *J Cell Physiol* **228**, 1487-1495 (2013).
223. N. A. Atai *et al.*, Heparin blocks transfer of extracellular vesicles between donor and recipient cells. *J Neurooncol* **115**, 343-351 (2013).
224. M. Cerezo-Magaña, A. Bång-Rudenstam, M. Belting, The pleiotropic role of proteoglycans in extracellular vesicle mediated communication in the tumor microenvironment. *Semin Cancer Biol* **62**, 99-107 (2020).
225. H. C. Christianson, K. J. Svensson, T. H. van Kuppevelt, J.-P. Li, M. Belting, Cancer cell exosomes depend on cell-surface heparan sulfate proteoglycans for their internalization and functional activity. *Proceedings of the National Academy of Sciences* **110**, 17380 (2013).
226. M. Tkach *et al.*, Qualitative differences in T-cell activation by dendritic cell-derived extracellular vesicle subtypes. *Embo j* **36**, 3012-3028 (2017).
227. A. Sobo-Vujanovic, S. Munich, N. L. Vujanovic, Dendritic-cell exosomes cross-present Toll-like receptor-ligands and activate bystander dendritic cells. *Cell Immunol* **289**, 119-127 (2014).
228. J. Hakulinen, S. Junnikkala, T. Sorsa, S. Meri, Complement inhibitor membrane cofactor protein (MCP; CD46) is constitutively shed from cancer cell membranes in vesicles and converted by a metalloproteinase to a functionally active soluble form. *Eur J Immunol* **34**, 2620-2629 (2004).
229. C. Barrès *et al.*, Galectin-5 is bound onto the surface of rat reticulocyte exosomes and modulates vesicle uptake by macrophages. *Blood* **115**, 696-705 (2010).
230. D. Feng *et al.*, Cellular internalization of exosomes occurs through phagocytosis. *Traffic* **11**, 675-687 (2010).
231. D. Fitzner *et al.*, Selective transfer of exosomes from oligodendrocytes to microglia by macropinocytosis. *J Cell Sci* **124**, 447-458 (2011).

232. A. Montecalvo *et al.*, Mechanism of transfer of functional microRNAs between mouse dendritic cells via exosomes. *Blood* **119**, 756-766 (2012).
233. A. E. Morelli *et al.*, Endocytosis, intracellular sorting, and processing of exosomes by dendritic cells. *Blood* **104**, 3257-3266 (2004).
234. C. Frühbeis *et al.*, Neurotransmitter-triggered transfer of exosomes mediates oligodendrocyte-neuron communication. *PLoS Biol* **11**, e1001604 (2013).
235. K. J. Svensson *et al.*, Exosome uptake depends on ERK1/2-heat shock protein 27 signaling and lipid Raft-mediated endocytosis negatively regulated by caveolin-1. *J Biol Chem* **288**, 17713-17724 (2013).
236. A. Nanbo, E. Kawanishi, R. Yoshida, H. Yoshiyama, Exosomes derived from Epstein-Barr virus-infected cells are internalized via caveola-dependent endocytosis and promote phenotypic modulation in target cells. *J Virol* **87**, 10334-10347 (2013).
237. H. Costa Verdera, J. J. Gitz-Francois, R. M. Schiffelers, P. Vader, Cellular uptake of extracellular vesicles is mediated by clathrin-independent endocytosis and macropinocytosis. *J Control Release* **266**, 100-108 (2017).
238. J. C. Gross, V. Chaudhary, K. Bartscherer, M. Boutros, Active Wnt proteins are secreted on exosomes. *Nature Cell Biology* **14**, 1036-1045 (2012).
239. V. Luga *et al.*, Exosomes Mediate Stromal Mobilization of Autocrine Wnt-PCP Signaling in Breast Cancer Cell Migration. *Cell* **151**, 1542-1556 (2012).
240. S. Paget, The distribution of secondary growths in cancer of the breast. 1889. *Cancer Metastasis Rev* **8**, 98-101 (1989).
241. I. J. Fidler, G. Poste, The "seed and soil" hypothesis revisited. *Lancet Oncol* **9**, 808 (2008).
242. Q. Liu *et al.*, Factors involved in cancer metastasis: a better understanding to "seed and soil" hypothesis. *Mol Cancer* **16**, 176 (2017).
243. A. J. Minn *et al.*, Distinct organ-specific metastatic potential of individual breast cancer cells and primary tumors. *J Clin Invest* **115**, 44-55 (2005).
244. A. Müller *et al.*, Involvement of chemokine receptors in breast cancer metastasis. *Nature* **410**, 50-56 (2001).
245. P. K. Myint, E. J. Park, A. Gaowa, E. Kawamoto, M. Shimaoka, Targeted remodeling of breast cancer and immune cell homing niches by exosomal integrins. *Diagn Pathol* **15**, 38 (2020).
246. I. Häuselmann, L. Borsig, Altered tumor-cell glycosylation promotes metastasis. *Front Oncol* **4**, 28 (2014).
247. W. Li, J. M. Ng, C. C. Wong, E. K. W. Ng, J. Yu, Molecular alterations of cancer cell and tumour microenvironment in metastatic gastric cancer. *Oncogene* **37**, 4903-4920 (2018).

248. G. Gandaglia *et al.*, Impact of the Site of Metastases on Survival in Patients with Metastatic Prostate Cancer. *Eur Urol* **68**, 325-334 (2015).
249. Q. Liu *et al.*, Surgery for synchronous and metachronous single-organ metastasis of pancreatic cancer: a SEER database analysis and systematic literature review. *Scientific Reports* **10**, 4444 (2020).
250. J. Yang, D. K. Manson, B. P. Marr, R. D. Carvajal, Treatment of uveal melanoma: where are we now? *Ther Adv Med Oncol* **10**, 1758834018757175 (2018).
251. J. Urosevic *et al.*, Colon cancer cells colonize the lung from established liver metastases through p38 MAPK signalling and PTHLH. *Nat Cell Biol* **16**, 685-694 (2014).
252. Y. Gao *et al.*, Metastasis Organotropism: Redefining the Congenial Soil. *Dev Cell* **49**, 375-391 (2019).
253. D. X. Nguyen, P. D. Bos, J. Massagué, Metastasis: from dissemination to organ-specific colonization. *Nat Rev Cancer* **9**, 274-284 (2009).
254. A. C. Obenauf, J. Massagué, Surviving at a Distance: Organ-Specific Metastasis. *Trends Cancer* **1**, 76-91 (2015).
255. T. Schild, V. Low, J. Blenis, A. P. Gomes, Unique Metabolic Adaptations Dictate Distal Organ-Specific Metastatic Colonization. *Cancer Cell* **33**, 347-354 (2018).
256. M. Morishita, Y. Takahashi, M. Nishikawa, Y. Takakura, Pharmacokinetics of Exosomes-An Important Factor for Elucidating the Biological Roles of Exosomes and for the Development of Exosome-Based Therapeutics. *J Pharm Sci* **106**, 2265-2269 (2017).
257. C. Charoenviriyakul *et al.*, Cell type-specific and common characteristics of exosomes derived from mouse cell lines: Yield, physicochemical properties, and pharmacokinetics. *Eur J Pharm Sci* **96**, 316-322 (2017).
258. A. Chow *et al.*, Macrophage immunomodulation by breast cancer-derived exosomes requires Toll-like receptor 2-mediated activation of NF-κB. *Sci Rep* **4**, 5750 (2014).
259. S. H. Kim, N. R. Bianco, W. J. Shufesky, A. E. Morelli, P. D. Robbins, Effective treatment of inflammatory disease models with exosomes derived from dendritic cells genetically modified to express IL-4. *J Immunol* **179**, 2242-2249 (2007).
260. H. Peinado *et al.*, Pre-metastatic niches: organ-specific homes for metastases. *Nat Rev Cancer* **17**, 302-317 (2017).
261. A. Zomer *et al.*, In Vivo imaging reveals extracellular vesicle-mediated phenocopying of metastatic behavior. *Cell* **161**, 1046-1057 (2015).
262. H. Peinado *et al.*, Melanoma exosomes educate bone marrow progenitor cells toward a pro-metastatic phenotype through MET. *Nat Med* **18**, 883-891 (2012).

263. A. Hoshino *et al.*, Tumour exosome integrins determine organotropic metastasis. *Nature* **527**, 329-335 (2015).
264. J. N. Higginbotham *et al.*, Amphiregulin exosomes increase cancer cell invasion. *Curr Biol* **21**, 779-786 (2011).
265. N. Tarbé, S. Lösch, H. Burtscher, M. Jarsch, U. H. Weidle, Identification of rat pancreatic carcinoma genes associated with lymphogenous metastasis. *Anticancer Res* **22**, 2015-2027 (2002).
266. W. Mu, S. Rana, M. Zöller, Host matrix modulation by tumor exosomes promotes motility and invasiveness. *Neoplasia* **15**, 875-887 (2013).
267. A. Bobrie *et al.*, Rab27a Supports Exosome-Dependent and -Independent Mechanisms That Modify the Tumor Microenvironment and Can Promote Tumor Progression. *Cancer Research* **72**, 4920-4930 (2012).
268. D. Guo *et al.*, RAB27A promotes melanoma cell invasion and metastasis via regulation of pro-invasive exosomes. *Int J Cancer* **144**, 3070-3085 (2019).
269. J. I. Zwicker *et al.*, Prediction and prevention of thromboembolic events with enoxaparin in cancer patients with elevated tissue factor-bearing microparticles: a randomized-controlled phase II trial (the Microtec study). *British Journal of Haematology* **160**, 530-537 (2013).
270. M. Tkach, C. Théry, Communication by Extracellular Vesicles: Where We Are and Where We Need to Go. *Cell* **164**, 1226-1232 (2016).
271. E. Gezelius *et al.*, Circulating Levels of the Cardiovascular Biomarkers ST2 and Adrenomedullin Predict Outcome within a Randomized Phase III Lung Cancer Trial (RASTEN). *Cancers (Basel)* **14** (2022).
272. E. Gezelius *et al.*, Low-molecular-weight heparin adherence and effects on survival within a randomised phase III lung cancer trial (RASTEN). *Eur J Cancer* **118**, 82-90 (2019).
273. E. Gezelius *et al.*, Coagulation biomarkers and prediction of venous thromboembolism and survival in small cell lung cancer: A sub-study of RASTEN - A randomized trial with low molecular weight heparin. *PLoS One* **13**, e0207387 (2018).
274. G. O. Griffiths *et al.*, FRAGMATIC: a randomised phase III clinical trial investigating the effect of fragmin added to standard therapy in patients with lung cancer. *BMC Cancer* **9**, 355 (2009).
275. S. A. Dusoswa *et al.*, Glycan modification of glioblastoma-derived extracellular vesicles enhances receptor-mediated targeting of dendritic cells. *J Extracell Vesicles* **8**, 1648995 (2019).

276. S. A. Dusoswa *et al.*, Glioblastomas exploit truncated O-linked glycans for local and distant immune modulation via the macrophage galactose-type lectin. *Proc Natl Acad Sci U S A* **117**, 3693-3703 (2020).
277. S. K. Horrevorts *et al.*, Glycan-Modified Apoptotic Melanoma-Derived Extracellular Vesicles as Antigen Source for Anti-Tumor Vaccination. *Cancers (Basel)* **11** (2019).
278. N. Nishida-Aoki, N. Tominaga, N. Kosaka, T. Ochiya, Altered biodistribution of deglycosylated extracellular vesicles through enhanced cellular uptake. *J Extracell Vesicles* **9**, 1713527 (2020).
279. F. Royo, U. Cossío, A. Ruiz de Angulo, J. Llop, J. M. Falcon-Perez, Modification of the glycosylation of extracellular vesicles alters their biodistribution in mice. *Nanoscale* **11**, 1531-1537 (2019).
280. Y. Uen *et al.*, Mining of potential microRNAs with clinical correlation - regulation of syndecan-1 expression by miR-122-5p altered mobility of breast cancer cells and possible correlation with liver injury. *Oncotarget* **9**, 28165-28175 (2018).
281. H. Liu *et al.*, The Effect of Triptolide-Loaded Exosomes on the Proliferation and Apoptosis of Human Ovarian Cancer SKOV3 Cells. *Biomed Res Int* **2019**, 2595801 (2019).
282. D. Gajria, S. Chandarlapaty, HER2-amplified breast cancer: mechanisms of trastuzumab resistance and novel targeted therapies. *Expert Rev Anticancer Ther* **11**, 263-275 (2011).
283. V. G. Martinez *et al.*, Resistance to HER2-targeted anti-cancer drugs is associated with immune evasion in cancer cells and their derived extracellular vesicles. *Oncoimmunology* **6**, e1362530 (2017).
284. G. P. Adams, L. M. Weiner, Monoclonal antibody therapy of cancer. *Nat Biotechnol* **23**, 1147-1157 (2005).
285. K. Nazimek, K. Bryniarski, Perspectives in Manipulating EVs for Therapeutic Applications: Focus on Cancer Treatment. *Int J Mol Sci* **21** (2020).
286. S. Najafi, J. Majidpoor, K. Mortezaee, Extracellular vesicle-based drug delivery in cancer immunotherapy. *Drug Deliv Transl Res* 10.1007/s13346-023-01370-3, 1-17 (2023).
287. A. Słomka *et al.*, EVs as Potential New Therapeutic Tool/Target in Gastrointestinal Cancer and HCC. *Cancers (Basel)* **12** (2020).
288. S. H. Lo, Focal adhesions: What's new inside. *Developmental Biology* **294**, 280-291 (2006).
289. L. A. Lonowski *et al.*, Genome editing using FACS enrichment of nuclease-expressing cells and indel detection by amplicon analysis. *Nat Protoc* **12**, 581-603 (2017).

290. C. E. Turner, Paxillin and focal adhesion signalling. *Nature Cell Biology* **2**, E231-E236 (2000).
291. D. K. Greene, S. Tumova, J. R. Couchman, A. Woods, Syndecan-4 associates with alpha-actinin. *J Biol Chem* **278**, 7617-7623 (2003).
292. S.-T. Lim, R. L. Longley, J. R. Couchman, A. Woods, Direct Binding of Syndecan-4 Cytoplasmic Domain to the Catalytic Domain of Protein Kinase Cα (PKCα) Increases Focal Adhesion Localization of PKCα*. *Journal of Biological Chemistry* **278**, 13795-13802 (2003).
293. E. S. Oh, A. Woods, J. R. Couchman, Syndecan-4 proteoglycan regulates the distribution and activity of protein kinase C. *J Biol Chem* **272**, 8133-8136 (1997).
294. S. Saoncella *et al.*, Syndecan-4 signals cooperatively with integrins in a Rho-dependent manner in the assembly of focal adhesions and actin stress fibers. *Proc Natl Acad Sci U S A* **96**, 2805-2810 (1999).
295. S. A. Wilcox-Adelman, F. Denhez, P. F. Goetinck, Syndecan-4 modulates focal adhesion kinase phosphorylation. *J Biol Chem* **277**, 32970-32977 (2002).
296. A. Woods, R. L. Longley, S. Tumova, J. R. Couchman, Syndecan-4 binding to the high affinity heparin-binding domain of fibronectin drives focal adhesion formation in fibroblasts. *Arch Biochem Biophys* **374**, 66-72 (2000).
297. D. Freitas *et al.*, Different isolation approaches lead to diverse glycosylated extracellular vesicle populations. *J Extracell Vesicles* **8**, 1621131 (2019).
298. B. Costa-Silva *et al.*, Pancreatic cancer exosomes initiate pre-metastatic niche formation in the liver. *Nat Cell Biol* **17**, 816-826 (2015).
299. J. Poças, M. Belting, Analysis of Extracellular Vesicle-Associated Proteoglycans. *Methods Mol Biol* **2619**, 125-139 (2023).
300. E. Panizza, R. M. M. Branca, P. Oliviusson, L. M. Orre, J. Lehtiö, Isoelectric point-based fractionation by HiRIEF coupled to LC-MS allows for in-depth quantitative analysis of the phosphoproteome. *Scientific Reports* **7**, 4513 (2017).
301. V. Indira Chandran *et al.*, Ultrasensitive Immunoprofiling of Plasma Extracellular Vesicles Identifies Syndecan-1 as a Potential Tool for Minimally Invasive Diagnosis of Glioma. *Clin Cancer Res* **25**, 3115-3127 (2019).
302. P. Correa, M. B. Piazuelo, The gastric precancerous cascade. *J Dig Dis* **13**, 2-9 (2012).
303. J. K. Sung, Diagnosis and management of gastric dysplasia. *Korean J Intern Med* **31**, 201-209 (2016).
304. S. H. Imran, E. Olivier, Challenges in Using ctDNA to Achieve Early Detection of Cancer. *bioRxiv* 10.1101/237578, 237578 (2017).

305. J. Phallen *et al.*, Direct detection of early-stage cancers using circulating tumor DNA. *Sci Transl Med* **9** (2017).
306. J. D. Cohen *et al.*, Detection and localization of surgically resectable cancers with a multi-analyte blood test. *Science* **359**, 926-930 (2018).
307. A. R. Parikh *et al.*, Liquid versus tissue biopsy for detecting acquired resistance and tumor heterogeneity in gastrointestinal cancers. *Nature Medicine* **25**, 1415-1421 (2019).
308. C. Foroni *et al.*, When Less Is More: Specific Capture and Analysis of Tumor Exosomes in Plasma Increases the Sensitivity of Liquid Biopsy for Comprehensive Detection of Multiple Androgen Receptor Phenotypes in Advanced Prostate Cancer Patients. *Biomedicines* **8** (2020).
309. J. Skog *et al.*, Glioblastoma microvesicles transport RNA and proteins that promote tumour growth and provide diagnostic biomarkers. *Nature Cell Biology* **10**, 1470-1476 (2008).
310. S. Singh *et al.*, Proteomic Signatures of Diffuse and Intestinal Subtypes of Gastric Cancer. *Cancers (Basel)* **13** (2021).
311. A. M. Moreira *et al.*, Proteomic Identification of a Gastric Tumor ECM Signature Associated With Cancer Progression. *Front Mol Biosci* **9**, 818552 (2022).
312. S. Ge *et al.*, A proteomic landscape of diffuse-type gastric cancer. *Nature Communications* **9**, 1012 (2018).
313. A. I. Tsonis *et al.*, Evaluation of the coordinated actions of estrogen receptors with epidermal growth factor receptor and insulin-like growth factor receptor in the expression of cell surface heparan sulfate proteoglycans and cell motility in breast cancer cells. *Febs j* **280**, 2248-2259 (2013).
314. S. M. Kim *et al.*, Protective Effects of Female Reproductive Factors on Lauren Intestinal-Type Gastric Adenocarcinoma. *Yonsei Med J* **59**, 28-34 (2018).
315. P. Muti, The role of endogenous hormones in the etiology and prevention of breast cancer: the epidemiological evidence. *Recent Results Cancer Res* **166**, 245-256 (2005).
316. S. L. Klein, K. L. Flanagan, Sex differences in immune responses. *Nature Reviews Immunology* **16**, 626-638 (2016).
317. C. Habes, G. Weber, C. Goupille, Sulfated Glycoaminoglycans and Proteoglycan Syndecan-4 Are Involved in Membrane Fixation of LL-37 and Its Pro-Migratory Effect in Breast Cancer Cells. *Biomolecules* **9** (2019).
318. F. Charni *et al.*, Syndecan-1 and syndecan-4 are involved in RANTES/CCL5-induced migration and invasion of human hepatoma cells. *Biochim Biophys Acta* **1790**, 1314-1326 (2009).

319. S. Adepu *et al.*, Incipient renal transplant dysfunction associates with tubular syndecan-1 expression and shedding. *Am J Physiol Renal Physiol* **309**, F137-145 (2015).
320. T. Manon-Jensen, Y. Itoh, J. R. Couchman, Proteoglycans in health and disease: the multiple roles of syndecan shedding. *The FEBS Journal* **277**, 3876-3889 (2010).
321. P. W. Park *et al.*, Activation of syndecan-1 ectodomain shedding by Staphylococcus aureus alpha-toxin and beta-toxin. *J Biol Chem* **279**, 251-258 (2004).
322. T. T. Vuong, T. M. Reine, A. Sudworth, T. G. Jenssen, S. O. Kolset, Syndecan-4 is a major syndecan in primary human endothelial cells in vitro, modulated by inflammatory stimuli and involved in wound healing. *J Histochem Cytochem* **63**, 280-292 (2015).
323. T. Pasqualon *et al.*, A transmembrane C-terminal fragment of syndecan-1 is generated by the metalloproteinase ADAM17 and promotes lung epithelial tumor cell migration and lung metastasis formation. *Cell Mol Life Sci* **72**, 3783-3801 (2015).
324. R. Kashyap *et al.*, Syntenin-knock out reduces exosome turnover and viral transduction. *Scientific Reports* **11**, 4083 (2021).
325. R. J. Petrie, A. D. Doyle, K. M. Yamada, Random versus directionally persistent cell migration. *Nature Reviews Molecular Cell Biology* **10**, 538-549 (2009).
326. B. H. Sung, T. Ketova, D. Hoshino, A. Zijlstra, A. M. Weaver, Directional cell movement through tissues is controlled by exosome secretion. *Nature Communications* **6**, 7164 (2015).
327. T. Parimon *et al.*, Syndecan-1 Controls Lung Tumorigenesis by Regulating miRNAs Packaged in Exosomes. *Am J Pathol* **188**, 1094-1103 (2018).
328. U. Barash *et al.*, Proteoglycans in health and disease: new concepts for heparanase function in tumor progression and metastasis. *Febs j* **277**, 3890-3903 (2010).
329. Z. Piperigkou, K. Kyriakopoulou, C. Koutsakis, S. Mastronikolis, N. K. Karamanos, Key Matrix Remodeling Enzymes: Functions and Targeting in Cancer. *Cancers (Basel)* **13** (2021).
330. R. R. Wei *et al.*, CTC clusters induced by heparanase enhance breast cancer metastasis. *Acta Pharmacol Sin* **39**, 1326-1337 (2018).
331. F. Teixeira, M. Götte, Involvement of Syndecan-1 and Heparanase in Cancer and Inflammation. *Adv Exp Med Biol* **1221**, 97-135 (2020).
332. E. M. Putz *et al.*, NK cell heparanase controls tumor invasion and immune surveillance. *J Clin Invest* **127**, 2777-2788 (2017).
333. I. Doweck, N. Feibish, Opposing Effects of Heparanase and Heparanase-2 in Head & Neck Cancer. *Adv Exp Med Biol* **1221**, 847-856 (2020).

334. L. P. Liu *et al.*, Helicobacter pylori promotes invasion and metastasis of gastric cancer by enhancing heparanase expression. *World J Gastroenterol* **24**, 4565-4577 (2018).
335. W. J. Yang, L. Shi, X. M. Wang, G. W. Yang, Heparanase is a novel biomarker for immune infiltration and prognosis in breast cancer. *Aging (Albany NY)* **13**, 20836-20852 (2021).
336. T. Li *et al.*, TGF-β1-SOX9 axis-inducible COL10A1 promotes invasion and metastasis in gastric cancer via epithelial-to-mesenchymal transition. *Cell Death Dis* **9**, 849 (2018).
337. L. Zhang, K. W. Peng, B. Wang, X. F. Yang, Z. M. Zhang, EDIL3 regulates gastric cancer cell migration, invasion and epithelial-mesenchymal transition via TGF-β1/XIST/miR-137 feedback loop. *Transl Cancer Res* **9**, 6313-6330 (2020).
338. F. Yang *et al.*, Interaction with CD68 and Regulation of GAS6 Expression by Endosialin in Fibroblasts Drives Recruitment and Polarization of Macrophages in Hepatocellular Carcinoma. *Cancer Res* **80**, 3892-3905 (2020).
339. D. Zdżalik-Bielecka *et al.*, The GAS6-AXL signaling pathway triggers actin remodeling that drives membrane ruffling, macropinocytosis, and cancer-cell invasion. *Proceedings of the National Academy of Sciences* **118**, e2024596118 (2021).
340. N. G. Seidah, R. Day, M. Marcinkiewicz, M. Chrétien, Precursor convertases: an evolutionary ancient, cell-specific, combinatorial mechanism yielding diverse bioactive peptides and proteins. *Ann N Y Acad Sci* **839**, 9-24 (1998).
341. T. Nakajima *et al.*, Prohormone convertase furin has a role in gastric cancer cell proliferation with parathyroid hormone-related peptide in a reciprocal manner. *Dig Dis Sci* **47**, 2729-2737 (2002).
342. L. G. Lima *et al.*, Tumor microenvironmental cytokines bound to cancer exosomes determine uptake by cytokine receptor-expressing cells and biodistribution. *Nature Communications* **12**, 3543 (2021).
343. C. Williams *et al.*, Assessing the role of surface glycans of extracellular vesicles on cellular uptake. *Scientific Reports* **9**, 11920 (2019).
344. W. F. Altei *et al.*, Inhibition of αvβ3 integrin impairs adhesion and uptake of tumor-derived small extracellular vesicles. *Cell Communication and Signaling* **18**, 158 (2020).
345. H. I. Choi *et al.*, Helicobacter pylori-derived extracellular vesicles increased in the gastric juices of gastric adenocarcinoma patients and induced inflammation mainly via specific targeting of gastric epithelial cells. *Exp Mol Med* **49**, e330 (2017).

346. A. S. Chung, Q. Gao, W. J. Kao, Either integrin subunit beta1 or beta3 is involved in mediating monocyte adhesion, IL-1beta protein and mRNA expression in response to surfaces functionalized with fibronectin-derived peptides. *J Biomater Sci Polym Ed* **18**, 713-729 (2007).
347. P. Fuentes *et al.*, ITGB3-mediated uptake of small extracellular vesicles facilitates intercellular communication in breast cancer cells. *Nat Commun* **11**, 4261 (2020).
348. A. Ito *et al.*, Extracellular vesicles shed from gastric cancer mediate protumor macrophage differentiation. *BMC Cancer* **21**, 102 (2021).
349. C. L. Chaffer, R. A. Weinberg, A perspective on cancer cell metastasis. *Science* **331**, 1559-1564 (2011).
350. S. Hiratsuka, A. Watanabe, H. Aburatani, Y. Maru, Tumour-mediated upregulation of chemoattractants and recruitment of myeloid cells predetermines lung metastasis. *Nature Cell Biology* **8**, 1369-1375 (2006).
351. R. N. Kaplan *et al.*, VEGFR1-positive haematopoietic bone marrow progenitors initiate the pre-metastatic niche. *Nature* **438**, 820-827 (2005).
352. Y. Liu, X. Cao, Characteristics and Significance of the Pre-metastatic Niche. *Cancer Cell* **30**, 668-681 (2016).
353. K. Yanagihara *et al.*, Development and biological analysis of peritoneal metastasis mouse models for human scirrhous stomach cancer. *Cancer Sci* **96**, 323-332 (2005).
354. K. Yanagihara *et al.*, Establishment of two cell lines from human gastric scirrhous carcinoma that possess the potential to metastasize spontaneously in nude mice. *Cancer Sci* **95**, 575-582 (2004).
355. D. Shukla *et al.*, A novel role for 3-O-sulfated heparan sulfate in herpes simplex virus 1 entry. *Cell* **99**, 13-22 (1999).
356. S. A. Melo *et al.*, Author Correction: Glypican-1 identifies cancer exosomes and detects early pancreatic cancer. *Nature* **610**, E15-E17 (2022).
357. M. Clos-Sansalvador, M. Monguió-Tortajada, S. Roura, M. Franquesa, F. E. Borràs, Commonly used methods for extracellular vesicles' enrichment: Implications in downstream analyses and use. *European Journal of Cell Biology* **101**, 151227 (2022).
358. Y. Jia *et al.*, Small extracellular vesicles isolation and separation: Current techniques, pending questions and clinical applications. *Theranostics* **12**, 6548-6575 (2022).
359. R. E. Veerman *et al.*, Molecular evaluation of five different isolation methods for extracellular vesicles reveals different clinical applicability and subcellular origin. *Journal of Extracellular Vesicles* **10**, e12128 (2021).

360. H. Zhang *et al.*, Exosome-delivered EGFR regulates liver microenvironment to promote gastric cancer liver metastasis. *Nat Commun* **8**, 15016 (2017).
361. B. Février, G. Raposo, Exosomes: endosomal-derived vesicles shipping extracellular messages. *Curr Opin Cell Biol* **16**, 415-421 (2004).
362. J. Ratajczak, M. Wysoczynski, F. Hayek, A. Janowska-Wieczorek, M. Z. Ratajczak, Membrane-derived microvesicles: important and underappreciated mediators of cell-to-cell communication. *Leukemia* **20**, 1487-1495 (2006).
363. J. C. Akers, D. Gonda, R. Kim, B. S. Carter, C. C. Chen, Biogenesis of extracellular vesicles (EV): exosomes, microvesicles, retrovirus-like vesicles, and apoptotic bodies. *J Neurooncol* **113**, 1-11 (2013).
364. S. Pant, H. Hilton, M. E. Burczynski, The multifaceted exosome: biogenesis, role in normal and aberrant cellular function, and frontiers for pharmacological and biomarker opportunities. *Biochem Pharmacol* **83**, 1484-1494 (2012).
365. A. V. Vlassov, S. Magdaleno, R. Setterquist, R. Conrad, Exosomes: current knowledge of their composition, biological functions, and diagnostic and therapeutic potentials. *Biochim Biophys Acta* **1820**, 940-948 (2012).
366. S. Bratulic *et al.*, Noninvasive detection of any-stage cancer using free glycosaminoglycans. *Proceedings of the National Academy of Sciences* **119**, e2115328119 (2022).